UNIVERSITÀ DEGLI STUDI DI CAGLIARI

DIPARTIMENTO DI CHIMICA INORGANICA ED ANALITICA

PhD thesis of

Anna Pintus

Design, Synthesis and Characterisation of Homoleptic and Heteroleptic 1,2-Dichalcogenolene Platinum and Gold Complexes with Potential ICT Applications: an Experimental and Theoretical Study.

Supervisor: Coordinator:

Dr. Massimiliano Arca   Prof. Mariano Casu

Scuola di Dottorato in Scienze e Tecnologie Chimiche e Farmaceutiche

XXIII Ciclo, 2008-2010

Acknowledgments

I would like to express my gratitude to my supervisor, Dr. Massimiliano Arca, whose expertise, understanding, and patience, enriched considerably my research experience.

I wish to thank all the other members of the research group I have been working with, namely Prof. Francesco A. Devillanova, Prof. Vito Lippolis, Dr. M. Carla Aragoni, Prof. Francesco Isaia, Prof. Gaetano Verani, Dr. Claudia Caltagirone, Dr. Alessandra Garau, and Dr. Greta De Filippo, for the assistance and encouragement they provided at all levels of the research project.

I would also like to acknowledge Prof. Dominique Lorcy from Rennes 1 University and Prof. M. Agostina Cinellu from Sassari University for their crucial contribution to this work, and Prof. Mike Ward, Dr. Mike J. Morris and Dr. Julia Weinstein, who gave me the opportunity of spending a productive and stimulating research stay at the University of Sheffield. I also wish to acknowledge Prof. Francesco Lelj for my useful and educational stay at the University of Basilicata.

Prof. Mike Hursthouse, Dr. Susanne Huth, Dr. Samantha Callear, Dr. Simon J. Coles, Prof. J. Derek Woollins, and Prof. Alexandra M. Z. Slawin are acknowledged for the structural characterisations, and Prof. Marco Sampietro and Dr. Dario Natali for the photophysical measurements.

My thanks to Mr. Antonio Sabeddu, who performed the elemental analysis measurements reported in this work.

Finally I would like to thank Dr. Annalisa Mancini and Ms Lucia Ambrosio for their contribution to this work, and all the students I worked with for providing a stimulating and fun environment in which to learn and grow.

Contents

Contents

II

List of Compounds

1	[Ni(Ph$_2$-edt)$_2$]
2	[Ni(mnt)$_2$]
3	[Ni(H$_2$-edt)$_2$]
4	[Pd(H$_2$-edt)$_2$]
5	[Pt(H$_2$-edt)$_2$]
6	[Ni(dfcdt)$_2$]
7	[Ni(fcdt)$_2$]
8	[Ni(dfcvt)$_2$]
9	[Ni(Et-dmet)$_2$]
10	[Pd(Et-dmet)$_2$]
11	[Pt(Et-dmet)$_2$]
12	[Ni(dmit)$_2$]
13	[Ni(Et$_2$-timdt)$_2$]
14	[Pt(mnt)$_2$]
15	[Au(mnt)$_2$]
16	[Pt(2,2′-bipy)(tds)]
17	[Pt(ppy)(mnt)]
18	[Pt(tpy)(mnt)]
19	[Au(ppy)(tdt)]
20	[Au(Ph,H-edt)$_2$]
21	[Au(Naph,H-edt)$_2$]
22	[Au(Pyr,H-edt)$_2$]
23	*O*-Isopropyl *S*-Phenyl Dithiocarbonate
24	*O*-Isopropyl *S*-Nahthyl Dithiocarbonate
25	*O*-Isopropyl *S*-Pyrenyl Dithiocarbonate
26	Phenyl-1,3-dithiol-2-one
27	2-Naphthyl-1,3-dithiol-2-one
28	1-Pyrenyl-1,3-dithiol-2-one
29	[Au(2-Py,H-edt)$_2$]
30	[Au(3-Py,H-edt)$_2$]
31	[Au(4-Py,H-edt)$_2$]
32	[Au(C$_6$H$_4$S$_2$)$_2$]
33	[Au(Ph$_2$-edt)$_2$]
34	2,5-*Bis*(naphthyl)-thiophene
35	[Zn(Me-dmet)$_2$]
36	[Ni(Me-dmet)$_2$]
37	[Pd(Me-dmet)$_2$]
38	[Zn(Me-dset)$_2$]
39	[Ni(Me-dset)$_2$]
40	[Pd(Me-dset)$_2$]
41	[Pt(2,2′-bipy)Cl$_2$]
42	[Pt(1,10-phen)Cl$_2$]
43	[Pt(5,5′-Me$_2$-bipy)Cl$_2$]

List of Compounds

44	[Pt(4,4′-Me$_2$-bipy)Cl$_2$]
45	[Pt(4,4′-tBu$_2$-bipy)Cl$_2$]
46	[Pt(4,4′-Ph$_2$-bipy)Cl$_2$]
47	[Pt(3,7-Ph$_2$-phen)Cl$_2$]
48	[Pt(3,4,7,8-Me$_4$-bipy)Cl$_2$]
49	*N*-Methyl-4,5-*bis*(2′-cyanoethylthio)-1,3-thiazol-2-thione
50	*N*-Ethyl-4,5-*bis*(2′-cyanoethylthio)-1,3-thiazol-2-thione
51	*N*-Phenyl-4,5-*bis*(2′-cyanoethylthio)-1,3-thiazol-2-thione
52	*N*-Methyl-4,5-*bis*(2′-cyanoethylseleno)-1,3-thiazol-2-thione
53	[Pt(2,2′-bipy)(Ph,H-edt)]
54	[Pt(2,2′-bipy)(Naph,H-edt)]
55	[Pt(2,2′-bipy)(Pyr,H-edt)]
56	[Pt(2,2′-bipy)(Me-dmet)]
57	[Pt(2,2′-bipy)(Et-dmet)]
58	[Pt(2,2′-bipy)(Ph-dmet)]
59	[Pt(2,2′-bipy)(Me-dset)]
60	[Pt(1,10-phen)(Ph,H-edt)]
61	[Pt(1,10-phen)(Naph,H-edt)]
62	[Pt(1,10-phen)(Pyr,H-edt)]
63	[Pt(1,10-phen)(Me-dmet)]
64	[Pt(1,10-phen)(Et-dmet)]
65	[Pt(1,10-phen)(Ph-dmet)]
66	[Pt(1,10-phen)(Me-dset)]
67	[Pt(5,5′-Me$_2$-bipy)(Me-dmet)]
68	[Pt(4,4′-Me$_2$-bipy)(Me-dmet)]
69	[Pt(4,4′-tBu$_2$-bipy)(Me-dmet)]
70	[Pt(4,4′-Ph$_2$-bipy)(Me-dmet)]
71	[Pt(3,7-Ph$_2$-phen)(Me-dmet)]
72	[Pt(3,4,7,8-Me$_4$-phen)(Me-dmet)]
73	[Pt(4,4′-tBu$_2$-bipy)(Fc,H-edt)]
74	Ferrocenyl-1,3-dithiol-2-one
75	[Pt(phen)(tdt)]
76	[Au(Py[1])(mnt)]
77	[Au(Py[1])Cl$_2$]

1. *Introduction*

Metal 1,2-dithiolenes are a well-studied class of coordination compounds, featuring 1,2-dialkene- or 1,2-diaryl dithiolates ligands. The name of 1,2-dithiolene was originally introduced by Mc Cleverty[1] as a simple nomenclature to describe the metal complexes bearing bidentate sulphur-donor ligands connected via an unsaturated carbon-carbon bond (Scheme 1.1), and refer neither to a specific molecular charge nor to the oxidation state of the central metal ion.

edt   tfd   mnt   mant   madt   dtsq

mdt   dmt   dmit   dmio   dmise

α-tpdt   btdt   dtcs   midt

tds   R-dmet   R,R'-timdt   qdt   pdt

dddt   ddt   cddt   medt

phdt   dphdt   bdt   tdt

ddtdt   ttdt   diod   F₂pdt
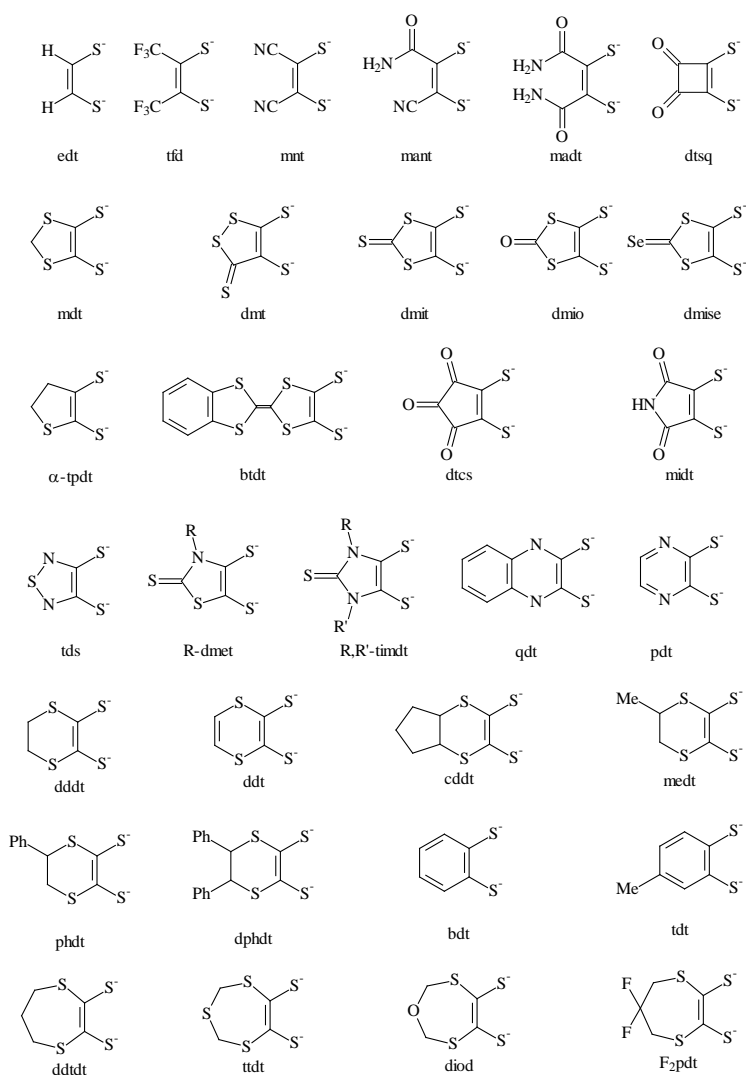
Scheme 1.1. *Selected 1,2-dithiolene ligands and commonly used acronyms. All ligands have been drawn in their 1,2-dithiolato form.*

The chemistry of 1,2-dithiolene ligands has been finding increasing interest in the scientific community over the past 40 years, although unsaturated 1,2-dithiolates, such as toluene-3,4-dithiolate (tdt^{2-}, Scheme 1.1), and their reactivity towards several metal ions have been subject of study since the mid-1930s by Clarck and coworkers.[2] In 1957, Bähr and Schleitzer[3] first reported a Pd complex deriving from the sodium salt of a ligand they had prepared, Na_2mnt (mnt^{2-} = 1,2-maleonitrile-1,2-dithiolate, Scheme 1.1), and observed that the complex could be oxidised to an unidentified product. Two years later, Stevancevic and Drazic[4] reported some dianionc metal complexes derived from quinoxaline-2,3-dithiol (H_2qdt, Scheme 1.1). Nevertheless, it was only in the mid-1960s with the seminal works by Schrauzer and Mayweg[5] on $[Ni(Ph_2-edt)_2]$ (**1**, Ph_2-edt^{2-} = 1,2-diphenyl-ethylene-1,2-dithiolato), and by Gray on nickel maleonitrile-1,2-dithiolate complexes[6] (**2**) that the chemistry of 1,2-dithiolene complexes started to attract the interest of researchers. Since then, a very large variety of different 1,2-dithiolene ligands and their complexes with numerous metal ions has been reported, and the interest in 1,2-dithiolene chemistry has been continuously increasing,[7] also because of the discovery of a large number of applications, in fields as varied as c3onductivity, magnetism, linear and nonlinear optical properties, and due to the role of 1,2-dithiolene systems in biology.[8]

In 1967, in view of interest focusing on the chemistry of 1,2-dithiolene complexes, Davison and Shawl thought it was reasonable to prepare the corresponding selenium-containing complexes, and synthesised several 1,2-diselenolene transition metal complexes.[9] The number of scientific works addressing metal complexes bearing 1,2-diselenolene ligands (Scheme 1.2) is much smaller than that regarding 1,2-dithiolene complexes, both because of synthetic difficulties and because the properties of these complexes are very similar to those of the fully sulphured congeners.[10] Descending

along the chalcogen group, only very few publications have addressed the synthesis and characterisation of 1,2-ditellurolene complexes.[11]
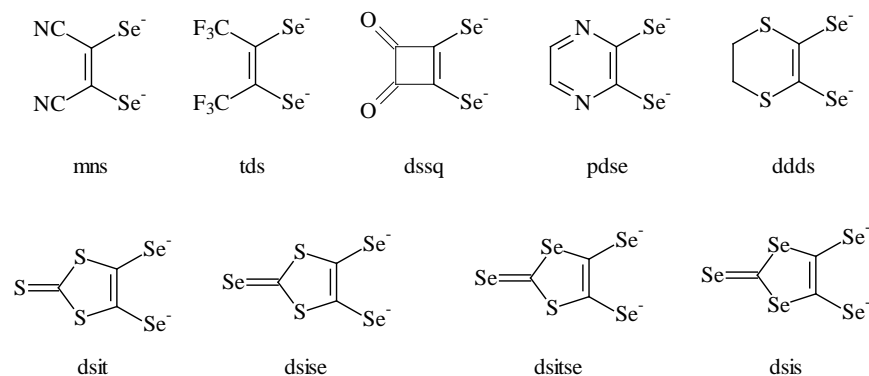
Scheme 1.2. *Selected 1,2-diselenolene ligands and commonly used acronyms. All ligands have been drawn in their 1,2-diselenolato form.*

Due to the great variety of application fields, 1,2-dichalcogenolene ligands appear in a huge number of both homoleptic and heteroleptic complexes. In this chapter, an overview on the synthesis of different 1,2-dichalcogenolene ligands and the synthesis, properties and applications of their metal homoleptic and heteroleptic complexes will be briefly provided.

1.1. Synthesis of 1,2-dichalcogenolene ligands and precursors

The synthesis of metal complexes deriving from 1,2-dichalcogenolato ligands is generally complicated by the tendency of these ligands to polymerise or decompose.[12] A plethora of different and specific synthetic routes to 1,2-dichalcogenolene ligands has been reported, but some general routes can be identified.[13]

1.1.1. Synthesis of arene-1,2-dichalcogenolato ligands

Arene-1,2-dichalcogenolene ligands are generally stable as 1,2-dichalcogenolato sodium salts,[14] and can be prepared by following two different synthetic approaches, as shown in Scheme 1.3 for bdt^{2-}.
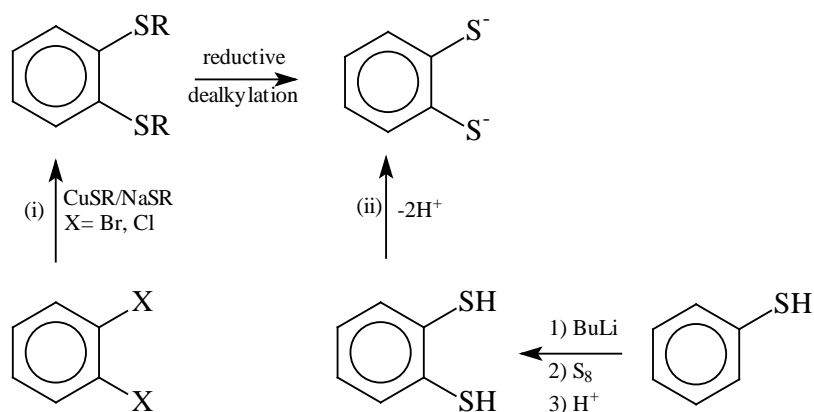
Scheme 1.3. *Strategies for the synthesis of 1,2-benzenedithiolate (bdt^{2-}) and related ligands.*

According to the former synthetic route, the desired dihalo-arene is reacted with cuprous or sodium thiolates to give the corresponding vicinal thioether, which can be reductively dealkylated to give the dithiol.[15] Alternatively, the appropriate arenethiol is reacted with *n*-BuLi, and the resulting lithiated product is made to react with elemental sulphur to give the corresponding 1,2-dithiolate salt.

The corresponding diselenolene ligand can be obtained by reacting the desired 1,2-dibromoarene with Na$_2$Se to give a poly(*o*-arylenediselenide), which can be reduced by NaBH$_4$, yielding a arene-1,2-diselenolate anion.[16]

1.1.2. Synthesis of alkene-1,2-dichalcogenolato ligands

Compared to arene-1,2-dithiols, alkene-1,2-dithiols and the corresponding dithiolates are generally much less stable, and must be protected until reacted with the metal salt. Also in this case, several synthetic routes are available, as summarised in Scheme 1.4.
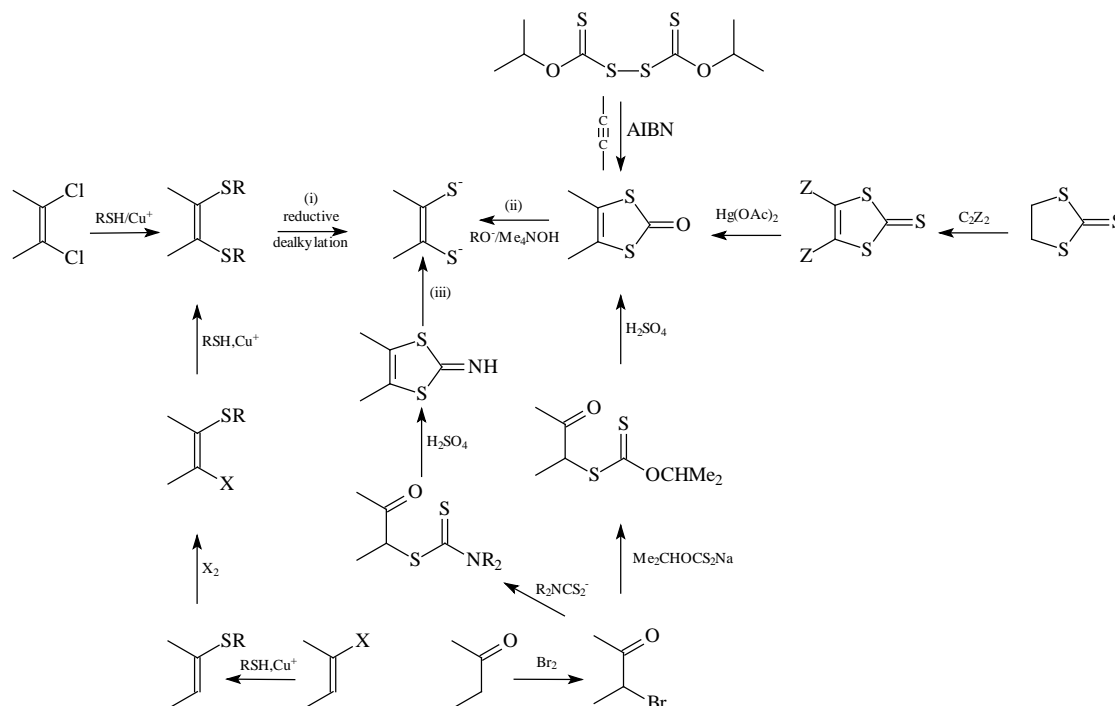
Scheme 1.4. *Strategies for the synthesis of ethylene-1,2-dithiolato ligands.*

A first method [(i) in Scheme 1.4] is analogous to that described for arene-1,2-dithiolates: an appropriate dithioether, such as a *cis*-1,2-*bis*(benzylthio)alkene (R′ = CH$_2$Ph in Scheme 1.4), is made to react with a strongly reducing agent to give the corresponding *cis*-alkene-1,2-dithiolato. The dithioether can be obtained starting from mono- or 1,2-dihaloalkenes.

In the second method, α-bromoketones, obtainable by direct halogenation of the desired ketones, are reacted with alkylxanthate or *N,N′*-dialkyldithiocarbamate salts [typically

^{i}PrOCS$_2$Na and (^{i}Pr)$_2$NCS$_2$Na, respectively][17] to give the corresponding α-ketoxanthate or α-ketodithiocarbamate esters, which undergo cyclisation in strongly acid medium to give the vinylene dithiocarbonate or iminiumdithiocarbonate. Both types of compounds lead to the desired symmetrically or asymmetrically substituted alkene-1,2-dithiolate when reacted with strong bases [reactions (ii) and (iii) in Scheme 1.4].[17,18]

Alternatively, 1,3-dithiol-2-ones can be obtained by reacting diisopropylxanthogen disulfide with unsaturated substrates, such as disubstituted alkynes R$_2$C$_2$, in the presence of AIBN [azo bis (isobutyronitrile)], a radical initiator.[19]

Finally, vinylene dithiocarbonates can be obtained by reacting mercury(II) acetate with the corresponding trithiocarbonates, generated by reaction of electrophilic alkynes with ethylene trithiocarbonate.[20] Analogously, disubstituted vinylene triselenocarbonates have been obtained by reacting the corresponding ethylenetriselenocarbonates with activated alkynes R$_2$C$_2$.[21]

1.1.3. Synthesis of mnt^{2-}, dmit^{2-}, and isologs

Specific procedures have been used for the synthesis of the two most commonly adopted 1,2-dithiolene ligands, mnt^{2-} and dmit^{2-}, and their selenium isologs (Schemes 1.1 and 1.2). The disodium salt of mnt^{2-} (Na$_2$mnt) is synthesised by reacting NaCN with CS$_2$, which leads to the formation of [S$_2$CCN]$^-$ as intermediate. This species undergoes a coupling reaction accompanied by loss of sulphur to give the desired ligand.[22]

The dmit^{2-} ligand and its selenated analogue dsis^{2-} are obtained through the chemical or electrochemical reduction of CS$_2$ and CSe$_2$ respectively, along with the corresponding trichalcogenocarbonate (Scheme 1.5). Both anions can be isolated as air stable quaternary ammonium salts of the corresponding Zn complexes, [Zn(dmit)$_2$]$^{2-}$ and [Zn(dsis)$_2$]$^{2-}$.[23]
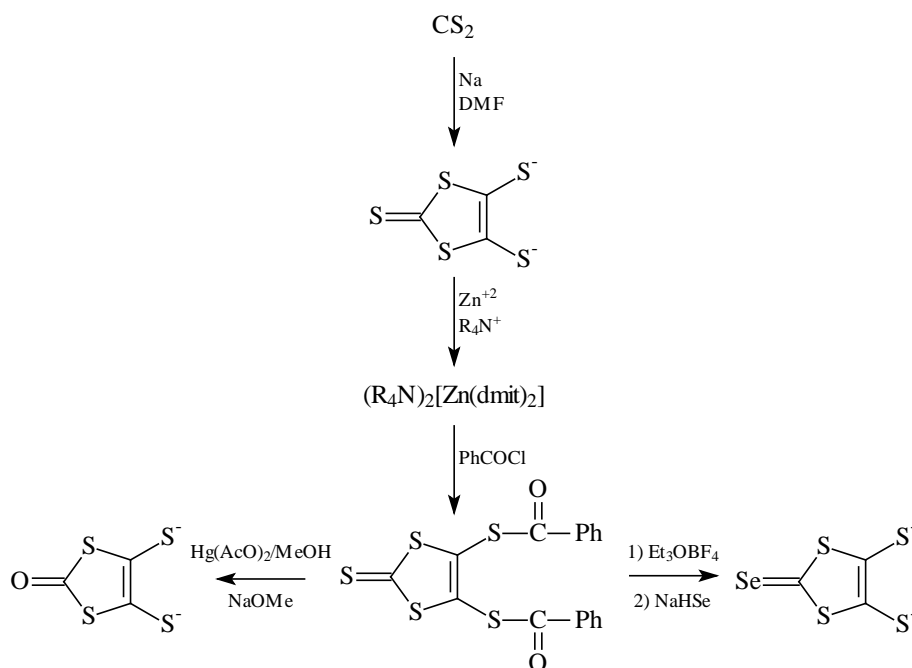
Scheme 1.5. *Strategies for the synthesis of dmit^{2-}, dmid^{2-}, and dmise^{2-} ligands.*

In addition, $[Zn(dmit)_2]^{2-}$ and $[Zn(dsis)_2]^{2-}$ can be reacted with PhCOCl to give the thioesters dmit[C(O)Ph]$_2$ and dsis[C(O)Ph]$_2$, whose hydrolysis with NaOMe yields Na$_2$dmit and Na$_2$dsis respectively.[24] Replacement of the terminal sulphur of the dmit^{2-} ligand with oxygen or selenium has been performed to prepare the dmid^{2-} and dmise^{2-} ligands.[25]

1.1.4. Synthesis of R,R'-timdt^{2-} and R–dmet^{2-}

In recent years, another synthetic strategy for obtaining a new class of ligands related to dmit^{2-}, namely R,R′-timdt^{2-} (*N,N'*-disubstituted 2-thioxoimidazoline-4,5-dithiolate, Scheme 1.1), was developed.[12,26] This route does not allow for isolating the ligand, but consists in the preparation of the ligand and in the *in situ* formation of the complex in a one-pot reaction. The corresponding complexes of Ni, Pd, and Pt were in fact synthesised by sulphuration with Lawesson's reagent [2,4-*bis*(4-methoxyphenyl)-

1,3,2,4-dithiadiphosphetane-2,4-disulfide] of *N,N'*-disubstituted 2-thioxoimidazolidine-4,5-diones [(i) in Scheme 1.6], in the presence of the desired metal introduced as powder (M = Ni) or halide (M = Pd, Pt). This synthetic procedure was extended by our research group to an ulterior related class of ligands with highly delocalised π-systems (R-dmet^{2-} or R-thiazdt^{2-}, as recently reported; *N*-substituted 2-thioxo-thiazoline-4,5-dithiolate; Scheme 1.1),[27,28] and an alternative method for the preparation of these ligands (and their selenated analogues, R-dset^{2-}) has been recently reported, involving the direct sulphuration/selenation of a thiazolidine-4,5-dione through a lithiating agent [(ii) in Scheme 1.6].[28]
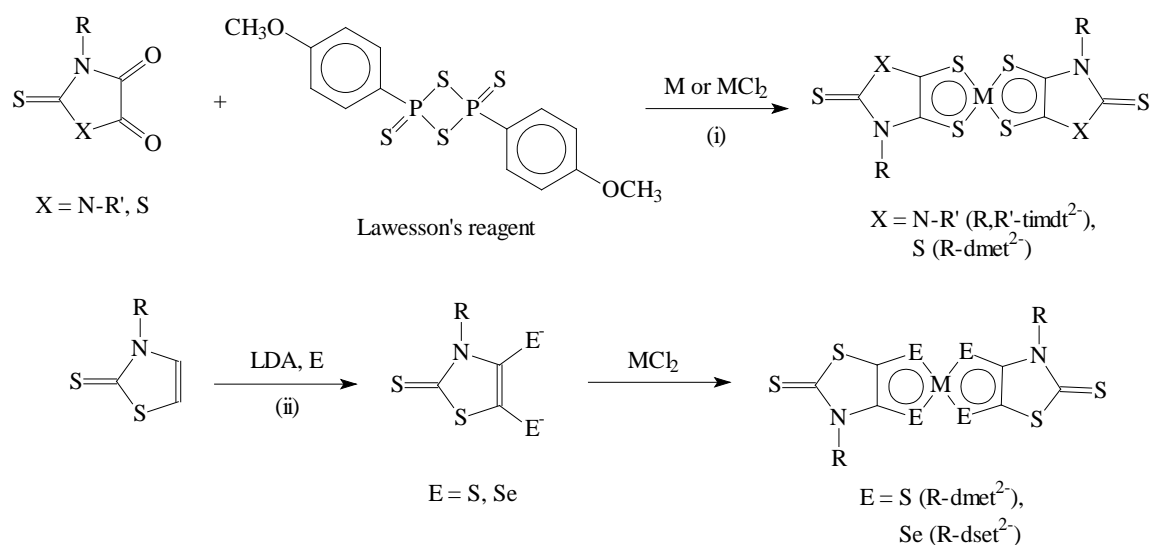
Scheme 1.6. *Strategies for the synthesis of R,R'-timdt^{2-} and R-dmet^{2-} ligands and their metal complexes.*

1.2. Homoleptic 1,2-dichalcogenolene metal complexes

1,2-Dichalcogenolene ligands form complexes with main group and *d* transition metal ions. *Bis*(1,2-dithiolene) complexes have been obtained for metals such as Cr, Mn, Ni,

Cu, Zn for the first row, Pd, Ag, and Cd for the second row, and Pt, Au, and Hg for the

third row.[13] On the other hand, homoleptic *tris*(1,2-dithiolene) complexes were obtained

for Ti, V, Cr, Zn, Mo, Tc, Ru, Ta, W, Re and Os. Fe and Co were found both in *bis* and

tris(1,2-dithiolene) complexes.

Bis(1,2-dichalcogenolene) complexes of d^8 transition metals, exhibiting square-planar

structures, have been particularly investigated in the past. The simplest *bis*(1,2-

dithiolene) complex is [M(H$_2$-edt)$_2$] [M = Ni (**3**), Pd (**4**), Pt (**5**), H$_2$-edt^{2-} = ethylene-1,2-

dithiolate, Scheme 1.1], commonly called "parent dithiolene" (Figure 1.1).
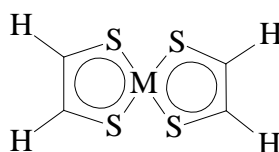
Figure 1.1. *Molecular scheme for [M(H$_2$-edt)$_2$] complexes of d^8 metal ions.*

All *bis*(1,2-dithiolene) complexes can be considered as formally derived from the parent

dithiolene by substitution of one or both of its hydrogen pendants with different alkyl or

aryl groups, except those containing the 1,2-dithiolene ligand condensed with a five- or

six-membered ring, such as the well known benzene-1,2-dithiolate (bdt^{2-}) and 2-thioxo-

1,2-dithiole-4,5-dithiolate (dmit^{2-}) ligands (Scheme 1.1).

One of the peculiar properties of this class of compounds is the ability of the molecular

entity to carry a charge which can vary considerably between anionic and neutral or

cationic states, the different molecular oxidation states being reversibly accessible by

chemical or electrochemical means (Scheme 1.7 for group 10 metal ions).
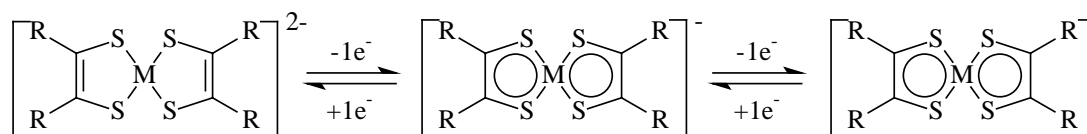
Scheme 1.7. *Redox processes involving bis(1,2-dithiolene) complexes of group 10 metal ions.*

This makes it difficult to assign clearly separated formal charges to the metal and to the ligand, (Scheme 1.8 for a neutral diamagnetic complex), so that 1,2-dithiolene ligands can be considered as ene-1,2-dithiolate dianions, neutral dithioketones, or mixed-valence thioketone-radical thiolate monoanions. This behaviour led in the past to a vivid debate on the nature of 1,2-dithiolene ligands, that have been regarded both as *"innocent"* and *"noninnocent"* ligands.[29] A ligand is considered innocent when it allows to define unambiguously the oxidation state of the central metal ion in the complex, according to the definition provided by Jørgeson.[30] More recently Ward and McCleverty pointed out that the term noninnocent is applied properly when referred to a particular combination of the metal and the ligand rather than to redox-active ligands alone.[31] When the metal- and ligand-centred molecular orbitals of the complex lie at different energies, their redox potentials are separated, and the related redox processes can be clearly assigned to the metal or to the ligand; on the other hand, if a significant mixing between the metal- and ligand-centred molecular orbitals occurs, ambiguity is found in assigning the redox processes of the complex.[32]
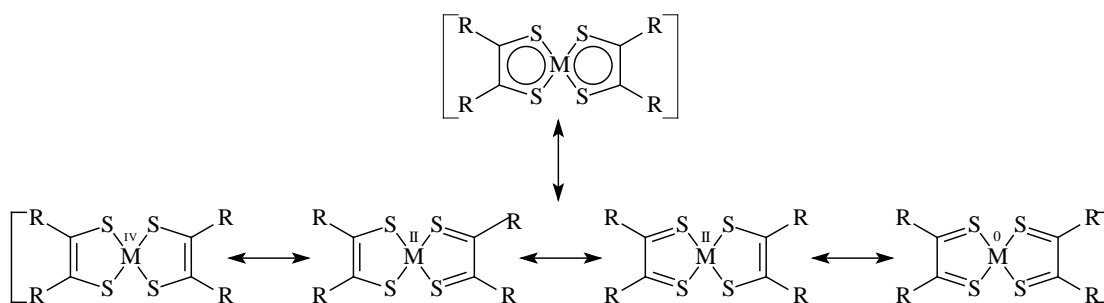
Scheme 1.8. *Lewis structures for neutral bis(1,2-dithiolene) complexes of d^8 metal ions.*

1.2.1 Synthesis

Bis and *tris*(1,2-dichalcogenolene) complexes are usually obtained as anionic species, by adopting different synthetic routes, which vary depending upon the nature of the starting 1,2-dichalcogenolene ligands or precursors, as summarised in Scheme 1.9.[13]

(i) Stable 1,2-dichalcogenolene salts, such as those of mnt^{2-} or arene-1,2-dithiolates, directly give the corresponding homoleptic *bis* or *tris*(1,2-dichalcogenolene) complexes when reacted with the appropriate metal halides.[33] (ii) As previously mentioned, the isolation of dmit^{2-} and isologs in the form of quaternary ammonium salts of the corresponding Zn-complexes made it possible to obtain a large variety of different anionic complexes through ligand exchange reactions.[34] (iii) As already mentioned, metal 1,2-dichalcogenolene complexes can also be obtained by hydrolysing precursors of the 1,2-dichalcogenolene ligands such as vinylene dichalcogenocarbonates in alkaline media in the presence of a suitable metal salt.[21,35] (iv) As regards the tdf^{2-} and tds^{2-} ligands, the corresponding *bis*(1,2-dichalcogenolene) complexes can be synthesised starting from 1,2-dithietes or 1,2-diselenoletes, four-membered R$_2$C$_2$E$_2$ rings formally deriving from the oxidation of the corresponding alkene-1,2-dichalcogenolates[36] (E = S, Se).[13,37] Correlated is the sulphuration of α-hydroxyketones (acyloins)[13,38] and 1,2-diketones with reagents such as P$_4$S$_{10}$ or Lawesson's reagent[39] in the presence of metal

11

salts or elemental metals.[13,37,40] This method was used to prepare several diaryl substituted 1,2-dichalcogenolene complexes, as well as to synthesise neutral complexes belonging to the classes $[M(R,R'\text{-timdt})_2]$[12] and $[M(R\text{-dmet})_2]$[27] (see above, M = Ni, Pd, Pt). (v) The reaction of electrophilic alkynes, such as DMAD (dimethyl acetylenedicarboxylate), with metal per- and poly-chalcogenido complexes was also exploited for the synthesis of 1,2-dichalcogenolene complexes.[13,41]
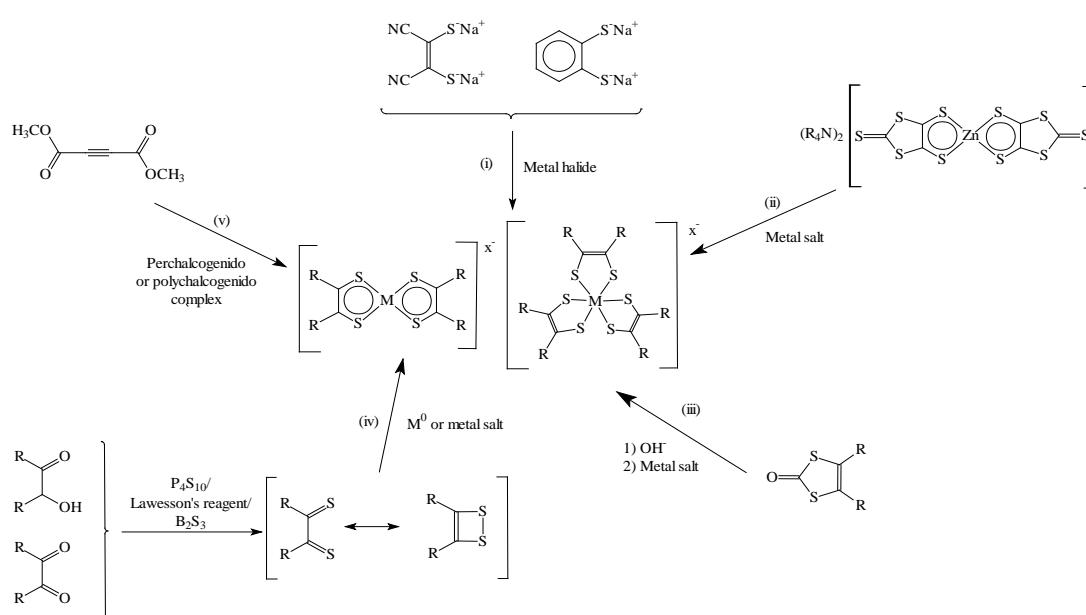
Scheme 1.9. *Strategies for the synthesis of homoleptic bis and tris(1,2-dithiolene) complexes.*

Whatever the synthetic route adopted, the isolated *bis* or *tris*(1,2-dichalcogenolene) complexes can be further exploited as starting materials for exchange reactions, involving both redox and non-redox processes.[23h,42]

1.2.2. General structural features

Solid state diffraction techniques play a primary role in the understanding of the structural features of metal 1,2-dichalcogenolene complexes, also in view of the

importance of solid-state properties of these compounds. In fact, as previously pointed out, 1,2-dichalcogenolene ligands possess the ability to carry variable molecular charges, and in this context interatomic distances within the chelate rings, along with the frequencies of the related stretching vibrations, have been used as indicators to elucidate the electronic configuration of the complexes, and to distinguish between the 1,2-dichalcogenolate and 1,2-dichalcogenone limit forms of the ligands. In particular, for 1,2-dithiolene ligands, C-C distances in the range of 1.30–1.36 Å and C-S distances in the range 1.71–1.75 Å are considered to be typical of C=C double and C-S single bonds respectively, thus suggesting a ene-1,2-dithiolate form ($^-$S-C=C-S$^-$) for the ligand, while longer C-C and shorter C-S distances indicate the presence of the 1,2-dithioketone (S=C-C=S) form.[43]

Since the first structural reports on complexes **1** and **2**$^{2-}$ were published,[5,44] several reviews have focused on the structural features and packing effects of 1,2-dichalcogenolene complexes[1,40,45] and an examination of the structural reports allows to deduce some features common to the large variety of compounds examined.[46]
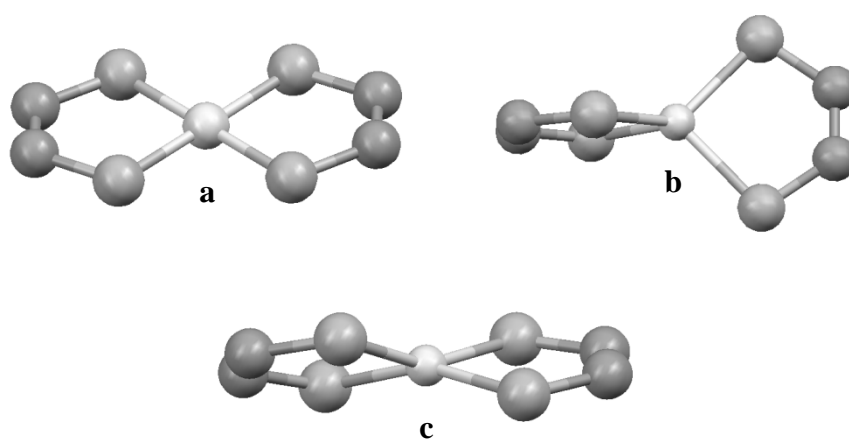
Figure 1.2. *Examples of common coordination geometries in homoleptic bis(1,2-dithiolene) metal complexes: a) square-planar; b) tetrahedral; c) distorted tetrahedral.*

(1) In *bis*(1,2-dichalcogenolene) complexes the central metal ion adopts square-planar, tetrahedral or near tetrahedral coordination geometries (Figure 1.2).

Several structural parameters, such as the dihedral angle between the two E-M-E planes, the angle c_1-M-c_2 (where c_1 and c_2 represent the midpoints between the two coordinating chalcogen atoms of the two ligand units), and the bend angle between the E-M-E and E-C-C-E planes, have been used to better define the coordination geometry of the metal and qualify the distortions with respect to idealised geometries (Figure 1.3, for E = S).[46]
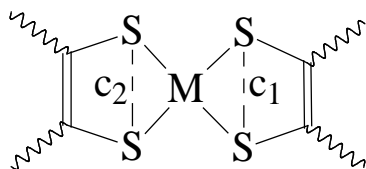
Figure 1.3. *Definition of the c_1-M-c_2 angle in bis(1,2-dithiolene) complexes*.

An examination of the Cambridge Crystallographic Database[47] allows to evidence that the nature of the central metal ion shows a great influence on the structural parameters of the *bis*(1,2-dichalcogenolene) complexes, especially as regards M-E bond lengths.[48]

On the other hand, the other bond lengths are quite constant in *bis*(1,2-dichalcogenolene) complexes. For example, in *bis*(1,2-dithiolene) complexes C-S distances cover a range of 0.135 Å (1.642-1.777 Å), while C=C distances fall within a 0.236 Å range (1.284-1.520 Å).[46] As far as angles are concerned, S-M-S angles have been found to range between 86.5 and 96.4°, and tend to be smaller for longer M-S distances.[46] Ranges for M-S-C and S-C-C angles are between 92.1 and 107.3° and between 117.7 and 129.5° respectively, and larger M-S-C angles are offset by smaller S-C-C angles (Figure 1.4).[46]
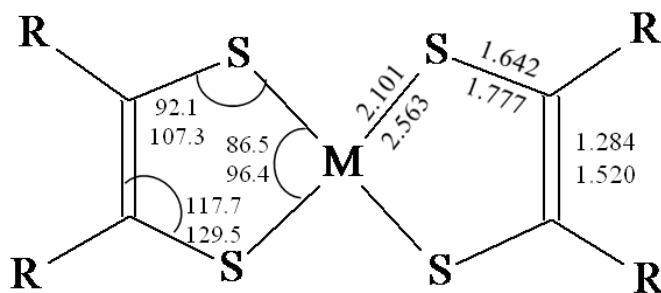
Figure 1.4. *Smallest and largest bond distances (Å) and angles (°) for bis(1,2-dithiolene) transition metal structures.*

Depending on the central metal ion, and especially when the transition metal features a formal configuration ranging between d^5 and d^8, *bis*(1,2-dithiolene) and *bis*(1,2-diselenolene) complexes with a square-planar coordination may exhibit a tendency to form dimeric[33,35a,46] or trimeric[46] structures. These aggregates are held together by strong intermolecular M-E or M-M bonds, as shown in Figure 1.5 for E = S.
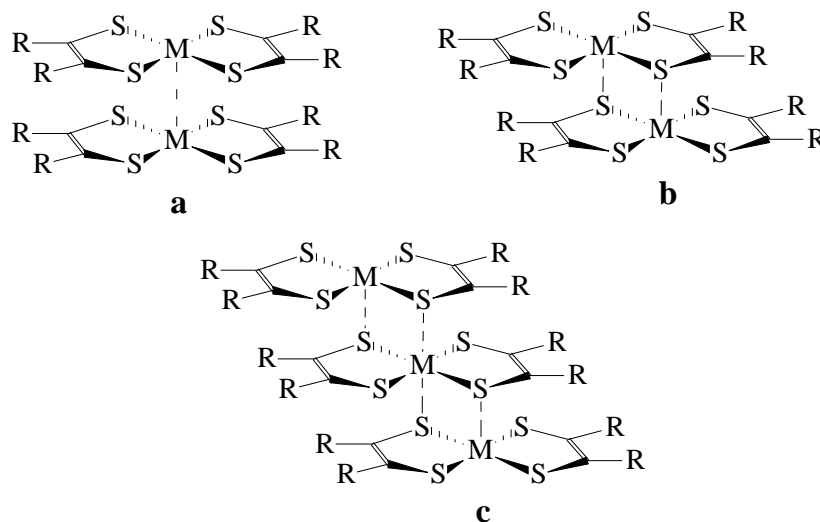
Figure 1.5. *Examples of structural types of multimeric bis(1,2-dithiolene) units: a) M-M dimer; b) M-S dimer; c) M-S trimer.*

Within the dimers, the monomeric units maintain the structural characteristics of the monomers.[46] Different dimers or trimers can interact with each other,[49] and the difference between interacting dimers or trimers and stacked polymeric structures can be uncertain. In the case of anionic complexes, the nature and size of the countercations can play a crucial role in the formation of the stacks.[50] The tendency to form stacks increases with the extension the complex π-system, as observed in dmit^{2-} *bis*(1,2-dithiolene) complexes.[51]

(2) In *tris*(1,2-dichalcogenolene) complexes the central metal ion adopts an octahedral or a distorted trigonal prismatic coordination geometry[52] (Figure 1.6). A number of geometrical parameters have been proposed to discriminate between these two possibilities: (i) the twist angle between chalcogen E atoms in the two dimensional projection along the threefold axes, (ii) the dihedral angle between the ligand E-M-E plane and the E-E-E plane formed by three coordinating chalcogen atoms from the three units lying on the same side with respect to the metal centre, or (iii) the dihedral angle between the two E-E-E planes defined as described above (E = S, Se).[52a,53]
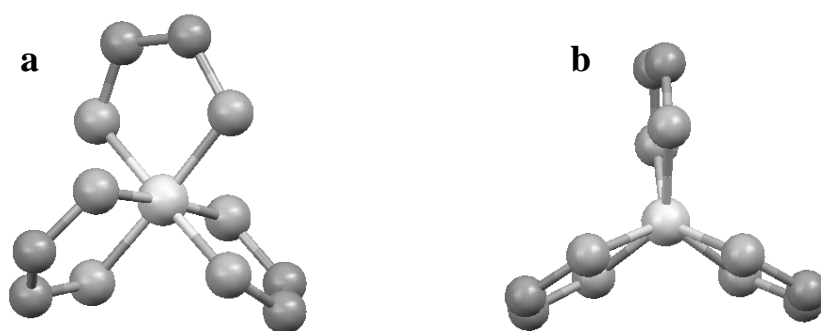
Figure 1.6. *Examples of coordination geometries in tris(1,2-dithiolene) metal complexes: a) octahedral; b) trigonal prismatic.*

Average bond lengths and angles for homoleptic *tris*(1,2-chalcogenolene) complexes are less sensitive to the identity of the transition metal or 1,2-dichalcogenolene ligand than those of *bis*(1,2-dichalcogenolene) complexes. As summarised in Figure 1.7 for *tris*(1,2-dithiolene) complexes, M-S bond lengths span between 2.263 and 2.543 Å, while the ranges for S-C and C-C distances are 1.665-1.785 and 1.304-1.524 Å respectively.[46] Concerning the angles describing the C_2S_2M metallacycle, ranges of 79.2-91.1, 100.7-111.1, and 118.5-123.9° have been reported for S-M-S, M-S-C and S-C-C angles respectively.[46]
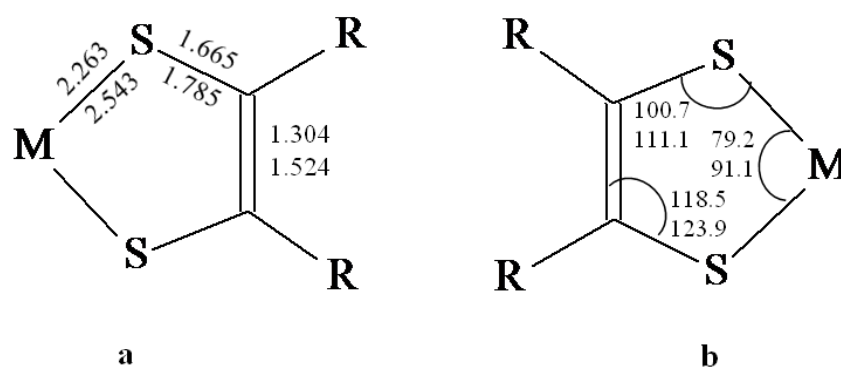
Figure 1.7. *Smallest and largest bond distances (Å) and angles (°) for tris(1,2-dithiolene) transition metal structures*

(3) In general, the different ligands feature typical geometrical parameters over a wide range of 1,2-dichalcogenolene complexes.[46]

1.2.3. Electronic structure

The understanding of the electronic structure of homoleptic metallo-dichalcogenolenes has always been an important goal of theoretical research.[54] Since the first theoretical investigations, dating to 1964,[55] there have been a considerable number of publications

reporting calculations [mainly performed on *bis*(1,2-dithiolene) complexes featuring the metal ion in a square-planar coordination] at different levels of theory, ranging from Extended Hückel Theory (EHT)[56] to, in recent years, Density Functional Theory (DFT).[57]

One of the first theoretical calculations in this field were performed by Hoffman and collaborators at EHT level,[56] with the main goal of developing a satisfying bonding and molecular orbital (MO) description for nickel *bis*(1,2-dithiolene) complexes. They therefore provided an elegant, yet simple, description of the bonding in neutral [Ni(H$_2$-edt)$_2$] (**3**, Figure 1.8).

This electronic structure description is exactly what one would expect for two dianionic dithiolene ligands bound to a nickel ion in the IV oxidation state. The d_{xy} (b_{1g}) and d_{xz} (b_{2g}) orbitals are both empty in this scheme, and six of the eight out-of-plane π-type (only the six highest energy orbitals are shown) and all four of the in-plane σ-type dithiolene ligand orbitals are occupied. Furthermore, the filled ligand orbitals lie at energies below the five 3d orbitals of Ni, indicating that they are primarily acting as σ and π-donor ligands. The d_{xy} (b_{1g}) orbital is raised considerably in energy due to a high degree of mixing with a σ-type dithiolene orbital of the same symmetry. The severe destabilisation of the d_{xy} orbital precludes electron occupation of this orbital, and neither Ni^I (d^9) or Ni^0 (d^{10}) electron configurations are anticipated to be encountered for these complexes.
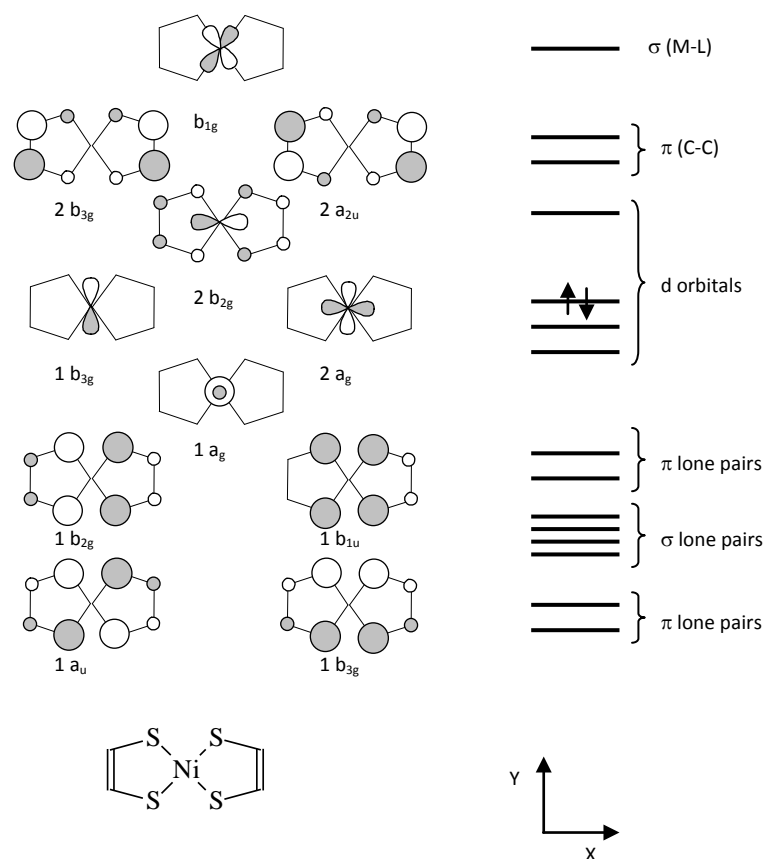
Figure 1.8. *MO scheme of **3** calculated at EHT level (Ref. 56).*

The electronic structure of *bis*(1,2-dithiolene) complexes with a square-planar coordination is however better described by *ab-initio,* post-SCF or DFT approaches, as first shown in 1998.[26d,58] As an example, the MO scheme of **3** calculated at hybrid DFT level by our group is depicted in Figure 1.9,[12] showing that the HOMO is a π orbital deriving from the in-phase combination of $2p_z$ atomic orbitals of C atoms, and the antibonding combination of these with $3p_z$ atomic orbitals of S atoms. On the other hand, the LUMO, having a π-nature as well, is antibonding with respect to the metal, and derives from the combination of the same atomic orbitals described above for the HOMO (but with the C_2S_2 units assuming a opposite phase), with a participation of the $3d_{yz}$ atomic orbital of the metal.

<div align="center">50</div>

<div align="center">54</div>

<div align="center">58</div>

<div align="center">49</div>

<div align="center">53</div>

<div align="center">57</div>

<div align="center">48</div>

<div align="center">52</div>

<div align="center">56 LUMO</div>

<div align="center">47</div>

<div align="center">51</div>

<div align="center">55 HOMO</div>
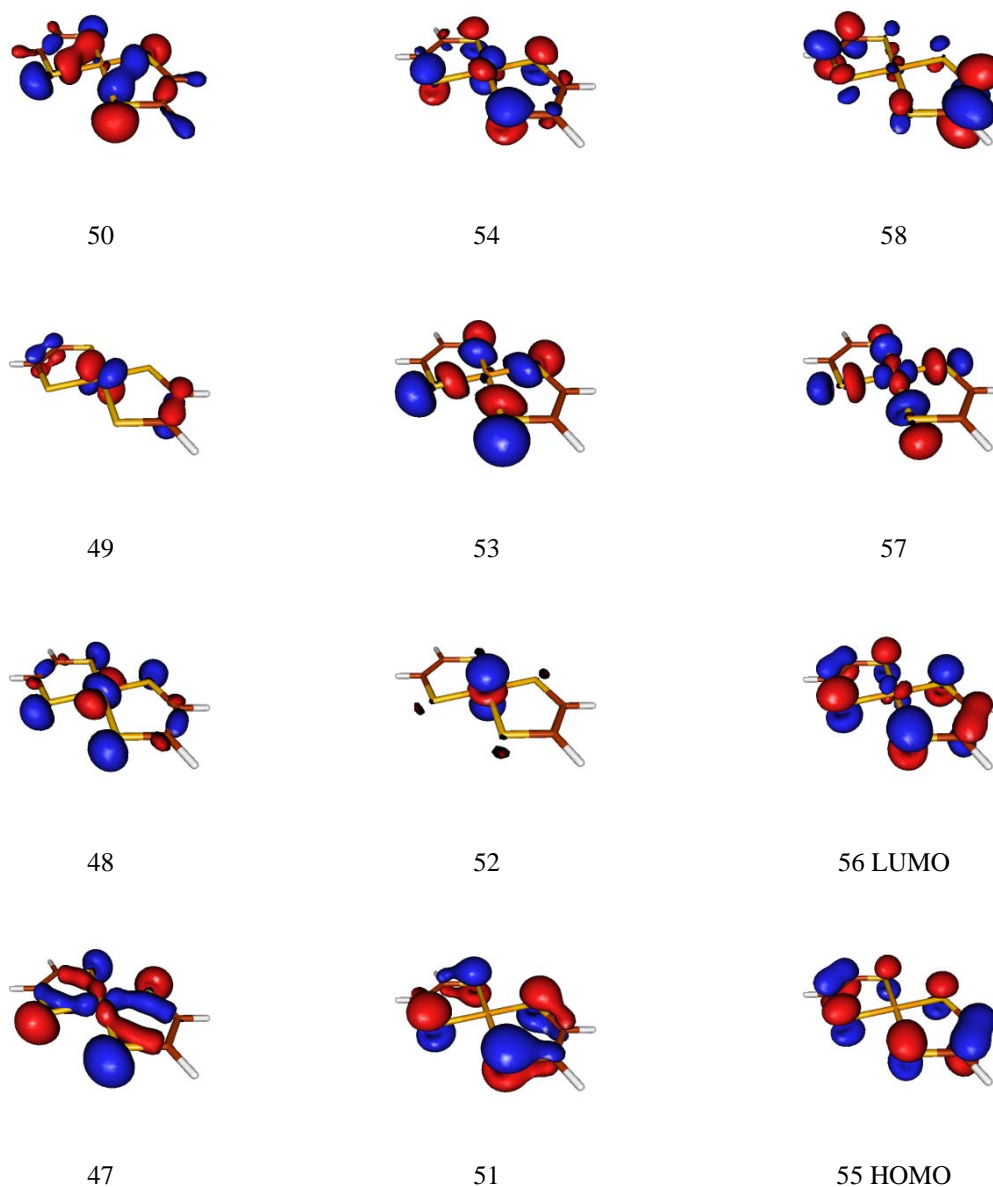
Figure 1.9. *Frontier MOs calculated for 3 at DFT level[B3LYP//LanL2DZ+ECP(Ni)/Ahlrichs (C, H, S); cutoff = 0.05 e; Ref. 12].*

More recently, theoretical calculations have been exploited to get an insight into other aspects of 1,2-dithiolene chemistry. As an example, Holm and coworkers performed in 2001 a study on $[Ni(S_2C_2Me_2)]^{x-}$ ($x = 0, 1, 2$) at DFT level,[59] thus deducing a correlation between the electronic and geometric structures of the entire electron-transfer-series. This study provided the first theoretical interpretation of both electrochemical and spectroscopic features of 1,2-dithiolene complexes (see below).

Theoretical calculations were also exploited to elucidate the intensely debated question of whether dichalcogenolene ligands can exist as neutral dichalcogenoketones, radical monoanions or dianionic dichalcogenolate. In this context, neutral nickel *bis*(1,2-dithiolene) complexes have been particularly studied in the past, and two principal models for the electronic structure of these complexes, resulting in an oxidation state of II for the metal, were first discussed in the literature.[60] Stiefel et al. proposed a diradical singlet ground state (open-shell, Scheme 1.10), whereas Schrauzer and Mayweg[5] and Bach and Holm[61] proposed a singlet closed shell ground state based on either a fully delocalised structure or on two resonance hybrid structures (Scheme 1.8). The ability to describe the diradical character of such complexes is clearly the most challenging task for theoretical calculations, and the work performed by Bachler et al.[62] using broken symmetry DFT formalism,[63] or more recently by other researchers,[64] exemplifies the difficulties to find the most appropriate theoretical method to describe these systems. Very recently, persuasive considerations were deduced on this topic by Wieghardt and coworkers, by means of an analysis of $[M(bdt)_2]$ complexes featuring different transition metal ions (Cr, Fe, Co, Ni, Cu, Pd, Pt, and Au),[65] through the combined adoption of various spectroscopic methods (MCD, absorption, resonance Raman, EPR, and sulphur K-edge XAS) and theoretical calculations at different levels of theory (DFT or *ab initio*). The authors concluded that the *noninnocent* nature of the 1,2-dithiolene ligand in these systems is strongly dependent on the nature of the transition metal ion present in the complex, analogously to what hypotesised by Ward and McCleverty (see above).[31] Vibrational spectra of these systems have also been used for the interpretation of their electronic structure.[26d,46,66]
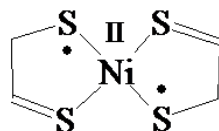
Scheme 1.10. *Diradical open-shell structure for the neutral form of **3**.*

1.2.4. Properties and applications

Homoleptic metal 1,2-dithiolene and 1,2-diselenolene complexes have been exploited for a large variety of diverse applications, thanks to their unique molecular properties exhibited both in solution and in the solid state.

1.2.4.1 Properties in solution

1.2.4.1.1. Electrochemical properties

As previously mentioned, one of the peculiar properties of metal *bis*(1,2-dichalcogenolenes) is the ability to assume different molecular charges, the different molecular oxidation states being reversibly accessible by chemical or electrochemical means (Scheme 1.7 for metal ions of group 10).

The redox potentials, and in particular the half-wave potentials $E_{1/2}$, can serve as a guide for the synthesis of differently charged dithiolene complexes, and several generalisations can be made about the electrochemical behaviour of homoleptic *bis*(1,2-dithiolene) complexes (all potentials below are referenced to SCE): [67]

(i) For couples with $E_{1/2} < 0.00$ V, the reduced species is susceptible to air oxidation in solution, whereas if $E_{1/2} > 0.00$ V the reduced species is air-stable.

(ii) When $E_{1/2} > 0.20$ V, the oxidised species can be reduced by weakly basic solvents (e.g. ketones or alcohols), but when $-0.12 < E_{1/2} < +0.20$ V, the oxidised form can be reduced by stronger bases (e.g. aromatic amines).

(iii) When $E_{1/2} <$ -0.12 V, the oxidised form is readily reduced by strong reducing species such as hydrazine, sodium amalgam, and $NaBH_4$.

(iv) The reduced form can be oxidised by molecular iodine when $E_{1/2} <$ +0.40 V, otherwise stronger oxidants are required.

However, it must be emphasised that the values listed above are only indicative, and in the course of reactions where oxidation or reduction processes are involved, a proper selection of the oxidising or reducing agents is crucial, along with the choice of appropriate reaction conditions. Side reactions such as ligand exchange may indeed occur, and reducing agents like amines can act themselves as coordinating ligands. Moreover, the reduction of oxidised species in couples with $E_{1/2} <$ -0.95 V or oxidation of the reduced form in couples with $E_{1/2} >$ +0.95 V is generally difficult by chemical means, and hence electrochemical methods are more suitable.[68]

A particular behaviour is shown by some cobalt and iron complexes which exist as partially reduced dimers, and dissociate into monomers upon full reduction (Equation 1.1).[61,69]

$$[M(S \wedge S)_2]_2^0 \underset{-e^-}{\overset{+e^-}{\rightleftharpoons}} [M(S \wedge S)_2]_2^- \underset{-e^-}{\overset{+e^-}{\rightleftharpoons}} [M(S \wedge S)_2]_2^{2-} \underset{-e^-}{\overset{+e^-}{\rightleftharpoons}} 2\,[M(S \wedge S)_2]^{2-}$$

$(S \wedge S = \text{dithiolene ligand, } M = Fe, Co)$ (1.1)
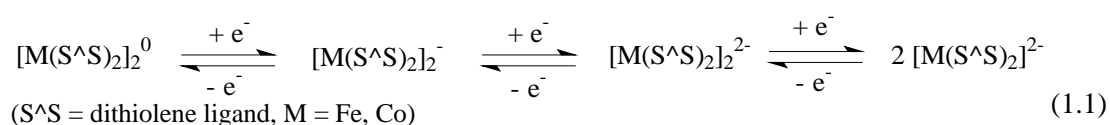
Furthermore, few *bis*(1,2-dithiolene) complexes bear redox-active substituents directly bonded to the dithiolene core, or connected to it through a spacer, so that the interpretation of their redox behaviour is particularly complicated. An example is given by some nickel *bis*(1,2-dithiolene) complexes reported by Mueller-Westerhoff,[70] Underhill,[71] and Lee,[72] bearing ferrocenyl groups as substituents at the 1,2-dithiolene ligands (Figure 1.10).
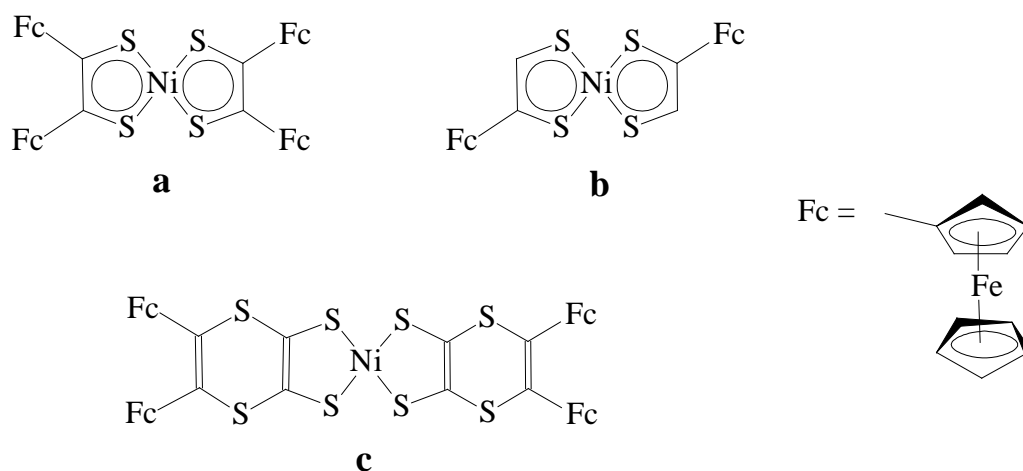
Figure 1.10. *Redox-active substituted metal 1,2-dithiolenes: a) [Ni(dfcdt)$_2$] (**6**); b) [Ni(fcdt)$_2$] (**7**); c) [Ni(dfcvt)$_2$] (**8**, Refs. 70, 71, and 72, respectively).*

For example, the tetrakis(ferrocenyl)-nickel dithiolene [Ni(dfctd)$_2$] (**6**) shows up to six monoelectronic redox processes, four of which are centred on the ferrocenyl units, while the remaining two involve the dithiolene system (Equation 1.2).[73]

(1.2)
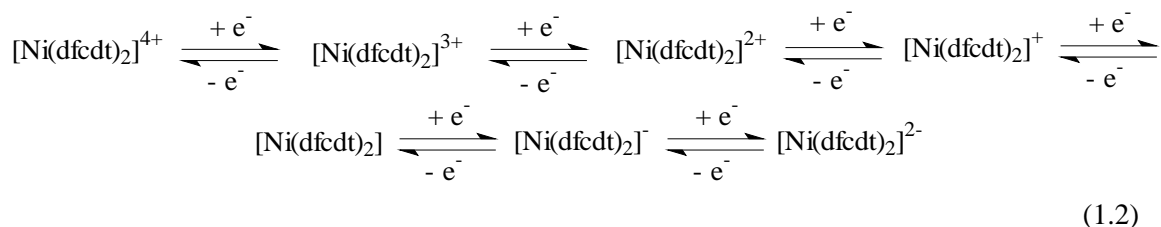
1.2.4.1.2. Optical properties

One of the most striking properties of 1,2-dithiolene and 1,2-diselenolene complexes, and in particular of *bis*(1,2-dichalcogene) complexes of d^8 metal ions, is their intense molecular absorption in the Visible-Near Infrared (Vis-NIR) region.[1,35b,37,40,54,74]

This absorption has been extensively studied for metals belonging to group 10, and for Ni in particular, while it has been only recently evidenced for *bis*(1,2-dithiolene)

complexes of Au^{III}.[75] The absorption maximum (λ_{max}) of this band falls between 700 and 1750 nm, depending on the nature of the substituents, on the central metal ion, on the coordination geometry, on the global charge of the complex (electrochromism), and on the solvent (solvatochromism). The absorption intensity, with extinction coefficients ε ranging between 15000 and 120000 M^{-1} cm^{-1},[12] is unmatched in most transition metal compounds, whose low energy absorptions have been generally assigned to *d-d* transitions.[37] On the contrary, Vis-NIR absorption is well known to be due to a $\pi-\pi*$ electronic transition involving the frontier molecular orbitals, and, as previously mentioned, its nature has been studied at different levels of theory.

As just mentioned, the nature of substituents on the 1,2-dichalcogenolene ligands plays an important role in determining the position of the Vis-NIR absorption in these systems. As regards neutral 1,2-dithiolene complexes, as compared to the nickel parent dithiolene (**3**, λ_{max} = 720 nm in hexane),[76] donor substituents cause a bathochromic shift in the λ_{max} value, while acceptor substituents do not markedly affect the energy of the Vis-NIR absorption band. According to the qualitative interpretation proposed by Mueller-Westerhoff,[40] acceptor substituents lower the energies of the HOMO and the LUMO by similar amounts of energy, not resulting in drastic shifts in transition energies, while donor substituents raise the energy of the former MO more than that of the latter, thus reducing the HOMO-LUMO energy gap, and therefore causing the bathochromic shift observed for the corresponding absorption. As a consequence, the lowering of the LUMO energy induced by acceptor substituents causes a stabilisation of *bis*(1,2-dithiolene) anionic forms, while donor substituents tend to stabilise neutral or, in some cases, cationic forms.[37,40] Due to the applicative interest in low energy absorptions, one of researchers' main goals has been that of lowering the energy of this absorption as much as possible by systematically varying the substituents on the 1,2-

dithiolene ligands. Mueller-Westerhoff and co-workers found that this aim could be achieved in nickel complexes by introducing aromatic substituents coplanar with the dithiolene core, in order to enhance the extension of the π-system, and containing amino-donor groups. Examples of this type of ligands are julolidinyl-ethylene-1,2-dithiolate (JUL1^{2-}), 1,2-*bis*(julolidinyl)-ethylene-1,2-dithiolate (JUL2^{2-}), and *bis*(3-*N,N'*-diethyltetrahydroquinazolyl)-ethylene-1,2-dithiolate (DETHQ^{2-}, Scheme 1.11), whose nickel complexes were reported to feature low-energy NIR absorptions at 1180, 1270, and 1370 nm, respectively in CH_2Cl_2.[40,74b]
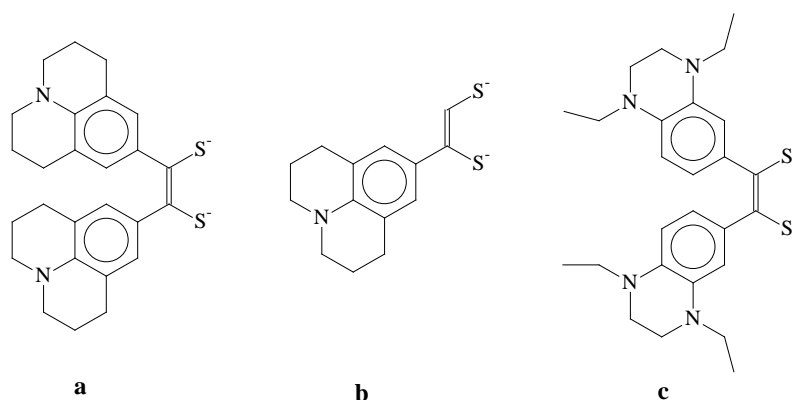
Scheme 1.11. *Examples of 1,2-dithiolene ligands featuring aromatic substituents and containing amino-donor groups: a) JUL1^{2-}, b) JUL2^{2-}, c) DETHQ^{2-} (Refs. 40 and 74b).*

NIR absorptions around 1000 nm were also obtained in nickel complexes by adopting the 1,2-dithiolene ligands dmit^{2-},[26c] medt^{2-},[77] bddt^{2-},[77] and cddt^{2-}.[35b]

As already mentioned, our research group has been active too in this field since about fifteen years, with the synthesis and the characterisation of more than sixty members belonging to the class [M(R,R'-timdt)$_2$] (M = Ni, Pd, Pt),[12] whose NIR absorptions fall around 1000 nm and change upon varying R, R', and M (Table 1.1).[78]

Table 1.1. *Experimental NIR absorption maxima* λ_{max} *(nm) for neutral [M(R,R'-timdt)$_2$] complexes in CHCl$_3$ (Ref. 78).*

M	R	R′	λ_{max}
Ni	*m*-CF$_3$-Bz	Me	992
Pd	*m*-CF$_3$-Bz	Me	1017
Pt	*m*-CF$_3$-Bz	Me	1010
Ni	*m*-CF$_3$-Ph	Pr^i	1008
Pd	*m*-CF$_3$-Ph	Pr^i	1033
Pt	*m*-CF$_3$-Ph	Pr^i	1010
Ni	*p*-CF$_3$O-Ph	Et	1010
Pd	*p*-CF$_3$O-Ph	Et	1032
Pt	*p*-CF$_3$O-Ph	Et	1010
Pd	*p*-F-Ph	*p*-F-Ph	1027
Pt	*p*-F-Ph	*p*-F-Ph	1012
Pd	*p*-F-Ph	*p*-NO$_2$-Ph	1042
Pt	*p*-F-Ph	*p*-NO$_2$-Ph	1021
Ni	Ph	Ph	1023
Pd	Ph	Ph	1043
Pt	Ph	Ph	1022
Ni	Naph	Et	1007
Pd	Naph	Et	1033
Pt	Naph	Et	1011
Pd	*p*-F-Ph	*m,m,p*-(CH$_3$O)$_3$-Ph	1052
Pt	*p*-F-Ph	*m,m,p*-(CH$_3$O)$_3$-Ph	1025
Ni	*p*-F-Ph	Naph	1019
Pd	*p*-F-Ph	Naph	1047
Pt	*p*-F-Ph	Naph	1021
Ni	ClCH$_2$CH$_2$	Et	1001
Pd	ClCH$_2$CH$_2$	Et	1027
Pt	ClCH$_2$CH$_2$	Et	1006

An in depth investigation on the effects induced on the energy of this absorption by changing M, R, and R′ has allowed for the recognition of the additive contributions of the central metal ion and of the substituents to the λ_{max} position of the NIR absorption maximum.[78] The considerations derived from this analysis can be summarised as follows: (i) in complexes featuring aryl substituents the NIR absorption is bathochromically shifted with respect to alkyl substituted ones; (ii) among complexes bearing aliphatic R and R′ groups, the λ_{max} position tends to shift towards shortest wavelengths as the length of the alkyl chain increases; (iii) the presence of electron-withdrawing substituents at the aromatic ring of complexes bearing aryl pendants induces a bathochromic effect on the position of the NIR absorption, while electron-releasing groups show the opposite effect; (iv) complexes with M = Pd feature the NIR absorption at lower energies with respect to nickel and platinum complexes (Figure 1.11).

More recently, to further investigate the possibility of tuning the position of the NIR absorption in systems with a highly delocalised π-system, the first three *bis*(1,2-dithiolene) complexes belonging to the class [M(R-dmet)$_2$] [R = Et; M = Ni (**9**), Pd (**10**), Pt (**11**)] were prepared by our group,[27] and several ulterior members of this class have been also obtained by Lorcy and collaborators (M = Pt, Zn, Au; R = Me, Et, Ph).[28,79] As predictable, the energies of the NIR absorptions in these complexes were found to be intermediate between those of *bis*(1,2-dithiolenes) belonging to the classes [M(R,R′-timdt)$_2$] and [M(dmit)$_2$] [λ_{max} = 1023, 1003, and 1010 nm in toluene for [Ni(dmit)$_2$] (**12**), [Ni(Et$_2$-timdt)$_2$] (**13**), and **9**, respectively].[27]
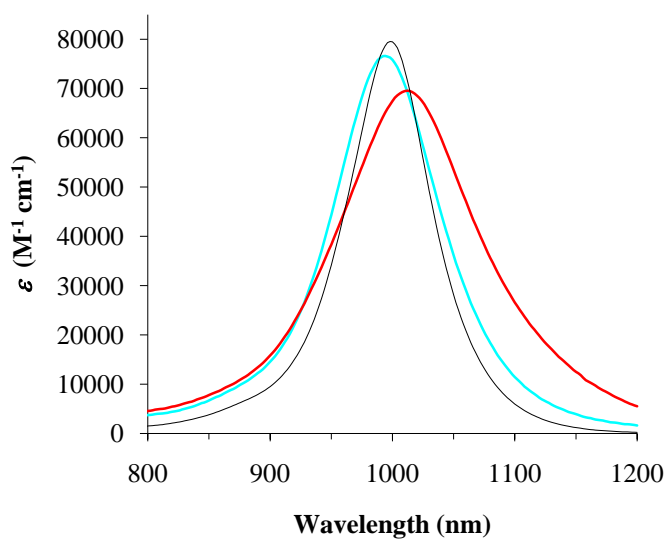
Figure 1.11. *NIR absorption spectra of [M(Et₂-timdt)₂] in CHCl₃ [M = Ni (black line), Pd (red), Pt(blue)] (Ref. 12).*

Absorption energies falling at even lower values were observed in nickel complexes containing ferrocenyl substituents bonded to the 1,2-dithiolene ligands (Figure 1.10),[80] or, more recently, in a *bis*-double-decker complex assembled from the nickel *bis*(1,2-dithiolene) complex $[Ni(S_2C_2Me_2)_2]^{-1/-2}$ and two $[Cp^*Fe]^+$ units ($Cp^* = C_5Me_5$, Figure 1.12).[81]
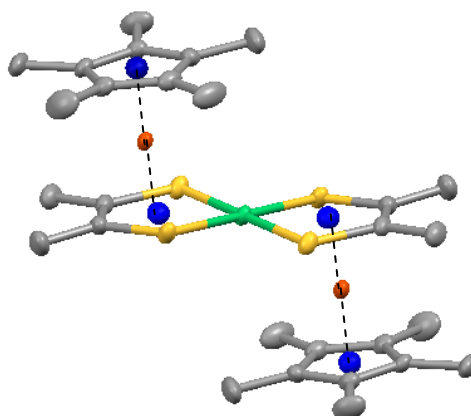
Figure 1.12. *ORTEP drawing of the cationic complex $[\eta^5\text{-}Cp^*\text{-}Fe\text{-}\mu\text{-}\eta^5\text{-}\eta^5\text{-}((S_2C_2Me_2)_2Ni)Fe\text{-}\eta^5\text{-}Cp^*]^+$ (Ref. 81). Ellipsoids are shown at the 50% probability level. Hydrogen atoms are omitted for clarity.*

Concerning the role of the oxidation state of the complex in tuning the energy of the Vis-NIR absorption band, it was observed that electronic absorptions featured by monoanionic *bis*(1,2-dithiolene) complexes of metal ions belonging to the 10 group are generally bathochromically shifted as compared to those of corresponding neutral species.[77,82] These observations were also confirmed by our group in the case of the [M(R,R′-timdt)$_2$][83] and [M(R-dmet)$_2$],[27] whose NIR absorption in the monoanionic form is bathochromically shifted by about 400 and 200 nm respectively with respect to neutral complexes.

The intense NIR absorption peculiar to neutral and monoanionic *bis*(1,2-dithiolene) complexes of Ni, Pd and Pt has been exploited for several applications.

(a) *Q-Switching*. Laser emission consists of a continuous output of coherent radiation, that can be turned into ultra-short pulses of extremely high energy[84] by using "Q-switching" dyes,[40] provided that (1) the dye has a significant absorption close to the same energy; (2) the dye has no significant absorption close to the laser emission energy; (3) the excited state lifetime is long enough to allow for bleaching of the laser; and (4) the dye is thermally and photochemically stable. *Bis*(1,2-dithiolene) complexes are generally thermally and photochemically stable and their Vis-NIR absorption can be tuned in order to reach the wavelength ranges of interest for NIR lasers, such as Nd:YAG, Nd-YLF, and Er:Glass solid-state lasers (emission wavelengths = 1064, 1053, and 1540 nm, respectively). In this context, many groups of researchers devoted their efforts to synthesising 1,2-dithiolene complexes for this type of application, and indeed some complexes were patented and are commercially available.[74,85]

(b) *Nonlinear Optics*. Metal 1,2-dithiolene complexes have been studied for applications in the field of second- and third-order nonlinear optical (NLO) properties.[86] Since materials for second-order nonlinear optics (SONLO) must not be

centrosymmetric,[87] heteroleptic *bis*(1,2-dithiolene) complexes are mainly involved in this field,[74a] although homoleptic *bis*(1,2-dithiolene) complexes featuring asymmetric substituents in the *cis* conformation are good candidates as well (see below). On the other hand, third-order NLO effects impose no symmetry constraints, though requiring higher energy sources. Thus, studies on this type of nonlinearity have addressed both homoleptic and heteroleptic *bis*(1,2-dithiolene) complexes.[88]

(c) *Optical Technology*. Several publications and patents have dealt with application of 1,2-dithiolene complexes to the various branches of optical information technology. Thus, 1,2-dithiolene systems have been exploited in materials used for optical data storage such as CD-ROM or LD-ROM media, as ink components for copiers,[89] or as photodetectors.[90] Recently, the applications of 1,2-dithiolene complexes to wavelength sensitive NIR-photocondictivity have been investigated, and working prototypes converting trains of impinging NIR-pulses into electrical signals have been created (see below).[91]

1.2.4.1.3. Reactivity

Compared with the large body of electrochemical and spectroscopic data, there have been fewer studies on the chemical reactivity of *bis*(1,2-dithiolene) complexes. In light of the redox chemistry of *bis*(1,2-dithiolene) complexes and the redox-active nature of the 1,2-dithiolene ligands, it is not surprising that the reactivity is largely related to the redox properties. The observed reactions can be summarised as follows.[67]

(a) *Ligand Exchange Reactions.* Although most 1,2-dithiolene complexes are stable compounds and many do not react with strong acids or bases, *bis*(1,2-dithiolene) complexes featuring a square-planar coordination are nevertheless reactive enough to undergo linear-exchange reactions with other *bis*-chelating ligands, according to Equation 1.3.[92]

$$M^1(S^\wedge S)_2 + M^2(L^\wedge L)_2 \rightleftharpoons M^1(S^\wedge S)(L^\wedge L) + M^2(L^\wedge L)(S^\wedge S) \tag{1.3}$$

(S^S = 1,2-dithiolene ligand; L^L = bidentate ligand)

Reactions of these type can also occur between homoleptic complexes in different oxidation states (e.g. 0 and -2), so that the dianionic compound acts as reducing agent toward the neutral one, according to Equation 1.4.[42c]

$$[M(S^\wedge S)_2]^{2-} + [M(L^\wedge L)_2] \rightarrow 2\,[M(S^\wedge S)(L^\wedge L)]^- \tag{1.4}$$

(S^S = 1,2-dithiolene ligand; L^L = bidentate ligand)

(b) *Ligand Addition and Substitution Reactions*. *Bis*(1,2-dithiolene) complexes of group VIII and IX metals generally exist in their dimeric forms $[M(S_2C_2R_2)_2]_2^{x-}$ (M = Fe, Co, x = 0-2). By treating these species with Lewis bases L such as pyridine, phosphine, stibline, CN^-, or N^{3-} results in dissociation of the dimer and formation of five-coordinate adducts $[M(L)(S_2C_2R_2)_2]^{x/2}$.[93]

(c) *Alkylation*. Reduction of *bis*(1,2-dithiolene) complexes to their dianions increases the nucleophilicity of sulphur atoms, facilitating electrophilic attack by alkyl halides. As an example, Schrauzer at al.[94] described the formation of the neutral complex $[Ni(MeS_2C_2Ph_2)_2]$ when $[Ni(sdt)_2]^{2-}$ (sdt^{2-} = stilbene-1,2-dithiolato) is made to react with methyl iodide. In this complex, the methyl groups are in *trans* position, and further reaction with MeI results in fully methylation of all four sulphur atoms, yielding $[Ni(Me_2S_2C_2Ph_2)I_2]$, in which the six-coordinate nickel atom is equatorially coordinated by two iodide ligands.

(d) *Cycloaddition with Unsaturated Compounds.* Schrauzer and Mayweg[38a] first reported that $[M(sdt)_2]$ (M = Ni, Pd, Pt) reacts with alkynes and alkenes to give

cycloaddition to the dithiolene ligand (Figure 1.13 for nickel). Wing et al.[95] further

investigated the reaction of olefins with 1,2-dithiolene complexes, and found that

[Ni(tdf)$_2$] not only reacts with dienes, but also reacts with highly strained mono-olefins,

such as norbornene, forming a 1:1 adduct. Addition of other unsaturated compounds,

such as SO$_2$[96] and O$_2$,[97] has also been reported.
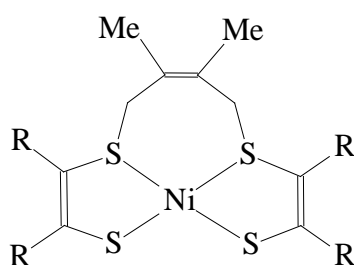
Figure 1.13. *Product of the reaction between a nickel 1,2-dithiolene complex and olefins (Ref. 38a).*

1.2.4.2 Solid state properties

1.2.4.2.1. Electrical properties

The solid state conducting properties of 1,2-dithiolene and 1,2-diselenolene complexes

have been the subject of a vast number of publications and reviews.[40,74a,98,99] In all

cases, conducting properties (insulating, semi-conducting, metal-like, or even

superconducting) have been rationalised in terms of their structural features, which in

turn are affected by temperature and applied pressure.[100] For conducting molecular one-

dimensional (1D) systems, some criteria were proved to be necessarily satisfied in order

to make observation of solid state conductivity possible:[74a] (i) the existence of stacking

structures, (ii) a spatial extension of the electronic system so as to allow for a significant

overlap between stacked units, and (iii) the partial filling of the conducting band,

achieved by means of non-integral oxidation or CT processes. Metal 1,2-

dichalcogenolene complexes are a very suitable source of open-shell stable systems and are able to satisfy these criteria provided that a sufficient extended planar system is present in the ligands. In particular, open-shell systems deriving from both *bis*(1,2-dithiolene) and *bis*(1,2-diselenolene) systems of d^8 metal ions feature a marked tendency to form intermolecular stack-interactions with short metal-metal distances. However, in the first 1,2-dicalcogenolene complex showing metal-like behaviour, $(Per)_2[Pt(mnt)_2]$ [$(Per)_2$(**14**); Per = perylene],[101] the stacking of perylene units was responsible for the conducting properties, while the first compound containing a 1,2-dichalcogenolene complex responsible for the metal-like conductivity was $(H_3O)_{0.33}Li_{0.82}$(**14**)·$1.67H_2O$.[102] In order to avoid Peierls instability, predicted in 1962 by McConnell and collaboratotrs,[100] and first reported in $(TTF)[M(tfd)_2]$ complexes (M = Cu, Au; TTF = tetrathiafulvalene),[74a, 103] much effort has been devoted to enhancing the structural dimensionality beyond 1D. BEDT-TTF [*bis*(ethylenedithio)tetrathiafulvalene] indeed provided a variety of 2D-metallic systems, thanks to the possibility of intermolecular interactions guaranteed by the peripheral sulphur atoms.[98, 104] Several 1,2-dichalcogenolene complexes can behave as molecular acceptors in charge-transfer (CT) complexes with donors such as TTF and related species, or originate Non Integral Oxidation State (NIOS) compounds, and the possibility of forming transverse short E···E (E = S, Se) contacts between different stacks could avoid the mono-dimensionality of the stacking structure.[105] Moreover, due to the greater orbital spatial extension of Se compared to S, the replacement of sulphur with selenium has been proposed as a tool for achieving greater interanionic interactions.[106]

The complex TBA_2(**12**)$_7$·2MeCN was the first reported conducting $dmit^{2-}$ salt,[107] while (TFF)(**12**)[108] was the first superconductor containing a dithiolene system. Several other compounds based on 1,2-dithiolene complexes and exhibiting superconducting

properties have been further identified, and notably all of them contain the dmit^{2-} ligand.[109,110]

More common are 1,2-dichalcogenolene-based compounds showing metal-like behaviour. These systems are generally either NIOS salts or CT-complexes, which contain donors of various type, such as Per or TTF, and also in this case the majority of complexes are based on dmit^{2-} ligand.[74a] Recent literature also reports many examples of *bis*(1,2-dithiolene) complexes deriving from mnt^{2-}, tdf^{2-}, dddt^{2-}, dmise^{2-}, dcit^{2-}, and dmbit^{2-} (Scheme 1.1) showing metal-like conductivity properties.[74a,98,111] Some examples of CT-salts containing 1,2-diselenolene complexes with metal-like conductivity have also been reported.[106b,112]

1.2.4.2.2. *Magnetic properties*

Solid-state magnetic properties of 1,2-dithiolene and 1,2-diselenolene complexes have been dealt with in several reviews.[1,37,74a,98,111b,113] The most common magnetic behaviour is antiferromagnetism.[35a,49a,74a,114] More unusual are the systems featuring spin-Peierls (SP) transitions, spin-ladder (SL) transitions, or ferromagnetic properties.

SP transitions are temperature-dependent magnetoelastic transitions involving quasi 1D insulating systems, and were reported for (TTF)[M(tfd)$_2$][103a] (M = Cu, Au) and (TTF)[Cu(tfs)$_2$][115] complexes. The definition of SL systems is related to crystalline frameworks resulting from the interaction between a finite number of S = 1/2 strongly magnetically coupled chains arranged each next to the other.[74a] Among the most important systems, it is worth recalling (*p*-EPYNN)(**12**)[116] (*p*-EPYNN = *p-N*-pyrimidine α-nitronyl nitroxide) and (DT-TTF)$_2$[Au(mnt)$_2$][117] [(DT-TTF)$_2$(**15**); DT-TTF = dithiophenetetrathiafulvalene).

Short-range order ferromagnetic interactions were reported for several compounds containing 1,2-dichalcogenolene complexes,[74a,118] while long-range ferromagnetic

behaviour was reported for $(NH_4)(\mathbf{12}) \cdot H_2O$[111c,119] and $(Cp_2{}^*Mn)(\mathbf{12})$ (Cp* = pentamethylcyclopentadienyl).[120]

1.3. Heteroleptic 1,2-dichalcogenolene metal complexes

Different mixed-ligand 1,2-dithiolene complexes have been synthesised in the past with the aim of obtaining new materials suitable for NLO applications, given the lack of inversion centre proper of these compounds. The majority of these complexes belongs to two classes: the mixed-ligand *bis*(1,2-dithiolene) metal complexes and the diimine-dichalcogenolate metal complexes.

1.3.1. Mixed-ligand bis(1,2-dithiolene) complexes

In these complexes, two different 1,2-dithiolene ligands, featuring different substituents, coordinate the central metal ion to give a non-centrosymmetric complex. When the two ligands feature remarkably different electron-donor properties, the resulting complexes are considered as *push/pull* systems, where the ligand with more electron-donor character acts as a *push* ligand, while the other one represents the *pull* ligand. In neutral complexes, the different behaviour of the two ligands gives rise to a charge separation between the two units, usually reflected in a not negligible dipole moment. The entity of this separation depends on the difference in the *push/pull* character of the ligands: the largest the differences in the electron-donor properties of the ligands' substituents, the highest the charge separation.

Accordingly, if the differences in the *push/pull* character of the two ligands are small, the resulting mixed-ligand complex will show, in the neutral form, a ground state

similar to that of corresponding homoleptic *bis*(1,2-dithiolene) complexes, and describable with the limit form **b** in Scheme 1.12; otherwise, one ligand will tend to coordinate the central metal ion in the neutral dithioketone form, while the other one acts as a ene-1,2-dithiolate dianion (forms **a** and **c** in Scheme 1.12). In this case, a redistribution of frontier molecular orbitals is also observed, with the HOMO mainly centred on the *pull* ligand and the LUMO localised on the *push* ligand.[121]
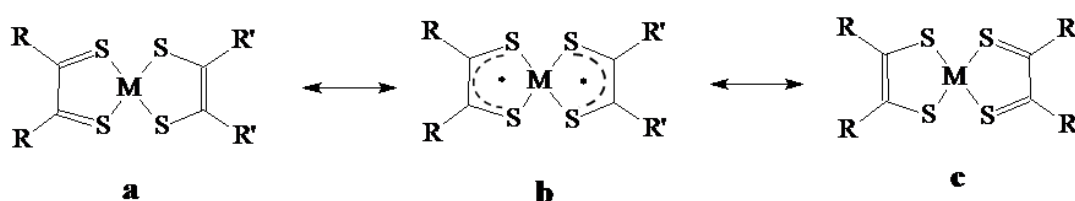
Scheme 1.12. *Lewis limit structures for neutral heteroleptic bis(1,2-dithiolene) complexes of d^8 metal ions.*

As a consequence, the peculiar monoelectronic HOMO-LUMO transition can be considered as an interligand charge-transfer process with some metal mixing, and this is reflected in the solvatochromic behaviour of the corresponding absorption band.[122]

Several well-documented mixed-ligand 1,2-dithiolene complexes have been reported, the majority of which featuring nickel as central metal ion,[42c,92a,122,123] while complexes based on different group 10 metals are far rarer.[124] Beside NLO applications,[125] these complexes have been exploited as components of molecular materials with optical or electrical properties,[98,111c,126] similarly to homoleptic *bis*(dithiolene) complexes.

Different synthetic routes have been exploited to obtain these complexes, and, as mentioned above, some of these methods involve scrambling reactions between symmetrical *bis*(1,2-dithiolene) complexes bearing different substituents, as reported in Equation 1.5:

$$[M(S^\wedge S^1)_2]^{x1} \quad + \quad [M(S^\wedge S^2)_2]^{x2} \quad \rightarrow \quad 2[M(S^\wedge S^1)(S^\wedge S^2)]^{x3} \tag{1.5}$$
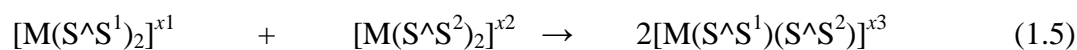
$(x = 0, -1, -2)$

The reactions between homoleptic *bis*(dithiolene) complexes in different oxidation states (e.g. $x_1 = 0$ and $x_2 = -2$) have been also exploited, so that the dianionic compound acts as reducing agent toward the neutral one, leading to the formation of symmetrical monoanionic intermediates which react to produce the mixed-ligand complex as a monoanion ($x_3 = -1$, Equation 1.5).[42c]

Another method consists in cross-coupling reactions summarised in Equation 1.6:[123g-i,124a]

$$S^\wedge S^1 + S^\wedge S^2 + MCl_2 \quad \rightarrow \quad [M(S^\wedge S^1)(S^\wedge S^2)] + [M(S^\wedge S^1)_2] + [M(S^\wedge S^2)_2] \tag{1.6}$$
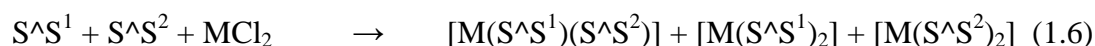
where $S^\wedge S^1$ and $S^\wedge S^2$ represent stable 1,2-dithiolates or their precursors.

An alternative synthetic pathway consists in the reaction between a *mono*(dithiolene) of the type $[M(S^\wedge S)(NH_3)_2]$ and a stable 1,2-dithiolene ligand, leading to the substitution of the NH_3 ligand of the complex (Equation 1.7):[123c]

$$[M(S^\wedge S^1)(NH_3)_2] \quad + \quad S^\wedge S^2 \quad \rightarrow \quad [M(S^\wedge S^1)(S^\wedge S^2)] \tag{1.7}$$
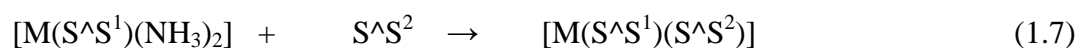
Arca and co-workers also reported a method based on a substitution reaction, in which the starting complex bears two bromide substituents (Equation 1.8).[124c] Through this method, the first palladium mixed-ligand *bis*(1,2-dithiolene) complex was obtained ($S^\wedge S^1 = Et_2$-timdt^{2-}; $S^\wedge S^2 = mnt^{2-}$).

$$[M(S\char`\^S^1)Br_2] \quad + \quad S\char`\^S^2 \quad \rightarrow \quad [M(S\char`\^S^1)(S\char`\^S^2)] \qquad (1.8)$$
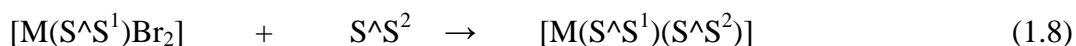
Mixed-ligand 1,2-dithiolene complexes of group 10 metals usually show a square-planar coordination, and in the case of nickel complexes, four similar M-S distances are generally found. On the contrary, in [Pd(Et$_2$-timdt)(mnt)][124c] significantly different Pd-S distances were observed for the two ligands. The analysis of bond distances in the 1,2-dithiolene core shows that, as expected, in complexes bearing ligands with similar *push/pull* character the C-C and C-S bond lengths are very similar in the two ligands, according to the Lewis structure **b** proposed in Scheme 1.12, while significantly different bond lengths are observed in complexes with ligands showing different *push/pull* character (better described with the Lewis structures **a** and **c** of Scheme 1.12).[121]

As mentioned above, absorption spectra of mixed-ligand 1,2-dithiolene complexes are characterised by an absorption band in the Vis-NIR region showing negative solvatochromism. The position of this band depends, again, on the *push/pull* character of the two ligands: if the *push/pull* character of the two ligands is similar, the absorption band falls in the NIR region, similarly to what observed for homoleptic *bis*(1,2-ditiholene) complexes of group 10 metals, while if the ligands bear substituents with significantly different electron-withdrawing character, the band shifts to shorter wavelengths, and shows a larger solvatochromism.[121]

Similarly to homoleptic *bis*(1,2-dithiolene) complexes, mixed-ligand complexes are redox-active species, and their redox properties are usually intermediate between those of symmetrical precursors.[121]

1.3.2. M(diimine)(dichalcogenolate) complexes

In diimine-dichalcogenolate metal complexes, the central metal ion is coordinated by two different types of ligands, a 1,2-dichalcogenolene ligand and a chelating diimine ligand, usually aromatic in nature, such as 2,2′-bipyridine, 1,10-phenanthroline and derivatives.[127]

Several complexes of this class have been synthesised in the past, mostly with group 10 metal ions, but diimine-dichalcogenolene complexes were also obtained for metals such as Co,[128] Au,[129] Zn,[130] Cd,[130f,131] Ru,[132] and Cu.[133] The majority of these complexes show the central metal ion in a four-coordinated fashion, with one 1,2-dichalcogenolene ligand and one diimine ligand, and are often schematised as [Pt(N^N)(E^E)] (where N^N is the diimine ligand, while E^E represent the 1,2-dichalcogenolate one), but six-coordinated complexes, with one 1,2-dichalcogenolene ligand and two diimine ones or *vice versa* are not unusual and were reported for Co,[128] Zn,[130g,f] Cd,[130f] Ru,[132] and Ni.[134]

To date, all diimine-dichalcogenolate complexes characterised structurally show 1,2-dithiolene ligands, beside [Pt(2,2′-bipy)(bds)] (**16**, bipy = 2,2′-bipyridine; bds^{2-} = benzene-1,2-diselenolate).[135]

In contrast to what specified above for homoleptic and heteroleptic *bis*(1,2-dithiolene) complexes, in this class of compounds it is possible to identify unambiguously the state of the 1,2-dithiolene ligand, which is in all cases in the 1,2-dithiolato form, as reflected in the name of the complexes. Therefore, diimine-dithiolate complexes of d^8 metal ions can always be conventionally described with the limit form shown in Figure 1.14.
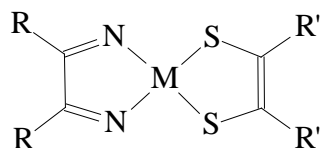
Figure 1.14. *Lewis structure for diimine-dithiolate complexes of d^8 metal dications.*

Platinum(II) diimine-dithiolate complexes have particularly attracted researchers' attention in the past few years, due to their wide range of possible applications. In the following section, the features of metal [M(N^N)(S^S)] complexes bearing aromatic diimine ligands will be summarised.

1.3.2.1. Synthesis

[M(S^S)(N^N)] complexes are usually synthesised as neutral species starting from the corresponding metal diimine-dichloro-complex, by displacement of the two chlorides with the desired 1,2-dithiolate ligand, as first reported by Vogler and coworkers (Equation 1.9).[136] In order to adopt this synthetic pathway, 1,2-dithiolene ligands or precursors existing in a stable form are required.

$$[M(N\char`\^N)Cl_2] \quad + \quad S\char`\^S \quad \rightarrow \quad [M(N\char`\^N)(S\char`\^S)] \tag{1.9}$$
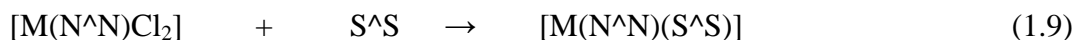
An alternative method consists of the reaction of the homoleptic *bis*(1,2-dithiolene) complex of the desired ligand with the appropriate diimine ligand (Equation 1.10). [137]

$$[M(S\char`\^S)_2] + \quad N\char`\^N \quad \rightarrow \quad [M(N\char`\^N)(S\char`\^S)] \tag{1.10}$$
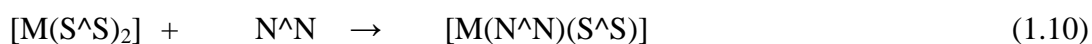
1.3.2.2. General structural features

Up to now less than fifty structures of [M(N^N)(S^S)], [M(N^N)(S^S)$_2$] and [M(N^N)$_2$(S^S)] complexes have been reported, as revealed by a search in the Cambridge Crystallographic Database, approximately half of which regarding platinum(II) complexes. An examination of these structural reports allows to deduce some general features for this class of compounds.

(i) In diimine-dithiolate complexes of the type [M(N^N)(S^S)], featuring one 1,2-dithiolene ligand a one diimine ligand, the central metal ion adopts a square-planar or distorted square-planar coordination, except for Zn complexes, where a tetrahedral or near-tetrahedral coordination is observed.[130a,b,f]

Analogously to what observed for homoleptic *bis*(1,2-dichalcogenolene) complexes (see above), the central metal ion has a great influence on the structural parameters of the complexes.[138,139] C-S distances within the 1,2-dithiolene ligands fit in a 0.113 Å range (1.687-1.800 Å), and tend to be longer than in homoleptic complexes, while the C-C bond lengths fall within a 0.177 Å range (1.283-1.460 Å), and their average lengths are shorter than in homoleptic complexes (Figure 1.15). This is in agreement with the fact that, as mentioned above, 1,2-dithiolene ligands in these complexes always behave as 1,2-dithiolates ($^-$S-C=C-S$^-$), while in *bis*(1,2-dithiolene) complexes they can assume a partial character of 1,2-dithioketones (Figure 1.14).
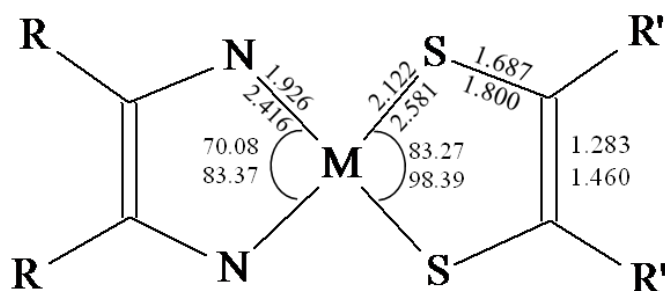
Figure 1.15. *Ranges of bond distances (Å) and angles (°) for diimine-dithiolate complexes of transition metals.*

Focusing on the most studied and promising platinum diimine-dithiolate complexes, Pt-S distances in the range 2.236-2.288 Å (average 2.256 Å)[140,141] and Pt-N distances in the range 2.010-2.065 Å (average 2.046 Å)[142,143] were reported, while C-S bond lengths and C-C distances fit in a 0.110 (1.690-1.800 Å, average 1.744 Å) [143,144] and 0.177 Å (1.283-1.460 Å, average 1.373 Å)[145,146] range, respectively. S-Pt-S and N-Pt-N angles range between 87.44-90.59 (average 89.38°)[140,143] and 77.54-80.65° (average 79.22°),[142,143] respectively (Figure 1.16).
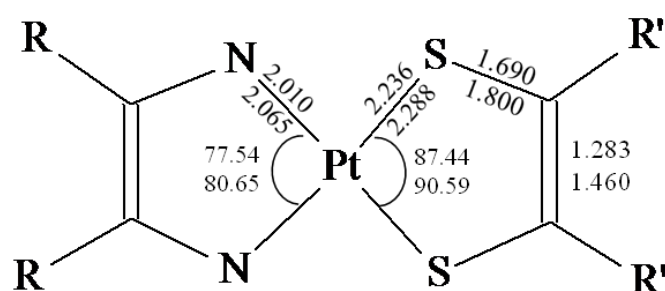
Figura 1.16. *Ranges of bond distances (Å) and angles (°) for platinum diimine-dithiolate complexes.*

Diimine-dithiolate complexes featuring both square-planar and tetrahedric coordination geometries at the metal ions exhibit a tendency to form dimeric structures, analogously to what observed for *bis*(1,2-dithiolene) complexes, and these aggregates are usually

held together by intermolecular M-S bonds between layered complexes in a head-to-tail orientation (Figure 1.17).[130d-e,131,140,147]
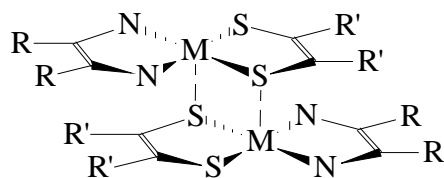
Figure 1.17. *Example of [M(N^N)(S^S)] dimeric structure.*

The complex units in the solid state are otherwise connected through stacking interactions, and also in this case for cationic and anionic complexes, the nature and size of the countercations can play a crucial role in the formation of the stacks.[129,148]

(ii) In the few structural reports on complexes of the type [M(N^N)$_2$(S^S)] or [M(N^N)(S^S)$_2$], the central metal ion is coordinated in an octahedral or distorted octahedral fashion. Bond lengths and angles have been found in the ranges summarised in Figure 1.18.[149]
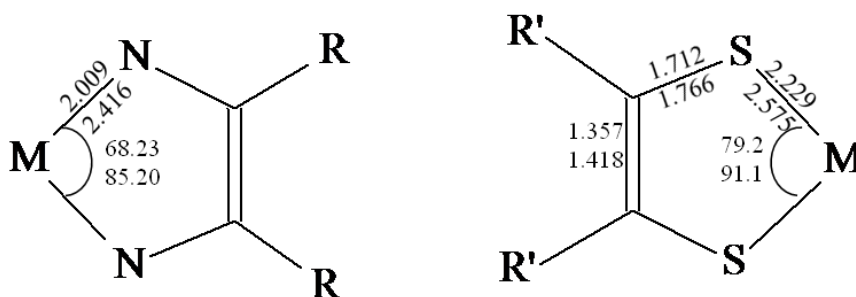
Figure 1.18. *Ranges of bond distances (Å) and angles (°) for octahedral diimine-dithiolate complexes of transition metals.*

1.3.2.3. Properties

The most striking feature of [M(diimine)(dithiolate)] complexes with square-planar coordination is the presence of an absorption band in the visible region showing a solvatochromic behavior, similar to that observed for heteroleptic *bis*(1,2-dithiolene) complexes (see above), but featuring a much larger range of energies.[121]

The assignment of this absorption band, deriving from a monoelectronic HOMO-LUMO vertical transition, has been extensively debated in the past. In the early works by Vogler,[136] the solvatochromic absorption band was assigned to a ligand-to-ligand charge-transfer (LL′CT) electronic transition, on the base of the assumption that the HOMO was mainly localised on the 1,2-dithiolene ligand, while the LUMO was centred on the diimine. More recently, the absorption band has been assigned by Eisenberg and coworkers[127,150] to a mixed metal-ligand-to-ligand charge-transfer (MMLL′CT, or MLCT/LLCT as recently abbreviated).[151] According to this interpretation, the HOMO in this complexes shows a not negligible metal character, as confirmed by the theoretical works performed by Mitsopoulou et al., and recently reviewed by the same authors.[152] In any case, the negative solvatochromism of this absorption band is due to the fact that the charge-transfer axis is collinear but antiparallel to the ground state of the dipole of the molecule, and thus excited state is less polar than the ground state.[121] Since the energy of the absorption band does not depend linearly on the polarity of the solvent, Eisenberg and coworkers developed an empirical solvent scale for platinum(II) diimine-dithiolate complexes.[127] Systematic variation in the nature of both the diimine and the dithiolate ligands can be used to tune the energy of this absorption band.[127,150] Eisenberg and coworkers, by testing the effects of several diimines and of a restricted number of well-known 1,2-dithiolene (namely edt^{2-}, mnt^{2-}, tdt^{2-}, and dmqdt^{2-}, Scheme 1.1) and other dithiolate ligands on the resulting complexes, concluded that the energy

of the absorption maximum in the visible region depends on both the dithiolate and diimine ligand. In particular diimines that possess electron-donating substituents were found to raise the energy of the LUMO (without affecting that of the HOMO), and consequently the HOMO-LUMO energy gap, while diimines featuring electron-withdrawing groups lower the energy of the LUMO and hence the energy gap between the frontier orbitals, while less accurate conclusions were formulated on the effect of the dithiolate, because of the limited number of 1,2-dithiolene ligands considered in the study.

The nature of the metal ion also affects the energy of the transition, as rationalised also by means of DFT calculations which showed that the energy of the transition decreases in the order Pd > Ni > Pt.[153]

Another important feature of diimine-dithiolate complexes featuring the metal ion in a square-planar coordination is their luminescence in solution, solid state, and frozen solvent glasses.[127] This emission occurs in the visible region, and has been assigned to a charge-transfer-to-diimine state, and accordingly its energy is solvent-dependent. Moreover, also in this case, a dependence of the emission features on the nature of the ligands was observed for platinum(II) complexes.[127] In particular, both the diimines and dithiolates influence the energy, emission lifetime and quantum yield of the Pt(diimine)(dithiolate) chromophore.[127] The analysis of the luminescence properties of these complexes also allowed to discover that they undergo both oxidative and reductive electron-transfer quenching, and, again, the excited-state redox potentials were found to depend on the nature of the ligands.[127] Moreover, it was observed that, depending on the concentration of the solutions, these complexes undergo self-quenching, attributed to the formation of stacks in solution.[154]

Similarly to homoleptic and heteroleptic *bis*(1,2-dithiolene) complexes, [M(N^N)(S^S)] complexes are redox-active species, and they usually feature two redox processes.[127]

The reversibility and the half-wave potentials of these processes depend, also in this case, on the nature of both the diimine and the dithiolato ligands. In particular, the nature of the N^N ligand affects the reduction potential (according to the localisation of the LUMO on this ligand), while the oxidation one depends on the S^S ligand (because of the localisation of the HOMO on this part of the complex),[127] though the tunability of this variable has not been investigated as thoroughly as those of absorption spectroscopic features.

Finally, another peculiar property of these systems is their photoreactivity. It is in fact well known that group 10 metals diimine-dithiolate complexes undergo photolysis in the presence of molecular oxygen, as illustrated for Pt^{II} complexes in Scheme 1.13.[155]
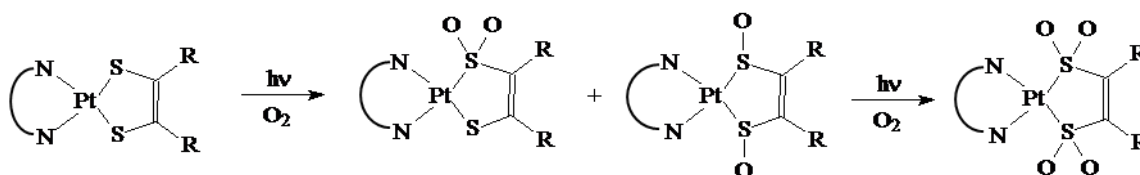
Scheme 1.13. *Photoreactivity of [Pt(N^N)(S^S)] complexes (adapted from Ref. 155).*

1.3.2.4. Applications

Due to their peculiar properties, diimine-dithiolate complexes, and in particular Pt^{II} ones, have been exploited for a wide range of applications, in fields ranging from material chemistry to biology.

(1) *Nonlinear Optics*. Given their lack of inversion centre, the molecular first hyperpolarisability (β) of diimine-dithiolate complexes is nonzero, so that they can be exploited for SONLO applications. Molecular first hyperpolarisabilities of a restricted number of Pt^{II} and Ni^{II} diimine-dithiolate complexes were evaluated from electric field induced second harmonic generation (EFISH) measurements, using the two-state

approximation.[87a,130,137a,156] The values of β determined for these complexes were found to reach as much as $-37 \cdot 10^{-30}$ esu,[130c] a value comparable to that of other NLO-active materials, so that these complexes represent one of the most promising class of complexes containing 1,2-dithiolene ligands for NLO applications. Also in this case, an influence of the nature of both the diimine and the dithiolate on the entity of β was found,[130c] and, interestingly, the Pt[II] complexes were identified as the most promising candidates for these applications, both experimentally[130c] and at a theoretical level.[153]

(2) *Applications in dye-sensitised solar cells*. In recent years the synthesis of transition-metal dye molecules for use as solar cells sensitisers has received much interest.[157] Dye molecules anchored to the surface of nanocrystalline TiO_2 absorb visible light and in their excited state they inject an electron into the conduction band of the TiO_2.[158] [Pt(N^N)(S^S)] compounds were investigated for their use in solar cells as they were shown to possess a number of key features that render them of interest as sensitisers. These features include their intense absorption band in the visible region, and their luminescent properties in solution, the tunability of which is particularly important in this context, since the electrochemical and photophysical properties of the dye generally affect the overall performance of the solar cell.[158] In order to be exploitable in this field, the dyes must contain a functional group to anchor them to the TiO_2 surface, such as a carboxyl group bound at the diimine ligand. The diimine-dithiolate complexes tested so far in a solar cell arrangement were found to efficiently convert light into electricity over the entire visible region, with overall efficiencies (η) up to 3%.[159]

(3) *Photogeneration of H_2.* The development of a molecular-based system for light-to-chemical energy conversion remains a key research objective for molecular scientists focused on energy production and utilisation. These studies employed multiple component systems that involved electron-transfer quenching of the chromophore, subsequent electron-transfer from the quencher to the dark catalyst, proton reduction to

yield H_2, and irreversible reaction of a sacrificial electron-donor.[160] [Pt(N^N)(S^S)] complexes were exploited for the design of molecular-based systems for light-driven, energy-storing reactions. In these systems, the diimine-dithiolate complexes are envisioned as the chromophores, having a directional charge-transfer excited state for electron-hole creation and substituent flexibility for tuning the excited state and connection to donor and acceptor groups. Eisenberg and collaborators successfully prepared some molecular photochemical devices (MPDs) based on [Pt(N^N)(S^S)] systems.[161]

(4) *Applications as conductive and magnetic materials.* Analogously to homoleptic and heteroleptic *bis*(1,2-dithiolene) complexes, the magnetic and electric properties of diimine-dithiolate complexes in the solid state have been tested. In particular, Matsubayashi and co-workers demonstrated that planar sulphur-rich dithiolate metal complexes of the [Pt(N^N)(S^S)] type (an example is drawn in Figure 1.19) can form, in their cationic form, columnar molecular stackings and/or layered interactions in the solid state through metal-metal and/or sulphur-sulphur contacts, giving rise to high electrical conductivities.[148b,162]
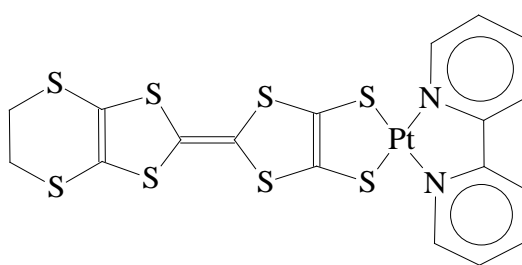
Figure 1.19. *Example of sulphur-rich 1,2-dithiolene metal complex with conductive properties: [Pt(bipy)($C_8H_4S_8$)] (Ref. 162).*

On the other hand, Omary recently reported on some charge-transfer products of [M(*t*Bu$_2$-bipy)(dmid)] (M = Pd, Pt; *t*Bu$_2$-bipy = 4,4′-*tert*-Bu$_2$-2,2′-bipyridine) complexes with organic acceptors such as TCNQ, TCNQF and TCNE (Figure 1.20, **a**, **b**, and **c**,

respectively), and demonstrated their magnetic susceptibilities and conductivities are nonzero, suggesting that these systems could be exploited as multifunctional molecular materials.[143]
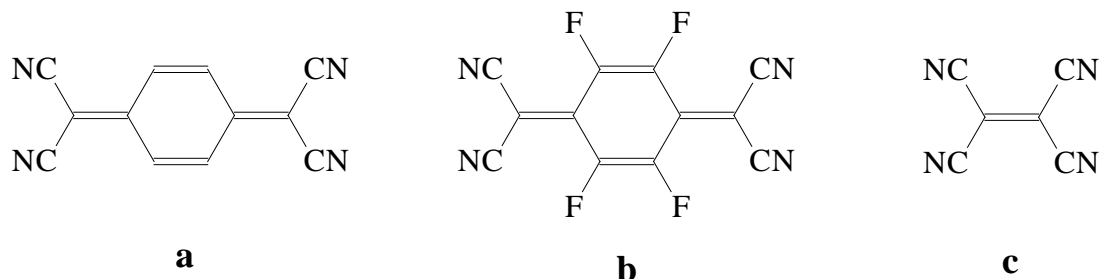
Figure 1.20. *Organic acceptors used for the formation of charge-transfer products with [M(tBu$_2$-bipy)(dmid)]: a) TCNQ; b) TCNQF; c) TCNE (Ref. 143).*

(5) *Applications as Sensors.* [M(diimine)(dithiolate)] complexes have been recently exploited as optical/electrochemical sensors for alkali metals. In particular Zuo[142,163] and co-workers reported some [Pt(N^N)(S^S)] complexes bearing crown-ether annelated dithiolene systems (Figure 1.21), and underlined that these systems undergo a potential shift of their redox processes and a colour change in the presence of Na$^+$ cations, demonstrating that these complexes represent highly selective sensors for the naked-eye detection of these metal ions.
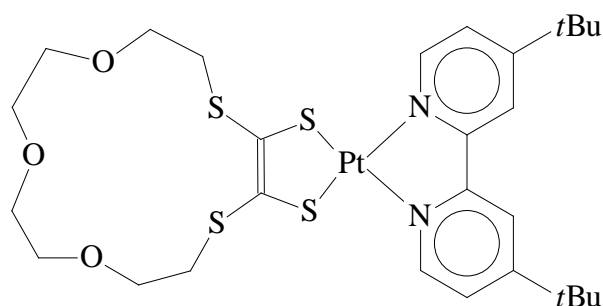
Figure 1.21. *Example of a [Pt(N^N)(S^S)] complex a bearing crown-ether annelated dithiolene system and used as Na$^+$ sensor: [Pt(dbbpy)(3O-C$_2$S$_4$)] (3O-C$_2$S$_4$ = 1,4,7-trioxa-10,13-dithiacyclopentadec-11-ene-11,12-dithiolate; dbbpy = 4,4'-di-tert-butyl-2,2'-bipyridine; Ref. 163).*

(6) *Biological applications.* Finally, a Pt^{II} diimine-dithiolate complex containing a quinoxaline ligand (Figure 1.22) was recently exploited as antiproliferative agent toward human tumour cells, given its ability to undergo DNA binding and photo-induced cleavage.[164]
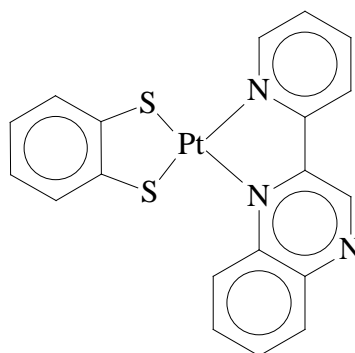
Figure 1.22. *Molecular drawing of the complex [Pt(pq)(bdt)] [pq = 2-(2'-pyridyl)quinoxaline and bdt^{2-} =benzene-1,2-dithiolato] (Ref. 164).*

1.3.3. Other systems containing 1,2-dichalcogenolene ligands.

1.3.3.1. Other mixed-ligand complexes featuring 1,2-dichalcogenolene ligands

1,2-Dichalcogenolene ligands have been also exploited for the synthesis of the following classes of compounds.

(1) *Cyclometalated complexes.* Some complexes schematised as [M(C^N)(S^S)] and related to M(diimine)(dithiolate) were synthesised in the past, bearing an arylpyridine chelating ligand in place of the diimine one, with several metal ions, such as Ni,[92d] Pd,[92d] Pt[165] and Au,[129] (See few examples in Figure 1.23), and they showed absorption and emission spectroscopic features very similar to those of [M(N^N)(S^S)] complexes.
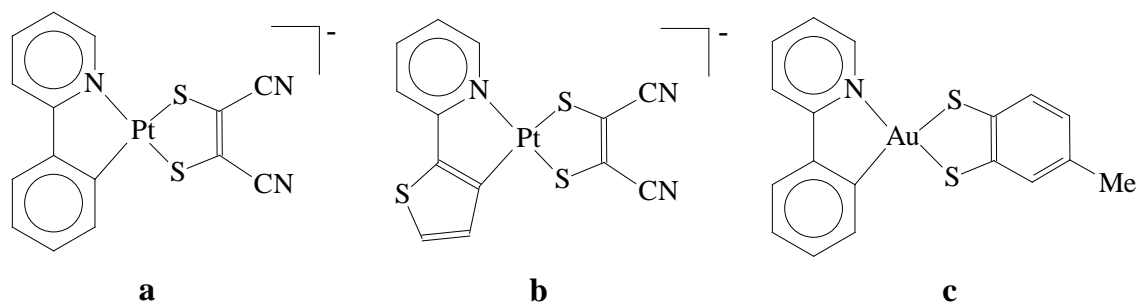
Figure 1.23. *Examples of cyclometalate complexes featuring arylpyridine chelating ligands along with 1,2-dithiolenes: a) (Bu₄N)[Pt(ppy)(mnt)]* (**17**)*, b) (Bu₄N)([Pt(tpy)(mnt)]* (**18**)*, c) [Au(ppy)(tdt)]* (**19**)*. Refs. 129 and 165.*

(2) *Carbonyl complexes.* Ultraviolet or visible light irradiation of a mixture of group 6 metal hexacarbonyl complexes $M(CO)_6$ (M = Cr, Mo, W) and $Ni(S_2C_2Z_2)_2$ (Z = alkyl or aryl) affords carbonyl complexes $[M(CO)_4(S_2C_2Z_2)]$ and $[M(CO)_2(S_2C_2Z_2)_2]$ (Figure 1.24).[107] The carbonyl groups in the *bis*(carbonyl)-*bis*(1,2-dithiolene) complexes are sufficiently labile to be displaced by a variety of other ligands, such as chalcogenides,[166] phosphines, 1,2-dithiolenes or halides.[167]
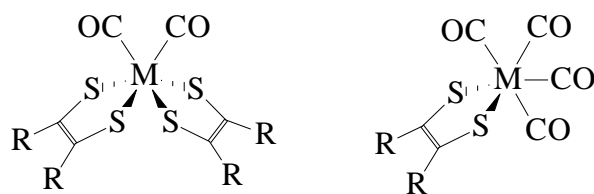
Figure 1.24. *Mono- and bis-(1,2-dithiolene) carbonyl metal complexes.*

(3) *Nitrosyl complexes.* McCleverty and co-workers found that dimeric dianions of the type $[Fe(S^\wedge S)_2]_2^{2-}$ are useful intermediates in the synthesis of iron mono-nitrosyl complexes. In fact, by treating the dimers with NO in nonpolar or weakly coordinating solvents, the corresponding complexes $[Fe(NO)(S^\wedge S)_2]^-$ were obtained (Figure 1.25).[168] Similar complexes were obtained with Co[168] and Mo.[169]
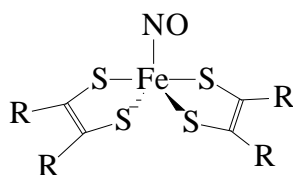
Figure 1.25. *Molecular drawing of a [Fe(NO)(S^S)]⁻ complex (Ref. 168).*

(4) *Cyclopentadienyl complexes*. A large number of mixed-ligand 1,2-dithiolene complexes including cyclopentadienyl (Cp) ligands have been prepared, both in their neutral or anionic state.[170] Extensive work on these systems was performed and recently reviewed by Sugimori.[171] The coexistence of aromaticity and unsaturation in the metalladithiolene ring confers unique reactivity to this class of complexes, which undergo electrophilic or radical substitution reactions, typical of aromatic rings. Recently, a *bis*(cyclopentadienyl) Ti complex featuring *N*-methyl-2-thioxo-1,3-thiazoline-4,5-diselenolate (Me-dset^{2-}) was also reported (Figure 1.26).[172]
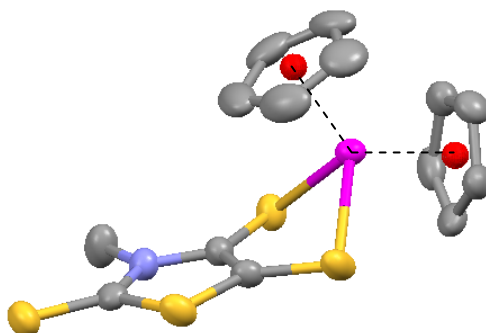
Figure 1.26. *ORTEP drawing of [Ti(Cp)$_2$(Me-dset)]. Ellipsoids are shown at the 50% probability level. Hydrogen atoms were omitted for clarity (Ref. 172).*

(5) *Phosphine-dithiolene complexes*. Pilato and co-workers synthesised a series of platinum(II) complexes of dppe (diphenylphosphinoethane) with 1,2-dithiolene ligands

(Figure 1.27).[173] These complexes present several interesting properties, such as solvatochromic absorption bands and luminescence in solution at room temperature, which make them candidates for applications as molecular probes and sensors.[174] The lowest energy excited state was characterised in these systems as a ene-1,2-dithiolate π→heterocycle π* ILCT, based on the solvatochromic absorption band that is independent of substituting Pt with Pd or Ni, but sensitive to changes on the heterocycle ring. The luminescence could be quenched by oxygen and organic electron-donors or acceptors, as well as by weak organic acids.[175]
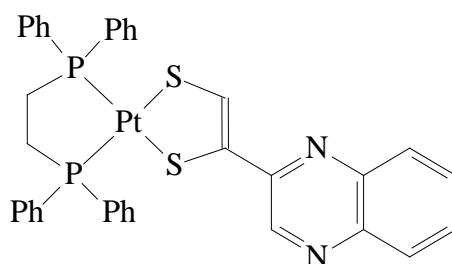
Figure 1.27. *Example of phosphine-dithiolene complex: Pt(dppe)[S₂C₂(2-quinoxaline)(H)] (Ref. 174).*

1.3.3.2. 1,2-Dithiolenes in nature

1,2-Dithiolenes play an important role in natural systems, since they are included in several metalloenzymes as integral components of their cofactors, and the role of dithiolenes in biological systems has been the subject of a vast number of publications and reviews.[8,176]

In particular, dithiolene groups are present in molybdenum- and tungsten-containing enzymes, which play an important role in the biochemical cycles of carbon, nitrogen and sulphur, and are present in all living systems.[176b] In particular, the molybdenum- and tungsten-containing enzymes featuring dithiolene systems are oxotranferases that

catalyse the transfer of an oxygen atom to a substrate X, or from a substrate XO, according to Equation 1.11:[8]

$$XO + 2H^+ + 2e^- \leftrightarrow X + H_2O \qquad (1.11)$$

The reactions catalysed involve a wide variety of substrates, including: (i) the oxidation of sulfite to sulfate, xanthine to uric acids, and an aldehyde to the corresponding carboxylic acid; (ii) the reduction of nitrate to nitrite and DMSO to DMS.[177] Several of these enzymes were structurally characterised,[178] and each catalytic centre showed to involve a single metal ion bound to one or two molecules of a special moiety, molybdopterin (MPT), that is unique to these enzymes (Figure 1.28).[179]
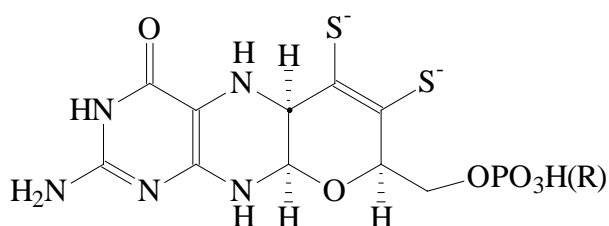
Figure 1.28. *Molecular structure of molybdopterin (MTP), the ligand that coordinates molybdenum or tungsten at the catalytic centre of the oxotransferase enzymes (R = H or nucleotide, Ref. 178).*

MTP is a triclinic pyranopterin, the pyran ring of which embeds the 1,2-dithiolene group and a phosphate side chain. The remainder of the coordination sphere of the metal is represented by a selection of ligands, including oxo-, dioxo-, hydroxo-, water-, or sulphide-groups and aminoacid side chains, and the molybdenum- and tungsten-containing enzymes structurally characterised so far have been classified on the basis of the number and nature of these ligands.[176b]

Spectroscopic informations indicate that the oxygen atom transfer reaction takes place at the metal centre, the oxidation state of which changes from M^{VI} to M^{IV} or *vice-versa*.[176d]

This chemistry has been mimicked by low molecular weight analogues of these centres, which were used as structural and reactivity models;[8,180] however, challenges remain in understanding the coordination chemistry of these centres, not the least of these is the role of the pterin and pyran ring that, together with the dithiolene, form MPT. In this context, theoretical calculations could play a crucial role, as testified by the recent publication of several works on this topic.[181]

2. *Objectives*

Since many years, the research group I have been working with has been focusing its attention on the chemistry of metal (1,2-dithiolene) complexes, and, in particular on the synthesis of complexes with square-planar coordination containing 1,2-dithiolene ligands, and the study of their chemical-physical properties, with particular regard to the linear and nonlinear optical features of these systems.

As already mentioned, during the past years, *bis*(1,2-dithiolene) complexes of the type [M(R,R′-timdt)$_2$] (M = Ni, Pd, Pt; R,R′-timdt^{2-} = *N,N′*-disubstituted 2-thioxoimidazoline-4,5-dithiolate)[12,26d,78,83,91] have been particularly studied. These complexes show interesting features, and in particular a NIR absorption whose energy suggested a possible use of these systems in Nd-based lasers, and NLO properties such as saturable absorption.[78,182,183] Moreover, these complexes feature a wavelength-selective photoconductivity coupled to the near-IR absorption, which allowed for the fabrication of solid-state photodetectors operating between the first and third optical-fiber windows.[91]

In the past few years, the research has been focusing on asymmetrically substituted 1,2-dithiolene ligands, whose complexes in their *cis* conformation, as already mentioned, are candidates for SONLO application. This was first achieved by modifying the R,R′-timdt^{2-} ligands through the introduction of R and R′ substituents remarkably different in nature.[78] Subsequently, as mentioned in Chapter 1 (Sections 1.1.4 and 1.2.4.1.2), homoleptic *bis*(1,2-dithiolene) complexes based on a class of ligands intermediate between R,R′-timdt^{2-} and dmit^{2-}, namely R-dmet^{2-} (*N*-substituted 2-thioxo-thiazoline-4,5-dithiolate), were obtained and characterised.[27] [M(R-dmet)$_2$] complexes (M = Ni, Pd, Pt), analogously to related [M(R,R′-timdt)$_2$] ones, were found to be good candidates for near-IR-laser applications and for near-IR-photoconductivity.[91d]

More recently, a study on mono-arylsubstituted 1,2-dithiolene ligands of the class Ar,H-edt^{2-} (aryl-substituted ethylene-1,2-dithiolate) has also been started,[184] with particular focus on the possibility of combining in the resulting metal complex the properties of the dithiolene system with those peculiar to the ligand substituents.

In this context, the present doctorate has been aimed at continuing the research on the topic of asymmetrically substituted 1,2-dichalcogenolene ligands, with the main aim of designing new SONLO-active materials. In particular, the work has been focused on the following goals:

a) Synthesis and characterisation of new homoleptic *bis*(1,2-dithiolene) complexes featuring monosubstituted 1,2-dithiolene ligands, and, in particular, monoarylsubstituted ligands of the type Ar,H-edt^{2-} capable of combining in a single molecular compound the luminescence of the substituents with the linear and nonlinear optical properties of the dithiolene core.

b) Synthesis and characterisation of a series of new mixed-ligand complexes containing both Ar,H-edt^{2-} and R-dmet^{2-} ligands (including selenated analogues), and in particular of platinum(II) diimine-dichalcogenolate complexes, in order to investigate the structure-properties relationships within the series of complexes obtained. [Pt(N^N)(S^S)] complexes were chosen as the focus of the investigation because, among all the mixed-ligand complexes featuring 1,2-dichalcogenolene ligands obtained so far, they represent the most promising candidates for NLO applications.

c) Study of the electronic structure of the synthesised complexes by means of DFT calculations. In this context, our goal is to evaluate the static first hyperpolarisability (β) of the synthesised compounds, in order to identify the best candidates for experimental NLO measurements and study, also in this case, the structure-properties relationships of these systems.

d) Study of other possible applications of the obtained compounds in the field of Information and Communication Technology (ICT), through the analysis of properties previously encountered for complexes based on 1,2-dichalcogenolene ligands, such as photoconduction.

3. Results and Discussion

The present work has been focused on the synthesis and characterisation of noncentrosymmetric complexes bearing 1,2-dichalcogenolene ligands for NLO applications, mainly employing asymmetrically substituted ligands belonging to the classes Ar,H-edt^{2-} (edt^{2-} = ethylene-1,2-dithiolato; Ar = aryl group) and R-dmet^{2-} (*N*-substituted 2-thioxo-thiazoline-4,5-dithiolate) or the isolog R-dset^{2-} (*N*-substituted 2-thioxo-thiazoline-4,5-diselenolate).

As far as homoleptic *bis*(1,2-dithiolene) complexes are concerned, those deriving from R-dmet^{2-} ligands have been extensively investigated by our research group and by Prof. Lorcy and coworkers in Rennes.[27,28,79,91c,172]

Homoleptic *bis*-dithiolenes of the type [M(Ar,H-edt)$_2$]$^{x-}$ were investigated in depth for M = Ni.[184] During the present work we have therefore extended this work to M = Au, a metal ion that in *bis*(1,2-dithiolene) complexes exhibits many common structural, electrochemical and spectroscopic aspects with the corresponding ones of group 10 metals.

Passing to heteroleptic complexes, in view of our interest for NLO potential applications and on the ground of the state of the art on this topic, we have turned to combining asymmetrical 1,2-dichalcogenolene ligands with symmetric aromatic diimines, to form the corresponding noncentrosymmetric Pt(diimine)(dichalcogenolate) complexes. For this purpose, 1,2-dichalcogenolene ligands belonging to both classes mentioned above were adopted, to give [Pt(N^N)(E^E)] complexes (E = S, Se).

In addition, few other complexes, not belonging to the classes of products just mentioned, have been prepared, and will be discussed in the following Sections.

3.1. Synthesis and characterisation of [Au(Ar,H-edt)₂]ˣ⁻ complexes (20ˣ⁻ - 22ˣ⁻)

3.1. Synthesis and characterisation of [Au(Ar,H-edt)₂]$^{x-}$ complexes (20^{x-}- 22^{x-})

Notwithstanding the large number of both experimental and theoretical studies on 1,2-dithiolene complexes, luminescence has been only occasionally tapped,[173] although such investigations are invaluable in understanding the electronic structure of both ground and excited states. Weak emission processes ($\Phi = 1 \cdot 10^{-5}$) have been reported for some *bis*(1,2-dithiolene) complexes,[150b] but more commonly studies have concerned either mixed-ligand monodithiolene complexes,[173,185] as previously mentioned, or negatively charged *bis*(1,2-dithiolene) complexes counterbalanced by fluorogenic cations.[186]

Consequently, impelled by the low-energy electronic NIR absorption of neutral d^8 metal complexes, and by the capability of asymmetrically substituted 1,2-dithiolene ligands to form noncentrosymmetric systems, the possibility of attaching a single fluorogenic substituent to each 1,2-dithiolene ligand has been investigated, so as to include in a single molecular compound the peculiar properties of the luminescent substituents along with the linear and NLO properties of the dithiolene core.

During the research described in this thesis, attention has been focused on the Au^{III} complexes **20**, **21**, and **22**, featuring monoaryl substituted ethylene-1,2-dithiolates with aromatic substituents of increasing complexity, namely phenyl, 2-napthyl, and 1-pyrenyl, respectively.

3.1.1. Synthesis

As mentioned in section 1.1.2., one of the most commonly adopted methods for the synthesis of stable open-ring 1,2-dithiolene ligands consists of the reaction of α-

haloketones with alkylxanthate anions to give the corresponding α-ketoxanthate esthers.[17] In a subsequent reaction, these esthers can undergo cyclisation in strongly acidic media to give the corresponding vinylene dithiocarbonates. The heterocycles are then reacted with strong bases, leading to the ethylene-1,2-dithiolates, that can be reacted with the desired metal ion to give the desired 1,2-dithiolene complexes.

According to this synthetic strategy, adopted previously to synthesise the salt (PPh$_4^+$)(**20**$^-$),[18b] a three-step synthetic route has been exploited for the synthesis of the complexes (Scheme 3.1). In this work, our interest has been focused on three aryl substituents of increasing extension, namely phenyl, 2-naphthyl, and 1-pyrenyl.

In the first step (i in Scheme 3.1), potassium isopropyl xanthate was reacted with the desired bromoacetylarene in acetone solution, to give the corresponding *O*-isopropyl-*S*-aryldithiocarbonate [Aryl = Ph (**23**), Naph (**24**), Pyr (**25**)].

This step is followed by the cyclisation of the obtained *O*-isopropyl-*S*-arylcarbonates **23-25** (ii in Scheme 3.1), performed in a 1:2 diethyl ether/chloroform mixture in the presence of HClO$_4$, leading to the formation of the corresponding aryl-1,3-dithiol-2-ones [aryl = Ph (**26**), Naph (**27**), Pyr (**28**)]. These heterocycles were subsequently suspended in ethyl alcohol in the presence of an excess of KOH, to give the corresponding monoaryl ethylene-1,2-dithiolates, which were readily reacted *in situ* with KAuCl$_4$ in the presence of tetrabutylammonium iodide. This led to the formation of the desired gold(III) *bis*(1,2-dithiolene) complexes **20-22** as monoanions, counterbalanced by tetrabutylammonium (TBA$^+$) cations (step iii in Scheme 3.1).

Ar = Ph (**23**), Naph (**24**), Pyr (**25**)

Ar = Ph (**26**), Naph (**27**), Pyr (**28**)

Ar = Ph (**20**), Naph (**21**), Pyr (**22**).
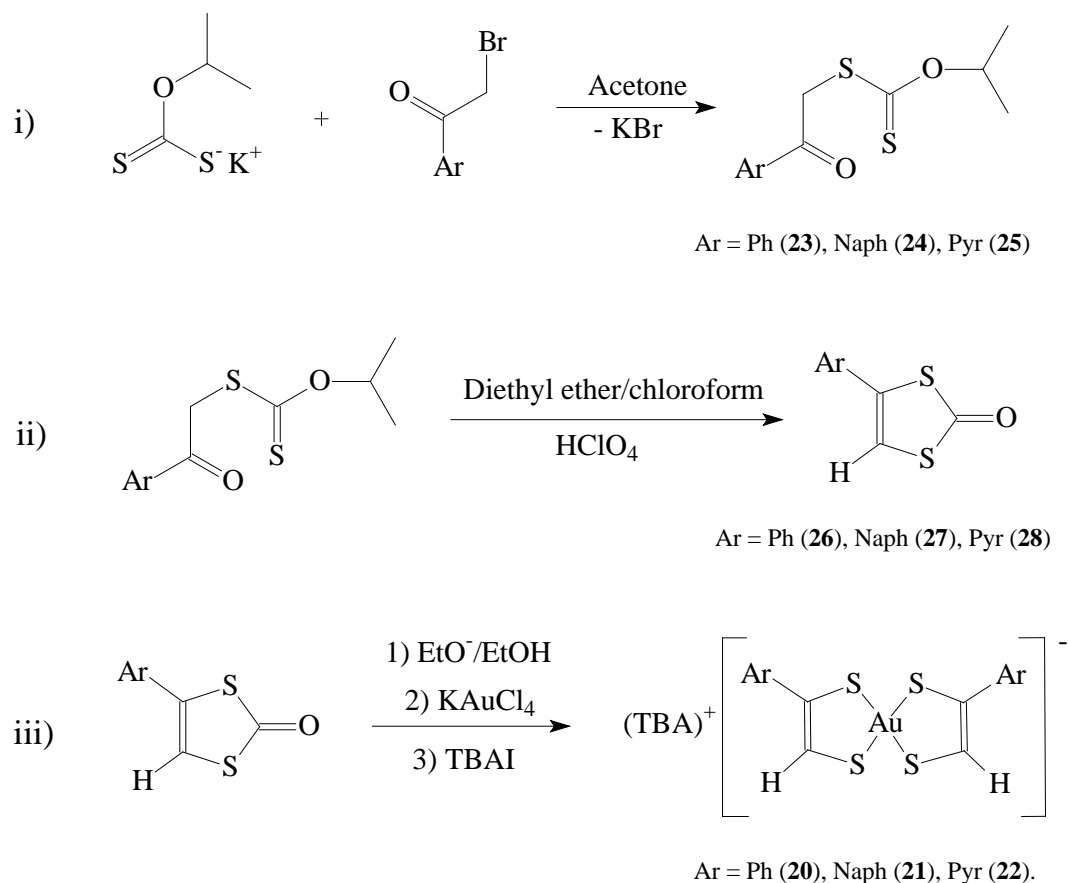
Scheme 3.1. *Synthesis of (TBA$^+$)[Au(Ar,H-edt)$_2$]$^-$ compounds.*

The complexes, obtained in yields ranging between 18 and 36%, were found to be thermally stable, with melting points above 110° C.

3.1.2. Structural characterisation

X-ray diffraction-quality crystals were obtained for one of the aryl-1,3-dithiol-2-one precursors, namely **26** (Figure 3.1, Table 3.1).
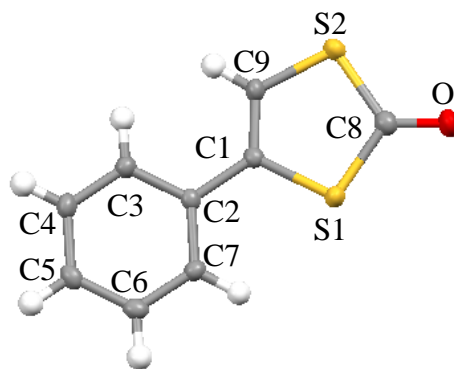
Figure 3.1. *ORTEP drawing and atom labelling scheme for **26**. Thermal ellipsoids are shown at the 50% probability level.*

Table 3.1. *Crystal data for **26**.[a]*

Empirical Formula	$C_9H_6OS_2$
Formula weight	194.26
Crystal size (mm)	0.36 x 0.12 x 0.02
Crystal system	Orthorhombic
Space group	Pbca
a (Å)	10.3779(6)
b (Å)	7.8316(3)
c (Å)	20.3844(12)
Volume (Å^3)	1656.75(15)
Z	8
Calculated density (Mg m^{-3})	1.558
Reflections unique	1900
R_{int}	0.0594
Parameters	109
Final R indices [$I > 2\sigma (I)$]	0.0400
$wR2$ (all data)	0.0966

[a] $T = 120(2)$ K. Mo$_{K\alpha}$ radiation ($\lambda = 0.71073$ Å).

The diffractometric analysis shows that the compound features the expected structure, with the phenyl substituent slightly twisted with respect to the plane of the heterocycle [9.18(12)°; Table 3.2] Concerning the bond lengths in the heterocycle, a C-C distance of 1.344(3) Å was observed, while the average C(1,9)-S(1,2) and C8-S(1,2) bond distances were found to be 1.742 and 1.771 Å, respectively (Table 3.2).

Table 3.2. *Selected bond lengths (Å), angles and dihedrals (°) for* **26.**[a]

S1-C8	1.770(2)
S2-C8	1.773(2)
C8-O	1.213(3)
C1-C9	1.344(3)
S1-C1	1.756(2)
S2-C9	1.729(2)
C1-C2	1.400(3)
C9-C1-S1	115.37(17)
C1-C9-S2	119.21(17)
C1-S1-C8	96.99(11)
C9-S2-C8	96.11(11)
S1-C8-S2	112.30(13)
C3-C2-C1-C9	9.18(12)

[a] Atom labeling scheme as in Figure 3.1.

Such metric parameters are in good agreement with the average experimental distances reported so far for differently substituted 1,3-dithiol-2-ones [1.346 (14), 1.739 (23), and 1.766 (7) Å for C1-C9, C(1,9)-S(1,2), and C8-S(1,2) bond lengths, respectively].[187]

Among the gold complexes deriving from the precursors **26-28**, crystals suitable for X-ray diffraction were obtained for the complex $(TBA^+)(21^-)$. The crystal structure (Figure 3.2, Table 3.3) shows that the compound contains discrete complexes featuring the central metal ion coordinated in a square-planar fashion, with the ligands assuming a *cis* conformation.
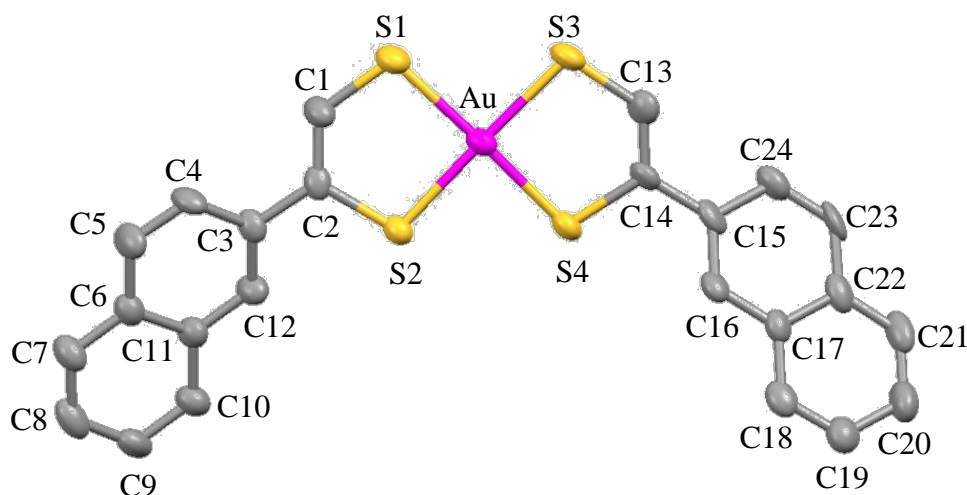
Figure 3.2. *ORTEP drawing and atom labelling scheme for the dithiolene unit in $(TBA^+)(21^-)$. Thermal ellipsoids are shown at the 50% probability level. Hydrogen atoms have been omitted for clarity.*

Although several examples of monoanionic homoleptic nickel *bis*(1,2-dithiolene) complexes derived from asymmetrically substituted ligands have been characterised structurally,[188] only two examples of gold 1,2-ditholenes with a *cis* [Ar = phenyl (**20**⁻), pyridin-2-yl (**29**⁻)] and two with a *trans* configuration [Ar = pyridin-3- (**30**⁻) and 4-yl (**31**⁻)] have been described to date (Figure 3.3).[18b, 189]
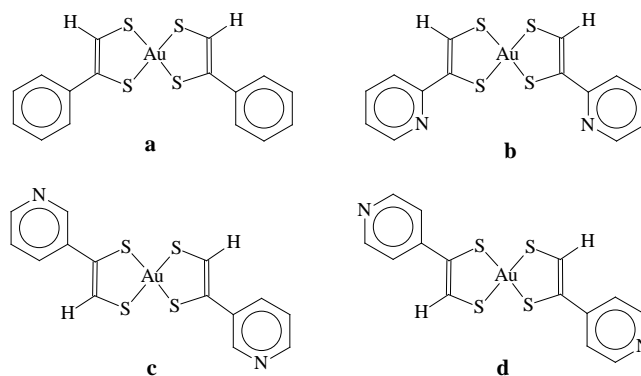
Figure 3.3. *Structures of monoanionic gold bis(1,2-dithiolene) complexes featuring monosubstituted ligands characterised structurally: a) [Au(Ph,H-edt)$_2$]$^-$ (**20**); b) [Au(2-Py,H-edt)$_2$]$^-$ (**29**$^-$); c) [Au(3-Py,H-edt)$_2$]$^-$ (**30**$^-$); d) [Au(4-Py,H-edt)$_2$]$^-$ (**31**$^-$, Refs. 18b and 189).*

Table 3.3. *Crystal data for (TBA$^+$)(**21**$^-$).^{a}*

Empirical Formula	$C_{40}H_{52}AuNS_4$
Formula weight	872.03
Crystal size (mm)	0.46 x 0.06 x 0.02
Crystal system	Orthorhombic
Space group	$P2_12_12_1$
a (Å)	12.1719(8)
b (Å)	16.2337(10)
c (Å)	19.4449(8)
Volume (Å^3)	3842.2(4)
Z	4
Calculated density (Mg m^{-3})	1.508
Total number of data	38594
Reflections unique	8772
R_{int}	0.1182
Parameters	419
Final R indices [$I > 2\sigma(I)$]	0.0506
$wR2$ (all data)	0.0979

^{a} T = 120(2) K. Mo$_{K\alpha}$ radiation (λ = 0.71073 Å).

Table 3.4. *Selected bond lengths (Å), angles and dihedrals (°) for (TBA⁺)(**21⁻**).*[a]

Au-S1	2.314 (2)
Au-S2	2.306 (2)
Au-S3	2.318 (2)
Au-S4	2.312 (2)
C1-C2	1.327 (12)
C13-C14	1.358 (12)
S1-C1	1.747 (9)
S2-C2	1.765 (8)
S3-C13	1.721 (9)
S4-C14	1.775 (8)
S1-Au-S2	89.93(8)
S3-Au-S4	89.98(8)
S1-Au-S3	91.78(8)
S2-Au-S4	88.42(8)
Au-S1-C1	100.8(3)
Au-S3-C13	100.7(3)
Au-S2-C2	102.6(3)
Au-S4-C14	102.3(3)
S1-C1-C2	127.3(7)
S2-C2-C1	119.3(7)
S3-C13-C14	125.9(8)
S4-C14-C13	121.2(7)
C1-C2-C3-C4	26.5(12)
C13-C14-C15-C24	25.7(12)

[a] Atom labeling scheme as in Figure 3.3.

The two naphthyl substituents are twisted with respect to the ethylene-1,2-dithiolato core by 25.7(12) and 26.5(12)°, analogously to what found for all the other homoleptic monoanionic or neutral gold *bis*(1,2-dithiolene) complexes that feature aromatic substituents structurally characterised so far, in which the aromatic rings show torsion angles ranging between 11.69(4)[18b] and 60.2(2)°.[75a]

A closer examination of the $Au(C_2S_2)_2$ core shows that the two units are remarkably different to each other as far as C-C and C-S bonds are concerned (Table 3.4). However, the average C-C and C-S bond lengths (1.342 and 1.752 Å, respectively) in **21⁻** are indeed close to the corresponding mean values [1.344(38) and 1.743(23) Å, respectively] found for the other monoanionic gold complexes of 1,2-dithiolene ligands found in the Cambridge Structural Database. These distances are also very close to those determined for compound **26**, discussed above. As previously pointed out, C-C and C-S bond lengths have been indicated as a criterion for discriminating between the ene-1,2-dithiolate (⁻S-C=C-S⁻) and the 1,2-dithioketone (S=C-C=S) possible limit forms of a 1,2-dithiolene ligand, and hence to estimate the oxidation state of the central metal. The bond lengths found in the crystal structure of **21⁻** indicate the presence of C=C double and C-S single bonds, respectively, suggesting that monoanionic gold *bis*(1,2-dithiolene) complexes should be formulated as Au[III] *bis*(ene-1,2-dithiolato) complexes, in agreement with what was proposed by Wieghardt and co-workers for $[Au(C_6H_4S_2)_2]^-$ (**32⁻**)[190] and $[Au(Ph_2-edt)_2]^-$ (**33⁻**) derivatives,[75a] by Tunney et al.[18b] for **20⁻**, and [Au(*n*-Py,H-edt)₂]⁻ [*n* = 2 (**29⁻**), 4 (**31⁻**); Py = *n*-pyridyl), and, more recently, by Rabaça et al. for **31⁻**.[189]

In the crystal packing, weak S···H (2.928–2.983 Å) and C···H (2.880–2.885 Å) contacts are responsible for the interactions between organic cations and the complex anions. Although the complex molecules are aligned along the cell axis directions, no significant stacking interactions between the complex units are present, the shortest

Au⋯Au distances of the complex molecules corresponding just to the cell axis dimensions.

Finally, during an attempt of crystallising (TBA⁺)(**21**⁻), single crystals of an unknown product were isolated. X-ray diffraction analysis established this to be 2,5-*bis*(naphthyl)-thiophene (**34),** a reaction by-product deriving from the condensation of two ligand units (Figure 3.4 and Table 3.5), previously synthesised from 2,5-dibromothiophene.[191]
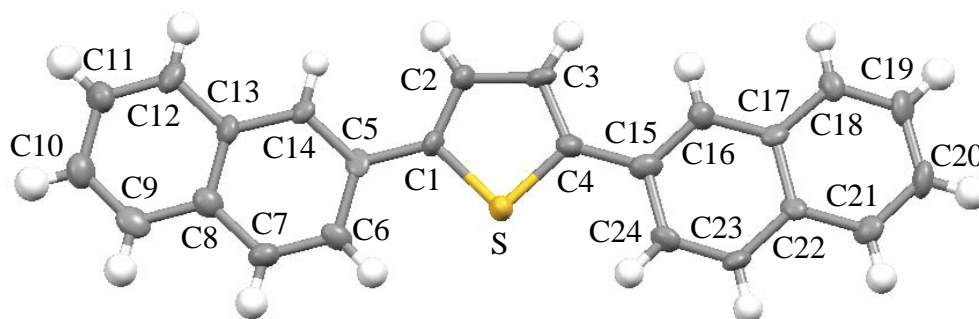
Figure 3.4. *ORTEP drawing and atom labelling scheme for **34**. Thermal ellipsoids are shown at the 50% probability level.*

Table 3.5. *Crystal data for 34.*[a]

Empirical Formula	$C_{24}H_{16}S$
Formula weight	336.43
Crystal size (mm)	0.06 x 0.06 x 0.02
Crystal system	Monoclinic
Space group	P21
a (Å)	7.7369(7)
b (Å)	5.8173(5)
c (Å)	36.365(3)
Volume ($Å^3$)	1627.7(2)
Z	4
Calculated density (Mg m^{-3})	1.373
Reflections unique	4844
R_{int}	0.0930
Parameters	452
Final R indices [$I > 2\sigma (I)$]	0.0764
$wR2$ (all data)	0.1848

[a] $T = 120(2)$ K. Mo$_{K\alpha}$ radiation ($\lambda = 0.71073$ Å).

The molecule is almost completely planar, with dihedral angles C2-C1-C5-C14 and C3-C4-C15-C16 of 3.11(10) and 0.58 (12)°, respectively. Selected structural parameters are listed in Table 3.6.

Notably, the isolation of **34** may be considered as a proof of the instability of aryl-ethylene-1,2-dithiolates, and its formation might be at least partially responsible for the rather modest reaction yields of the synthesis of complexes **20⁻-22⁻**.

Table 3.6. *Selected bond lengths (Å), angles and dihedrals (°) for **34**.[a]*

C1-C2	1.385(11)
C2-C3	1.427(11)
C3-C4	1.350(12)
C1-S	1.729(8)
C4-S	1.736(8)
C1-C5	1.459(12)
C4-C15	1.444(11)
C1-C2-C3	111.87(8)
C2-C3-C4	115.00(8)
C3-C4-S	109.82(6)
C4-S-C1	93.02(4)
S-C1-C2	110.3(7)
C2-C1-C5-C14	3.11(10)
C3-C4-C15-C16	0.58(12)

[a] Atom labeling scheme as in Figure 3.4.

3.1.3. Electrochemistry

As already mentioned, gold(III) *bis*(1,2-dithiolene) complexes, like all complexes of d^8 metals of the same type, are members of an electron-transfer series, which allows them to assume molecular charges x ranging between –2 and 1,[75a] the relative stability of each species being largely determined by the nature the of substituents at the 1,2-dithiolene ligand. Cyclic voltammetry (CV) and differential pulse voltammetry (DPV) measurements were performed in CH_2Cl_2 on $(TBA^+)(\textbf{20}^-)$, $(TBA^+)(\textbf{21}^-)$, and $(TBA^+)(\textbf{22}^-)$. Each of the compounds exhibits two one-electron DPV-tested redox

waves, at about -2.0 and -0.13 V versus the Fc$^+$/Fc couple [Table 3.7; Figure 3.5 for (TBA$^+$)(**22**$^-$)].
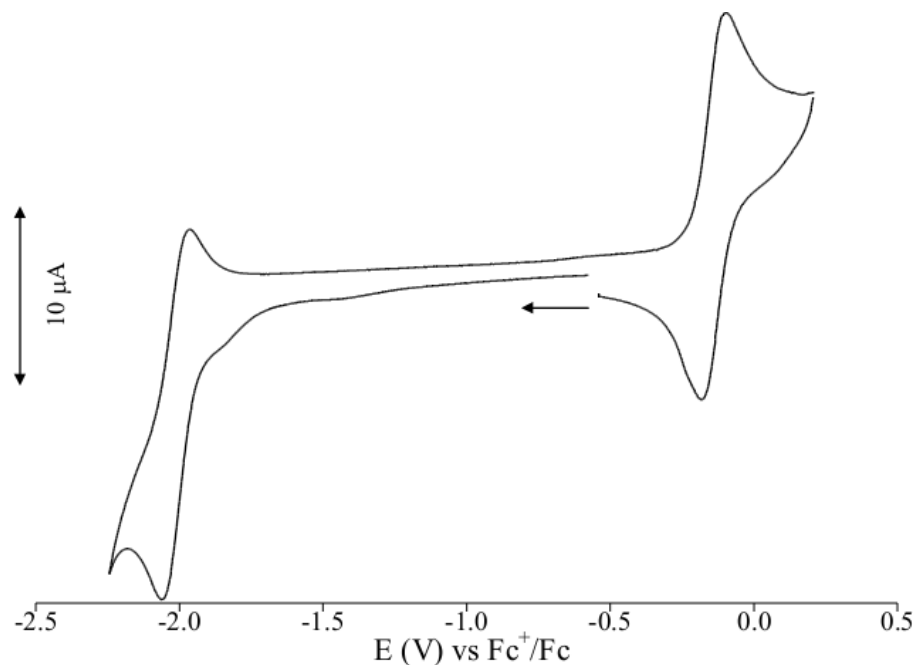
Figure 3.5. *Cyclic voltammogram recorded for a solution of (TBA$^+$)(**22**$^-$) at a platinum electrode in anhydrous CH$_2$Cl$_2$ [298 K; scan rate 100 mV s^{-1}; supporting electrolyte (TBA$^+$)(PF$_6^-$) 0.1 M].*

Following the interpretation provided by Wieghardt,[75a] these waves should be ascribed to the processes shown in Equation 3.1:

$$[\text{Au}^{\text{III}}(\text{L})(\text{L}^{\cdot})] \rightleftharpoons [\text{Au}^{\text{III}}(\text{L})_2]^- \rightleftharpoons [\text{Au}^{\text{II}}(\text{L})_2]^{2-} \qquad (3.1)$$
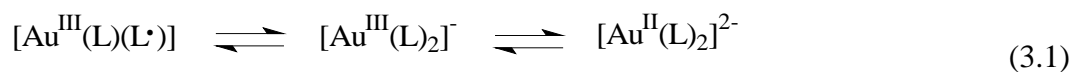
in which L represents the dianionic ene-1,2-dithiolate form ($^-$S-C=C-S$^-$) and L$^{\cdot}$ the corresponding monoanionic radical form of the ligand. Notably, in the explored potential range no waves indicating a further oxidation to cationic species [Au$^{\text{III}}$(L$^{\cdot}$)$_2$]$^+$ were found.

Table 3.7. *Half-wave potentials $E_{1/2}$ (V vs Fc^+/Fc) recorded by CV for complexes $(TBA^+)(20^- \text{-} 22^-)$.*

	$E_{1/2}$ $^{(-1/-2)}$	$E_{1/2}$ $^{(0/-1)}$	i_{pc}/i_{pa} $^{(-1/-2)}$	i_{pc}/i_{pa} $^{(0/-1)}$	$\|E_{pc}-E_{pa}\|^{(-1/-2)}$	$\|E_{pc}-E_{pa}\|^{(0/-1)}$
$(TBA^+)(\mathbf{20^-})$	-2.04	-0.13	1.2	1.0	0.135	0.093
$(TBA^+)(\mathbf{21^-})$	-2.01	-0.12	1.1	1.0	0.129	0.083
$(TBA^+)(\mathbf{22^-})$	-2.01	-0.14	0.8	1.0	0.100	0.078

An examination of i_{pc}/i_{pa} and peak separation values clearly indicates that oxidation of monoanionic species to the corresponding neutral ones is a fully reversible process (i_{pc}/i_{pa} = 0.8-1.2; $|E_{pc}-E_{pa}|$ about 100 mV at 100 mV s^{-1}), and it occurs without decomposition of the complexes. It should be noted that the redox behavior observed for $(TBA^+)(\mathbf{20^-})$ is different to that previously reported for $(PPh_4^+)(\mathbf{20^-})$,[18b] which, in DMF solution, showed an irreversible nature for both processes. CV data allowed to evaluate[192] the HOMO and the LUMO energies of the monoanionic species (HOMO: -4.89, -4.87, -5.25 eV; LUMO: -3.02, -2.91, -3.02 eV for $\mathbf{20^-}$, $\mathbf{21^-}$, and $\mathbf{22^-}$, respectively) and hence their HOMO–LUMO energy gaps ($\Delta E_{HOMO-LUMO}$ = 1.87, 1.96, and 2.24 eV for $\mathbf{20^-}$, $\mathbf{21^-}$, and $\mathbf{22^-}$, respectively), showing that the complex with the lowest HOMO-LUMO energy gap is $\mathbf{20^-}$. In Table 3.8, a comparison between the half-wave potentials determined for **20-22** and those reported for other $[Au(R_1,R_2\text{-edt})_2]$ complexes[18b,75,192a,193] is provided, and shows that on passing from electron-withdrawing (CN, CF$_3$) to electron-releasing substituents the potentials of the three redox processes in the series become progressively more negative, in agreement with what commonly observed for *bis*(1,2-dithiolene) complexes of d^8 metals (Section 1.2.4.1.1). Therefore, while for the gold *bis*(1,2-dithiolene) complexes that feature strongly or moderately electron-withdrawing R$_1$ and R$_2$ groups the redox process that leads to the monocation is not observed, for those that have electron-realising substituents, the redox step leading to the dianion falls outside the explorable

electrochemical window. Not surprisingly, an inspection of the Cambridge Structural Database shows that to date most of the crystal structures of gold *bis*(1,2-dithiolene) complexes concern monoanionic species, whereas only very few concern neutral species (8 out of 103).

Table 3.8. *Half-wave potentials $E_{1/2}$ (V vs Fc^+/Fc)[a] for* **20**–**22** *and some related [Au(R_1,R_2-edt)$_2$] complexes.*

	R_1	R_2	$E_{1/2}^{(-1/-2)}$	$E_{1/2}^{(0/-1)}$	$E_{1/2}^{(+1/0)}$	Solvent[b]	Ref.
	CF_3	CF_3	-1.36[a]	0.93[a]	-	CH_2Cl_2	75a
	CN	CF_3	-1.35	0.75	-	CH_2Cl_2	193c
15	CN	CN	-1.32[a]	0.71[a]	-	CH_2Cl_2	193b
29	2-Py [c]	H	-1.920	0.120[d]	-	DMF	18b
30	3-Py [c]	H	-1.880	0.180[d]	-	DMF	18b
31	4-Py [c]	H	-1.840	0.200	-	DMF	18b
20	Ph [c]	H	-1.970	0.050	-	DMF	18b
20	Ph [c]	H	-2.013	-0.127	-	CH_2Cl_2	This work
21	2-Naph [c]	H	-2.011	-0.120	-	CH_2Cl_2	This work
22	1-Pyr [c]	H	-2.038	-0.134	-	CH_2Cl_2	This work
	Ph-C_6H_4	Ph-C_6H_4	-2.03	-0.07	0.51	CH_2Cl_2	75a
33	Ph [b]	Ph	-2.061	-0.085	0.510	CH_2Cl_2	192a
	4-tBu-C_6H_4	4-tBu-C_6H_4	-2.09	-0.11	0.45	CH_2Cl_2	75a
	n-C_4H_9-O-C_6H_4	n-C_4H_9-O-C_6H_4	-	-1.390[a]	0.363[a]	CH_2Cl_2	75b
	n-C_8H_{17}-O-C_6H_4	n-C_8H_{17}-O-C_6H_4	-	-1.500[a]	0.375[a]	CH_2Cl_2	75b
	n-$C_{12}H_{25}$-O-C_6H_4	n-$C_{12}H_{25}$-O-C_6H_4	-	-1.460[a]	0.368[a]	CH_2Cl_2	75b

[a] For comparison purposes, data reported versus SCE were converted to versus Fc^+/Fc by subtracting 0.39 V.
[b] DMF = dimethylformammide; [c] Py=pyridyl; Ph = phenyl; Naph = naphthyl; Pyr = pyrenyl. [d] Anodic peak potential.

3.1.4. Absorption UV-Vis-NIR Spectroscopy

As already pointed out, one of the most striking property of *bis*(1,2-dithiolene) complexes of d^8 metals in a square-planar coordination is their intense absorption in the NIR region (Section 1.2.4.1.2.). This absorption has been particularly studied in *bis*(1,2-dithiolene) complexes of group 10 metals. In these systems, the NIR-absorption occurs both in their neutral form, where is mainly due to a monoelectronic HOMO-LUMO vertical transition, and in the monoanions. In the latter case, being the molecular orbital corresponding to the LUMO of the neutral form singly occupied, the electronic transition is HOMO-SOMO in nature, and is always found at lower energies than in neutral complexes, because of the stabilisation of the SOMO, and the subsequent lowering of the energy gap between the frontier molecular orbitals, determined by the partial filling of the former orbital (Figure 3.6). On the other hand, *bis*(1,2-dithiolene) complexes of group 11 metals, and in particular gold(III) ones featuring a square-planar coordination, due to their different electronic structure, show this band in their neutral state, corresponding, from an electronic point of view, to the monoanionic form of related *bis*(1,2-dithiolene) complexes of group 10 metals, and in the monocations, corresponding to neutral group 10 metal complexes (Figure 3.6). Therefore, the absorption is not present in the UV-Vis-NIR spectra of corresponding monoanionic complexes, where the orbital corresponding to the SOMO in the monoanion is completely occupied.

Group 10 metal *bis*(1,2-dithiolene) complexes

Group 11 metal *bis*(1,2-dithiolene) complexes
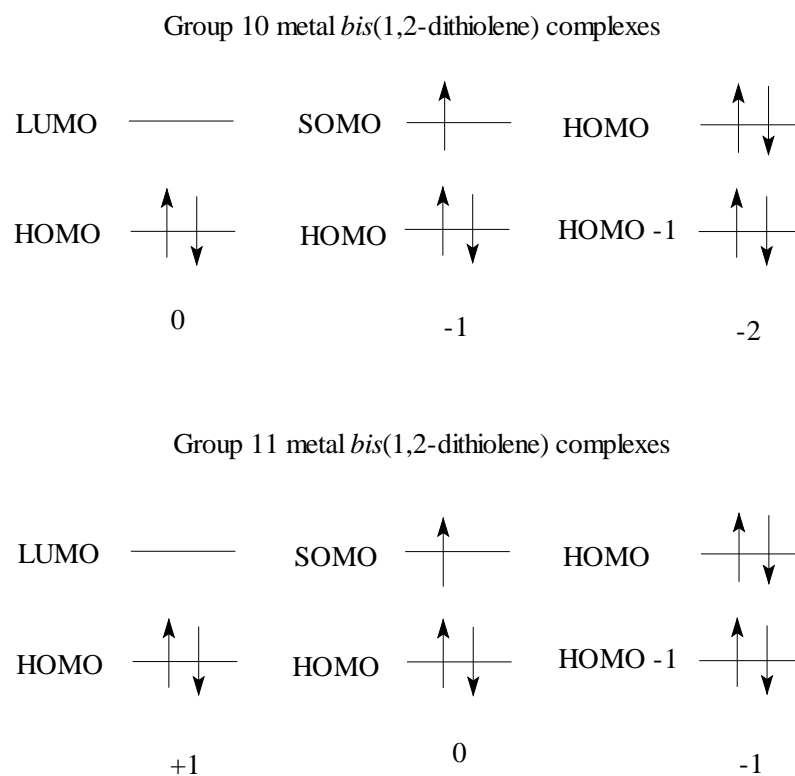
Figure 3.6. *Frontier molecular orbitals occupation diagram for differently charged bis(1,2-dithiolene) complexes of group 10 and 11 transition metals.*

The absorption band falls at energies remarkably lower than those of corresponding Ni, Pd and Pt complexes, and the maximum absorption wavelength λ_{max} depends on the electronic features of the substituents. Thus, whereas **15** features a NIR absorption band at 1110 nm,[75a] neutral gold *bis*(1,2-dithiolene) complexes that contain electron-releasing groups feature bands centered at almost 1600 nm.[75b] As predictable, the corresponding monocations feature very intense NIR bands with higher energies, at about 1100 nm (1066 and 1142 nm for $[Au\{(4\text{-}t\text{Bu-}C_6H_4)_2\text{-edt}\}_2]^+$ and $[Au\{(4\text{-}C_6H_5\text{-}C_6H_4)_2\text{-edt}\}_2]^+$, respectively, in CH_2Cl_2).[75a]

The UV-Vis-NIR electronic absorption spectra (200–2000 nm) in CH_2Cl_2 of the TBA^+ salts of complexes **20⁻-22⁻** all feature absorptions in the UV-Vis region, the maxima of which fall below 450 nm, with the band at the lowest energy featuring a maximum in all cases at about 350 nm (Figure 3.7 for **22⁻**).
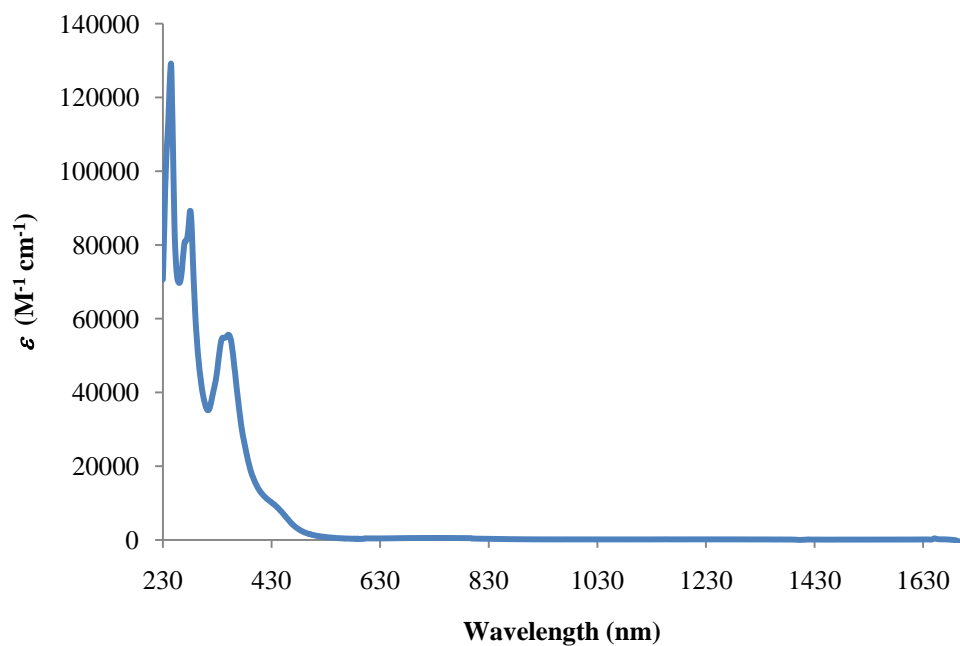
Figure 3.7. *UV-Vis-NIR absorption spectrum recorded in CH$_2$Cl$_2$ for (TBA$^+$)($\textbf{22}^-$).*

As expected, the corresponding neutral species, readily formed in solution by oxidation with I$_2$, feature intense NIR absorption bands falling at 1408, 1464, and 1432 nm in CH$_2$Cl$_2$ for **20$^-$**, **21$^-$**, and **22$^-$**, respectively, with molar extinction coefficients ε up to about 20000 M^{-1} cm^{-1} (Table 3.9 and Figure 3.8 for **21$^-$**).
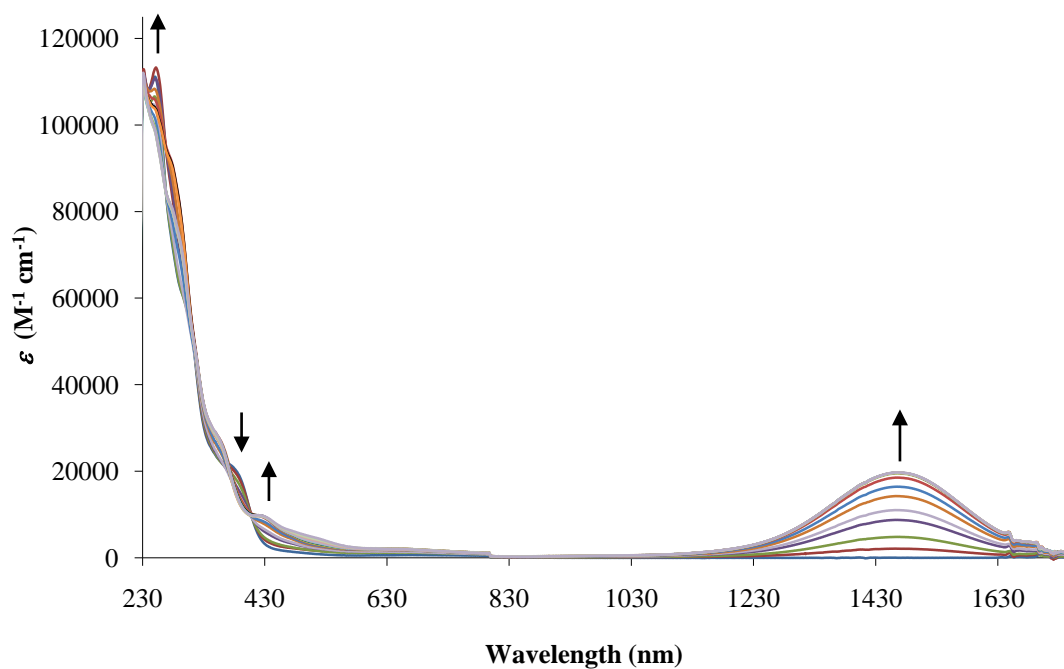
Figure 3.8. *Dilution corrected UV-Vis-NIR spectra recorded during the spectrophotometric titration of* *(TBA$^+$)(**21**$^-$) with I$_2$ in CH$_2$Cl$_2$ solution.*

The presence of well-defined isosbestic points in the titration spectra of the three complexes supports their stabilities in the neutral state, already proved in the CV timescale.

Table 3.9. *NIR absorption maxima (nm) and molar extinction coefficients (M^{-1} cm^{-1}) for complexes **20**$^-$-* *22$^-$ in CH$_2$Cl$_2$.*

	λ_{max}	ε
(TBA$^+$)(**20**$^-$)	1408	12400
(TBA$^+$)(**21**$^-$)	1464	19500
(TBA$^+$)(**22**$^-$)	1432	7950

3.1.5. Emission Spectroscopy

To the best of our knowledge, no investigations on the luminescence of gold 1,2-dithiolene complexes have been reported to date, whereas, as far as nickel 1,2-dithiolene complexes are concerned, the complex core is not luminescent itself and fluorescence was reported only when negatively charged 1,2-dithiolene complexes were counterbalanced by fluorescent cations.[186]

Fluorescence measurements carried out on $(TBA^+)(\mathbf{20^-}\text{-}\mathbf{22^-})$ in the range $\lambda_{exc} = 220\text{–}400$ nm showed in all cases a complex emission profile in the visible region (380–550 nm), with quantum yields (Φ) of about $1\cdot10^{-3}$ ($2.4\cdot10^{-3}$, $9.4\cdot10^{-4}$, and $1.0\cdot10^{-3}$ for $\mathbf{20^-}$, $\mathbf{21^-}$, and $\mathbf{22^-}$, respectively).

Table 3.10. *Excitation and emission wavelengths [λ_{exc} and λ_{em} (nm), respectively] for $\mathbf{20^{x-}}$–$\mathbf{22^{x-}}$ (x = 0, 1) in CH$_2$Cl$_2$ at room temperature.*

	Monoanion		Neutral form	
	λ_{exc}	λ_{em}	λ_{exc}	λ_{em}
20	333	390	300	390
21	360	426	360	424
22	343	410	343	473

As an example, in Figure 3.9 the UV-Vis absorption and the fluorescence emission spectra recorded for $\mathbf{21^-}$ in CH$_2$Cl$_2$ are compared.
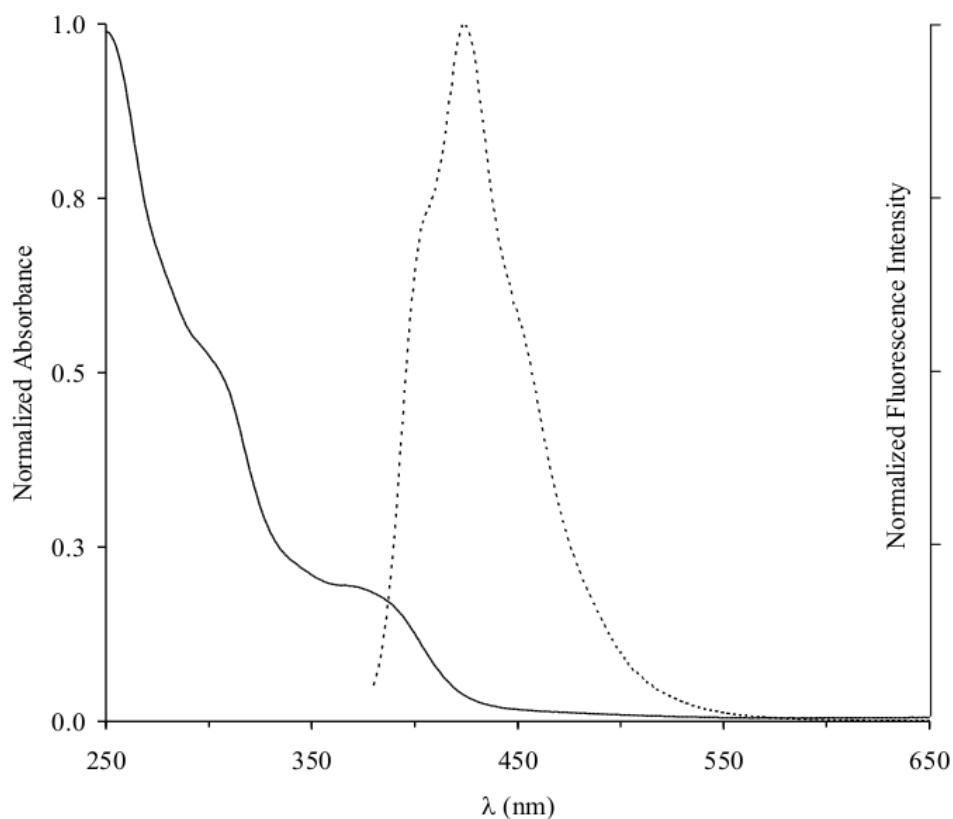
Figure 3.9. *Superimposed normalised UV-Vis (250-650 nm) absorption (continuous line) and emission (dotted line; λ_{exc} = 360 nm) spectra recorded for (TBA$^+$)(**21**$^-$) in CH$_2$Cl$_2$ solution.*

A spectral decomposition allowed us to evaluate the energy differences between the emission maxima of the single component peaks, which were found to be within the range 0.2–0.3 eV (Table 3.11; Figure 3.10 for **21**$^-$), so that the emission spectra should result from a vibronic progression[194] that derives from a single electronic relaxation path.
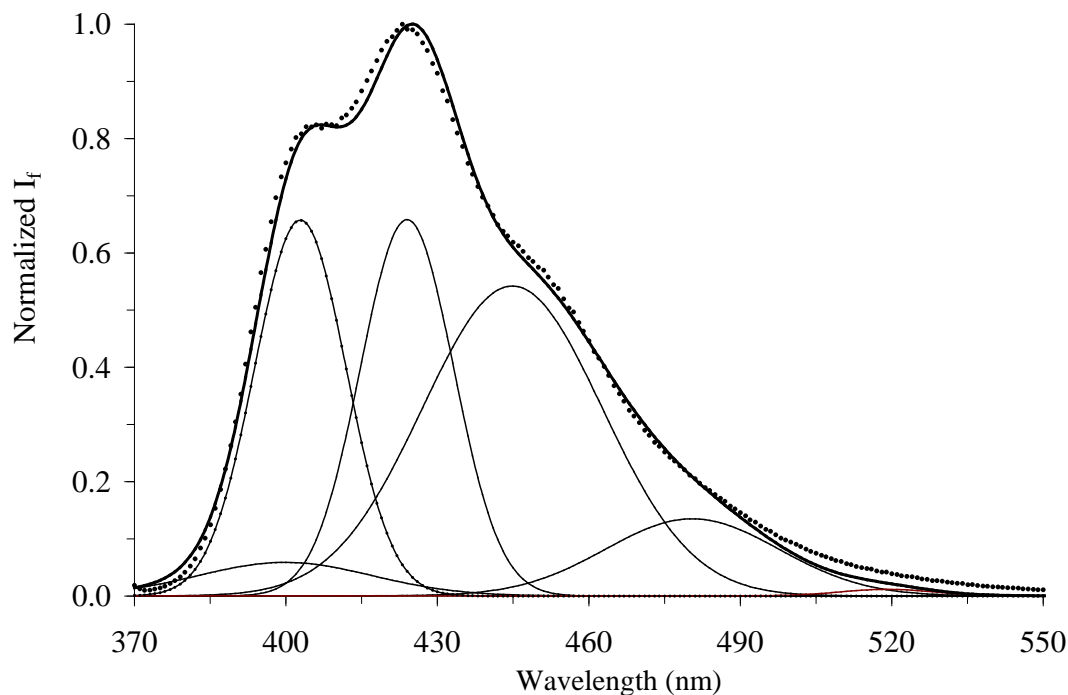
Figure 3.10. *Normalised emission spectrum recorded for (TBA⁺)(**21⁻**) in CH₂Cl₂ solution (dotted line) decomposed into the constituent Gaussian curves. C = 3.2·10⁻⁵ M. λₑₓc = 360 nm. Gaussian curves: maximum wavelengths λ = 400, 403, 424, 445, 480, 519 nm; full width at half maximum w = 20.3, 10.7, 10.9, 21.0, 20.2, 10.8 nm; relative intensity h = 0.09, 1.00, 1.00, 0.82, 0.20, 0.02.*

Table 3.11. *Results from the decomposition of the CH₂Cl₂ solution fluorescence spectra (350-500 nm) recorded for (TBA⁺)(**20⁻**)-(**22⁻**) in four constituent Gaussian components. Each curve is described in terms of wavelength position (λ, nm), full width at half maximum (w, nm) and relative intensity (h).*

	λ_1	λ_2	λ_3	λ_4	w_1	w_2	w_3	w_4	h_1	h_2	h_3	h_4
20⁻	370.0	388.1	407.5	408.1	5.5	12.6	22.9	99.3	0.7	0.8	0.8	0.3
21⁻	370.7	399.1	404.4	424.0	8.8	11.5	74.9	10.6	0.3	0.3	0.4	0.3
22⁻	386.4	400.6	447.6	501.8	2.7	20.5	53.9	142.0	0.4	0.6	0.4	0.1

Fluorimetric I₂ titrations showed that neutral complexes **20**–**22** (λ_{exc} = 300, 360, and 343 nm, respectively) feature emission spectra in the same region as the corresponding monoanionic species, as summarised in Table 3.10 (molar extinction coefficients ε

calculated at the excitation wavelengths remain almost unaltered on passing from the monoanions to the corresponding neutral species (Figure 3.8 for **21**⁻ and **21**). In the case of (TBA⁺)(**20**⁻) and (TBA⁺)(**21**⁻), an increase in the fluorescence intensity (I_f), linearly correlated to the increase in the NIR absorption, was observed during the titrations, with the Φ values roughly doubling on passing from **20**⁻/**21**⁻ to **20**/**21** [I_f(neutral species)/I_f(monoanion) = 1.92 and 1.90, corresponding to the emission maxima λ_{em}^{max} that fall at 390 and 424 nm for **20**⁻ and **21**⁻, respectively, Table 3.10].

More promising are the emission spectra of **22**, since on oxidation of (TBA⁺)(**22**⁻) an increase in the emission at 473 nm and a decrease in the region around 410 nm were observed (Table 3.10, Figure 3.11), thus resulting in a variation of the Stokes shift on passing from the monoanion to the neutral species.
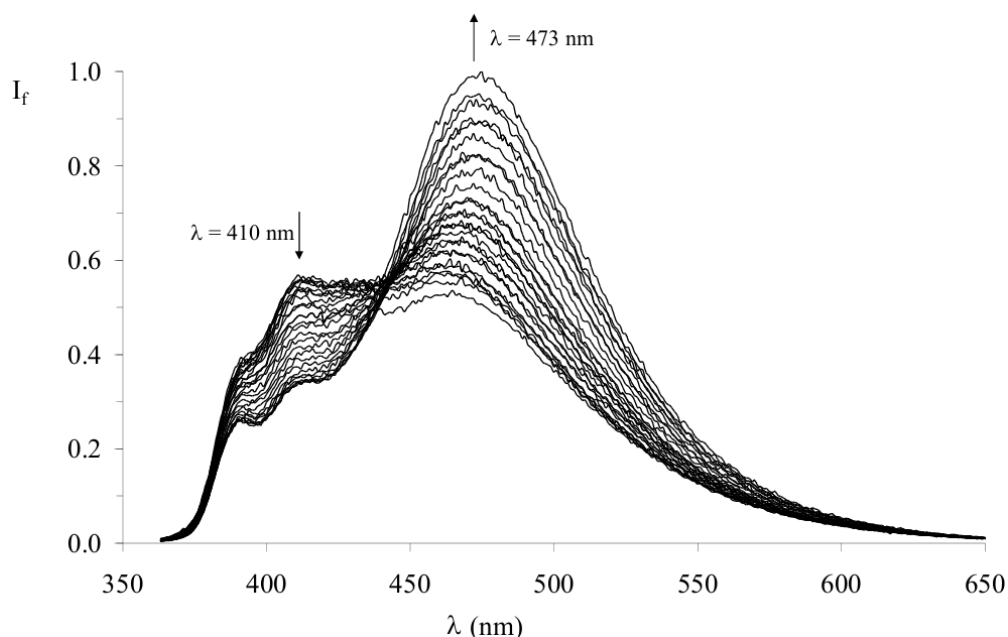
Figure 3.11. *Normalised corrected emission spectra (λ_{exc} = 343 nm) recorded during the titration of (TBA⁺)(**22**⁻) with I_2 in CH₂Cl₂.*

Thus, since spectroscopic and electrochemical measurements agree in the indication that no decomposition leading to fluorescent byproducts occurs upon oxidation of the

monoanionic complexes, in the case of $(TBA^+)(\mathbf{22}^-)$ the energy of the maximum in the emission spectrum is controlled by the applied redox potential.

3.1.6. DFT calculations

Theoretical calculations represent an imparallelable tool for the inspection of electronic features and the interpretation of physical-chemical properties of inorganic systems.

For this reason, with the aim of getting an insight into the structural, spectroscopic, and electrochemical features of the title complexes, quantum chemical calculations have been carried out at the density functional theory (DFT)[195] level. Following the results of previous studies, in which various functionals and basis sets were compared for 1,2-dithiolene[196] and different gold complexes,[197] Barone's and Adamo's mPW1PW functional[198] was adopted. For light atomic species (H, C, and S) the all-electron double-ζ basis sets (BSs) with polarisation functions from Schäfer, Horn, and Ahlrichs[199] were exploited, whereas for gold the LanL2DZ (d,p) BS with effective core potentials[200] was preferred so as to account for relativistic effects.

To give an interpretation of the different features shown by complexes $\mathbf{20}^{x-}$-$\mathbf{22}^{x-}$ in their different oxidation states, theoretical analysis has been performed on the former complexes considering different molecular charges x ranging between -2 and 0. Since, as previously pointed out, crystallographic reports on different $[Au(R,R'\text{-edt})_2]^{x-}$ complexes show these systems can exhibit *cis*/*trans* isomerism, both conformations were optimised for the nine model complexes considered.

3.1.6.1. Geometry optimisation

The optimised *cis* and *trans* isomers of complexes $\mathbf{20}^{x-}$-$\mathbf{22}^{x-}$ (x = 0-2) were found to show negligible differences in their total electronic energies (less than 0.2 kcal mol^{-1}, Table 3.12), in agreement with what has been recently reported.[193c]

Table 3.12. *Energy difference ΔE (kcal mol^{-1}) between cis/trans isomers of $\mathbf{20}^{x-}$-$\mathbf{22}^{x-}$ calculated at their optimised geometries.*

x	−2	−1	0
20	$1.67\cdot10^{-1}$	$2.87\cdot10^{-2}$	$7.01\cdot10^{-2}$
21	$8.72\cdot10^{-2}$	$1.04\cdot10^{-2}$	$1.19\cdot10^{-1}$
22	$0.59\cdot10^{-4}$	$1.36\cdot10^{-1}$	$4.70\cdot10^{-5}$

As an example, the optimised structure of the *cis* isomer of **22** is depicted in Figure 3.12.
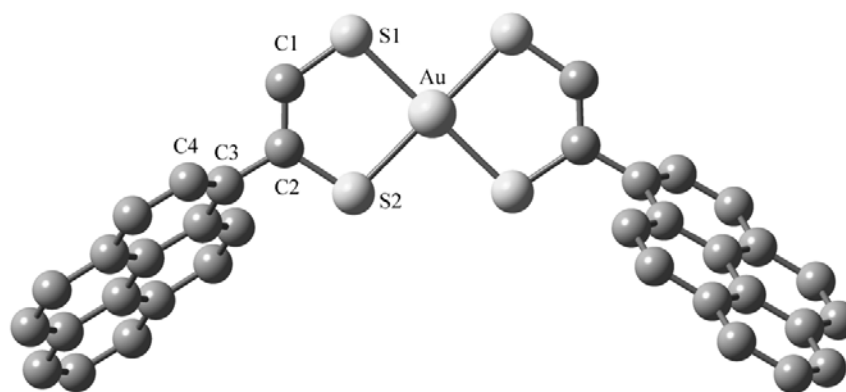
Figure 3.12. *Molecular drawing and atom labelling scheme for the cis isomer of **22** at the optimised geometry (C_2 point group).*

Selected optimised bond lengths and angles for the eighteen model compounds are listed in Table 3.13.

Table 3.13. *Selected optimised bond lengths (Å) and angles (°) for the cis and trans isomers of* **20**$^{x-}$*-***22**$^{x-}$ *(x = 0-2).*[a]

	20		20$^-$		20^{2-}		21		21$^-$		21^{2-}		22		22$^-$		22^{2-}	
	cis	*trans*	*cis*	*trans*	*cis*	*trans*	*cis*	*trans*	*cis*	*trans*	*cis*	*trans*	*cis*	*trans*	*cis*	*trans*	*cis*	*trans*
C1-C2	1.368	1.368	1.352	1.352	1.370	1.370	1.369	1.369	1.350	1.354	1.374	1.375	1.365	1.364	1.350	1.350	1.377	1.378
S1-Au	2.361	2.360	2.379	2.378	2.512	2.507	2.362	2.359	2.379	2.376	2.511	2.507	2.365	2.360	2.380	2.379	2.505	2.499
S2-Au	2.357	2.357	2.375	2.377	2.505	2.510	2.358	2.361	2.374	2.376	2.500	2.501	2.359	2.363	2.378	2.378	2.496	2.499
C1-S1	1.713	1.713	1.737	1.737	1.722	1.721	1.712	1.713	1.734	1.734	1.714	1.714	1.717	1.717	1.740	1.740	1.713	1.712
C2-S2	1.741	1.740	1.771	1.771	1.765	1.765	1.741	1.741	1.771	1.771	1.761	1.761	1.739	1.738	1.772	1.772	1.763	1.763
S1-Au-S2	88.86	88.85	88.71	88.74	85.14	85.12	88.79	88.8	88.66	88.66	85.00	85.06	88.94	89.00	88.95	88.97	85.20	85.16
S1-C1-C2	126.21	126.26	126.46	126.53	128.26	128.34	126.25	126.30	126.58	126.70	128.44	128.50	125.98	125.98	126.26	126.38	128.35	128.54
S2-C2-C1	121.95	121.87	121.97	121.92	122.79	122.67	121.85	121.81	121.72	121.59	122.32	122.28	122.50	122.58	122.50	122.36	122.24	121.93
Au-S1-C1	100.95	100.79	100.94	100.94	101.29	101.39	100.99	101.03	100.99	101.01	101.39	101.40	100.81	100.85	100.78	100.75	101.42	101.51
Au-S2-C2	102.02	102.00	101.90	101.86	102.47	102.41	102.08	102.00	102.03	102.02	102.83	102.76	101.74	101.59	101.44	101.47	102.72	102.78
C1-C2-C3-C4	36.64	35.90	30.12	30.18	23.87	23.61	33.86	33.98	25.01	23.42	14.48	16.20	64.63	68.67	56.03	55.54	40.95	39.43

[a] Numbering scheme as in Figure 3.12.

A comparison of optimised parameters (Table 3.13) with the corresponding structural data of the *cis* isomers of **20⁻** and **21⁻**,[18b] discussed above (Table 3.4), shows a very good agreement between the two sets of data, only the Au-S distances being slightly overestimated (by less than 0.08 Å, Table 3.14).

Table 3.14. *Comparison between optimised and experimental bond lengths (Å) and angles (°) for the cis isomers of 20⁻ and 21⁻.*

	Calculated		Experimental[a]	
	20⁻	**21⁻**	**20⁻**[b]	**21⁻**[c]
C1-C2	1.352	1.350	1.336	1.342
S1-Au	2.379	2.379	2.314	2.317
S2-Au	2.375	2.374	2.313	2.309
C1-S1	1.737	1.734	1.737	1.734
C2-S2	1.771	1.771	1.777	1.770
S1-Au-S2	88.71	88.66	89.66	89.96
S1-C1-C2	126.46	126.58	126.2	126.60
S2-C2-C1	121.97	121.72	120.3	120.25
Au-S1-C1	100.94	100.99	101.15	100.75
Au-S2-C2	101.90	102.03	102.32	102.45
C1-C2-C3-C4	30.12	25.01	24.01	26.10

[a] Numbering scheme as in Figure 3.12. [b] Ref.18b. [c] Average values (Table 3.4).

Given this very good agreement between the parameters optimised for the *cis* isomers of **20⁻** and **21⁻** and the corresponding structural data, the optimised data obtained for **22⁻** can be considered good estimates of the structural parameters as well.

Moreover, the average C-C, C-S, and Au-S bond lengths optimised for 22^{x-} are very close to the corresponding mean values found for the *bis*(1,2-dithiolene) gold complexes found on the Cambridge Crystallographic Database (Table 3.15).

Table 3.15. *Selected experimental and optimised structural bond distances (Å) of bis(1,2-dithiolene) gold complexes.*

Complex	C-C	C-S	Au-S
$[Au^{III}(R,R'\text{-edt})_2]$ [a]	1.366(8)	1.736(5)	2.300(4)
$[Au^{III}(R,R'\text{-edt})_2]^-$ [b]	1.361(4)	1.745(2)	2.310(2)
$[Au^{II}(R,R'\text{-edt})_2]^{2-}$ [c]	1.374(4)	1.731(3)	2.425(7)
22 [d]	1.365	1.728	2.362
22$^-$ [d]	1.350	1.756	2.379
22^{2-} [d]	1.377	1.738	2.500

[a] Mean value calculated on 9 crystal structures deposited at CCDC. [b] Mean value calculated on 82 crystal structures deposited at CCDC. [c] Taken from ref. 201 for L = mnt^{2-}. [d] Mean values of the optimised parameters calculated for the *cis* and *trans* isomers (Table 3.13).

It is worth noting that, for each oxidation state, both the isomerism of the complexes and the nature of the substituent at the carbon atom of the ethylene-1,2-dithiolate do not induce significant modifications in the optimised bond lengths and angles.

An examination of the calculated structural parameters for the different oxidation states of **20-22** can give an insight on the electronic structure of these complexes, and in particular on the form assumed by the 1,2-dithiolene ligands (ene-1,2-dithiolate, $^-$S-C=C-S$^-$, or 1,2-dithioketone, S=C-C=S). The C-S and C-C bond lengths calculated for

20⁻-22⁻ (Table 3.14) suggest that monoanionic gold *bis*(1,2-dithiolene) complexes should be formally considered as Au^{III} complexes of ene-1,2-dithiolato ligands, which, as a consequence, would behave as *innocent* ligands, in agreement with structural data. This is further supported by the very close values of the C-C distances found in monoanionic $[Au(R,R'\text{-edt})_2]^-$ complexes and in the corresponding 1,3-dithiol-2-ones, as discussed in Section 3.1.2 for **26** and **21⁻**. On the other hand, as expected, neutral complexes feature C-C and C-S optimised distances that are systematically longer and shorter, respectively, than those of the corresponding monoanions. This testifies that the ligands feature a more pronounced 1,2-dithioketone character in the neutral species than do the monoanions. These data support the hypothesis that oxidation of the monoanions should be ligand centered (Equation 3.1), without affecting the formal oxidation state of the central metal ion.

Concerning the features of the complexes in their oxidation state –2, the trends observed in the calculated C-S and C-C distances for **20²⁻-22²⁻** have been found to be in perfect agreement with the experimental ones determined for the only authentic dianionic *bis*(1,2-dithiolene) gold complex reported to date, $(TBA^+)_2(\mathbf{15}^{2-})$,[201] and suggest that reduction of monoanionic to dianionic forms of gold *bis*(1,2-dithiolenes) should not be considered simply as metal centered (Equation 3.1), but should significantly involve the ligands as well. Indeed, notwithstanding the authors' claims, the reported values calculated for $[Au(Ph_2\text{-edt})_2]^{x-}$ (**33ˣ⁻**, $x = 0$, 1, 2) reflect exactly the same trend (C-C = 1.383, 1.359, and 1.362 Å; C-S = 1.756, 1.788, and 1.780 Å; Au-S = 2.360, 2.362, and 2.410 Å, for $x = 0$, 1, and 2, respectively).[75a] This is in agreement with the conclusions drawn by Schlupp and Maki, who, on the grounds of electron paramagnetic resonance (EPR) measurements, considered $(TBA^+)_2(\mathbf{15}^{2-})$ as better described as a Au^{III} complex featuring a radical anion ligand,[202] and subsequently by Kokatam et al. in the case of **33²⁻**,[75a] which was considered as an intermediate Au^{II}/Au^{III} complex.

It is interesting to note that the torsion angle θ of the aryl substituent (C1-C2-C3-C4 dihedral angle in Figure 3.12) is also affected by the overall charge of the complexes, with the neutral species featuring θ values larger by 6-9° with respect to the corresponding monoanionic ones, which in turn feature torsion values larger by 6-16° with respect to dianionic species (Table 3.13). To further investigate this feature, a scan of the potential-energy surface (PES) was performed on $\mathbf{20}^{x-}$ ($x = 0, 1$) both in its neutral and monoanionic form (Figure 3.13), by calculating the variations ΔE in the total electronic energy of the complex optimised at various frozen θ values (-90 < θ < 90°).
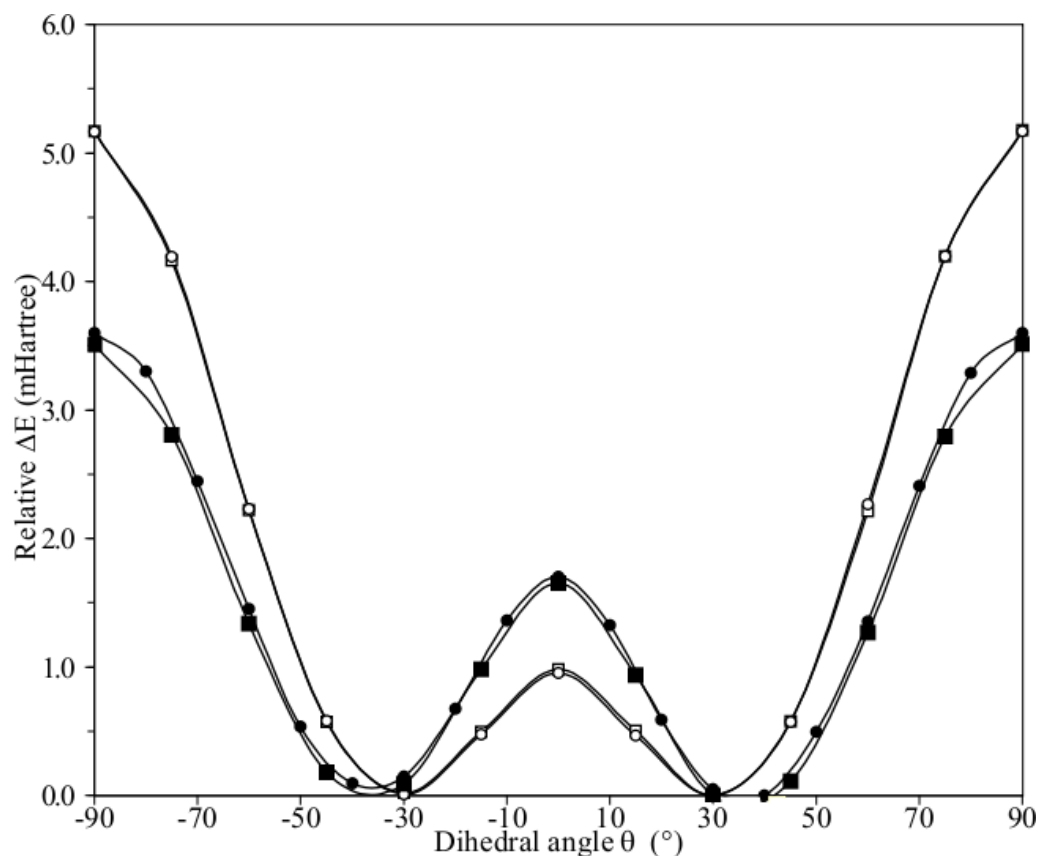
Figure 3.13. *Relative total electronic energy variation (ΔE) calculated as a function of the phenyl rotation (θ) for the cis and trans isomers of $\mathbf{20^-}$ (squares and circles, respectively) and $\mathbf{20}$ (filled squares and circles, respectively).*

This analysis shows that values of about 35 and 30° for neutral and monoanionic species, respectively, represent absolute energy minima, the rotational barrier being in any case small (about 3.5 kcal mol^{-1}).[203]

3.1.6.2. Ground state (GS)

The description of the ground-state (GS) bonding scheme of **20-22** (^2A and ^2B for *cis* and *trans* isomers, respectively) based on DFT calculations is in agreement with the results of previous calculations carried out on **33**.[75a]
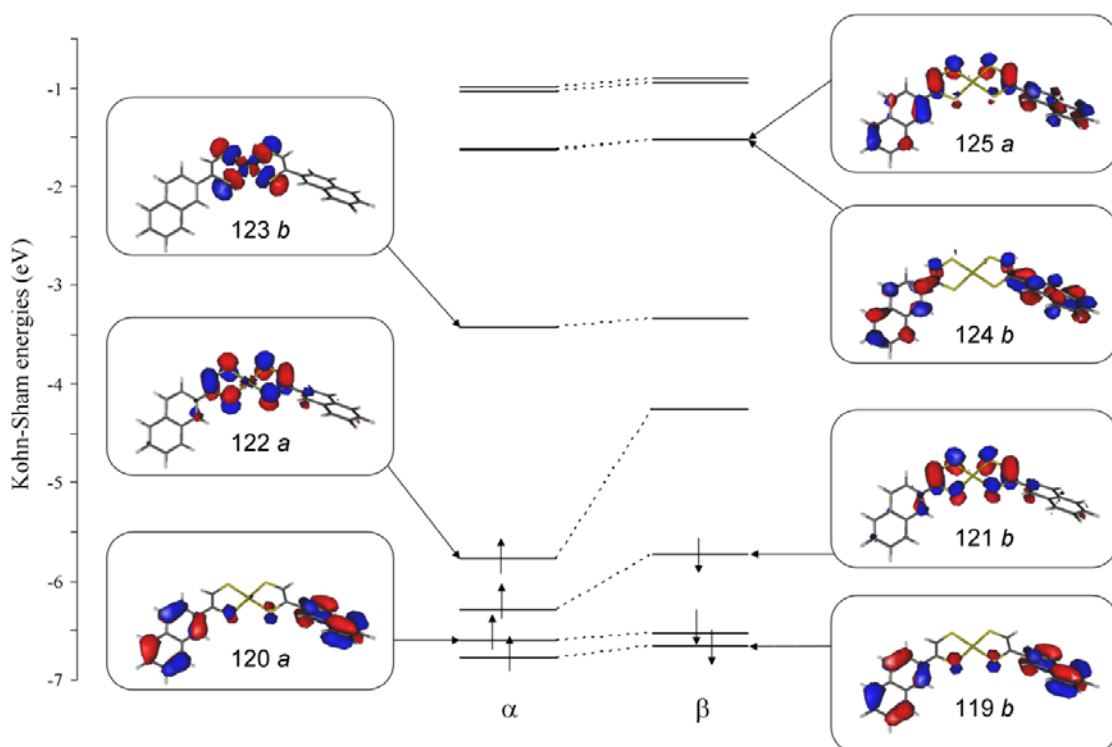
Figure 3.14. *KS-MO scheme and isosurface drawings calculated for **21** (cis isomer) at DFT mPW1PW level (C_2 point group). Contour value = 0.05 e.*

The examined complexes exhibit very similar Kohn–Sham molecular orbital (KS-MO) compositions, and it is remarkable that the order and the composition of KS-MOs does not significantly depend on the nature of the isomers. The frontier KS-MO scheme calculated for **21** in its *cis* form is depicted in Figure 3.14, and a correlation diagram showing the variation of the KS eigenvalues calculated for the frontier orbitals of the *cis* and *trans* isomers of **22**, **22$^-$** and **22^{2-}** is shown in Figure 3.15.
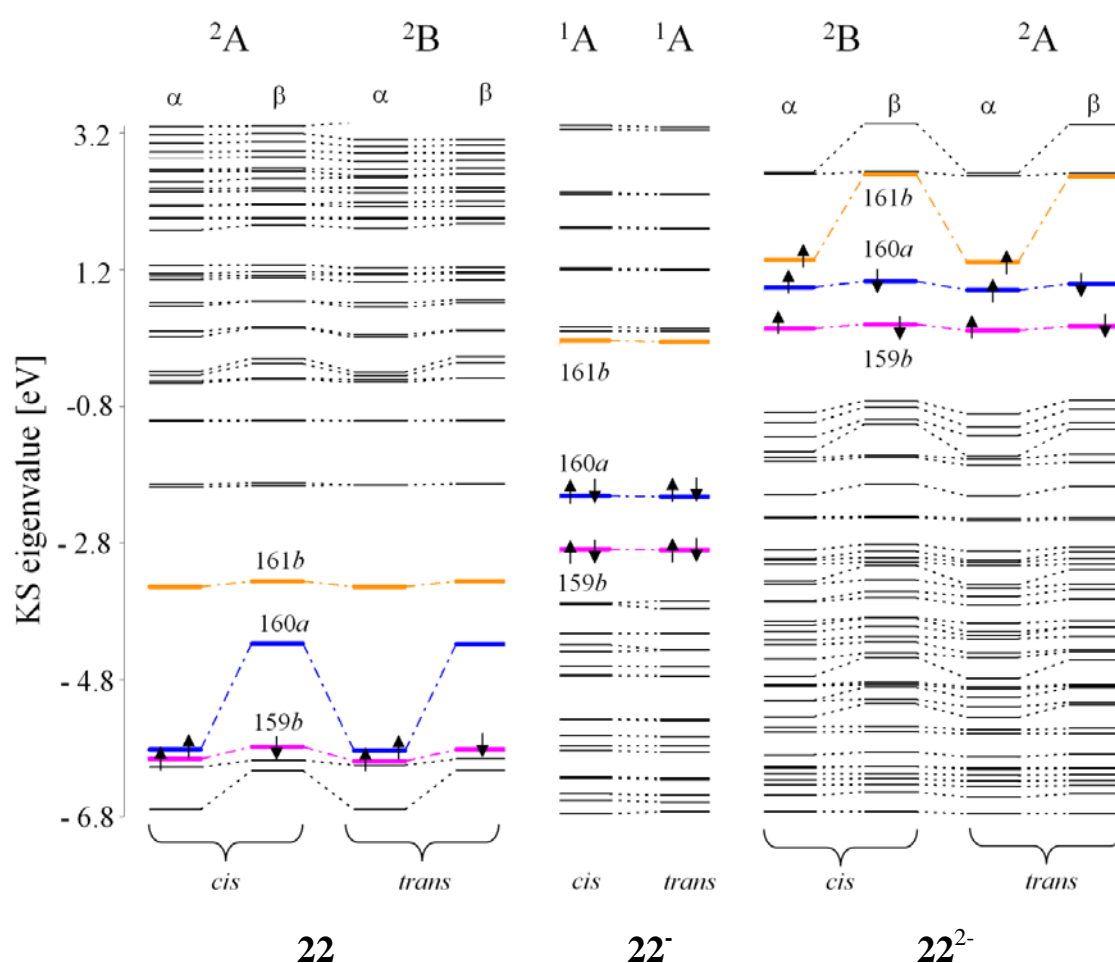
Figure 3.15. *Correlation diagram between the KS eigenvalues of selected MOs calculated for* **22**, **22$^-$**, *and* **22^{2-}** *(cis and trans isomers) in their ground states. Symmetry labels are referred to the C$_2$ point group.*

In addition, for each MO, the contributions from the central gold species, the C_2S_2 moiety, and the H and aryl substituents at the 1,2-dithiolene system have been calculated (Figures 3.16 and 3.17 for the *cis* isomers of **21** and **22,** respectively).

ALPHA

BETA
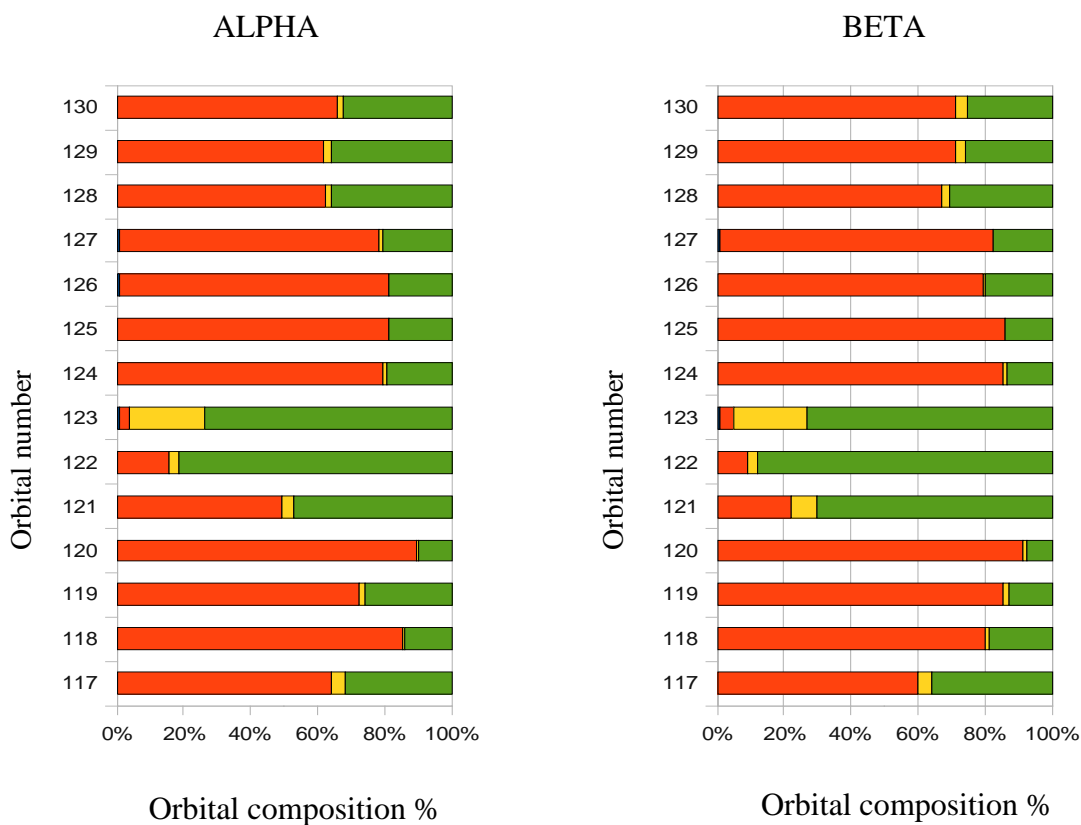
Figure 3.16. *Frontier molecular orbital (KS-MOs 117-130; SOMO = 122, LUMO = 123) composition calculated for 21 [cis isomer; fragments: gold atom (yellow), 2-naphthyl (red) and hydrogen (blue) substituents, ethylene-1,2-dithiolato (green)].*

ALPHA   BETA
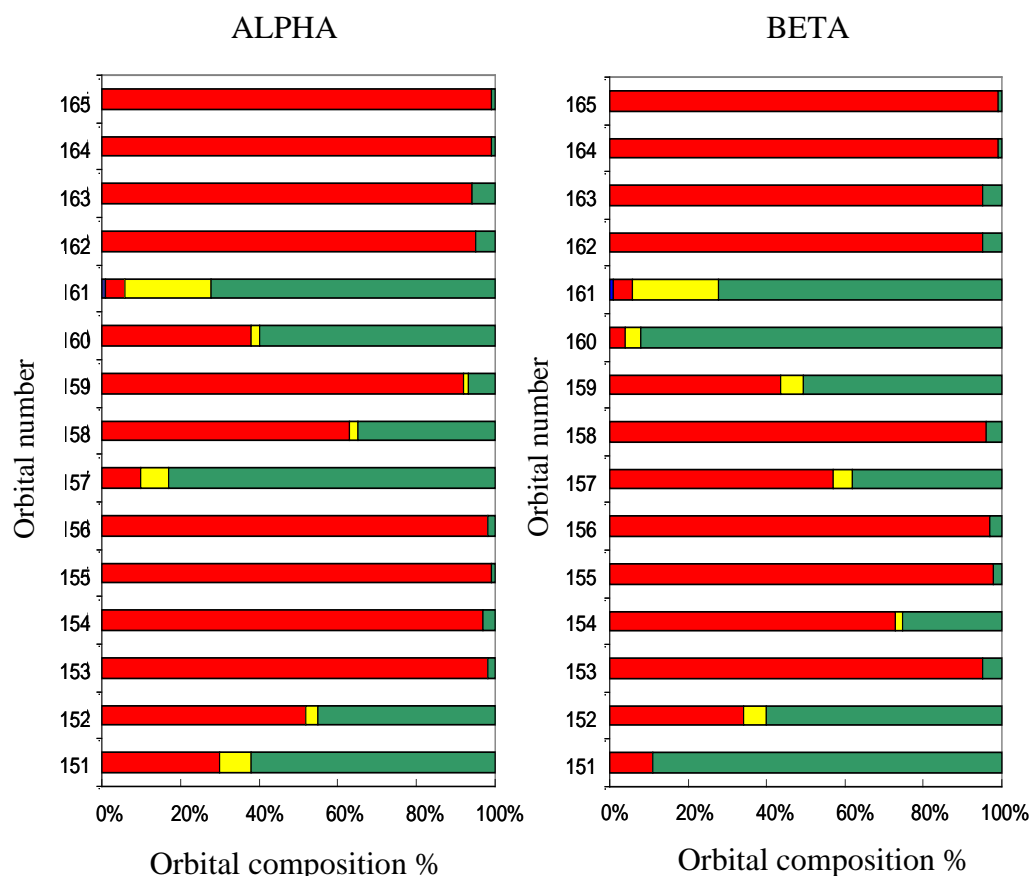
Figure 3.17. *Frontier molecular orbital (KS-MOs 151-165; SOMO = 159, LUMO = 160) composition calculated for* **22** *[cis isomer; fragments: gold atom (yellow), 1-pyrenyl (red) and hydrogen (blue) substituents, ethylene-1,2-dithiolato (green)].*

The energy separation between gold $5d$ orbitals and the π system of the ligands prevents the superexchange interaction reported for analogous *bis*(1,2-dithiolene) complexes of group 10 metals.[190b] As a consequence, in **20-22** the singly occupied molecular orbital (SOMO; orbitals 122 and 159 for **20** and **22**, respectively) is a π MO predominantly localised on the ethylene-1,2-dithiolato moiety (57-82%) with only minor participation of Au d character (2-3%; Figures 3.16 and 3.17). The LUMO (orbital 123 in Figure 3.14 for **21**) is an antibonding MO built up by the combination of the in-plane sulphur $2p$ atomic orbitals (74%) with the $5d$ atomic orbital (22%) of the metal species. The one-electron reduction, which leads to the corresponding monoanions (GS ^1A in the C_2 point group), corresponds to the introduction of a β electron in the SOMO. Notably, the small

94

contribution of gold atomic orbitals to this MO is responsible for the very moderate change in the Au-S distances observed on passing from **20-22** to **20⁻-22⁻**. This further confirms that the gold electron population is not remarkably altered with respect to the corresponding neutral species. On the contrary, since this MO is bonding with respect to the C-C bond and antibonding with respect to the C-S ones, the corresponding bond lengths undergo the remarkable structural variations discussed above.

Figure 3.15 shows that, on passing from monoanionic to dianionic species, the eigenvalues of the frontier MOs are progressively raised, and the mixing between the gold AOs and the ligand orbitals is increased in the dianion. This can be rationalised by considering that the progressively added charges stabilise the combinations of molecular orbitals on the ligands that are symmetry-allowed to interact with the gold $5d$ AOs, which results in a progressive lowering of the energy gap between the two groups of interacting orbitals. This gives rise to an increased overlap, which is reflected in the destabilisation of their antibonding combinations, represented by the frontier KS-MOs discussed above, and an increased participation of the gold AOs. Considering for example the case of **22**, on passing from the neutral species to the dianion, the contribution of the metal species to the singly occupied KS-MO 161 (α-SOMO for **22**$^{2-}$) is remarkably increased (22%), which leads to a lengthening of the Au-S bonds calculated for this species. This is in agreement with the structural data for dianionic *bis*(1,2-dithiolene) gold complexes (Table 3.14). The mixing of the gold $5d$ AOs with the MOs mostly localised on the dithiolene ligand justifies the uncertainty, discussed above, about the oxidation state of gold in dianionic complexes, and this suggests that the *innocent/noninnocent* behavior of 1,2-dithiolene ligands depends not only on the nature of the central metal ion, but also on the charge of the resulting complexes.

3.1.6.3. Mulliken charges

In Table 3.16, the results from a Mulliken population analysis are summarised for 20^{x-}-22^{x-} ($x = 0$-2) in their *cis* and *trans* conformations.

Table 3.16. *Mulliken charges Q (e) calculated on Au, C1, S1, the hydrogen atom H bonded to C1, the substituents Ar, and each ligand L for the cis and trans isomers of complexes 20^{x-}, 21^{x-} and 22^{x-} [L = Ar,H-edt^{2-}; Ar = phenyl (20), 2-naphthyl (21), 1-pyrenyl (22); x = 0, 1, 2].^{a}*

	Isomer	Q(Au)	Q(S1)	Q(S2)	Q(C1)	Q(C2)	Q(H)	Q(Ar)	Q(L)	ΔQ(L)^b	ΔQ(Au)^b
20	*cis*	-0.163	0.008	0.007	-0.052	-0.029	0.080	0.068	0.082	-	-
	trans	-0.162	0.008	0.005	-0.051	-0.029	0.080	0.068	0.081	-	-
20⁻	*cis*	-0.222	-0.109	-0.110	-0.089	-0.016	0.035	-0.100	-0.389	-0.471	-0.059
	trans	-0.221	-0.107	-0.113	-0.088	-0.017	0.035	-0.100	-0.390	-0.471	-0.059
20²⁻	*cis*	-0.304	-0.210	-0.220	-0.116	-0.021	-0.001	-0.280	-0.848	-0.459	-0.082
	trans	-0.304	-0.204	-0.225	-0.115	-0.022	0.000	-0.282	-0.848	-0.458	-0.083
21	*cis*	-0.161	0.007	0.002	-0.056	-0.023	0.080	0.071	0.081	-	-
	trans	-0.161	0.007	0.002	-0.055	-0.025	0.080	0.072	0.081	-	-
21⁻	*cis*	-0.210	-0.102	-0.109	-0.094	-0.006	0.039	-0.123	-0.395	-0.476	-0.049
	trans	-0.207	-0.113	-0.098	-0.094	-0.005	0.039	-0.126	-0.397	-0.477	-0.046
21²⁻	*cis*	-0.286	-0.190	-0.205	-0.117	-0.010	0.008	-0.327	-0.857	-0.462	-0.076
	trans	-0.286	-0.182	-0.212	-0.116	-0.012	0.009	-0.326	-0.857	-0.460	-0.079
22	*cis*	-0.197	0.008	0.035	-0.012	-0.128	0.079	0.116	0.098	-	-
	trans	-0.199	0.011	0.036	-0.007	-0.135	-0.027	0.116	0.099	-	-
22⁻	*cis*	-0.244	-1.104	-0.087	-0.0503	-0.106	0.037	-0.065	-0.378	-0.476	0.047
	trans	-0.243	-0.100	-0.090	-0.054	-0.103	0.038	-0.069	-0.378	-0.476	0.046
22²⁻	*cis*	-0.289	-0.176	-0.180	-0.086	-0.083	0.016	-0.345	-0.855	-0.477	0.045
	trans	-0.286	-0.166	-0.188	-0.087	-0.080	0.018	-0.354	-0.857	-0.479	0.043

^{a} Numbering scheme as in Figure 3.12. ^{b} Charge variation calculated on passing from the neutral species to the corresponding monoanions, and from the monoanions to the dianionic forms.

The charge on the central gold atom is scarcely affected by the nature of the substituents and by the conformation of the complex. As expected on the basis of the KS-MO analysis, the charge on the central Au ion does not undergo a large variation on passing from the neutral to the monoanionic species (about 0.05 e); the charge variation is instead assumed by the ligands (about 0.47 e for each ligand), thereby further confirming that the electron-transfer processes are largely ligand-based for this class of compounds.

Notably, calculated Mulliken charges indicate that the increased charges on passing from neutral to dianionic species are progressively distributed over the ligands.

3.1.6.4. Time dependent DFT (TD-DFT) calculations

With the aim of better understanding the spectroscopic absorption and emission properties of the title compounds, time-dependent DFT (TD-DFT) calculations were carried out on the *cis* and *trans* isomers of 21^{x-} and 22^{x-} ($x = 0$, 1)[204] at the optimised geometries (C_2 point group) in their GSs [singlet ^1A (S0) and doublet ^2A (D0) for $x = 1$ and 0, respectively]. TD-DFT calculations were carried out at the same theoretical level discussed previously.

Table 3.17. *Principal computed electronic transitions (f > 0.05) calculated for the cis and trans isomers of* **21**. *For each transition, the excitation energy E (eV), the oscillator strength f and molecular orbital composition of the excited-state functions, along with with the fragments where the involved KS-MO are mainly localised, are reported.*

		Exc. State	E	f	Spin	Composition[a]	%	Molecular Fragments[b]
21	*cis*	D1	0.792	0.135	β	121 → 122	88	edt (70%) → edt (87%)
		D14	2.587	0.110	α	120 → 123	56	naph (89%) → edt (74%)
		D31	3.610	0.169	α	122 → 124	36	edt (82%) → naph (80%)
					β	121 → 125	54	edt (70%) → naph (86%)
		D44	4.107	0.253	α	121 → 125	23	naph (49%) +edt (47%) → naph (81%)
					β	121 → l27	27	edt (70%) → naph (81%)
		D51	4.312	0.164	α	120 → 125	11	naph (89%) → naph (81%)
					β	119 → 124	17	naph (86%) → naph (86%)
					β	120 → 125	16	naph (91%) → naph (86%)
		D52	4.331	0.616	α	116 → 123	22	edt (87%) → edt (74%)
					β	114 → 123	22	edt (79%) → edt (74%)
					β	108 → 122	15	naph (76%) → edt (87%)
21	*trans*	D1	0.794	0.145	β	121 → 122	88	edt (71%) → edt (87%)
		D13	2.539	0.084	α	120 → 123	58	naph (88%) → edt (74%)
					β	120 → 123	22	naph (90%) → edt (74%)
		D18	2.739	0.110	α	116 → 123	12	edt (89%) → edt (74%)
					β	117 → 122	45	naph (71%) → edt (87%)
		D30	3.571	0.278	α	122 → 125	32	edt (81%) → naph (81%)
					β	121 → 125	48	edt (71%) → naph (85%)
		D48	4.218	0.170	α	118 → 125	8	naph (81%) → naph (81%)
					β	118 → 124	9	naph (73%) → naph (87%)
		D50	4.244	0.805	β	114 → 123	16	edt (81%) → edt (74%)

[a] The molecular orbitals are labelled according to Figure 3.16. [b] edt = ethylene-1,2-dithiolato; naph = 2-naphthyl substituent at the edt core.

Table 3.18. *Principal computed singlet-singlet electronic transitions (f > 0.05) calculated for the cis and trans isomers of **21⁻**. For each transition, the excitation energy E (eV), the oscillator strength f and composition of the excited-state functions, along with the fragments where the involved KS-MO are mainly localised, are reported.*

		Exc. State	E	f	Composition[a]	%	Molecular Fragments[b]
21⁻	*cis*	S3	2.487	0.154	122 → 124	93	edt (87%) → naph (93%)
		S4	2.525	0.057	122 → 125	92	edt (87%) → naph (93%)
		S7	3.053	0.090	122 → 127	87	edt (87%) → naph (84%)
		S9	3.264	0.067	121 → 124	87	edt (77%) → naph (93%)
		S10	3.272	0.153	121 → 125	88	edt (77%) → naph (93%)
		S12	3.812	0.371	118 → 123	13	edt (89%) → edt (73%)
					121 → 126	66	edt (77%) → naph (86%)
		S15	4.082	0.069	120 → 125	49	edt (64%) → naph (93%)
					119 → 124	33	naph (57%) → naph (93%)
		S17	4.125	0.143	115 → 123	36	edt (80%) → edt (73%)
		S18	4.200	0.409	116 → 123	32	naph (52%) + edt (47%) → edt (73%)
					118 → 123	28	edt (89%) → edt (73%)
					122 → 134	10	edt (87%) → Au (84%)
21⁻	*trans*	S3	2.491	0.249	122 → 124	93	edt (87%) → naph (93%)
		S6	3.042	0.121	122 → 127	88	edt (87%) → naph (85%)
		S9	3.267	0.204	121 → 124	89	edt (77%) → naph (93%)
		S12	3.789	0.399	118 → 123	24	edt (71%) → edt (74%)
					121 → 126	50	edt (77%) → naph (85%)
		S15	4.052	0.095	120 → 124	69	naph (40%) + edt (54%) → naph (93%)
		S16	4.073	0.382	115 → 123	31	edt (83%) → edt (74%)
					117 → 123	22	naph (44%)+edt (52%) → edt (74%)
					118 → 123	11	edt (71%) → edt (74%)
		S18	4.246	0.335	115 → 123	31	edt (83%) → edt (74%)
					117 → 123	22	naph (44%) + edt (52%) → edt (74%)
					118 → 123	11	edt (71%) → edt (74%)
					122 → 129	15	edt (87%) → naph (93%)

[a] The molecular orbitals are labelled according to Figure 3.16. [b] edt = ethylene-1,2-dithiolato; naph = 2-naphthyl substituent at the edt core.

In Tables 3.17 and 3.18, the main vertical electronic transitions calculated for the neutral and monoanionic forms, respectively, of **20** are summarised along with the most relevant MO contributions to each one-electron excitation. The same data are listed in Tables 3.19 and 3.20 for **22** and **22⁻**.

Table 3.19. *Principal computed electronic transitions (f > 0.05) calculated for the cis and trans isomers of **22**. The vertical excitation energies E (eV), the oscillator strengths f and molecular orbital compositions of the excited-state functions, along with the description of the fragments where the involved KS-MO are mainly localised, are reported.*

		Excited State	E	f	Spin	Composition[a]	%	Molecular fragments[b]
22	*cis*	D1	0.826	0.121	β	159 → 160	85	Pyr (44%) + edt (51%) → edt (92%)
		D12	2.072	0.058	β	158 → 161	76	Pyr (96%) → edt (73%)
		D33	3.284	0.051	β	147 → 160	45	Pyr (36%) + edt (55%) → edt (92%)
					β	149 → 160	46	Pyr (67%) → edt (92%)
		D34	3.310	0.118	β	159 → 162	50	Pyr (44%) + edt (51%) → Pyr (95%)
					α	160 → 163	29	Pyr (38%) +edt (60%) → Pyr (94%)
		D42	3.617	0.978	α	159 → 162	44	Pyr (93%) → Pyr (94%)
		D48	3.684	0.189	β	158 → 162	42	Pyr (96%) → Pyr (95%)
		D49	3.693	0.122	β	153 → 161	42	Pyr (95%) → edt (73%)
		D50	3.708	0.082	β	153 → 161	32	Pyr (95%) → edt (73%)
					β	158 → 163	14	Pyr (96%) → Pyr (95%)
		D66	4.097	0.231	α	152 → 161	36	Pyr (52%) + edt (45%) → edt (73%)
					β	150 → 161	21	Pyr (41%) + edt (55%) → edt (73%)
		D76	4.331	0.148	α	158 → 165	10	Pyr (63%) + edt (35%) → Pyr (99%)
					α	160 → 165	30	Pyr (38%) +edt (60%) → Pyr (99%)
					β	159 → 164	32	Pyr (44%) + edt (51%) → Pyr (99%)
		D78	4.400	0.516	α	149 → 161	10	Pyr (30%) + edt (68%) → edt (73%)
					β	135 → 160	12	Pyr (34%) + edt (63%) → edt (92%)
					β	148 → 161	20	Pyr (59%) + edt (39%) → edt (73%)
					α	147 → 161	9	Pyr (33%) + edt (67%) → edt (73%)
22	*trans*	D1	0.845	0.119	β	159 → 160	83	Pyr (40%) + edt (54%) → edt (93%)
		D9	2.015	0.084	α	158 → 161	40	Pyr (60%) + edt (38%) → edt (73%)
					α	160 → 161	17	Pyr (41%) + edt (57%) → edt (73%)

Excited State	E	f	Spin	Compositionᵃ	%	Molecular fragmentsᵇ
			β	155 → 160	13	Pyr (98%) → edt (93%)
D11	2.064	0.063	β	158 → 161	67	Pyr (96%) → edt (73%)
D34	3.347	0.089	α	160 → 162	24	Pyr (41%) + edt (57%) → Pyr (94%)
			β	159 → 162	58	Pyr (40%) + edt (54%) → Pyr (96%)
D41	3.614	0.156	α	154 → 161	54	Pyr (96%) → edt (73%)
D43	3.634	0.317	α	155 → 163	9	Pyr (99%) → Pyr (95%)
			α	156 → 162	9	Pyr (99%) → Pyr (96%)
			α	158 → 162	9	Pyr (60%) + edt (38%) → Pyr (96%)
			β	155 → 162	8	Pyr (98%) → Pyr (96%)
			β	156 → 163	8	Pyr (97%) → Pyr (94%)
			β	158 → 163	8	Pyr (96%) → Pyr (94%)
D49	3.705	0.057	α	160 → 163	11	Pyr (41%) + edt (57%)→ Pyr (95%)
			β	153 → 161	22	Pyr (94%) → edt (73%)
			β	158 → 162	16	Pyr (96%) → Pyr (92%)
D51	3.714	0.123	β	153 → 161	40	Pyr (94%) → edt (73%)
			β	158 → 162	20	Pyr (96%) → Pyr (92%)
D64	4.032	0.172	α	152 → 161	35	Pyr (57%) + edt (40%) → edt (73%)
			β	150 → 161	23	edt (91%) → edt (73%)
D69	4.180	0.083	β	138 → 160	20	Pyr (35%) + edt (59%) → edt (97%)
			β	142 → 160	22	Pyr (50%) + edt (31%) → edt (97%)
			β	144 → 160	17	Pyr (50%) + edt (31%) → edt (97%)
D76	4.326	0.139	β	157 → 161	17	Pyr (60%) + edt (35%) → edt (73%)
			β	159 → 164	59	Pyr (40%) + edt (54%) → Pyr (99%)
D78	4.399	0.467	α	149 → 161	11	edt (75%) → edt (73%)
			β	135 → 160	15	Pyr (30%) + edt (67%) → edt (93%)
			β	140 → 160	11	Pyr (84%) → edt (93%)
			β	148 → 161	11	edt (74%) → edt (73%)

ᵃ The molecular orbitals are labeled according to Figure 3.17. ᵇ edt = ethylene-1,2-dithiolato; Pyr = pyrenyl substituent at the edt core.

Table 3.20. *Principal computed electronic transitions (f > 0.05) calculated for the cis and trans isomers of 22⁻. The vertical excitation energies E (eV), the oscillator strengths f and molecular orbital compositions of the excited-state functions, along with the description of the fragments where the involved KS-MO are mainly localised, are reported.*

		Excited State	E	f	Composition[a]	%	Molecular Fragments[b]
22⁻	*cis*	S3	1.868	0.052	160 → 163	80	edt (91%) → Pyr (75%)
		S5	2.6703	0.059	159 → 162	94	edt (81%) → Pyr (96%)
		S10	3.127	0.064	158 → 161	62	Pyr (87%) → Pyr (27%) + edt (56%)
		S12	3.310	0.065	160 → 167	95	edt (91%) → Pyr (97%)
		S14	3.480	0.444	155 → 161	23	edt (88%)→ Pyr (27%) + edt (56%)
					157 → 162	14	Pyr (72%) → Pyr (96%)
					158 → 161	24	Pyr (87%)→ Pyr (27%) + edt (56%)
		S15	3.510	0.171	154 → 161	13	Pyr (84%)→ Pyr (27%) + edt (56%)
					157 → 162	36	Pyr (72%)→ Pyr (96%)
					158 → 163	15	Pyr (87%)→ Pyr (75%)
		S16	3.553	0.134	157 → 163	21	Pyr (72%)→ Pyr (75%)
					158 → 162	15	Pyr (87%)→ Pyr (96%)
					159 → 165	33	edt (81%) → Pyr (97%)
		S18	3.594	0.129	159 → 165	54	edt (81%)→ Pyr (97%)
		S28	4.041	0.097	154 → 161	23	Pyr (84%)→ Pyr (27%) + edt (56%)
					155 → 161	33	edt (88%)→ Pyr (27%) + edt (56%)
					155 → 163	22	edt (88%)→ Pyr (75%)
		S30	4.136	0.257	155 → 163	32	edt (88%)→ Pyr (75%)
					159 → 166	34	edt (81%) → Pyr (99%)
		S32	4.166	0.133	159 → 166	49	edt (81%)→ Pyr (97%)
		S34	4.354	0.053	151 → 161	39	Pyr (91%)→ Pyr (27%) + edt (56%)
					153 → 162	23	edt (78%)→ Pyr (96%)
22⁻	*trans*	S2	1.855	0.082	160 → 163	78	edt (90%) → Pyr (72%)
		S5	2.681	0.083	159 → 162	94	edt (80%) → Pyr (96%)
		S11	3.363	0.064	160 → 167	95	edt (90%) → Pyr (98%)
		S13	3.383	0.382	156 → 161	34	edt (74%) → Pyr (29%) + edt (54%)
					158 → 161	49	Pyr (79%) → Pyr (29%) + edt (54%)
		S14	3.502	0.427	158 → 163	53	Pyr (79%)→ Pyr (72%)
		S16	3.556	0.125	155 → 161	14	edt (81%) → Pyr (29%) + edt (54%)
					157 → 161	18	Pyr (82%) → Pyr (29%) + edt (54%)
					158 → 162	36	Pyr (79%) → Pyr (96%)

Excited State	E	f	Composition[a]	%	Molecular Fragments[b]
S17	3.557	0.074	$159 \rightarrow 164$	85	edt (80%) $\rightarrow$ Pyr (99%)
S19	3.718	0.060	$157 \rightarrow 162$	71	Pyr (82%) $\rightarrow$ Pyr (96%)
S27	4.025	0.089	$153 \rightarrow 161$	37	edt (77%) $\rightarrow$ Pyr (29%) + edt (54%)
			$160 \rightarrow 168$	25	edt (90%) $\rightarrow$ Pyr (89%)
S28	4.049	0.228	$154 \rightarrow 161$	57	edt (87%) $\rightarrow$ Pyr (29%) + edt (54%)
S30	4.139	0.101	$159 \rightarrow 166$	60	edt (80%) $\rightarrow$ Pyr (99%)
S32	4.194	0.239	$154 \rightarrow 163$	45	edt (87%) $\rightarrow$ Pyr (72%)
S37	4.363	0.058	$153 \rightarrow 163$	72	edt (77%) $\rightarrow$ Pyr (72%)

[a] The molecular orbitals are labeled according to Figure 3.17. [b] edt = ethylene-1,2-dithiolato; Pyr = pyrenyl substituent at the edt core.

These contributions allow to classify each excitation depending on the nature of the involved KS-MOs, as mainly localised on the aromatic substituents, on the C_2S_2 core (edt), or as consisting of an interligand charge-transfer (ILCT) process between the two moieties of the ligand. In the case of the closed-shell species **20** and **22**, in addition to singlet–singlet one-electron excitations, triplet–triplet excitations have been calculated.

TD-DFT calculations have been exploited to simulate the UV-Vis-NIR absorption spectra for the eight model complexes (Figure 3.18 for **21** and **21⁻**). An inspection of the absorption spectra (250–2000 nm) simulated for the *cis* and *trans* isomers of both complexes clearly shows that the spectroscopic features depend on the global charge of the complex, as shown by experimental UV-Vis-NIR spectroscopy, but are only very marginally affected by *cis*/*trans* isomerism.
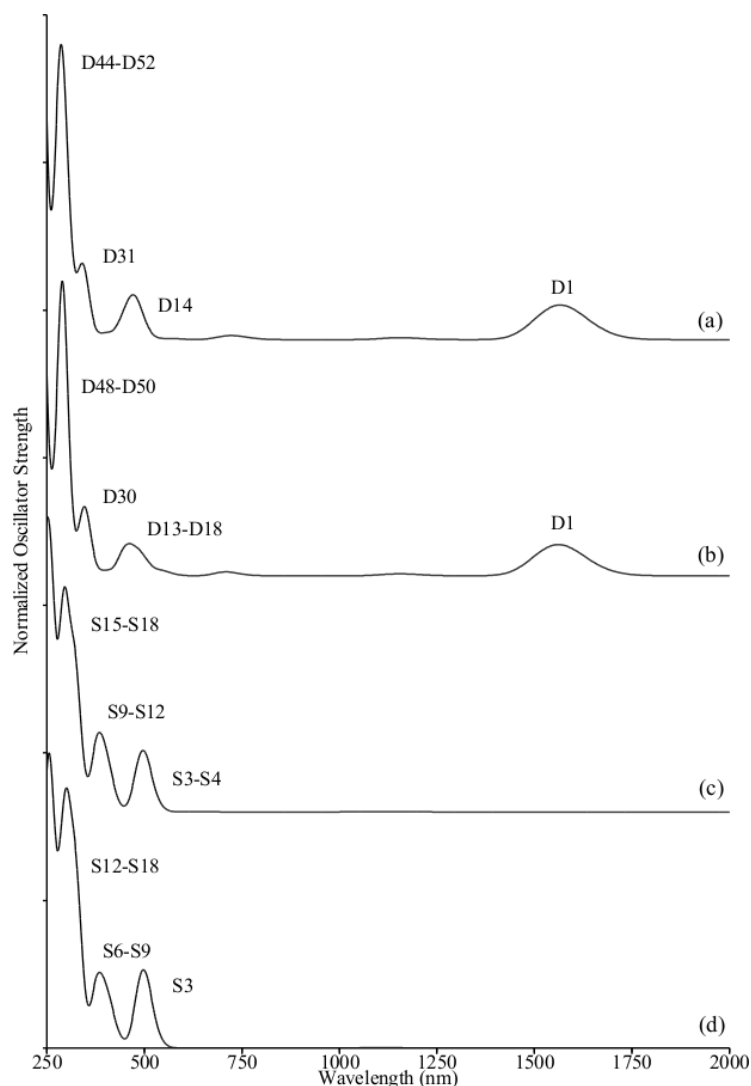
Figure 3.18. *Simulated UV-Vis-NIR spectra (250-2000 nm) based on TD-DFT calculations (Tables 3.17 and 3.18) calculated for the cis and trans isomers of 21 [(a) and (b), respectively] and 21⁻ [(c) and (d), respectively].*

A comparison of the simulated spectra with those recorded during the diiodine titration of (TBA⁺)(**21⁻-22⁻**) (Figure 3.8 for **21⁻**) evidences that, although transition energies are slightly underestimated, a very good agreement between experimental and simulated spectra holds. In particular, the D0→D1 vertical transition, responsible for the intense (f = 0.135 and 0.121 for **21** and **22**, respectively) NIR absorption in neutral species, should be attributed to an almost pure (85-88%) one-β-electron excitation involving the frontier molecular orbitals. In particular, KS-MOs 121 and 122, mainly localised on the

ethylene-1,2-dithiolato moiety, are involved in the case of **21** (Figure 3.16), while for **22** the transition occurs from KS-MO 159, which is mainly localised on the pyrenyl substituents, to 160 (Figure 3.17), which is mainly localised on the ethylene-1,2-dithiolato moiety.

For both monoanionic and neutral species of **21**, the electron absorptions in the visible region (bands in the range 350–440 nm) can be assigned to the intense transitions S0→S3 and D0→D13/D14 (*cis/trans* isomers, respectively) respectively, thereby resulting in a π-electron transfer process from the ethylene-1,2-dithiolate to the naphthyl substituents for the neutral species (corresponding to the 122→124 one-electron excitation) and *vice versa* for the monoanionic form (120→123, corresponding to a α-electron SOMO-2→LUMO excitation), falling at very similar energies. A second group of bands (S0→S9–S12/S6–S9 for the *cis/trans* isomers of **21⁻**; transitions D0→D31/D30 for the *cis/trans* isomers of **21**) are calculated at higher energies (in the range 3.0–3.3 eV for **21** and 3.5–4.3 eV for **21⁻**). These absorptions also involve electron excitations from filled KS–MOs localised on the ethylene-1,2-dithiolate and empty KS-MOs localised on the naphthyl substituents. Therefore, excitation at 360 nm, which results in the emission processes described above for both **21** and **21⁻**, should mainly involve transitions that have the same character of photoinduced electron-transfer processes edt→naphthyl. Only at higher energies can π–π* electron transitions involving KS-MOs exclusively localised on the edt moiety or the aryl substituents be found [**21⁻**: S0→S18 (4.200 eV, *f* = 0.409), S0→S30, not included in Table 3.18 (4.758 eV, *f* = 0.435); **21**, *cis* isomer: D0→D51 (4.312 eV, *f* = 0.164), D0→D52 (4.331 eV, *f* = 0.616); **21**, *trans* isomer: D0→D48 (4.218 eV, *f* = 0.170), D0→D50 (4.244 eV, *f* = 0.805)].

Concerning **22**, the series of relatively minor absorptions calculated in the visible region (2.1–3.3 eV) for both **22** and **22⁻** feature in the majority of cases a significant charge-

transfer character from the pyrenyl substituents to the edt core or *vice versa* (Tables 3.19 and 3.20), as observed for **21**. On the other hand, the very intense absorptions calculated at about 3.5 eV for both neutral and monoanionic species involve exclusively the π system of the pyrenyl pendant (S0→S14 and D0→D42/43–44 for **22⁻** and **22**, respectively), which corresponds to monoelectronic excitations from KS-MOs 155–158 and 156–159 to 161–163 and 162–163, respectively. Therefore, excitation at 343 nm, which results in the emission processes described above, in the case of **22** and **22⁻** should mainly involve transitions localised on the pyrenyl fragment.
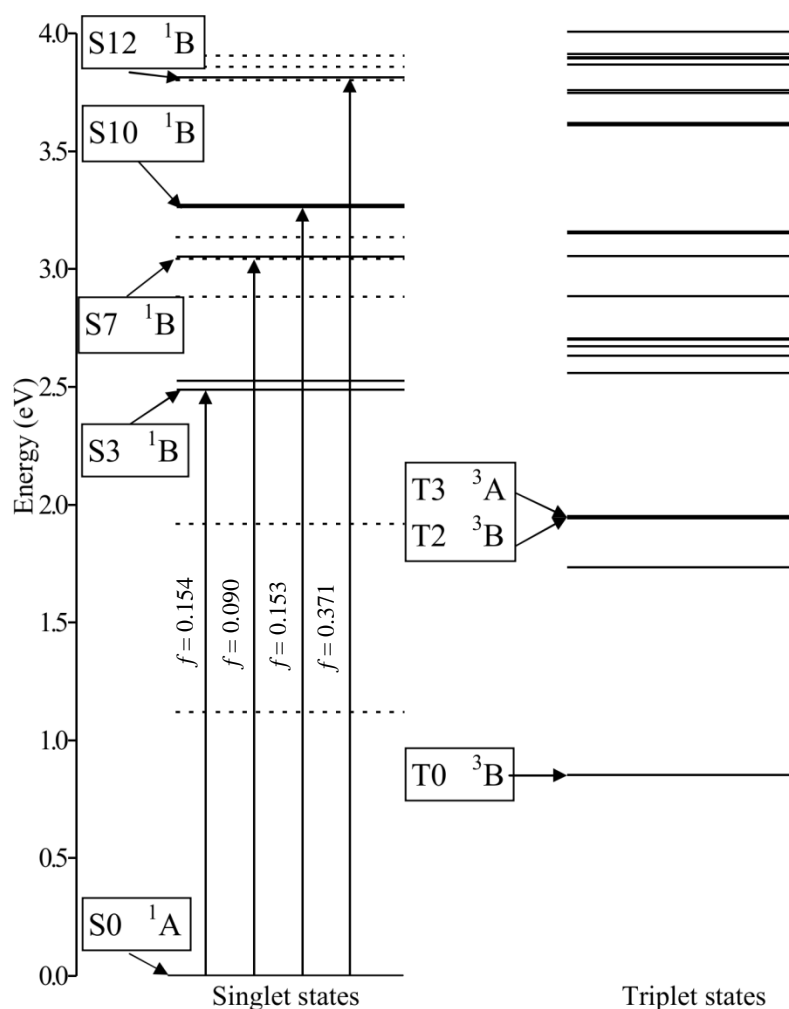
Figure 3.19. *Jablonsky diagram (0.0-4.0 eV) calculated for the cis isomer of **21⁻** at TD-DFT level (Table 3.18). The singlet transitions having oscillator strength values f < 0.05 are represented as dotted lines.*
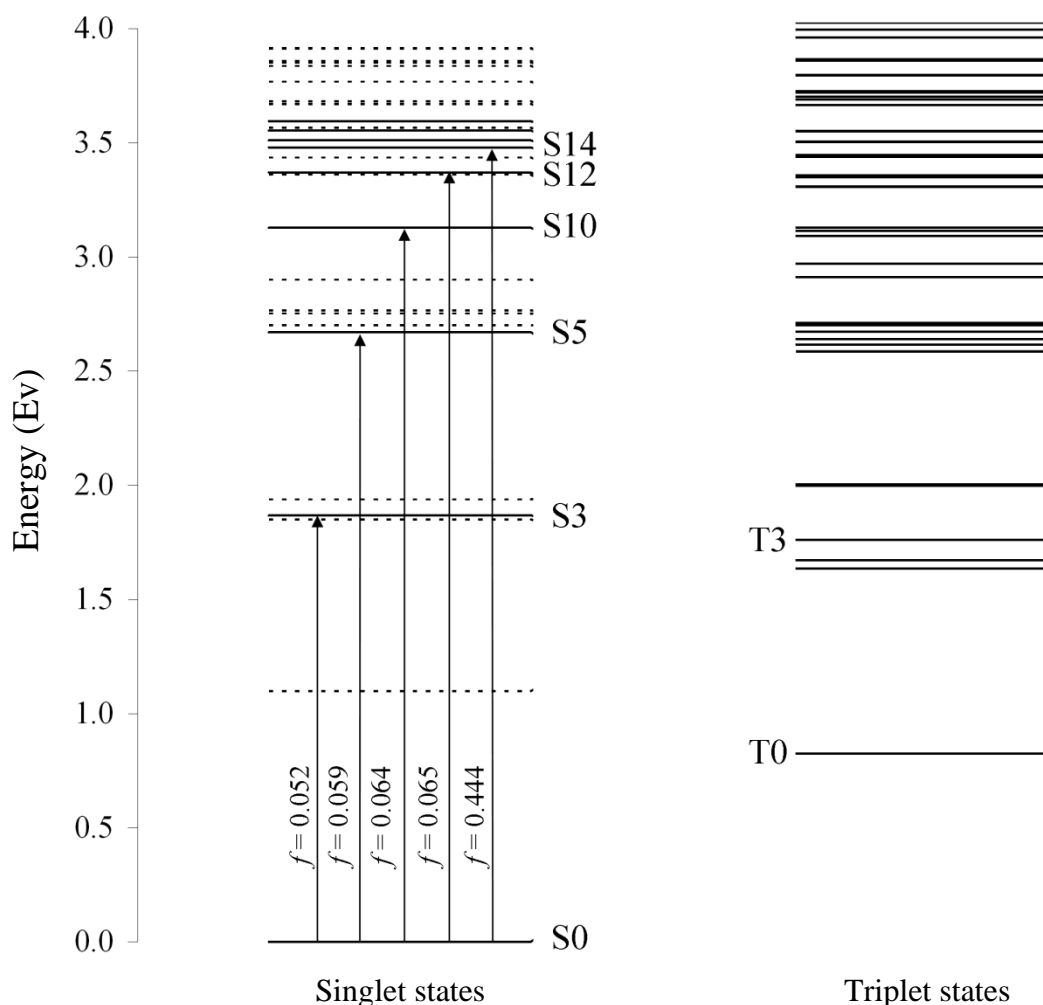
Figure 3.20. *Jablonsky diagram (0.0-4.0 eV) calculated for the cis isomer of 22⁻ at TD-DFT level (Table 3.20). The singlet excited states with oscillator strength values f < 0.05 are represented as dotted lines.*

As mentioned above, in the case of **21⁻** and **22⁻**, the pattern of triplet–triplet excitations have been calculated as well for both *cis* and *trans* isomers (Figures 3.19 and 3.20, for the *cis* isomers of **21⁻** and **22⁻**, respectively). A comparison of the energies of singlet and triplet excited states (ESs), shows that the singlet ESs accessible from the GS with the largest values of oscillator strengths (**21⁻**, *cis* isomer: S3, S7, S10, and S12; **21⁻**, *trans* isomer: S3, S6, S9, and S12; **22⁻**, *cis* isomer: S3, S5, S10, S12, and S14; **22⁻** *trans* isomer: S2, S5, S11, and S13, Tables 3.18 and 3.20) feature triplet ESs very close in energy, directly accessible through intersystem crossing (ISC) processes mediated by

spin–orbit coupling. Therefore, although monoanionic and neutral species feature very similar excitation energies, only the ESs of the former species can feature ISC relaxation paths, in agreement with the higher fluorescence quantum yields of the latter species evidenced experimentally and discussed above. In particular, the lowest singlet ES accessible from the GS S0 with a large oscillator strength (S3 for **20⁻**, and S3 and S2 for *cis* and *trans* isomers of **22⁻**, respectively) is close in energy to the triplet ESs T2 and T3 ($\Delta E_{S3\text{-}T3}$ = 0.536 and 0.548 eV for the *cis* and *trans* isomers of **20⁻**, respectively; $\Delta E_{S3\text{-}T3}$ = 0.108 eV and $\Delta E_{S2\text{-}T3}$ = 0.093 eV for *cis* and *trans* isomers of **22⁻**, respectively), which could therefore play a role in the ISC processes of both the isomers of both complexes **21⁻** and **22⁻**. As far as radiative paths are instead involved, after an internal conversion (IC) from the ESs accessible though UV excitation (**21⁻**, *cis* isomer: S10–S12; **21**, *cis* isomer: D31; **21⁻**, *trans* isomer: S9–S12; **21**, *trans* isomer: D30; **22⁻**, *cis* isomer: S14; **22**, *cis* isomer: D42; **22⁻**, *trans* isomer: S13–S14; **22**, *trans* isomer: D43–D44), relaxation processes responsible for fluorescence should occur from S3 and D14/D13 (*cis*/*trans* isomers) for **21⁻** and **21,** and from S2/S3 (*cis*/*trans* isomers) and D6 for **22⁻** and **22**, respectively. With regard to **22**, the vertical transition D0→D6 is calculated to occur with an almost negligible oscillator strength (f = 0.003). It could be tentatively hypotesised that both the geometry relaxation that occurred during IC processes and the libration of the pyrenyl substituents in solution, which lowers the symmetry of **22**, might increase the probability of the transition D6→D0.

In the case of **21**, the IC processes from D14 and D13 for the *cis* and *trans* isomers, respectively, could be prevented by the large energy difference between the two adjacent states D13 and D12, respectively (0.104 and 0.076 eV, respectively), thus justifying the apparent violation of Kasha's rule.[205] The same conclusions can be made for **22**, where the IC processes from D6 (0.980 and 0.988 eV, for the *cis* and *trans* isomers, respectively) could be prevented by the large energy difference between D6

and the doublet state D5 lying immediately below in energy ($\Delta E_{\text{D6-D5}}$ = 0.595 and 0.599 eV for the *cis* and *trans* isomers, respectively).

The very similar energies of the ESs S3 and D14/D13 for **20**, and S3/S2 and D6 for **22** with respect to the GSs S0 and D0 could account for the very close emission energies for both neutral and monoanionic species evidenced experimentally.

3.1.6.5. Calculation of static first hyperpolarisability (β)

As previously pointed out, the lack of an inversion center in the *cis* isomers of the title complexes suggests a possible application as second-order nonlinear optical (SONLO) materials. In this context, prompted by the results obtained by TD-DFT calculations, we calculated static dipole moments (μ) and static first (quadratic) hyperpolarisabilities (β) at the same level of theory described above.

In fact, as already mentioned, SONLO properties appear when the polarisability of a chemical species exposed to an intense electromagnetic field, is not simply proportional to the intensity of this field, so that it shows an additional second order polarisability proportional to the square of the field intensity (Equation 3.2), commonly called first or quadratic hyperpolarisability and indicated as β,[206] which is nonzero just in noncentrosymmetric systems.

$$\mu = \mu_0 + \sum_{ij} \alpha_{ij} E_j + \sum_{i \le j} \beta_{ijk} E_j E_k + ...$$

(3.2)

From a mathematical point of view, β is a third order tensor, summarisable as in Figure 3.21.

$$\beta = \begin{pmatrix} \beta_{xxx} & \beta_{xxy} & \beta_{xxz} & 0 & 0 & 0 & 0 & 0 & 0 \\ \beta_{xyx} & \beta_{xyy} & \beta_{xyz} & 0 & 0 & 0 & 0 & 0 & 0 \\ \beta_{xzx} & \beta_{xzy} & \beta_{xzz} & 0 & 0 & 0 & 0 & 0 & 0 \\ 0 & 0 & 0 & \beta_{yxx} & \beta_{yxy} & \beta_{yxz} & 0 & 0 & 0 \\ 0 & 0 & 0 & \beta_{yyx} & \beta_{yyy} & \beta_{yyz} & 0 & 0 & 0 \\ 0 & 0 & 0 & \beta_{yzx} & \beta_{yzy} & \beta_{yzz} & 0 & 0 & 0 \\ 0 & 0 & 0 & 0 & 0 & 0 & \beta_{zxx} & \beta_{zxy} & \beta_{zxz} \\ 0 & 0 & 0 & 0 & 0 & 0 & \beta_{zyx} & \beta_{zyy} & \beta_{zyz} \\ 0 & 0 & 0 & 0 & 0 & 0 & \beta_{zzx} & \beta_{zzy} & \beta_{zzz} \end{pmatrix}$$

Figure 3.21. *Matrix representation of the β_{ijk} components of the β tensor.*

According to Kleinman's symmetry rules[207] ($\beta_{xyy} = \beta_{yxy} = \beta_{yyx}$, $\beta_{yyz} = \beta_{yzy} = \beta_{zyy}$, …), some of the terms of the tensor are equivalent, so that the matrix is reduced to just 10 terms. The total value of β (β_{tot}) can be calculated from the 10 remaining terms according to equation 3.3:[208]

$$\beta_{tot} = \sqrt{\beta_x^2 + \beta_y^2 + \beta_z^2} \tag{3.3}$$

where $\beta_i = \beta_{iii} + \beta_{ijj} + \beta_{ikk}$.

The static dipole moments (μ) and static first hyperpolarisabilities (β_{tot}) were calculated in the gas phase at the optimised geometries for the *cis* and *trans* isomers of **20^{x-}-22^{x-}** (Table 3.21) in their neutral and monoanionic forms ($x = 0$ and 1 , respectively), easily obtained in CH_2Cl_2 (Sections 3.1.3 and 3.1.4).

Table 3.21. *Static dipole moment μ (D) and first hyperpolarisabilities β_{tot} (a.u. and esu) calculated for the cis and trans isomers of 20^{x-}-22^{x-} (x = 0, 1).*

		$\lvert \mu \rvert$ (D)	$\beta_{tot} \cdot 10^3$ (a.u.)	$\beta_{tot} \cdot 10^{-30}$ (esu)
20	*cis*	1.68	24.45	212
	trans	0.85	9.07	78
20⁻	*cis*	4.37	9.68	84
	trans	1.78	3.54	31
21	*cis*	0.61	13.19	114
	trans	0.21	3.74	32
21⁻	*cis*	0.94	9.66	83
	trans	0.15	1.40	12
22	*cis*	0.94	3.21	28
	trans	0.15	0.09	1
22⁻	*cis*	1.16	2.94	25
	trans	0.20	0.22	2

As expected, the *trans* isomers feature small β_{tot} values, although they are not zero because of the rotation of the aromatic substituents, which lower the molecular symmetry form D_{2h} to C_2. The *cis* isomers feature significantly larger β_{tot} values, in the range 25–210·10^{-30} esu, which are comparable to those of various NLO-active gold complexes.[209] On passing from **20** to **22**, the decrease in the extension of the aryl substituents is computed to be reflected in a remarkable decrease in both μ and β_{tot} values. An examination of the static hyperpolarisability components β_x, β_y, and β_z shows that, for both the monoanionic and neutral species, β_{tot} is determined by a single individual static component, the direction of which is aligned with that of the dipole

moment μ and is coincident with the C_2 symmetry axis (which lies on or perpendicular to the plane of the 1,2-dithiolene for *cis* and *trans* isomers, respectively). Note that, on passing from the neutral species to the corresponding monoanions, the increased charge is reflected in an increase in the $|\mu|$ values, whereas the first hyperpolarisabilities β_{tot} are decreased.

3.2. Synthesis and characterisation of heteroleptic 1,2-dichalcogenolene-complexes

As already pointed out, two different kinds of mixed-ligand 1,2-dichalcogenolene complexes have been obtained and fully characterised during the present research project: [Pt(N^N)(E^E)] complexes (E = S, Se) and a [Au(C^N)(S^S)] complex. The two kinds of systems will be treated separately in the two following sections.

3.2.1. Synthesis and characterisation of [Pt(N^N)(E^E)] complexes (53-73)

The 1,2-dithiolene ligands belonging to the classes Ar,H-edt^{2-} and R-dmet^{2-}/R-dset^{2-} were exploited for the synthesis of new diimine-dithiolate mixed-ligand complexes. Platinum(II) diimine-dichalcogenolate complexes were obtained from the combination of seven 1,2-dichalcogenolene ligands and eight aromatic diimine donors, listed in Tables 3.22 and 3.23, respectively.

Table 3.22. *1,2-dichalcogenolene ligands exploited in the present study for the synthesis of new [Pt(N^N)(E^E)] complexes.*
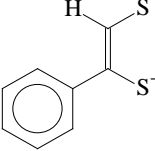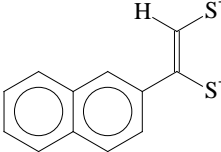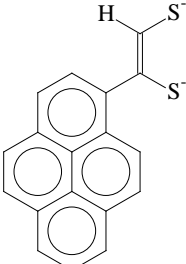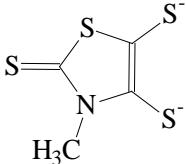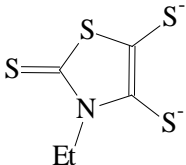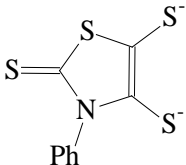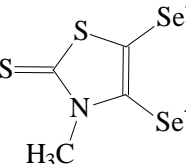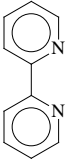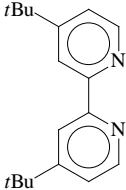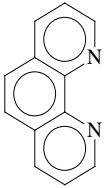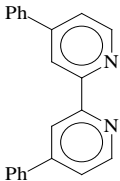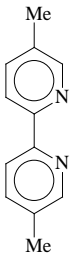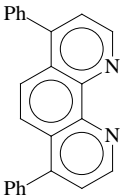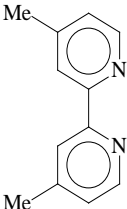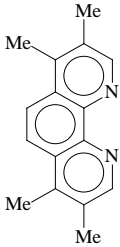
Ph,H-edt^{2-}

Naph,H-edt^{2-}

Pyr,H-edt^{2-}

Me-dmet^{2-}

Et-dmet^{2-}

Ph-dmet^{2-}

Me-dset^{2-}

Table 3.23. *Aromatic diimine ligands exploited in the present study for the synthesis of new [Pt(N^N)(E^E)] complexes.*

3.2.1.1. Synthesis

As already mentioned (Section 1.1.4), the ligands belonging to the classes R-dmet^{2-} and R-dset^{2-} (also known as R-thiazdt^{2-} and R-thiazds^{2-}, respectively)[28] were already exploited in the past for the synthesis of corresponding homoleptic *bis*(1,2-dithiolene) complexes [M(R-dmet)$_2$]$^{x-}$ and [M(R-dset)$_2$]$^{x-}$. In particular, the first complexes of this class were reported by our group in 2005 [R = Et, M = Ni (**9**), Pd (**10**), Pt (**11**), x = 0, 1, 2].[27] In that work, the complexes were synthesised by sulphuration of ethyl-2-thioxothiazolidine-4,5-dione with Lawesson's reagent in the presence of the metal as a

powder (M = Ni) or as chloride (M = Pd, Pt). By means of this synthetic pathway, the complexes were obtained in their neutral form (Scheme 1.6).

Recently, an alternative route was reported by Prof. Dominique Lorcy from Rennes 1 University, involving the direct sulphuration/selenation of a 1,3-thiazoline-2-thione, through a lithiating agent, followed by the addition of the metal as halide, and leading to the monoanionic form of the corresponding [M(R-dmet)$_2$] [R = Me, M = Zn (**35**), Ni (**36**), Pd (**37**)], and [M(R-dset)$_2$] [R = Me, M = Zn (**38**), Ni (**39**), Pd (**40**)] complexes (Scheme 3.2).[28]
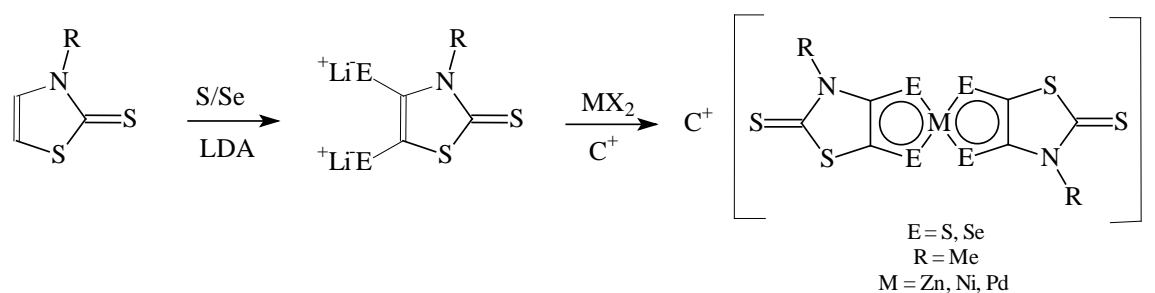
Scheme 3.2. *Synthetic route for the synthesis of [M(R-dmet)$_2$]⁻ (E = S) and [M(R-dset)$_2$]⁻ (E = Se) complexes (Ref. 28).*

From the zinc complexes **35** and **38**, the same authors obtained a stable form of the Me-dmet^{2-} and Me-dset^{2-} ligands, bearing cyanoethyl groups to protect the dichalcogenolate functions, by refluxing the complexes with 3-bromopropionitrile, and the method was recently extended to differently substituted R-dmet^{2-} ligands (R = Et, Ph). This stable form of the dithiolate ligand can be deprotected in basic medium and used to synthesise homoleptic or mixed-ligand complexes (Scheme 3.3).[28,79]
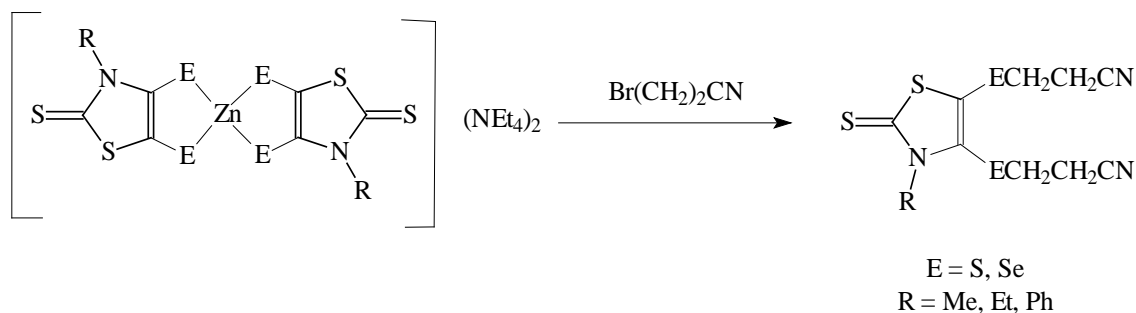
Scheme 3.3. *Synthesis of stable R-dmet^{2-} and R-dset^{2-} ligands from corresponding homoleptic zinc complexes (Refs. 28 and 79).*

This synthetic strategy was adopted to synthesise four R-dmet^{2-}/ R-dset^{2-} ligands (Table 3.22), obtained thanks to a collaboration from Prof. Lorcy.

Twenty new [Pt(N^N)(E^E)] complexes were obtained, synthesised according to the following steps:

1) Diimine donors (Table 3.23) were refluxed with K_2PtCl_4 to give the corresponding (N^N)PtCl$_2$ complexes[210] [N^N = 2,2′-bipyridine (**41**), 1,10-phenatroline (**42**), 5,5′-Me$_2$-bipyridine (**43**), 4,4′-Me$_2$-bipyridine (**44**), 4,4′-*t*Bu$_2$-bipyridine (**45**), 4,4′-Ph$_2$-bipyridine (**46**), 3,7-Ph$_2$-phenanthroline (**47**), 3,4,7,8-Me$_4$-phenanthroline (**48**)], with yields ranging from 39 to 88% (Scheme 3.4 and Table 3.24).
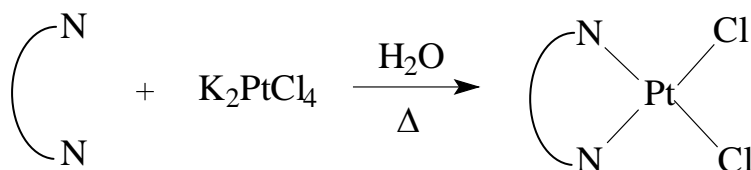
Scheme 3.4. *Synthesis of [Pt(N^N)Cl$_2$] complexes **41-48**.*

Table 3.24. *Yields (%) of [Pt(N^N)Cl₂] complexes **41-48**, synthesised according to Scheme 3.4.*

	N^N	Yield
41	2,2′-bipy	75%
42	1,10-phen	88%
44	4,4′-Me₂-bipy	88%
43	5,5′-Me₂-bipy	52%
45	4,4′,-*t*Bu₂-bipy	78%
46	4,4′-Ph₂-bipy	39%
47	4,7- Ph₂-phen	63%
48	3,4,7,8-Me₄-phen	53%

2) After the deprotection of the desired 1,2-dichalcogenolene precursor [arene-1,3-dithiol-2-one, Ar = Ph (**26**), Naph (**27**), Pyr (**28**); *N*-substituted-4,5-*bis*(2′-cyanoethylthio)-1,3-thiazol-2-thione, R = Me (**49**), Et (**50**), Ph (**51**); or *N*-substituted-4,5-*bis*(2′-cyanoethylseleno)-1,3-thiazol-2-thione, R = Me (**52**)] in basic medium, the obtained 1,2-dithiolato ligands were reacted with the platinum(II) dichloro diimine complexes. The corresponding [Pt(diimine)(dichalcogenolate)] complexes are formed by displacement of the two chlorides of the Pt^{II} precursor with the dichalcogenolate chelating ligand.
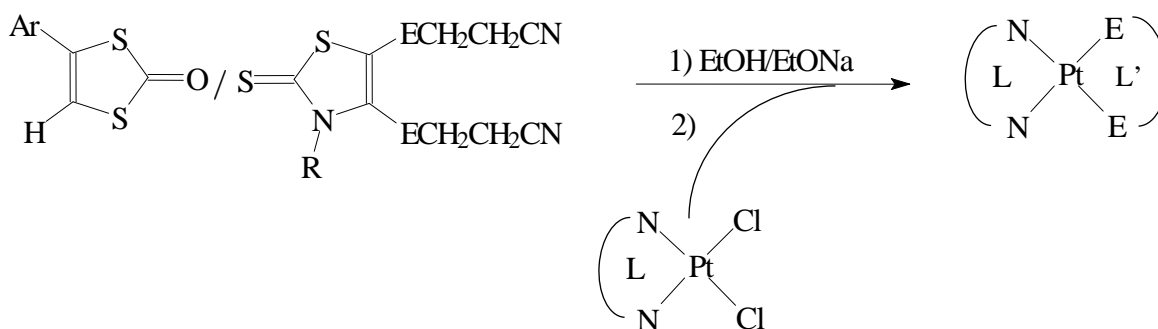
Scheme 3.5. *General procedure for the synthesis of [Pt(N^N)(E^E)] complexes.*

These complexes can be grouped into three different series. A first series of complexes was obtained by combining the seven different 1,2-dichalcogenolene ligands included in this study with 2,2′-bipyridine (Scheme 3.6). Therefore, in this series the complexes **53-59** differ only for the nature of the E^E ligand and all show N^N = 2,2′-bipyridine.
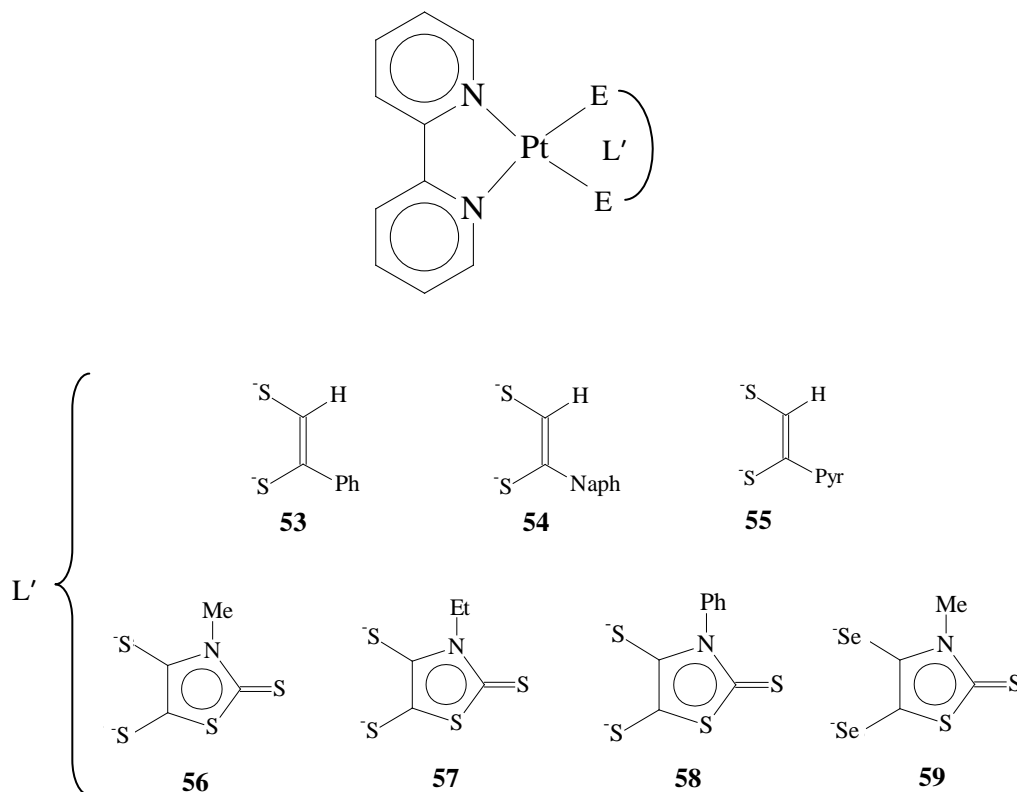
Scheme 3.6. *Complexes 53-59 belonging to Series 1 of neutral [Pt(2,2'-bipy)(E^E)] complexes.*

In a second series of complexes (**60-66**), the seven 1,2-dichalcogenolene ligands were combined with 1,10-phenanthroline (Scheme 3.7).
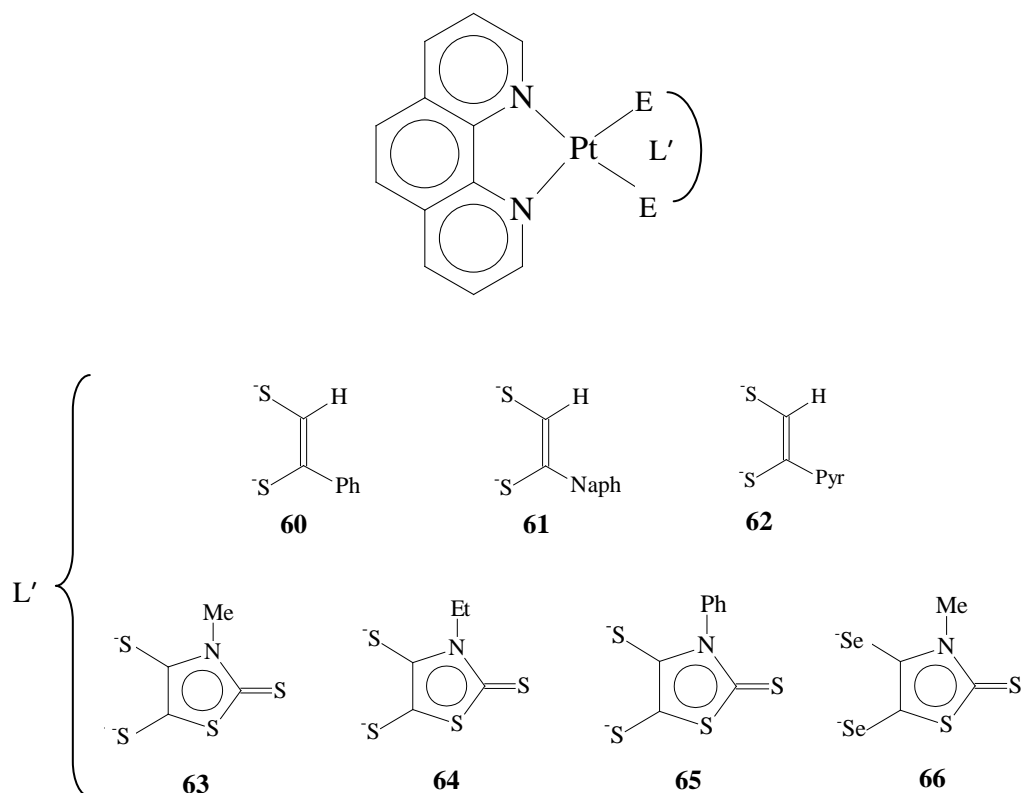
Scheme 3.7. *Complexes 60-66, belonging to Series 2 of neutral [Pt(1,10-phen)(E^E)] complexes.*

Finally, a third series of complexes was obtained by exploiting a single 1,2-dithiolate, namely Me-dmet^{2-}, and by systematically varying the diimine, in order to analyse the effect of differently substituted nitrogen ligands on the features of the corresponding complexes (Scheme 3.8; this series also comprises complexes **56** and **63**, included in the previous series).
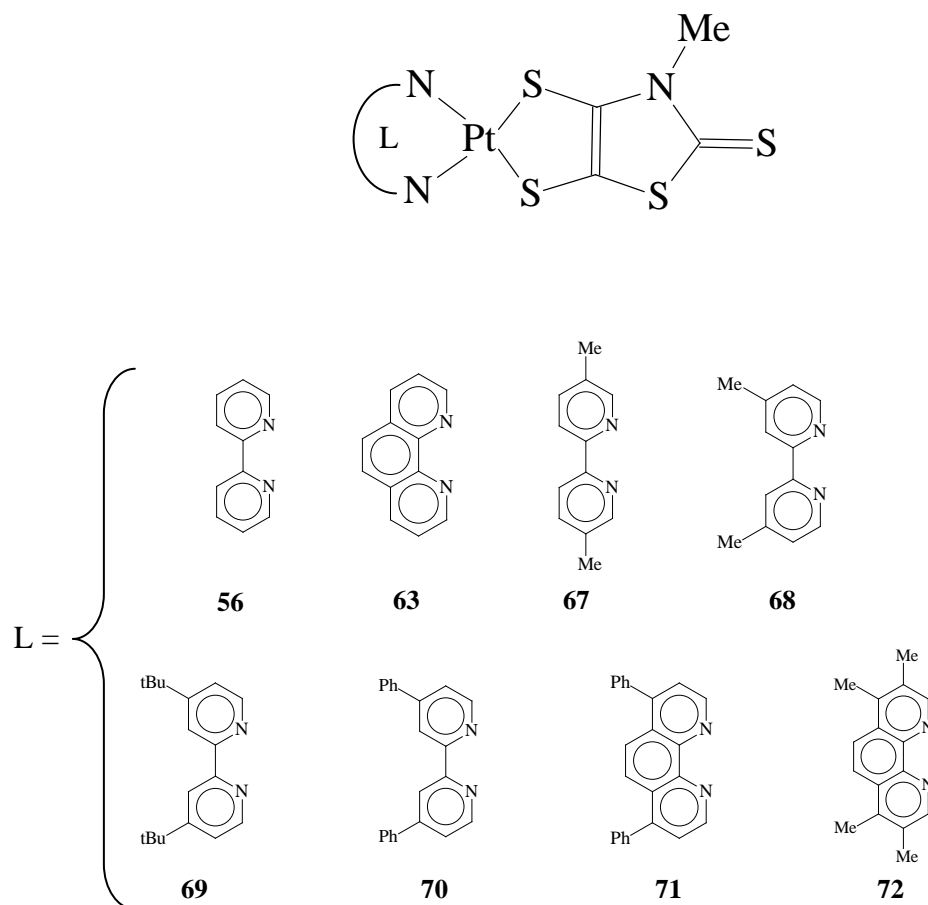
Scheme 3.8. *Complexes **56**, **63**, and **67-72**, belonging to Series 3 of neutral [Pt(N^N)(Me-dmet)] complexes.*

In addition, as already mentioned, to further investigate the effect of varying the 1,2-dichalcogenolene ligand on the properties of [Pt(N^N)(E^E)] complexes, an additional compound (**73**) was synthesised during a research visit at the University of Sheffield within the groups of Prof. M. Ward and Dr. M. Morris, by employing the Fc,H-edt^{2-} ligand (Fc = ferrocenyl).

This ligand was first reported by Underhill for the synthesis of the corresponding Ni^{II} complex (see above).[71] In the work reported by this author, the precursor of Fc,H-edt^{2-} ligand (ferrocenyl-1,3-dithiol-2-one, **74**) was synthesised through the classical synthetic route adopted for 1,3-dithiol-2-ones,[18] by reacting a α-bromoketone of ferrocene with

potassium ethylxanthate to give the corresponding α-ketoxanthate ester, which undergo

cyclisation in strongly acid mediums to give the desired heterocyclic precursor (Scheme

3.9).
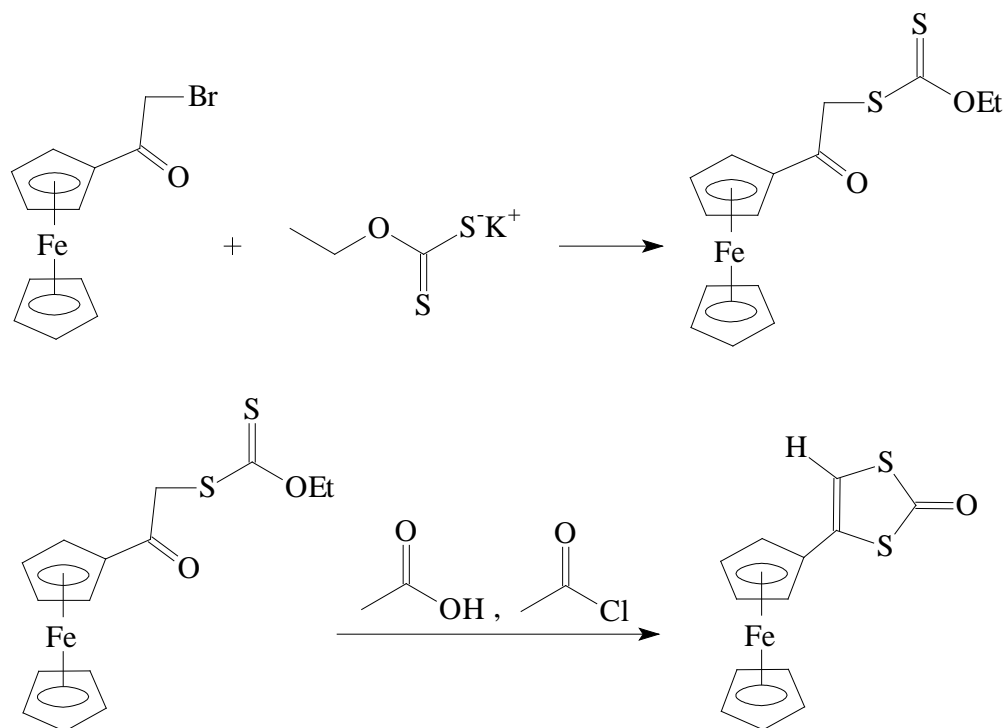
Scheme 3.9. *Synthetic route for the preparation of ferrocenyl-1,3-dithiol-2-one (**74**) according to the method reported by Underhill and co-workers (Ref. 71).*

For the present research project, an alternative synthetic method was employed, starting

from ethynylferrocene, prepared according to the route by Wang (Scheme 3.10):[211]

triphenylphosphine and iodoform were reacted in the presence of potassium *tert-*

butoxide to give the corresponding diiodomethyltriphenylphosphine ylide;

formylferrocene [obtained according to Tang et al.[212] by reacting ferrocene with

triethylorthoformate in the presence of AlCl$_3$, (i) in Scheme 3.10] was then added, and a

Wittig-type condensation occurred, to give 1,1′-diiodoferrocenylene; the addition of an

excess of *n*-BuLi at -15° C eventually leads to the formation of ethynylferrocene [(ii) in

Scheme 3.10].
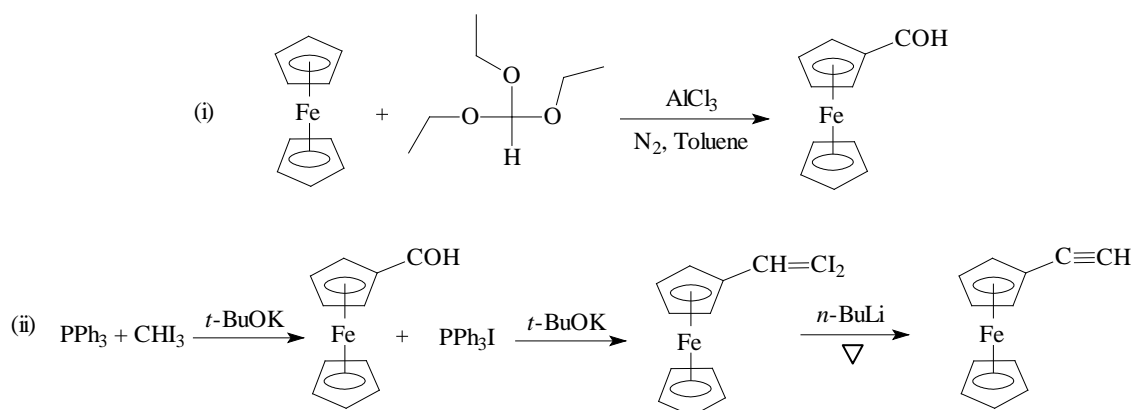
Scheme 3.10. *Synthesis of ethynylferrocene according to Wang (Ref. 211).*

Ethynylferrocene was then employed for the synthesis of the corresponding 1,3-dithiol-2-one **74**, following the general procedure reported by Gareau[19] (Section 1.1.2. and Scheme 3.11).
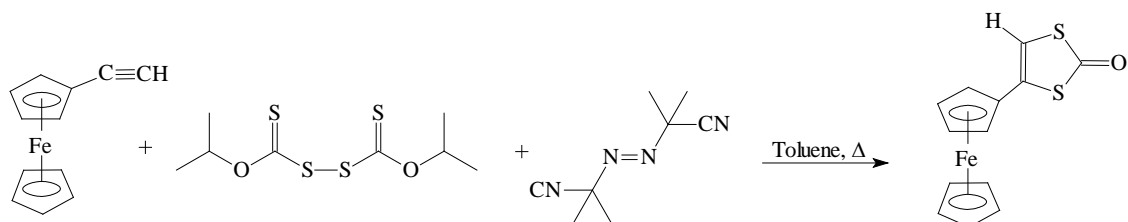
Scheme 3.11. *Synthesis of ferrocenyl-1,3-dithiol-2-one (**74**).*

According to this method, ethynylferrocene is reacted with diisopropyl xanthogen disulfide in the presence of AIBN (Scheme 3.11), which acts as a radical initiator, following the mechanism depicted in Scheme 3.12.[19,213]
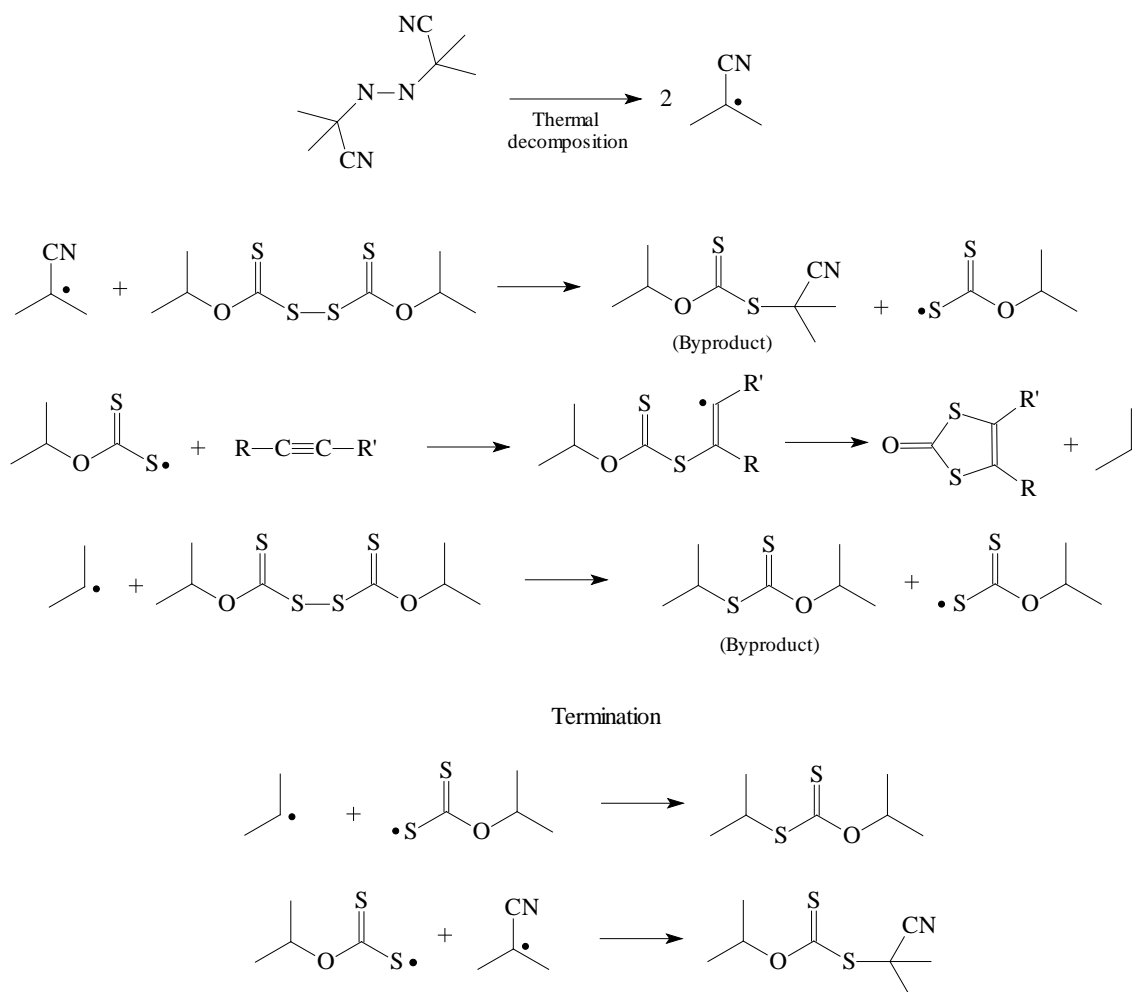
Scheme 3.12. *Radical reactions initiated by AIBN during the synthesis of ferrocenyl-1,3-dithiol-2-one (74), and relative termination (Refs. 19 and 213).*

From ferrocenyl-1,3-dithiol-2-one, the corresponding $[Pt(4,4'\text{-}t\text{Bu}_2\text{-bipy})(\text{Fc,H-edt})]$ (**73**) complex was obtained according to a modification of the general procedure summarised in Scheme 3.5, starting from $[Pt(4,4'\text{-}t\text{Bu}_2\text{-bipy})\text{Cl}_2]$ (Scheme 3.13). Notably, **73** represents the first example of a platinum(II) complex bearing this ferrocenyl-substituted ligand.

Scheme 3.13. *Synthesis of [Pt(4,4'-tBu$_2$-bipy)(Fc,H-edt)] (73).*
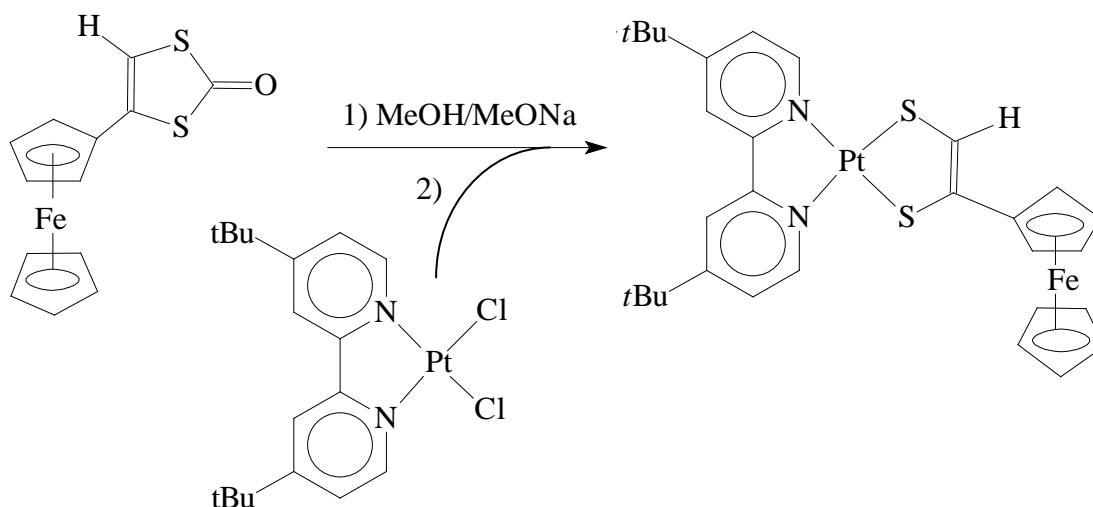
All the twenty-one complexes were found to have satisfying elemental analyses, except for **55** and **62**, which could not be obtained in a pure form notwithstanding the numerous attempts of purification. All complexes were obtained in yields ranging between 9 and 90%, and were found to be thermally stable, with melting points above 240° C. In all cases, a complete spectroscopic and electrochemical characterisation, summarised in the Experimental Section (Paragraph 5.2.2.2), was carried out.

3.2.1.2. Structural characterisation

Crystals suitable for X-ray diffraction measurements were collected for compounds **57-59**, **64**, **67**, and **69** (Figure 3.22, Tables 3.25 and 3.26). The quality of the structures, testified by the *R* indeces (Table 3.25), is in some cases not excellent, due to either disordered atoms unsuitable for splitting in the complex molecules (**64**, **67**) or solvent molecules encapsuled in the cavities (**57**, **59**).
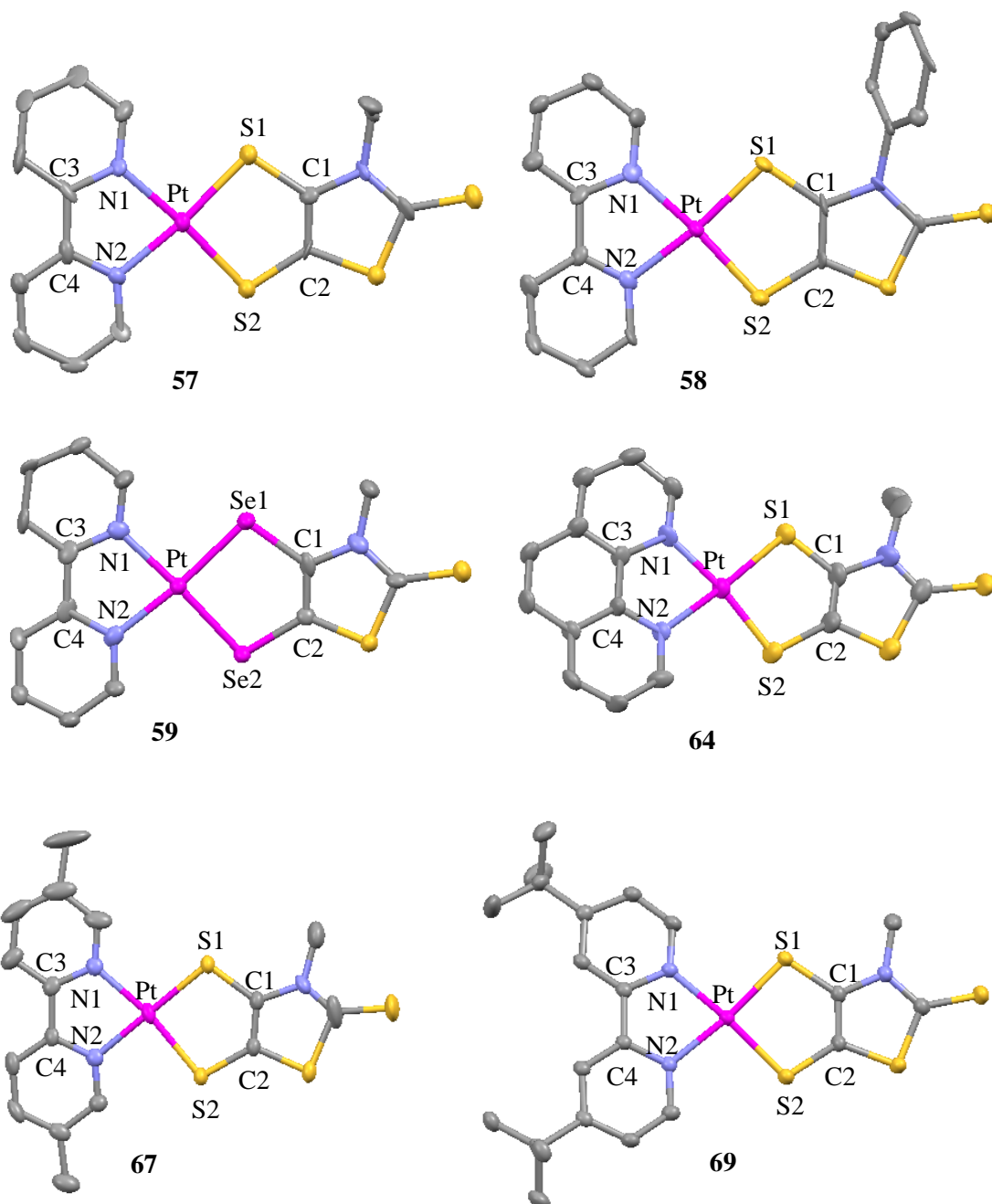
Figure 3.22 *ORTEP drawing and atom labelling scheme for the complex units in the crystal structures of 57·1/2THF, 58, 59·1/2CH₂Cl₂, 64, 67, and 69. Thermal ellipsoids are shown at the 50% probability level. Hydrogen atoms were omitted for clarity.*

In two cases, namely for complexes **57** and **59**, the structure determination established the crystallised compound as **57**·1/2 THF and **59**·1/2 CH$_2$Cl$_2$, respectively, due to the presence of co-crystallised solvent (Table 3.25). As an example, in the crystals of the

complex **57**, grown by slow evaporation of THF solutions, the unit cell consists of two independent specular [Pt(2,2′-bipy)(Et-dmet)] molecular units lying on parallel planes and slipped to each other, and a solvent molecule. Since the pattern of bond angles and distances within each complex unit shows significant differences, especially as far as the Et-dmet^{2-} ligand is regarded, in Table 3.26 the values for each molecular unit (labelled as A and B) are reported. Moreover, it is worth underlining that the structure of **67** features the simultaneous presence of two kinds of complex units (occupancies = 65% and 35%), differing for the parameters regarding the Me-dmet^{2-} ligand, and flipped by 180° with respect to the other.

An examination of the complex units in all the crystal structures (Figure 3.22, Table 3.26) shows the central metal ion coordinated in a square-planar fashion, and complexes are almost completely planar but for the substituents, with dihedral angles C3-N1-Pt-E1 ranging between 169.39 and 177.81° (Table. 3.26, numbering scheme as in Figure 3.22). For complexes **57**, **58**, **67**, and **69** bond lengths and angles describing Pt^{II} coordination are in good agreement with those reported for the [Pt(N^N)(S^S)] complexes structurally characterised so far [average experimental Pt-S, Pt-N, C-S and C-C distances = 2.256(14), 2.046(10), 1.744(23), and 1.373(41) Å, respectively; average experimental S-Pt-S and N-Pt-N angles = 89.38(8) and 79.22(8)°, respectively; Section 1.3.2.2]. In the case of **64**, Pt-S/Pt-N distances and S-Pt-S/N-Pt-N angles are shorter and larger, respectively, than those usually found for the other complexes structurally characterised. In particular, the comparison between bond lengths and angles in **57** and **64** (differing just for the identity of the diimine ligand), shows that the introduction of a 1,10-phenanthroline in place of a 2,2′-bipyridine determines significant differences in the structural features of [Pt(N^N)(S^S)] complexes. It is worth noting that, to best of our knowledge, only another [Pt(N^N)(S^S)] complex bearing a 1,10-phenanthroline ligand, namely [Pt(Ph$_2$-phen)(*t*Bu$_2$-tdt)] (Ph$_2$-phen: 4,7-diphenyl-phenanthroline, *t*Bu$_2$-

tdt: 3,5-di-*tert*-butyl-1,2-benzenedithiolato), was structurally characterised so far.[214] On the other hand, a comparison between **57**, **58**, **67**, and **69** shows that the addition of alkyl substituents to the 2,2′-bipyridine ligand does not induce significant changes into the crystal structure of the complex. Among the complexes characterised by X-ray diffraction, a particular mention is deserved by **59**, which represents the second example of a diimine-diselenolate ever characterised structurally.[135] As expected, due to the bigger radius of selenium as compared to sulphur, in the case of **59** the chalcogen-platinum distances are significantly longer than those determined for the corresponding sulphured compounds (as clearly appears from a comparison between the structural features of **59** and **57**).

Concerning the 1,2-dichalcogenolato system, C-C and C-S distances in the ranges 1.340-1.366 and 1.723-1.763 Å, respectively, were found for complexes **57**, **58**, **64**, **67**, and **69**, suggesting, as expected, a ene-1,2-dithiolato form ($^-$S-C=C-S$^-$) for the 1,2-dithiolene ligand. The same conclusions can been drawn for **59**, where C-Se bond lengths are remarkably longer (1.905 Å on average), due to the larger Van der Waals radius of Se compared to S.

Table 3.25. *Crystallographic data for 57·1/2THF, 58, 59·1/2CH$_2$Cl$_2$, 64, 67 and 69.*[a]

	57·1/2THF	58	59·1/2CH$_2$Cl$_2$	64	67	69
Empirical Formula	$C_{17}H_{13}N_3PtS_4$	$C_{19}H_{13}N_3PtS_4$	$C_{14.5}H_{11}ClN_3PtS_2Se_2$	$C_{17}H_{13}N_3PtS_4$	$C_{16}H_{15}S_4N_3Pt$	$C_{22}H_{27}N_3PtS_4$
Formula weight	592.66	606.67	679.85	582.65	572.66	656.82
Crystal size (mm)	0.06x0.03x0.01	0.12x0.09x0.03	0.15x0.03x0.03	0.27x0.15x0.03	0.15x0.13x0.07	0.23x0.14x0.08
Space group	P2$_1$/c	P-1	P-1	Pbca	P-1	P-1
Crystal system	Monoclinic	Triclinic	Triclinic	Orthorhombic	Triclinic	Triclinic
a (Å)	12.029(3)	7.640(6)	8.0202(13)	16.645(4)	8.3364(3)	10.8053(5)
b (Å)	15.048(3)	10.650(9)	8.2543(14)	16.525(4)	9.4820(4)	11.1233(5)
c (Å)	20.893(5)	12.300(10)	14.153(3)	13.150(3)	12.9422(5)	13.1623(6)
Volume (Å^3)	3770.4 (16)	918.4 (13)	872.2(3)	3616.8(14)	898.02(6)	1228.31(10)
Z	8	2	2	8	2	2
Calculated density (Mgm^{-3})	2.088	2.194	2.589	2.14	2.118	1.776
Temperature (K)	93(2)	125(2)	125(2)	125(2)	150(2)	150(2)
Total number of data	24784	11269	7214	25950	9762	10206
Reflections unique	7126	3674	3446	3286	4080	5503
Parameters	460	244	217	226	223	278
Rint	0.1	0.062		0.08	0.033	0.022
Final R indees [$I > 2\sigma(I)$]	0.0553	0.0513	0.0557	0.0619	0.0316	0.0235
wR2 (all data)	0.0812	0.1806	0.1634	0.1569	0.0708	0.0546

[a] T = 93(2) (**57**), 125(2) (**58, 59,** and **64**), or 150(2) (**67-69**) K; Mo$K\alpha$ radiation (λ = 0.7107 Å)

.

Table 3.26. *Selected bond lengths (Å) and angles (°) of complex units in the crystal structures of 57·1/2THF (units A and B), 58, 59·1/2CH₂Cl₂, 64, 67, and 69.*[a,b]

	57 A	57 B	58	59	64	67	69
Pt–E1	2.266(3)	2.266(3)	2.267(3)	2.382(15)	2.233(3)	2.257(2)	2.267(9)
Pt–E2	2.277(3)	2.275(3)	2.266(4)	2.392(13)	2.235(3)	2.360(3)	2.273(9)
Pt–N1	2.055(8)	2.055(8)	2.037(12)	2.079(11)	2.009(10)	2.050(5)	2.044(3)
Pt–N2	2.038(9)	2.043(8)	2.049(8)	2.056(13)	1.960(9)	2.045(4)	2.046(3)
E1–Pt–E2	91.04(10)	91.10(10)	90.98(12)	91.19(10)	97.11(12)	89.48(8)	90.85(3)
N1–Pt–N2	79.77(3)	79.58(3)	78.78(4)	81.35(3)	86.00(4)	80.1(18)	79.44(11)
C1–E1	1.763(11)	1.763(11)	1.746(14)	1.897(14)	1.733(14)	1.753(10)	1.738(4)
C2–E2	1.740(10)	1.740(11)	1.730(10)	1.906(13)	1.723(15)	1.739(9)	1.735(3)
C1–C2	1.341(15)	1.311(15)	1.350(18)	1.319(18)	1.343(19)	1.366(7)	1.340(5)
C3–N1–Pt–E1	177.56(12)	175.36(14)	169.39(10)	177.81(10)	174.86(12)	174.85(8)	173.70(10)

[a] E = S (**57, 58, 64, 67, 69**), Se (**59**). [b] Atom labelling scheme as in Figure 3.22.

Although the quality of some of the structures, as already mentioned, is not excellent, the interactions driving the crystals packing could be evaluated in all cases. An examination of the structures shows in all cases interactions between the electron π system of the diimine and the 1,2-dichalcogenolate.

In the case of **57**·1/2THF, the crystal packing originates from face-to-face π-π interactions between the 2,2′-bipyridine ligands of symmetry-related complex units disposed head-to-tail (1–x, 1–y, 1–z; intercentroid distance 3.70 Å) and between the 2,2′-bipyridine ligands and the C_2S_2Pt pentaatomic dithiolene rings (intercentroid distance 3.57 Å) that result in the formation of tetrameric aggregates (Figure 3.23). Slightly weaker interactions of the same type generate a complex network, leaving cavities that host the THF solvent molecules.
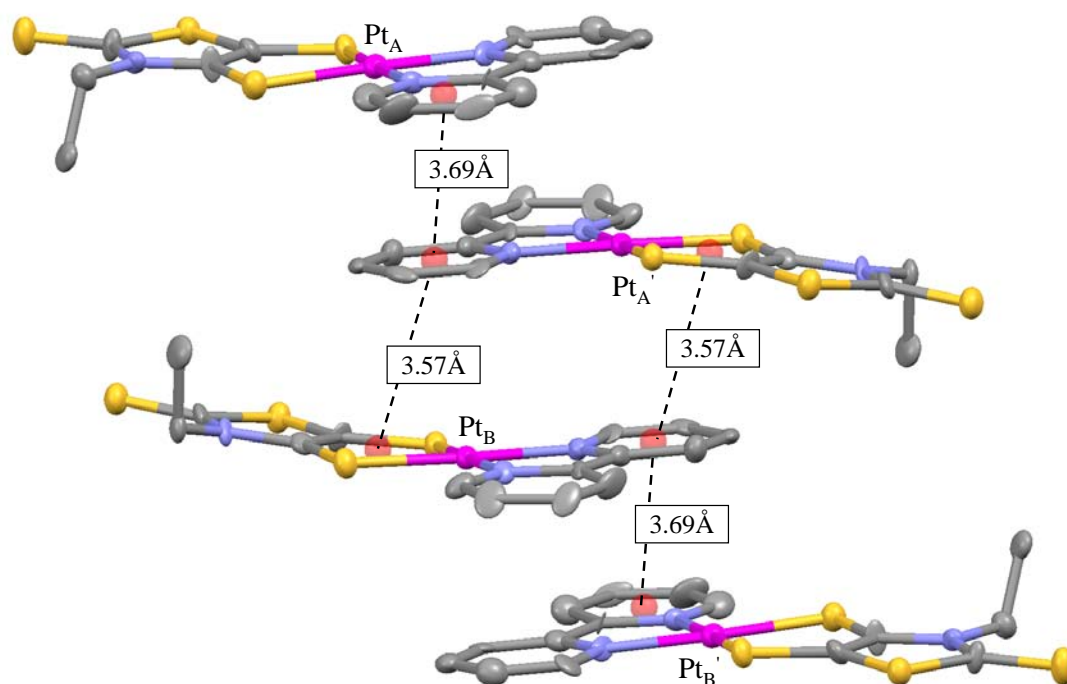
Figure 3.23. *ORTEP drawing of a portion of the crystal packing of **57**·1/2THF, showing the ring centroids in red. Hydrogen atoms have been omitted for clarity. Thermal ellipsoids have been drawn at 50% probability. ′ = 1–x, 1–y, 1–z.*

The crystal structure of **58** shows that also in this case weak π-π interactions lead to the formation of discrete aggregates. In fact, although the rotation of the phenyl substituent at the 1,3-thiazoline ring (65.73° between the average planes defined by the thiazoline and phenyl rings) prevents stacking interactions similar to those described for **57**, couples of interactions between the π system of the heterocyclic ring of the Ph-dmet^{2-} ligand and the Pt atom of a symmetry related molecule (1–*x*, 1–*y*, 1–*z*) lead to the formation of pairs (Pt-centroid distances 3.644 and 3.678 Å, Figure 3.24).
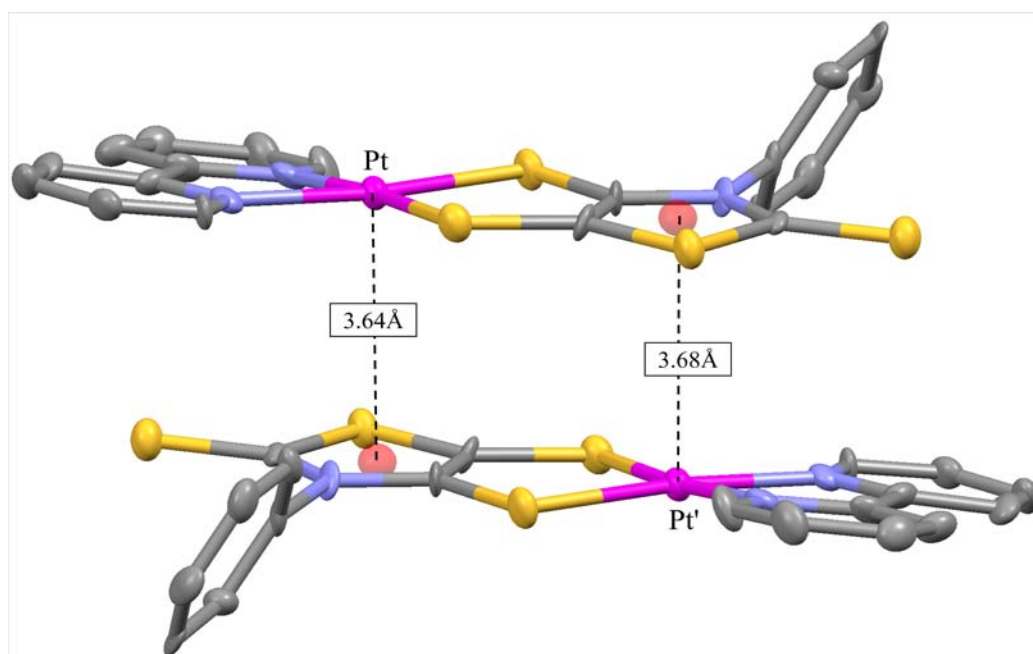
Figure 3.24. *ORTEP drawing of interacting symmetry related molecular units in the crystal structure of* **58**. *Ring centroids are drawn in red. Hydrogen atoms have been omitted for clarity. Thermal ellipsoids have been drawn at 50% probability. ' = 1–x, 1–y, 1–z.*

Two types of π-π supramolecular contacts extend the interactions between the units of **58**: (i) a slipped edge-to-edge interaction between the bipyridines results in the formation of ribbons running along the *a* vector (Figure 3.25). (ii) face-to-face π-π interactions between eclipsed couples of the phenyl substituents (distance between the planes described by the

phenyl rings 3.26 Å) keep together the ribbons to form stacks oriented along the *a* vector determining the overall three-dimensional structure.
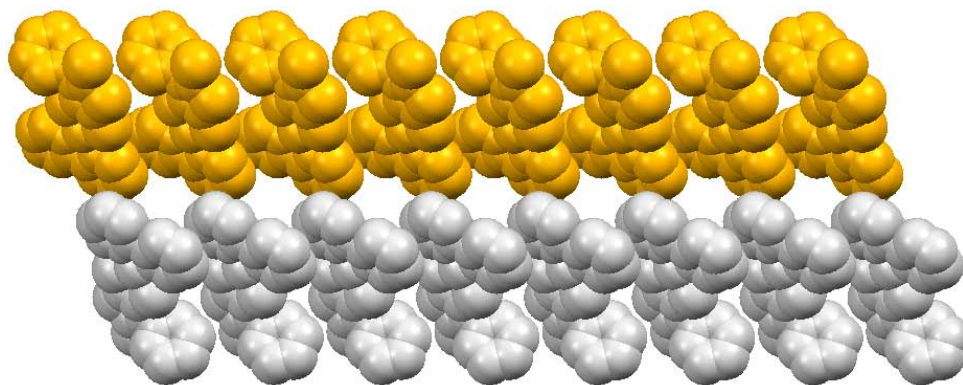
Figure 3.25. *Spacefill view along the c vector of the ribbons formed between symmetry related molecular units of 58 by means of the slipped edge-to-edge π-π interaction between the 2,2'-bipyridine ligands.*

The crystal packing of $59 \cdot 1/2CH_2Cl_2$ is originated from two main different types of interactions involving the diimine ligand, which features (i) face-to-face interactions with the C_3NS heterocycle of the Me-dset^{2-} ligand (intercentroid distance 3.50 Å), and, on the other side of the molecular plane, (ii) slipped π-π stacking interactions with the 2,2′-bipyridine of a symmetry related molecule (intercentroid distance 3.60 Å, Figure 3.26).
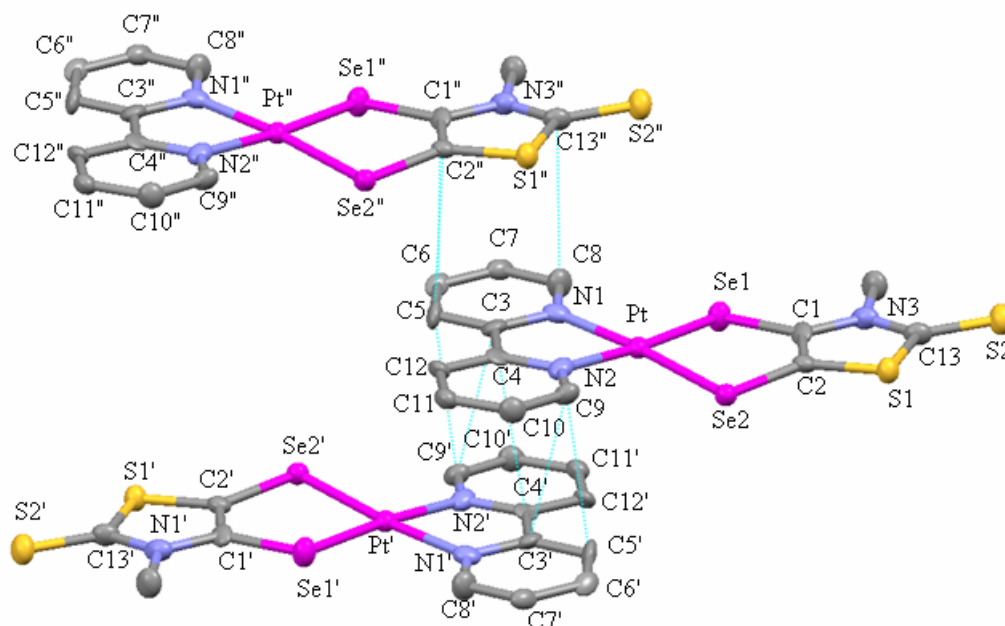
Figure 3.26. *ORTEP drawing of interacting symmetry related molecular units of **59** in the crystal structure of **59**·1/2CH$_2$Cl$_2$. Hydrogen atoms have been omitted for clarity. Thermal ellipsoids have been drawn at 50% probability. C5-C9' =3.34, C4-C9' = 3.44, C4-C4' = 3.37, C9-C3' = 3.44, C9-C5' = 3.34, C6-C1" = 3.50, C5-C2" = 3.46, C8-C13" = 3.48 Å. ' = 1–x, 1–y, 2–z; " = x, –1+y, z.*

The overall packing leaves cavities occupied by CH$_2$Cl$_2$ disordered solvent molecules, in molar ratio 1:2 with respect to **59**.

Although the crystals of **67** are of poor quality, it is possible to evaluate the connectivity within the molecule and confirm the hypothesised structure of the Pt^{II} complex. Monomeric units in the crystal are stacked along the *a* vector with a zig-zag motif by means of contacts closely related to those discussed above for **59**, i.e. slipped π-π stacking interactions between the 5,5′-Me$_2$-bipyridine ligands (intercentroid distance between pyridine units 3.62 Å) and face-to-face interactions with the C$_3$NS heterocycle of the Me-dmet^{2-} ligand (intercentroid distance 3.52 Å). Although such interactions result in Pt⋯Pt distances (4.18 Å) shorter than in the cases discussed above, these are largely above the sum of van der Waals radii (3.44 Å).[215] Weak contacts involving the

methyl substituents of the 1,2-dithiolates and the 2,2′-bipyridine units pack the stacks along the *b* and *c* axis.

The crystal structure of **64** shows that the same type of π–π interactions between the benzenoid ring of the 1,10-phenanthroline and the Et-dmet^{2-} ligands result in the formation of weakly bonded pairs of molecules (Figure 3.27).
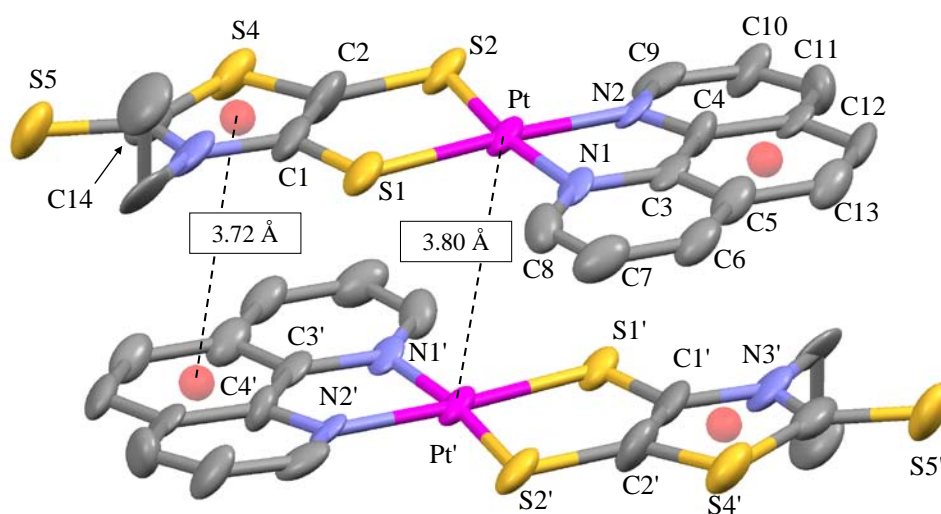
Figure 3.27. *ORTEP drawing of a portion of the crystal packing of **64**, showing the ring centroids in red. Only the atoms mentioned in the discussion are labelled. Hydrogen atoms have been omitted for clarity. Thermal ellipsoids have been drawn at 50% probability.* ′ = 2–x, –y, –z.

The endocyclic and the terminal sulphur atoms of the Et-dmet^{2-} ligand (S4 and S5, respectively, in Figure 3.27) are involved in weak contacts with hydrogen atoms of 1,10-phenanthroline ligands of different pairs of molecules disposed almost orthogonally (86.01°; S4···H7″ = 2.97, S4···H8″ = 2.86, S5···H9‴ = 2.97 Å; ″ = 1/2+*x*, *y*, 1/2–*z*, ‴ = 5/2–*x*, –*y*, 1/2+*z*).

Finally, in the crystal packing of **69** parallel molecular units can be envisaged with π-π face to face interactions between C_2N_2Pt metallacycles of couples of complex units

disposed head-to-tail (intercentroid distance 3.76 Å; symmetry operation $-x,-y,-z$).
Couples of weak intermolecular contacts involving the coordinating sulphur atoms and
the endocyclic chalcogen species of each Me-dmet^{2-} ligand (S2···S4" = 3.50 Å,
labelling scheme as in Figure 3.27 for **64**; " = $-1-x$, $-y$, $-z$), slightly shorter than the sum
of van der Waals radii (3.60 Å),[215] generate the ribbon depicted in Figure 3.28. Weak
minor hydrophobic contacts between parallel ribbons originate the crystal packing.
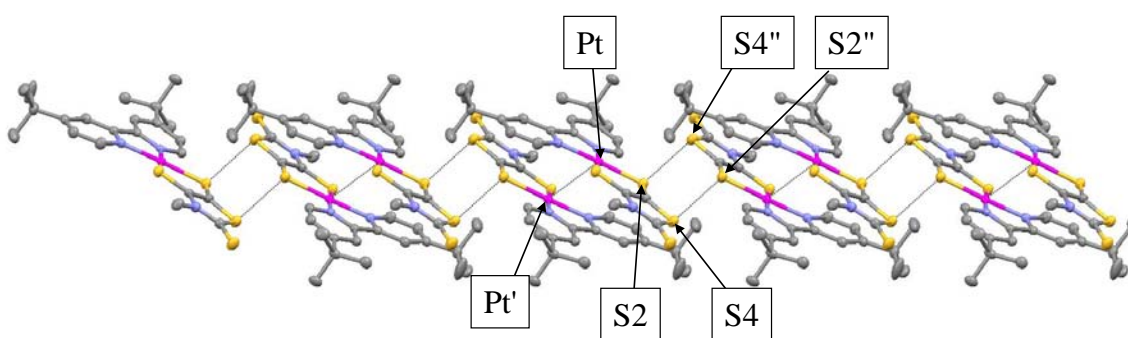
Figure 3.28. *ORTEP drawing of a portion of the ribbons, running along the a vector, formed by complex **69** by means of π−π interactions and S···S contacts seen along the c axis. Hydrogen atoms have been omitted for clarity. Thermal ellipsoids have been drawn at 50% probability.' = –x, –y, –z; " = –1–x, –y, –z.*

3.2.1.3. Electrochemistry

Cyclic Voltammetry (CV) measurements performed in DMSO on **53-72** show that, beside **72**, all the complexes feature two one-electron redox processes, at about -1.6 and 0.1 V versus the Fc$^+$/Fc couple (Table 3.27; Figure 3.29 for **54**).
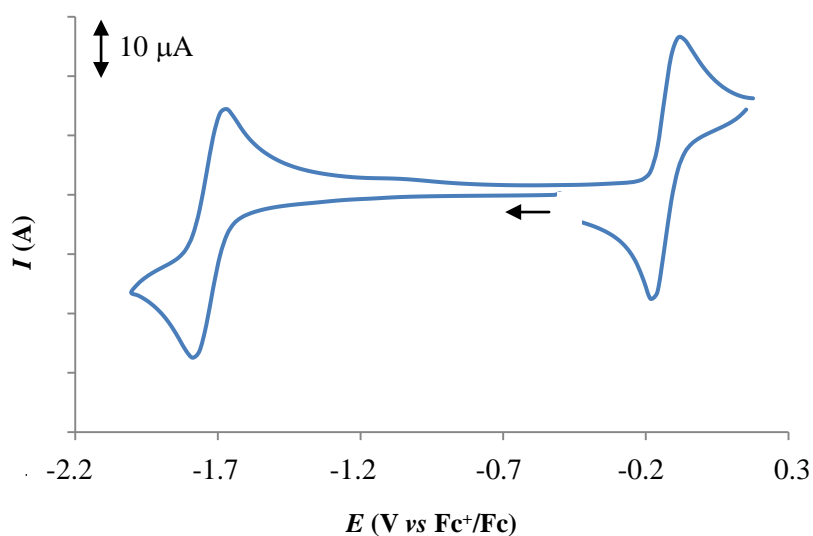
Figure 3.29. *Cyclic voltammetry recorded for a solution of **54** at a platinum electrode in anhydrous DMSO [298 K; scan rate 100 mV s^{-1}; supporting electrolyte (TBA$^+$)(PF$_6^-$) 0.1 M].*

Table 3.27. *Half-wave potentials $E_{1/2}$ (V vs Fc^+/Fc) recorded by CV for complexes **53-73** (scan rate 50 mV s^{-1}).*

	$E_{1/2}^{(-1/-2)}$	$E_{1/2}^{(0/-1)}$	$E_{1/2}^{(+1/0)}$
53	/	-1.741	-0.135
54	/	-1.727	-0.135
55	/	-1.618	-0.076
56	-2.270	-1.608	-0.004
57	-2.256	-1.609	0.008
58	-2.269	-1.622	0.046
59	-2.245	-1.607	0.044
60	/	-1.715	-0.147
61	/	-1.728	-0.161
62	/	-1.620	-0.076
63	/	-1.620	-0.017
64	/	-1.620	-0.027
65	/	-1.634	0.020
66	/	-1.620	-0.027
67	/	-1.730	-0.027
68	/	-1.740	-0.017
69	/	-1.692	-0.015
70	-2.112	-1.563	-0.040
71	/	-1.561	-0.002
72	/	-1.789	/
73[a]	/	-1.470	0.216

[a] Complex **73** features further redox processes not reported in this table.

Five of the complexes show an additional reduction process below -2.0 V (Table 3.27; Figure 3.30 for **56**).
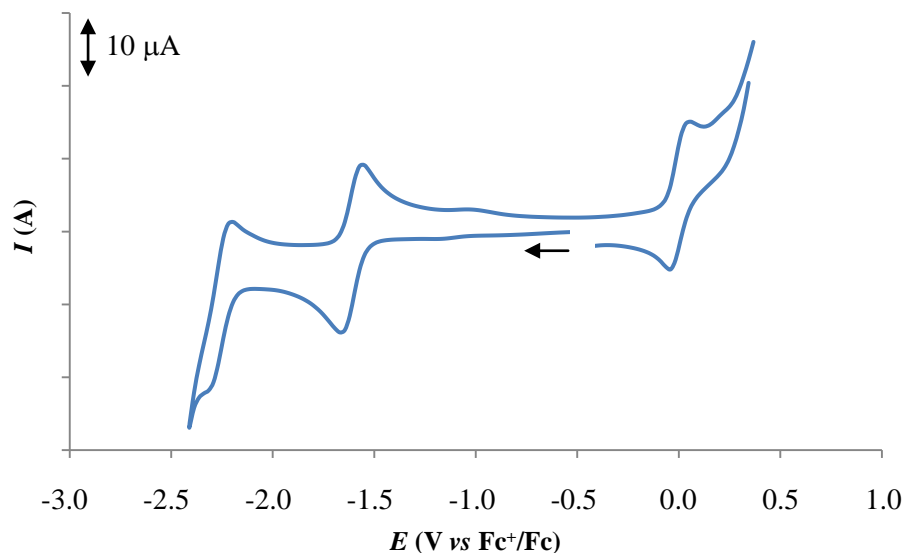
Figure 3.30. *Cyclic voltammetry recorded for a solution of **56** at a platinum electrode in anhydrous DMSO [298 K; scan rate 100 mV s^{-1}; supporting electrolyte (TBA$^+$)(PF$_6^-$) 0.1 M].*

An examination of i_{pc}/i_{pa} and peak separation values (Table 3.28) clearly indicates that reduction of neutral species to the corresponding monoanionic ones, common to all complexes, is a monoelectronic reversible process falling at about -1.6 V *vs* Fc$^+$/Fc, with i_{pc}/i_{pa} close to unity and $|E_{pc}-E_{pa}|$ = 49-79 mV at 50 mV s^{-1} for all complexes. The reduction process leading from the monoanionic to the dianionic form of complexes **56-59** and **70** occurs at about -2.1 V *vs* Fc$^+$/Fc, and is fully reversible as well ($i_{pc}/i_{pa} \approx 1$ and $|E_{pc}-E_{pa}|$ = 48-53 mV at 50 mV s^{-1}), thus suggesting both reduction processes occur without decomposition of the complexes. The oxidation occurring for all complexes beside **72** at about 0.1 V vs Fc$^+$/Fc, is also a reversible process, with i_{pc}/i_{pa} and $|E_{pc}-E_{pa}|$ ranging between 0.7 and 1.4, and 44 and 72 mV at 50 mV s^{-1}, respectively; only for **59** and **63** the i_{pc}/i_{pa} values fall out of the described ranges, so that, as concerns these complexes, the process should be considered as quasi-reversible.

Table 3.28. *Electrochemical data (V vs Fc$^+$/Fc) recorded by CV for complexes **53-73** (scan rate 50 mV s^{-1}).*

	$E_{1/2}$ $^{(-1/-2)}$		$E_{1/2}$ $^{(0/-1)}$		$E_{1/2}$ $^{(+1/0)}$	
	$\|E_{pc}-E_{pa}\|$	i_{pc}/i_{pa}	$\|E_{pc}-E_{pa}\|$	i_{pc}/i_{pa}	$\|E_{pc}-E_{pa}\|$	i_{pc}/i_{pa}
53	/	/	0.072	1.1	0.072	1.0
54	/	/	0.065	1.0	0.064	1.0
55	/	/	0.060	1.1	0.062	0.8
56	0.052	0.7	0.049	1.0	0.049	1.1
57	0.052	1.0	0.050	1.1	0.044	0.9
58	0.053	0.8	0.054	1.1	0.048	0.7
59	0.048	0.8	0.049	1.2	0.054	0.5
60	/	/	0.058	1.0	0.047	1.1
61	/	/	0.064	1.1	0.062	1.0
62	/	/	0.079	0.8	0.048	1.4
63	/	/	0.055	1.3	0.047	2.0
64	/	/	0.060	1.3	0.048	1.0
65	/	/	0.058	1.1	0.062	0.9
66	/	/	0.056	1.1	0.052	0.9
67	/	/	0.068	0.9	0.065	1.2
68	/	/	0.079	0.6	0.056	1.2
69	/	/	0.058	0.8	0.051	0.9
70	0.052	0.8	0.066	1.3	0.057	1.0
71	/	/	0.049	0.8	0.051	1.2
72	/	/	0.078	1.1	/	/
73[a]	/	/	0.075	1.0	0.048	1.0

[a] Complex **73** features further redox processes not reported in this table.

Concerning the features of the two redox processes common to all twenty complexes beside **72**, they can be rationalised by analysing separately the three series of complexes depicted in Schemes 3.6-3.8. In the first series, where all the complexes feature the same diimine ligand (2,2′-bipyridine), and differ for the identity of the 1,2-dichalcogenolene one, a dependence of the oxidation potential on the nature of the E^E ligand is observed, while the reduction potential is similar for all the complexes. This is

in agreement with the localisation of the HOMO on the 1,2-dichalcogenolene ligand hypotesised for [Pt(N^N)(E^E)] complexes (section 1.3.2.3).[152] In particular, in complexes **56-59**, bearing a R-dmet^{2-}/R-dset^{2-} ligand, the oxidation potential is systematically more positive than in **53-55**, where a Ar,H-edt^{2-} ligand is present, the latest complexes being therefore more easily oxidised (Figure 3.31, Table 3.27). These observations suggest that complexes **56-59** feature the HOMO at lowest energies with respect to **53-55**, while the variation of the substituent at the 1,2-dithiolene core within each class of ligands induce minor variations into the redox features of the corresponding complexes.
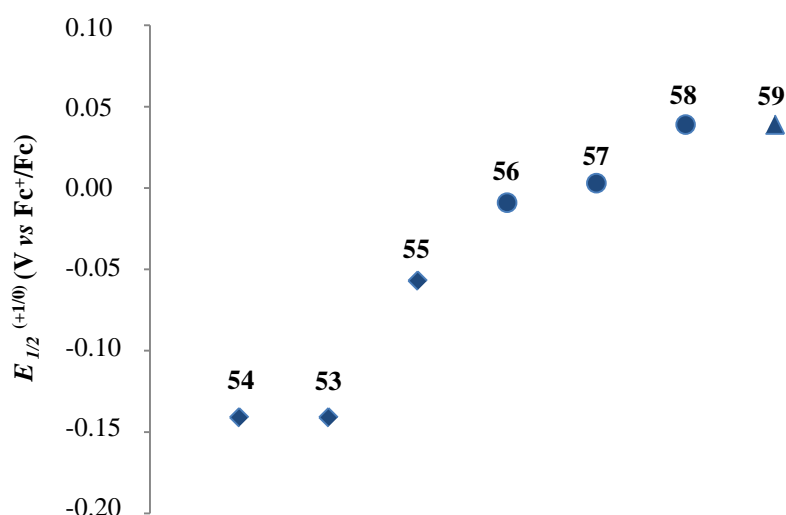
Figure 3.31. *Half-wave potentials (V vs Fc$^+$/Fc) of the oxidation process (Table 3.27) for complexes 53-59 (Series 1, Scheme 3.6). N^N = 2,2'-bipyridine; E^E = Ar,H-edt^{2-}(rhombs), R-dmet^{2-}(circles), Me-dset^{2-} (triangle).*

Similar observations can be drawn for Series 2, where 1,10-phenanthroline is present in place of 2,2′-bipyridine.

On the other hand, in Series 3, where Me-dmet^{2-} is combined with different diimine ligands, a dependence of the reduction potential on the nature of the N^N ligand is

observed, which can be related to the localisation of the LUMO on this fragment of the molecule assumed for these systems (Section 1.3.2.3).[152] In particular, the comparison between redox potentials of **56** and **63** suggest that, on passing from bipyridine to phenanthroline systems, no significant changes can be observed in the value of the reduction potential (Figure 3.32, Table 3.27).
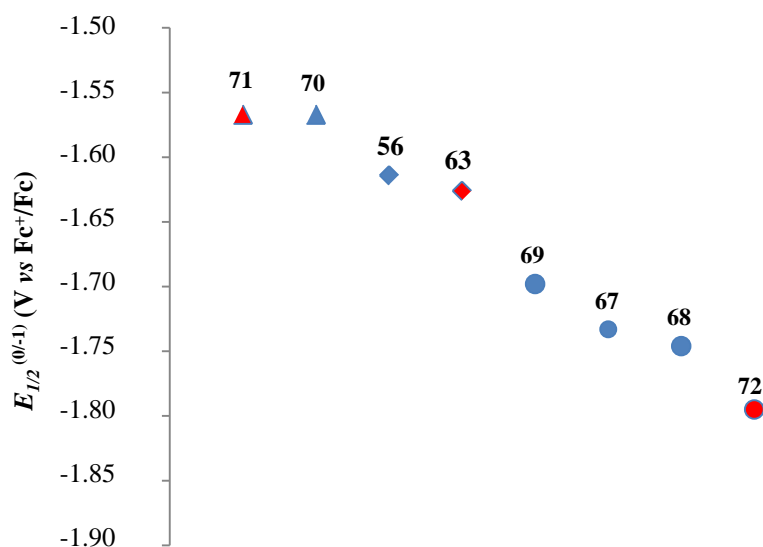
Figure 3.32. *Half-wave potentials (V vs Fc$^+$/Fc, Table 3.27) of the reduction process for complexes **56**, **63**, and **67-72** of Series 3 (Scheme 3.8). S^S = Me-dmet^{2-}; N^N = unsubstituted (rhombs) 2,2′-bipyridine (blue) or 1,10-phenanthroline (red) and alkyl (circles) or phenyl (triangles) derivatives.*

An examination of the reduction potentials of complexes bearing differently substituted 2,2′-bipyridine and 1,10-phenanthroline ligands (blue and red symbols, respectively in Figure 3.32) shows that systems bearing phenyl substituents feature the reduction at less negative potentials with respect to the unsubstituted systems, while the alkyl pendants induce the opposite effect.

Cyclic voltammetry measurements were also performed in CH$_2$Cl$_2$ for **73** (Figure 3.33). This complex features a monoelectronic reversible reduction wave at about -1.470 V *vs*

Fc$^+$/Fc (i_{pc}/i_{pa} = 1, |E_{pc}–E_{pa}| = 75 mV at 50 mV s^{-1}) and several oxidation waves. The number of processes should be due to the presence of the redox-active ferrocenyl substituent at the 1,2-dithiolene core. A first reversible process occurs at about 0.216 V *vs* Fc$^+$/Fc (i_{pc}/i_{pa} = 1, |E_{pc}-E_{pa}| = 48 mV at 50 mV s^{-1}), while at more positive potentials two more oxidations can apparently be found, at 0.613 and 0.773 V, respectively. A comparison of the voltammogram of **73** with those of the other related complexes discussed above, induces to hypothesise that the processes at -1.470 and 0.216 V *vs* Fc$^+$/Fc may be related to the formation of monoanionic and monocationic species respectively, and should be centred on the diimine-dithiolate core.

The two signals at more positive potentials could be tentatively assigned to a single oxidation process referable to the ferrocenyl substituent, whose wave would result split in two, possibly because of a deposition process at the electrode occurring during the measurements.
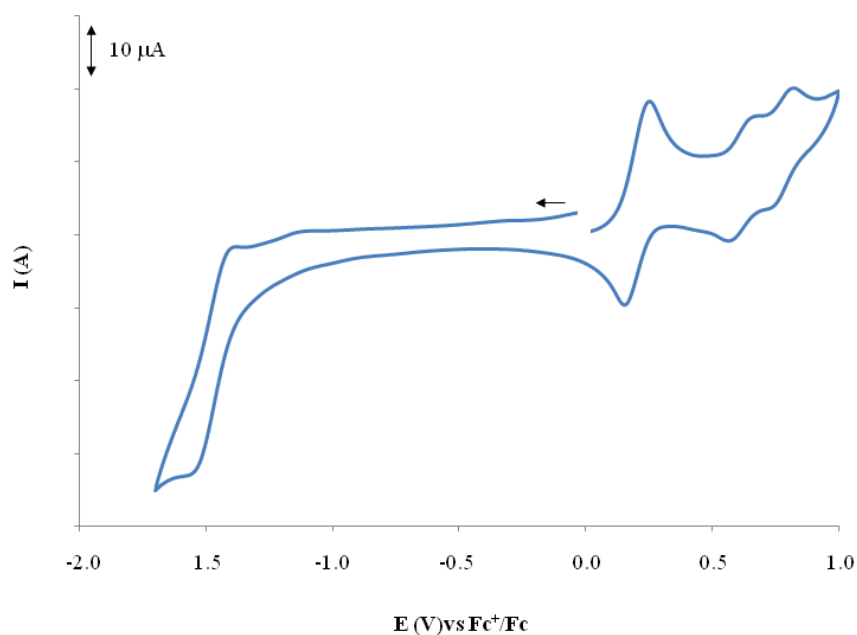
Figure 3.33. *Cyclic voltammetry recorded for a solution of **73** at a platinum electrode in anhydrous CH$_2$Cl$_2$ [298 K; scan rate 100 mV s^{-1}; supporting electrolyte (TBA$^+$)(PF6$^-$) 0.1 M].*

3.2.1.4. Absorption UV-Vis-NIR Spectroscopy

The UV-Vis-NIR absorption spectra (250-1100 nm) of complexes **53-73** recorded in DMSO feature a series of absorptions in the UV region, with λ_{max} ranging between 257 and 392 nm. In all cases, the band falling at highest energies and showing the highest extinction coefficient ε (15000-50000 M^{-1} cm^{-1}) is found at about 260 nm (Figures 3.34 and 3.35), both for the complexes bearing 2,2′-bipyridine and 1,10-phenanthroline ligands. Moreover, complexes bearing a substituted or unsubstituted 2,2′-bipyridine (**53-59**, and **67-70**) feature an absorption at about 300 nm, with $\varepsilon = $ 16000-40000 M^{-1} cm^{-1} (Figures 3.34 for **53** and 3.35 for **56**).

In the absorption spectra of complexes featuring Ar,H-edt^{2-} ligands (**53-55** and **60-62**), further absorptions with $\varepsilon = $ 8000-14000 M^{-1} cm^{-1} can be found in the region 320-380 nm (Figure 3.34 for **53**)
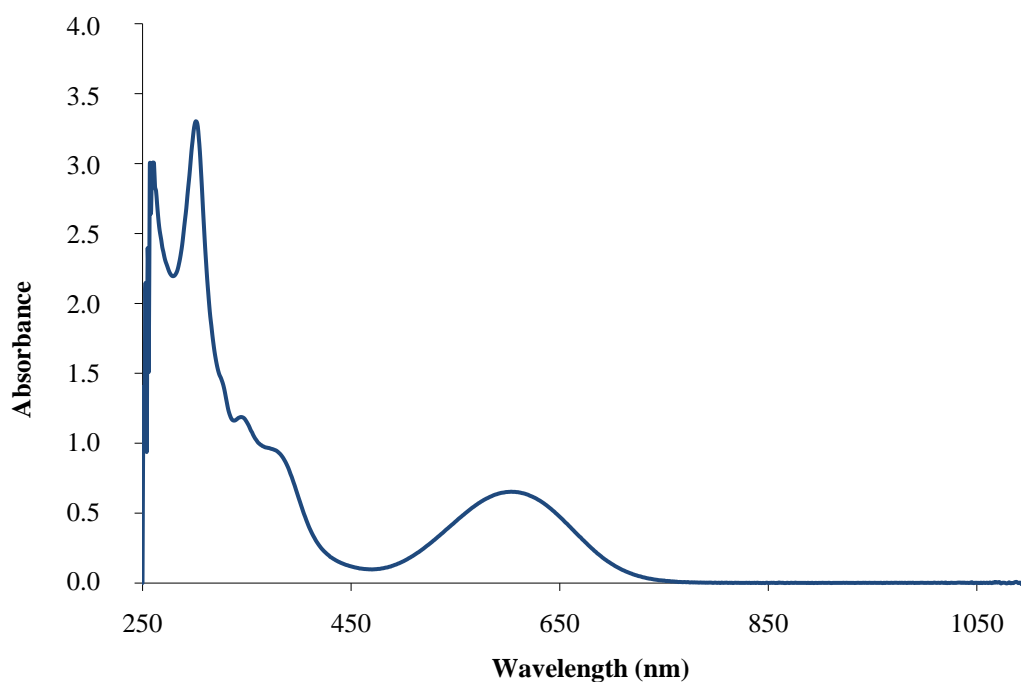
Figure 3.34. *UV-Vis-NIR absorption spectrum recorded for 53 in DMSO.*

On the other hand, all complexes featuring a R-dmet^{2-}/R-dset^{2-} ligand (**56-59**, **63-66**, and **67-72**) feature a relatively intense (ε = 6000-16000 M^{-1} cm^{-1}) absorption at about 370 nm (Figure 3.35 for **56**), and the complexes featuring the same ligands in combination with a substituted or unsubstituted 2,2′-bipyridine (**56-59**, **63-66**, and **67-70**) show two further narrow absorption bands at about 305 and 325 nm (ε = 6000-15000 M^{-1} cm^{-1}).
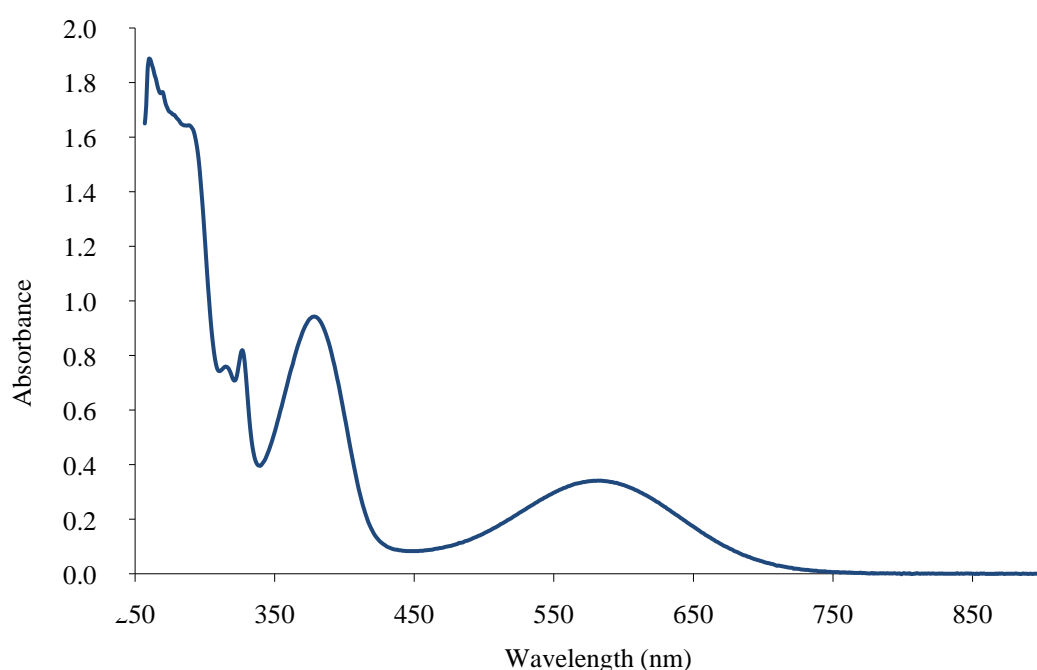
Figure 3.35. *UV-Vis-NIR absorption spectrum recorded for 56 in DMSO.*

As described in Section 1.3.2.3, a peculiar feature of [M(N^N)(E^E)] complexes is the presence of a solvatochromic absorption band in the visible region, assigned to a mixed metal-ligand-to-ligand charge-transfer (MMLL′CT, or MLCT/LLCT as recently abbreviated) occurring from the HOMO, which has a mixture of metal and dithiolate character, to the LUMO, centred on the diimine.[127] This absorption band is present in all

complexes of d^8 metals in a square-planar coordination belonging to this class, and the lowest energy and highest molar absorption coefficients are shown by Pt^{II} complexes. Accordingly, a broad absorption band in DMSO with $\varepsilon =$ 3500-6700 M^{-1} cm^{-1} can be found in spectra of complexes **53-73** in the visible region, with absorption maxima between 550 and 610 nm (Table 3.29 and Figures 3.34 and 3.35 for **53** and **56**, respectively). The absorption spectra of all complexes exhibit a remarkable negative solvatochromism, as proved by recording the absorption spectra in eight different solvents (dichloromethane, chloroform, acetonitrile, acetone, tetrahydrofurane, dimethylformammide, dimethylsulfoxide, and toluene; Table 3.29 and Figure 3.36 for **53**; due to solubility problems, the spectrum in toluene could not be recorded for some complexes). For each complex, the λ_{max} of the absorption band fits in a range of about 150 nm in the eight solvents considered, with the shortest wavelength shown in all cases in acetonitrile, and the longest one in toluene (Table 3.29 and Figure 3.36 for **53**). The molar extinction coefficient of the absorption is solvent-dependent as well (Table 3.29), reaching about 8000 M^{-1} cm^{-1} in toluene for **53**.

Table 3.29. *Visible absorption maxima* λ_{max} *(nm) and molar extinction coefficients* ε *(M^{-1} cm^{-1}, in parenthesis) for complexes **53-73** in different solvents.*

	CH$_2$Cl$_2$	CHCl$_3$	CH$_3$CN	Acetone	THF	DMF	DMSO	Toluene
53	636 (6100)	654 (4900)	598 (5500)	630 (6900)	672 (7800)	615 (6200)	604 (6700)	686, 743 (7200-8000)
54	637 (6200)	667 (5500)	601 (3900)	629 (5100)	675 (7100)	615 (6300)	603 (5900)	698, 760 (/)
55[a]	628 (/)	644 (/)	594 (/)	612 (/)	640 (/)	/	592 (/)	/
56	633 (5000)	660 (5200)	584 (3600)	610 (4100)	645 (3600)	591 (4300)	581 (4300)	740 (/)
57	635 (4800)	670 (4600)	577 (5900)	604 (4600)	652 (4800)	586 (3000)	582 (4500)	740 (4300)
58	630 (4400)	652 (4200)	579 (3200)	604 (3800)	651 (4600)	589 (3800)	580 (4000)	731 (4600)
59	622 (5100)	647 (5400)	578 (3200)	590 (3500)	635 (4200)	575 (4600)	569 (3500)	732 (/)
60	634 (6300)	653 (3600)	598 (3800)	632 (5400)	675 (6300)	618 (4300)	606 (5400)	677, 736 (5700, 7000)
61	632 (3300)	652 (5200)	598 (4000)	628 (4100)	675 (4100)	616 (5800)	603 (3600)	684, 732 (6100, 6800)
62[a]	620 (/)	/	/	606 (/)	/	596 (/)	/	/
63	631 (3600)	656 (2400)	589 (3100)	619 (5000)	654 (2700)	591 (4900)	581 (5000)	/
64	634 (4100)	660 (4500)	579 (3800)	606 (3500)	655 (3600)	589 (3800)	579 (4000)	757 (/)
65	628 (4900)	635 (4000)	577 (3700)	603 (4700)	652 (5300)	591 (4600)	581 (4600)	730 (4400)
66[b]	618 (4300)	644 (3600)	570 (3400)	601 (/)	637 (2800)	577 (5200)	570 (5000)	/
67	603 (5000)	623 (5300)	565 (3600)	585 (4700)	629 (6300)	570 (4900)	567 (4700)	687, 740 (/)
68	603 (5000)	623 (5300)	565 (3600)	585 (4700)	629 (6300)	570 (4900)	567 (4800)	/
69	607 (6200)	627 (4800)	564 (3500)	588 (4600)	564 (5000)	570 (5200)	631 (5300)	694, 755 (3900, 3700)
70	657 (5900)	675 (5500)	611 (3700)	637 (4500)	682 (5500)	615 (4600)	608 (5600)	/
71	642 (5700)	662 (5800)	600 (4200)	616 (4900)	672 (6200)	615 (5600)	602 (5700)	/
72[b]	633 (5000)	586 (4300)	543 (3700)	563 (/)	621 (/)	561 (3100)	549 (3800)	/
73	638 (5800)	659 (6100)	604 (6100)	637 (5900)	682 (5600)	623 (5700)	621 (5800)	/

[a] Molar extinction coefficients could not be determined for complexes **55** and **62** due to the presence of byproducts. [b]Molar extinction coefficients could not be determined in some solvents due to solubility reasons.

In the absorption spectra recorded in toluene, the solvatochromic absorption band is broadened or split into two bands, as already observed for other [Pt(N^N)(E^E)] complexes.[127]
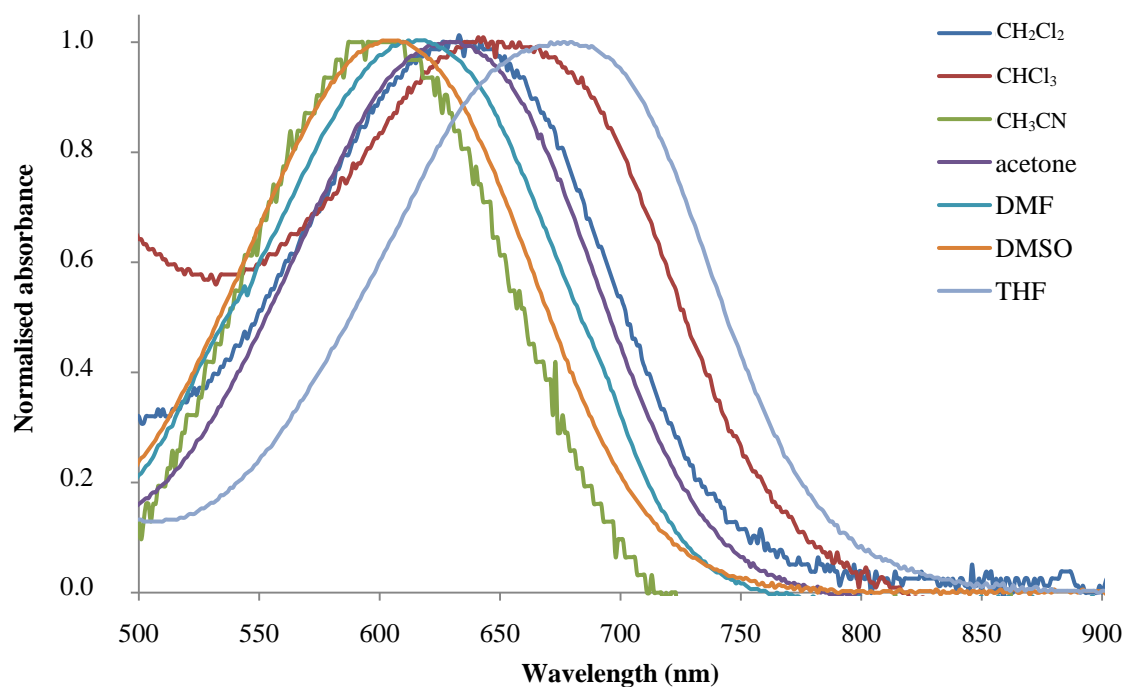
Figure 3.36. *Normalised absorption spectra in the Vis region (500-900 nm) recorded for **53** in selected solvents (Table 3.29).*

The trend of the position of λ_{max} in various solvents for a given compound is in perfect agreement with the empirical scale formulated by Eisenberg for [Pt(N^N)(E^E)] complexes,[127,216] as shown in Figure 3.37.
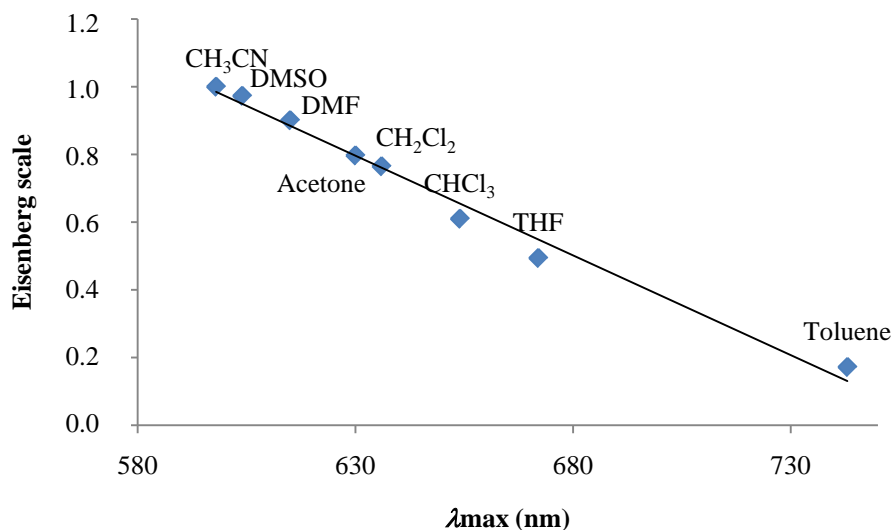
Figure 3.37. *Correlation between absorption wavelengths λ_{max} in different solvents for complex **53** and the empirical scale formulated by Eisenberg for [Pt(N^N)(S^S)] complexes ($R^2 = 0.99$; Ref. 127; Table 3.29).*

Moreover, the analysis of the absorption spectra of complexes **53-72** in a single solvent shows that the λ_{max} value of the absorption in the visible region depends on the nature of the ligands. In particular, the examination of λ_{max} in the absorption spectra registered in DMSO for the complexes belonging to Series 1, differing in the nature of the dichalcogenolate (Scheme 3.6), can give an insight into the dependence of this value on the nature of the E^E ligand (Figure 3.38). Complexes bearing a Ar,H-edt^{2-} ligand (**53-55**) feature the solvatochromic absorption band at wavelength values systematically longer than corresponding complexes featuring a R-dmet^{2-}/R-dset^{2-} ligand (**56-59**), suggesting that the HOMO-LUMO energy gap is smaller for the complexes featuring the former type of E^E ligands as compared to those featuring the latter. Within the complexes bearing a Ar,H-edt^{2-} ligand, **55** (Ar = Pyr) shows the shorter λ_{max}, while no remarkable differences in the position of the absorption band can be found between **53** and **54** (Ar = Ph and Naph, respectively). In the series **56-59**, the complex bearing Me-

dset^{2-} shows a lower value of λ_{max} with respect to all the complexes featuring R-dmet^{2-} ligands (Figure 3.38, Table 3.29).
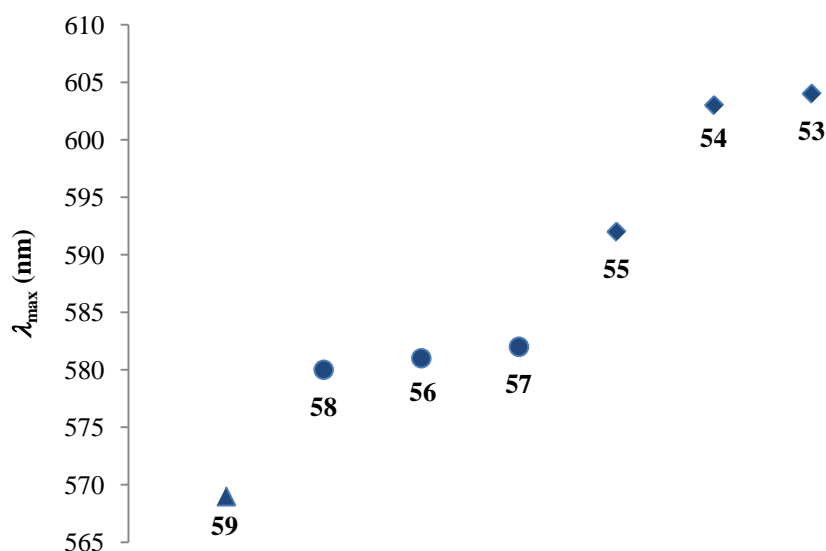
Figure 3.38. *Wavelength of the solvatochromic absorption band (nm, Table 3.29) in DMSO for complexes 53-59 (Series 1, Scheme 3.6). N^N = 2,2'-bipy; E^E = Ar,H-edt^{2-} (rhombs), R-dmet^{2-} (circles), Me-dset^{2-} (triangle).*

Similar considerations can be drawn for Series 2 (Scheme 3.7), while an examination of absorption spectra of the complexes belonging to Series 3 (Scheme 3.8) in DMSO, shows that the replacement of a 2,2′-bipyridine ligand with a 1,10-phenanthroline does not induce significant changes in the position of the solvatochromic absorption band (complexes **56-63** in Figure 3.39). A comparison of the λ_{max} value in complexes bearing differently substituted 2,2′-bipyridine and 1,10-phenanthroline ligands (blue and red symbols, respectively in Figure 3.39) suggests that the introduction of alkyl substituents in the diimine ligand causes a shift of the absorption band to higher energies, while the presence of a phenyl group induces the opposite effect, thus lowering the energy of the HOMO-LUMO energy gap (Figure 3.39, Table 3.29).
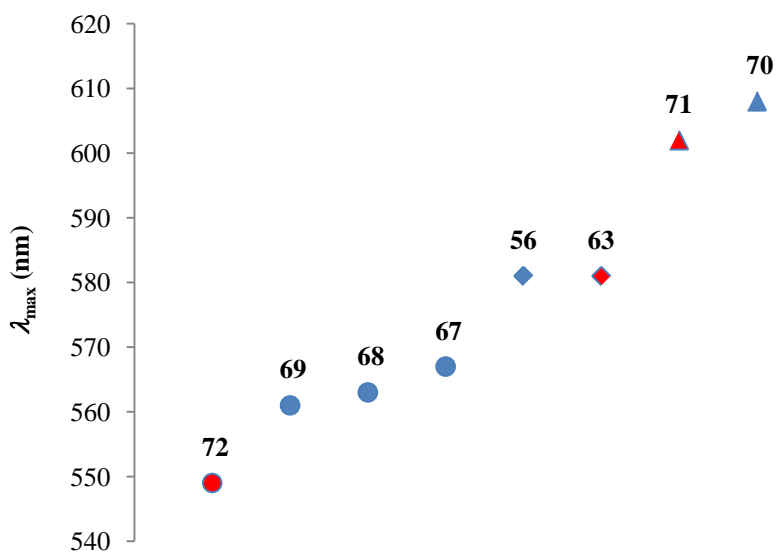
Figure 3.39. *Wavelength of the solvatochromic absorption band (nm) in DMSO (Table 3.29) for complexes 56, 63 and 67-72 (Series 3, Table 3.8). S^S = Me-dmet^{2-}; N^N = unsubstituted (rhombs) 2,2'-bipyridine (blue) or 1,10-phenanthroline (red) and alkyl (circles) or phenyl (triangles) derivatives.*

Since both the electrochemical data and the energy of the solvatochromic absorption band depend upon the HOMO and LUMO eigenvalues, the two sets of data have been compared.

Interestingly, a linear correlation holds between the position of the solvatochromic absorption band and the redox potentials for complexes **53-72**.

In particular, considering Series 1 (Scheme 3.6), a linear correlation ($R^2 = 0.93$) was found between the λ_{max} of the absorption and the oxidation potential $E_{1/2}^{(+1/0)}$ (Tables 3.27 and 3.29; Figure 3.40). Complexes bearing a R-dmet^{2-}/R-dset^{2-} ligand (**56-59**) feature the oxidation potentials and the λ_{max} value at more positive potentials and lower wavelengths, respectively, with respect to complexes featuring a Ar,H-edt^{2-} ligand (**53-55**), as shown in Figure 3.40. This suggests that the introduction of a R-dmet^{2-}/R-dset^{2-} ligand in place of a Ar,H-edt^{2-} dithiolene has the effect of lowering the energy of the

HOMO, and thus increasing the entity of the HOMO-LUMO energy gap. Concerning complexes **53-55**, the ligand bearing a pyrenyl substituent (featured by complex **55**) lowers the energy of the HOMO with respect to corresponding phenyl- and naphthyl-substituted systems (**53** and **54**, respectively). The replacement of S with Se as chelating atom in the 1,2-dichalcogenolene ligand has the same effect of lowering the energy of the HOMO, as shown by a comparison between **56** and **59** (Figure 3.40).
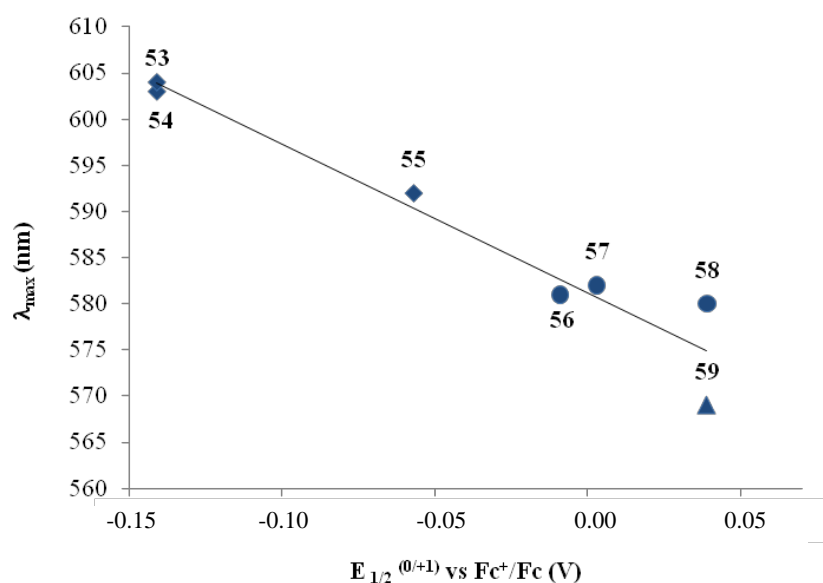
Figure 3.40. *Correlation between the $E_{1/2}^{(+1/0)}$ oxidation potentials (V vs Fc^+/Fc) and the λ_{max} of the solvatochromic absorption (nm) in complexes **53-59** (Scheme 3.6), belonging to Series 1 ($R^2 =0.93$; Tables 3.27 and 3.29). N^N = 2,2'-bipyridine; E^E = Ar,H-edt^{2-} (rhombs), R-dmet^{2-} (circles), and Me-dset^{2-} (triangle).*

On passing to Series 3 (Scheme 3.8), a linear correlation ($R^2 = 0.91$) can be found between the λ_{max} values of the solvatochromic absorption and the reduction potentials $E_{1/2}^{(0/-1)}$. In particular, considering the complexes bearing differently substituted 2,2'-bipyridine or 1,10-phenanthroline ligands (blue and red symbols, respectively, in Figure 3.41), the introduction of phenyl substituents in the diimine induces a lowering in the

energy of the solvatochromic absorption band and shifts the reduction potentials $E_{1/2}{}^{(0/-1)}$ to more negative values with respect to unsubstituted system, while alkyl substituents show the opposite effect. This suggests that the presence of phenyl, or more generally aryl, substituents at the diimine lowers the energy of the LUMO and thus of the HOMO-LUMO energy gap with respect to complexes bearing the corresponding unsubstituted nitrogen ligands, while the presence of alkyl groups increases the energy gap.
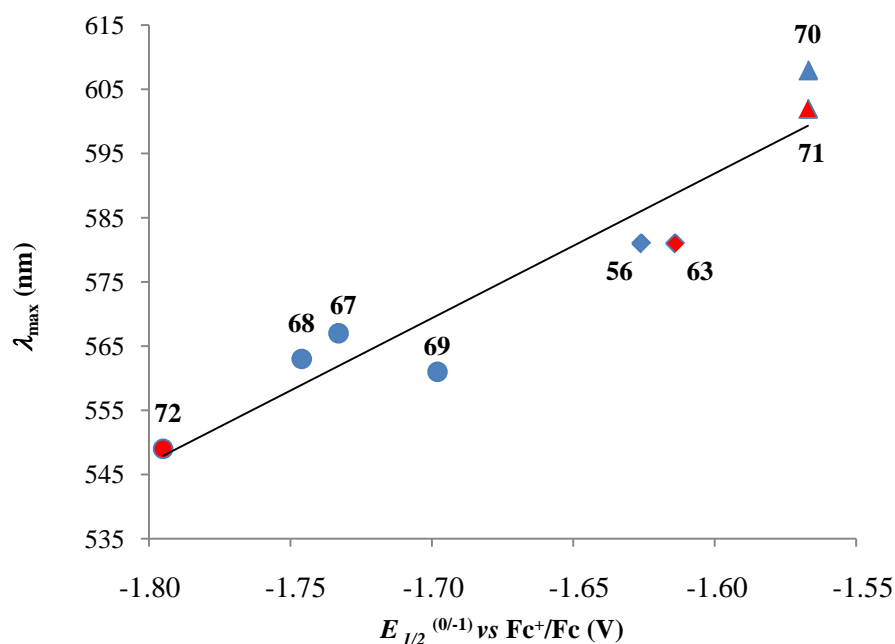
Figure 3.41. *Correlation between λ_{max} value of the solvatochromic absorption band (nm) and the reduction potentials $E_{1/2}{}^{(0/-1)}$ (V vs Fc$^+$/Fc) for complexes **56**, **63**, and **67-72** (Scheme 3.8), belonging to Series 3 ($R^2 = 0.91$; Tables 3.27 and 3.29). S^S = Me-dmet^{2-}; N^N = unsubstituted (rhombs) 2,2'-bipyridine (blue) or 1,10-phenanthroline (red) and alkyl (circles) or phenyl (triangles) derivatives.*

Finally, compound **73**, not included in Series 1-3, features the expected solvatochromic Vis absorption in the range 600-680 nm (Table 3.29), depending on the solvent. This notwithstanding, the spectral shape of the UV-Vis-NIR spectrum shows features quite

different from those of the other complexes, inducing to deepen the investigation by means of spectroelectrochemical measurements.

3.2.1.5. Spectroelectrochemical measurements

In order to get an insight into the nature of redox processes in complex **73**, spectroelectrochemical measurements were performed at the University of Sheffield, where the complex was synthesised, using an optically transparent thin-layer electrode (OTTLE) cell. In particular, in order to determine which of the two oxidation processes featured by **73** (Figure 3.33) is due to the ferrocenyl substituent, spectroelectrochemical measurements were performed on **73** and, for the sake of comparison, **53** (Ar = Ph). For these measurements, solutions of the two complexes and $(TBA^+)(PF_6^-)$ 0.1 M in CH_2Cl_2 were prepared, and the potentials corresponding to the first oxidation waves (Table 3.27) were applied (Figure 3.42 for **73**).

During the oxidation, both complexes underwent an increase in the absorption at about 380 nm accompanied by a progressive disappearing of the band at 600 nm, thus suggesting that the investigated redox process has the same nature for both complexes. Thus, for **73** this oxidation can be assigned to the [Pt(diimine)(dithiolate)] system as previously proposed, while the second one is due to the ferrocenyl pendant.
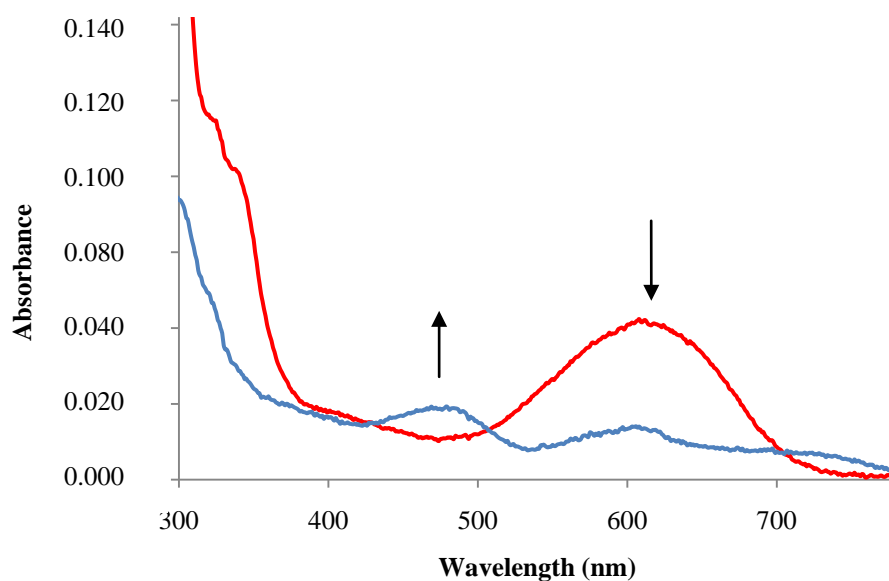
Figure 3.42. *Absorption spectra of the neutral (red) and cationic (blue) form of **73**, obtained at the beginning and the end, respectively, of a OTTLE spectroelectrochemical measurement recorded in CH$_2$Cl$_2$ at 0.216 V vs Fc$^+$/Fc [298 K; scan rate 100 mV s^{-1}; supporting electrolyte (TBA$^+$)(PF$_6^-$) 0.1 M].*

3.2.1.6. Emission Spectroscopy

As mentioned in Section 1.3.2.3, [Pt(N^N)(S^S)] complexes are fluorescent in solution, as reported by Eisenberg and collaborators.[127,150a,217] In particular, these authors reported that excitation in the range 350-500 nm resulted in a complex emission profile in the Vis region, with emission maxima in the range 500-800 nm. The energy and intensity of this emission could be tuned by varying the ligands, the temperature, or the solvent, and the process was attributed to a MMLL′CT.

Thus, fluorescence measurements were carried out at room temperature in DMSO on **53-54**, **56-61** and **63-73**, at concentrations ranging between $3 \cdot 10^{-7}$ and $3 \cdot 10^{-5}$ M. Measurements could not be performed on **55** and **62**, due to the scarce purity of the complexes.

All complexes were investigated by recording emission spectra obtained at excitation wavelengths corresponding to the absorption maxima observed from UV-Vis

spectroscopy measurements (Section 3.2.1.4), and thus in the range λ_{exc} = 260-600 nm, but emissive processes were observed just upon excitation in the UV region. Very similar emission features were observed for all complexes, and in particular excitation in the range λ_{exc} = 260-350 nm resulted in an emission profile in the UV-Vis region (350-450 nm), with quantum yields Φ ranging between $6 \cdot 10^{-3}$ and $3 \cdot 10^{-2}$ (Table 3.30). As an example, the absorption and the fluorescence spectra recorded for **53** are compared in Figure 3.43.
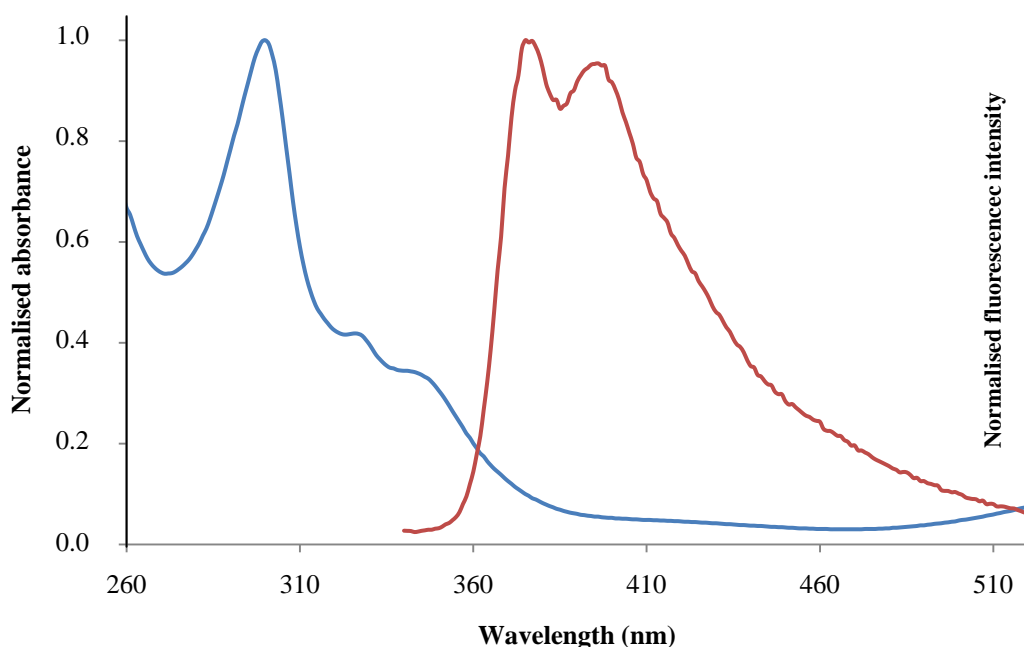
Figure 3.43. *Superimposed normalised UV-Vis (260-520 nm) absorption (blue line) and emission (red line; λ_{exc} = 327 nm) spectra recorded for **53** in DMSO solution.*

A dependence of the fluorescence intensity I_f on the concentration C of the solution was observed, the value of I_f decreasing when $C > 1 \cdot 10^{-6}$ M (Figure 3.44 for **53**), possibly due to self-quenching processes similar to those previously observed for different [Pt(N^N)(S^S)] complexes.[154]
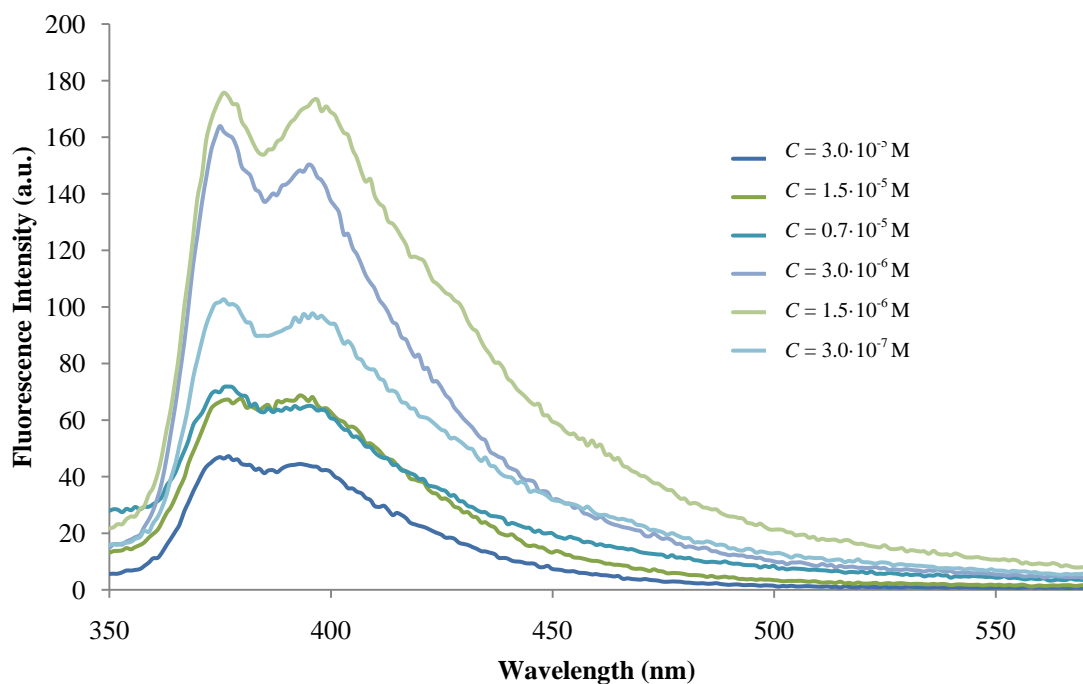
Figure 3.44. *Emission spectra recorded for **53** in DMSO solutions with different concentrations ($3 \cdot 10^{-7}$-$3 \cdot 10^{-5}$ M; λ_{exc} = 299 m).*

The emission spectra show approximately the same profile for all complexes, with two emission maxima at about 370 and 390 nm, respectively, suggesting the processes leading to the emission should have the same nature for all the compounds.[218] Interestingly, the emission energy is not affected by the nature of the ligand, while the fluorescence intensity varies upon changing both the diimine and the 1,2-dichalcogenolene ligand.
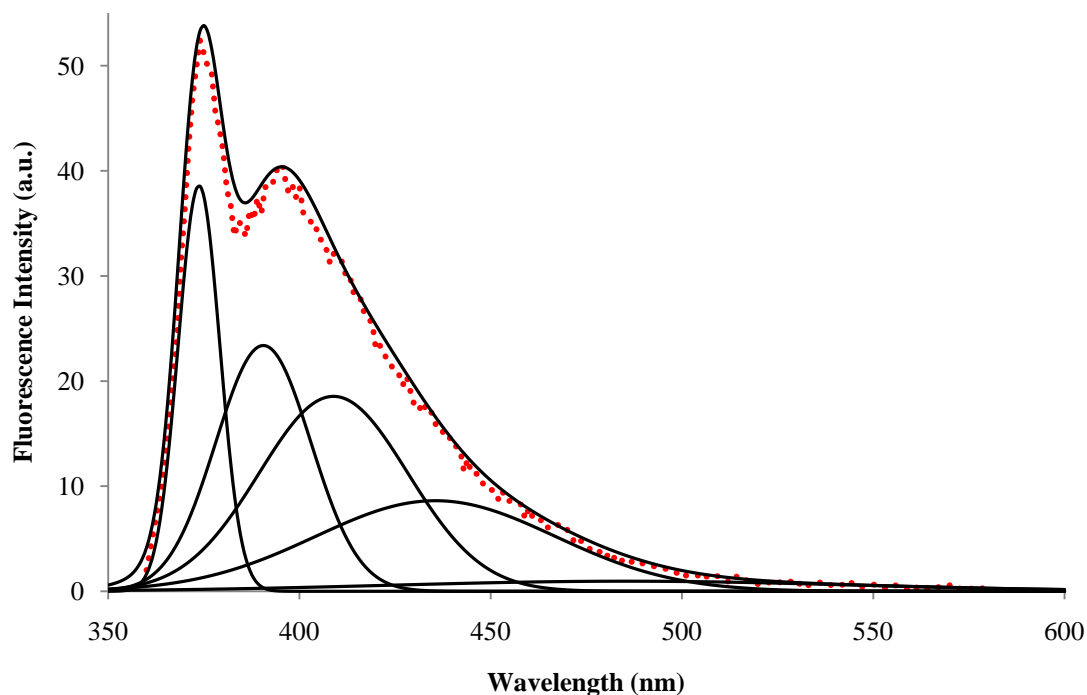
Figure 3.45. *Emission spectrum recorded for **70** in DMSO solution (dotted line) decomposed into five constituent Gaussian curves (Table 3.30; C = 3·10^{-6} M, λ_{exc} = 350 nm.).*

In fact, an examination of fluorescence quantum yields Φ, determined for all complexes relative to anthracene in ethyl alcohol (C = 1-5·10^{-6}; λ_{exc} = 334-359 nm) by calculating the integrated emission intensity of both the sample and the reference through a decomposition of the spectra in their constituents Gaussian curves (Table 3.30; Figure 3.45 for **70**), shows that for complexes **60**, **61** and **63-66** (Series 2, Scheme 3.7), featuring a 1,10-phenanthroline ligand, the fluorescence intensity is systematically larger than in corresponding complexes bearing a 2,2-bipyridine (**53**, **54** and **56-59**, Series 1; Scheme 3.6).[219]

Table 3.30. *Results from the decomposition of the DMSO solution fluorescence spectra (300-600 nm) recorded for* **53-73** *in five constituent Gaussian components, and relative quantum yields (Φ). Each curve is described in terms of wavelength position (λ, nm), full width at half maxima (w, nm) and relative intensity (h).*

	λ_1	λ_2	λ_3	λ_4	λ_5	w_1	w_2	w_3	w_4	w_5	h_1	h_2	h_3	h_4	h_5	Φ
53	374.2	406	394.4	424.9	461.4	18.8	15.7	17.3	46.1	237.8	17.2	13.1	12.9	7.3	0.18	$8.4 \cdot 10^{-3}$
54	399.9	433	399.8	373.5	429.3	226.1	76.4	30.8	16.4	25.7	1.7	5.1	14.5	14.9	3.38	$1.1 \cdot 10^{-2}$
56	374	390.5	411.4	438.5	479.6	11	36.7	55.5	95.8	240	27.5	22.6	15.2	5.2	1.29	$1.8 \cdot 10^{-2}$
57	376.2	397.5	425.9	429.3	447	16.8	34.6	25.8	70.6	234.3	15.6	12.8	2.6	3.9	0.94	$7.2 \cdot 10^{-3}$
58	372	549.6	420.6	472.6	704.3	14.2	45.4	74.4	137.2	311	14.8	45.4	6.9	1.3	0.29	$1.2 \cdot 10^{-2}$
59	376.7	395	400.9	426.9	474.6	14.9	13.3	48.6	81.3	177.7	13.5	3.6	8.4	4.1	0.68	$8.2 \cdot 10^{-3}$
60	373.6	404.5	423.2	382.4	447.8	8.9	32	24.3	16.8	16.1	16.5	37.2	15	15.7	2.3	$1.3 \cdot 10^{-2}$
61	376.1	402	431.2	426.9	448.6	21	30.4	20.3	81.6	195.5	21	22.9	5	9.5	1.58	$1.5 \cdot 10^{-2}$
63	374.4	404	425.8	431.6	444.6	10.4	18.6	20.6	74.1	149.2	14.1	33.8	22.6	35.7	5.44	$3.2 \cdot 10^{-2}$
64	375.7	390.9	403.7	433.8	486.4	15.5	10	46.5	79.4	153.2	6.3	5.2	7.3	4.8	0.92	$9.1 \cdot 10^{-3}$
65	374.3	403	429.3	423.2	442.2	10.9	31.1	17.2	86	190.5	19.1	21.6	10.2	28.5	2.91	$2.8 \cdot 10^{-2}$
66	410.4	436	464.7	471.9	391.2	26.3	31.7	24.9	61.3	15	22.7	20.5	5.4	5.7	5.43	$1.2 \cdot 10^{-2}$
67	373.6	394.4	422.1	461.3	541.5	19.6	33	52.1	94.7	155	13.6	9.5	6.9	2.6	0.65	$8.8 \cdot 10^{-3}$
68	375.1	398.8	423.4	449.2	501.5	23	33.5	42	75.8	144.9	17.2	12.9	6.9	4.9	1.69	$1.1 \cdot 10^{-2}$
69	374.7	392.4	414.9	448.3	507.3	17.5	31.9	47.3	80.5	142.3	19	13.8	11	6.6	2.26	$1.5 \cdot 10^{-2}$
70	373.7	390.5	408.9	435.5	485.2	12.9	29.3	45.8	73.7	143.8	38.6	23.4	18.5	8.6	0.97	$1.8 \cdot 10^{-2}$
71	373.5	393.4	418.6	453.4	412.9	12.3	31.3	55.5	103.1	10.6	41.1	29	17.4	3.8	2.51	$1.8 \cdot 10^{-2}$
72	383.9	409.8	428.3	449.2	448.7	30.2	19.3	30.1	62.3	209.6	7	3.6	2.6	2	0.86	$6.4 \cdot 10^{-3}$
73	373.3	392.2	405.6	426.8	451	10.3	7.4	55.2	95.8	184.8	4.8	4.1	8.4	10.3	2.67	$1.4 \cdot 10^{-2}$

3.2.1.7. DFT calculations

As mentioned in Section 1.3.2.3, the use of DFT as a tool for investigating the electronic structure of diimine-dithiolate complexes and identifying charge-transfer transitions was recently reviewed.[152] This notwithstanding, the availability of a complete set of structural, spectroscopic and electrochemical data for twenty-one completely new [Pt(N^N)(E^E)] complexes synthesised and characterised in this work represented a challenging opportunity to investigate in-depth the electronic features of this class of compounds at DFT[195] level.

In order to determine an appropriate computational setup for this class of complexes, preliminary calculations were performed on **56**, by adopting different functionals (both pure and hybrid) and various basis sets for the platinum atom (all featuring effective core potentials to account for relativistic effects),[200] while the all-electron double-ζ basis sets (BSs) with polarisation functions from Schäfer, Horn, and Ahlrichs[199] were exploited for light atomic species (C, H, N, S, Se, and Fe). The comparison between the optimised geometries obtained with different combinations of functionals and basis sets on the Pt atom, and the crystal structure of complex **57** (differing from **56** just for the presence of an ethyl in place of a methyl at the 1,2-dithiolene fragment), and between the simulated and experimental electronic spectra of **56**, allowed for identifying the best computational setup for these systems. Neglecting here the details of this setup, summarised in Annex A, the calculated data in best agreement with the experimental ones were obtained by adopting the hybrid PBE0 (PBE1PBE) functional by Adamo and Barone,[220] and the CRENBL+ECP basis set,[221] and therefore this computational setup was adopted for all the complexes included in this theoretical study. Moreover, given the solvent-dependence of some features of these complexes (see above), implicit solvation calculations were also carried out at the same level of theory, by using the

pure integral equation formalism of the polarisable continuous model (IEF-PCM) within

the Self Consistent Reaction Field (SCRF) approach.[222]

3.2.1.7.1. Geometry Optimisation

The geometry of complexes **53-73** were optimised both in the gas phase and under the

effect of the electric field of dichloromethane, modelled by using the IEF-PCM model

of SCRF theory. As an example, the optimised geometry of **53** in the gas phase is

depicted in Figure 3.46.
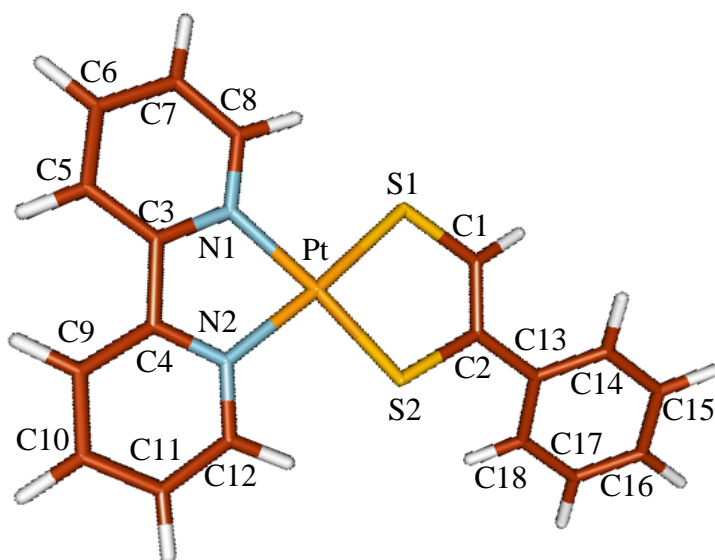
Figure 3.46. *Molecular drawing and atom labeling scheme of* **53** *at the optimised geometry in the gas phase.*

Selected optimised bond lengths and angles for the twenty-one model compounds in the

gas phase and in CH_2Cl_2 are listed in Table 3.31, and show that, in the presence of the

solvent, the structural parameters are affected by small variations (usually smaller than

0.02 Å and 1° for distances and angles, respectively) with respect to the ones optimised

in the gas phase. In particular, in the presence of the solvent a lengthening of Pt-E, Pt-N,

and E-C distances occurs (E = S, Se). A comparison of the gas-phase optimised parameters with the corresponding structural data determined by single crystal X-ray diffraction for **57-59**, **64**, **67** and **69**, discussed in Section 3.2.1.2, shows a very good agreement between the two sets of data, only the Pt-E (E = S, Se) distances being slightly overestimated (by less than 0.08 Å, Table 3.31). Moreover, a very good agreement was found between the average optimised bond lengths and angles for the sulphured model complexes (**54-58**, **60-65**, and **67-73**) and corresponding experimental mean values found for the crystal structures of the [Pt(N^N)(S^S)] complexes reported so far (Section 1.3.2.2), as summarised in Table 3.32.

Table 3.31. *Selected optimised bond lengths (Å) and angles (°) for complexes 53-73[a] in the gas phase and in CH$_2$Cl$_2$ (in parentheses).[b] Numbering scheme as in Figure 3.22.*

	Pt-E1	Pt-E2	Pt-N1	Pt-N2	E1-C1	E2-C2	C1-C2	E1-Pt-E2	N1-Pt-N2	N1-Pt-E1-C2	C1-C2-C13-C14
53	2.263 (2.276)	2.262 (2.277)	2.046 (2.056)	2.045 (2.056)	1.729 (1.738)	1.758 (1.769)	1.357 (1.355)	88.18 (88.21)	79.19 (79.21)	179.9 (179.6)	28.87 (24.72)
54	2.263 (2.277)	2.263 (2.263)	2.046 (2.056)	2.046 (2.056)	1.729 (1.738)	1.758 (1.769)	1.357 (1.357)	88.20 (88.20)	79.21 (79.21)	179.84 (179.85)	31.0 (27.86)
55	2.264 (2.277)	2.262 (2.277)	2.047 (2.055)	2.046 (2.055)	1.733 (1.742)	1.759 (1.769)	1.354 (1.352)	88.33 (88.31)	79.19 (79.20)	179.60 (179.41)	57.41 (55.15)
56	2.284 (2.299)	2.280 (2.298)	2.041 (2.051)	2.039 (2.049)	1.738 (1.744)	1.731 (1.740)	1.363 (1.361)	90.13 (90.38)	79.58 (79.56)	180.00 (180.00)	/
57	2.284 (2.299)	2.281 (2.299)	2.041 (2.051)	2.040 (2.049)	1.738 (1.745)	1.731 (1.739)	1.363 (1.360)	90.18 (90.44)	79.58 (79.58)	179.83 (179.34)	/
58	2.283 (2.299)	2.280 (2.299)	2.042 (2.051)	2.042 (2.050)	1.738 (1.742)	1.731 (1.739)	1.361 (1.359)	90.26 (90.56)	79.53 (79.58)	179.44 (179.55)	/
59	2.387 (2.401)	2.385 (2.401)	2.059 (2.051)	2.058 (2.050)	1.880 (1.887)	1.871 (1.879)	1.359 (1.358)	90.71 (90.97)	79.20 (79.21)	180.00 (180.00)	/
60	2.261 (2.274)	2.260 (2.274)	2.054 (2.063)	2.053 (2.064)	1.731 (1.739)	1.759 (1.770)	1.356 (1.355)	88.57 (88.89)	80.03 (80.02)	179.72 (179.88)	28.83 (25.08)
61	2.261 (2.275)	2.260 (2.275)	2.054 (2.063)	2.053 (2.063)	1.730 (1.738)	1.760 (1.770)	1.357 (1.355)	88.60 (88.60)	80.03 (80.02)	179.61 (179.93)	31.10 (27.96)
62	2.262 (2.276)	2.260 (2.274)	2.055 (2.063)	2.054 (2.063)	1.735 (1.743)	1.761 (1.771)	1.354 (1.352)	88.72 (88.70)	80.00 (80.01)	179.73 (179.75)	56.60 (54.07)
63	2.282 (2.296)	2.279 (2.296)	2.049 (2.059)	2.048 (2.058)	1.738 (1.744)	1.732 (1.740)	1.362 (1.360)	90.64 (90.89)	80.39 (80.35)	179.99 (179.99)	/
64	2.284 (2.296)	2.281 (2.296)	2.041 (2.059)	2.040 (2.056)	1.738 (1.746)	1.740 (1.740)	1.361 (1.361)	90.85 (90.85)	80.35 (80.39)	179.83 (179.22)	/
65	2.280 (2.297)	2.278 (2.296)	2.050 (2.059)	2.050 (2.057)	1.740 (1.743)	1.733 (1.740)	1.361 (1.359)	90.69 (90.96)	80.35 (80.37)	179.61 (179.91)	/
66	2.385 (2.398)	2.382 (2.398)	2.066 (2.075)	2.064 (2.072)	1.881 (1.888)	1.872 (1.880)	1.359 (1.358)	91.12 (91.38)	79.97 (79.97)	180.00 (180.00)	/
67	2.286 (2.398)	2.282 (2.398)	2.044 (2.054)	2.042 (2.050)	1.739 (1.745)	1.733 (1.740)	1.362 (1.361)	90.17 (90.39)	79.60 (79.60)	180.00 (180.00)	/
68	2.285 (2.300)	2.282 (2.299)	2.044 (2.051)	2.042 (2.049)	1.740 (1.745)	1.734 (1.740)	1.361 (1.361)	90.24 (90.45)	79.39 (79.46)	180.00 (180.00)	/
69	2.286 (2.300)	2.283 (2.299)	2.043 (2.051)	2.041 (2.049)	1.740 (1.745)	1.734 (1.740)	1.361 (1.361)	90.30 (90.45)	79.38 (79.42)	180.00 (180.00)	/
70	2.285 (2.299)	2.282 (2.299)	2.040 (2.048)	2.038 (2.047)	1.738 (1.743)	1.731 (1.739)	1.363 (1.360)	90.16 (90.51)	79.44 (79.44)	179.49 (178.85)	/
71	2.284 (2.298)	2.280 (2.297)	2.045 (2.053)	2.043 (2.051)	1.740 (1.744)	1.733 (1.740)	1.362 (1.360)	90.46 (90.78)	79.93 (79.91)	179.23 (179.41)	/
72	2.285 (2.300)	2.282 (2.299)	2.051 (2.058)	2.049 (2.057)	1.741 (1.745)	1.735 (1.740)	1.360 (1.360)	90.75 (90.89)	79.98 (80.02)	180.00 (179.99)	/
73	2.265 (2.279)	2.265 (2.279)	2.047 (2.055)	2.046 (2.055)	1.734 (1.743)	1.760 (1.768)	1.354 (1.353)	88.35 (88.35)	78.99 (79.03)	179.83 (179.82)	21.21 (20.44)

[a] E = S (**53-58, 60-65, 67-73**), Se (**59, 66**). [b] IEF-PCM SCRF model.

162

Table 3.32. *Selected experimental and optimised average bond distances (Å) and angles (°) for [Pt(N^N)(S^S)] complexes.*

	Pt-E	Pt-N	E-C	C-C	S-Pt-S	N-Pt-N
Experimental[a]	2.256 (14)	2.046(10)	1.744(23)	1.373(41)	89.38(8)	79.22(8)
Optimised[b]	2.275	2.046	1.739	1.360	89.64	79.65

[a] Mean values on 26 crystal structures deposited at the CCDC; [b] Mean values of the optimised parameters calculated for complexes **53-58**, **60-65**, and **67-73**.

As found experimentally, the optimised geometries of complexes **53-73** show the metal coordinated in a square-planar fashion, with the complexes completely planar but for the substituents (Figure 3.46 and Table 3.31). For complexes **53-55** and **60-62**, the torsion angles of the aromatic substituents at the 1,2-dithiolene ligand (dihedral angle C1-C2-C13-C14 in Figure 3.46) range between 28 and 57° depending on the nature of the aryl group [in agreement with what found for gold *bis*(1,2-dithiolene) complexes **20-22**, bearing the same ligands, Section 3.1.6.1], and undergo a reduction of about 2° when calculations are performed under the electrostatic field of CH_2Cl_2 (Table 3.31). Complexes **59** and **66**, featuring the Me-dset^{2-} ligand, show Pt-E and C-E distances longer (by about 0.1 and 0.12 Å, respectively, both in the gas phase and in CH_2Cl_2) with respect to corresponding sulphured complexes **56** and **63**, in agreement with structural data, due to the larger size of Se compared to S (Table 3.31). According to what found experimentally for complexes **57** and **64**, all the compounds featuring a 2,2′-bipyridine ligand show optimised Pt-S and Pt-N bond lengths systematically longer and shorter, respectively, than those of complexes bearing a 1,10-phenanthroline, both in the gas phase and in CH_2Cl_2 (Table 3.31). Moreover, focusing on Series 3 (Scheme 3.8), in complexes with aryl- and alkyl-substituted N^N ligands, the Pt-N distances are shorter and longer, respectively, than in unsubstituted systems.

As far as complexes **53-58** are regarded, a dependence of the bond lengths at the coordination core on the nature of the 1,2-dithiolene ligand can be observed, being Pt-S and Pt-N distances systematically longer and shorter, respectively, for complexes featuring a Ar,H-edt^{2-} ligand than for the ones with a R-dmet^{2-} system (Table 3.31 and Figure 3.47 for calculations performed in the gas phase).
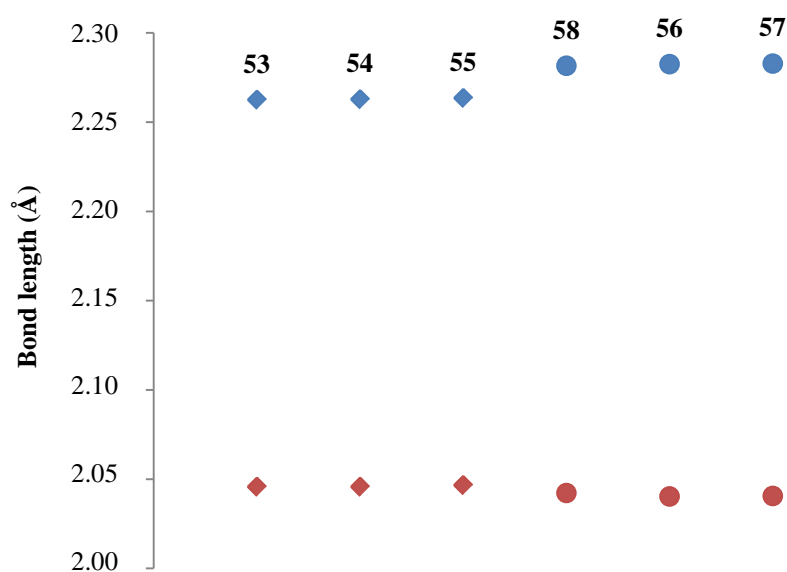
Figure 3.47. *Optimised Pt-S (blue) and Pt-N (red) distances (Å) for complexes 53-58 in the gas phase (Table 3.31). N^N = 2,2'-bipyridine; S^S = Ar,H-edt^{2-} (rhombs) or R-dmet^{2-} (circles).*

Complex **73** features optimised parameters very similar to those of **53-55** (Table 3.31). In order to get a deeper insight into the dependence of the complexes' features on the nature of the solvent, solvation DFT calculations were performed on **56** at the same level of theory discussed above, simulating the seven other solvents adopted for absorption spectroscopy measurements (Table 3.29), namely $CHCl_3$, CH_3CN, acetone, THF, DMF, DMSO, and toluene. As summarised in Table 3.33, optimised parameters vary only slightly upon changing the solvent, the Pt-S distances being the most affected (by only 0.01 Å), and showing the largest values in DMSO and DMF.

Table 3.33. *Selected optimised bond lengths (Å) and angles (°) for complex **56** in different solvents.*[a,b]

	CH_2Cl_2	$CHCl_3$	CH_3CN	Acetone	THF	DMF	DMSO	Toluene
Pt-S1	2.299	2.297	2.301	2.301	2.299	2.301	2.302	2.292
Pt-S2	2.298	2.296	2.300	2.300	2.298	2.300	2.301	2.292
Pt-N1	2.051	2.050	2.052	2.052	2.051	2.052	2.052	2.048
Pt-N2	2.049	2.048	2.050	2.050	2.049	2.050	2.049	2.045
S1-C1	1.744	1.744	1.744	1.744	1.744	1.745	1.745	1.742
S2-C2	1.740	1.739	1.740	1.740	1.739	1.740	1.740	1.737
C1-C2	1.361	1.360	1.361	1.361	1.361	1.361	1.361	1.360
S1-Pt-S2	90.38	90.38	90.38	90.37	90.38	90.38	90.39	90.31
N1-Pt-N2	79.56	79.56	79.57	79.58	79.57	79.57	79.59	79.55
N1-Pt-S1-C2	180.00	180.00	180.00	180.00	180.00	180.00	180.00	180.00

[a] IEF-PCM SCRF model. [b] Atom labeling scheme as in Figure 3.46.

3.2.1.7.2. Ground State (GS)

The description of the ground-state (GS) bonding scheme of **53-73** based on DFT calculations is in agreement with results of previous calculations carried out on [Pt(N^N)(S^S)] complexes.[152] In Figure 3.48, the frontier KS-MO scheme calculated in the gas phase for **56** is depicted, while in Figure 3.49 the contributions from the central platinum atom and the two ligands to the composition of each MO are summarised.
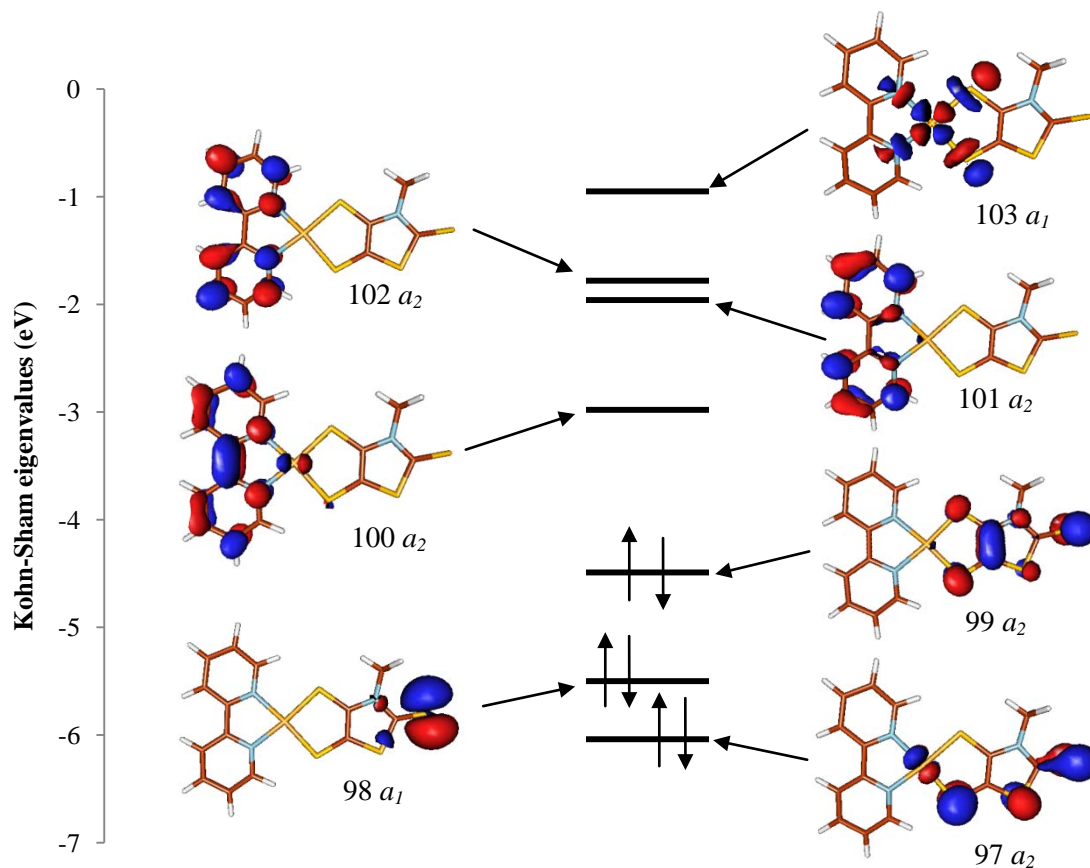
Figure 3.48. *KS-MO scheme and isosurface drawings calculated for **56** in the gas phase (C_s point group). Contour value = 0.05 e.*

Accordingly to what reported in the literature,[152] the highest occupied molecular orbital (orbital 99 in Figures 3.48 and 3.49), is a π MO predominantly localised on the S^S ligand, with only a minor participation of Pt $5d$ character (3%), while the LUMO (orbital 100 in Figures 3.48 and 3.49) is calculated to be almost exclusively located on the diimine, with a contribution of the metal similar to that observed for the HOMO (6%).
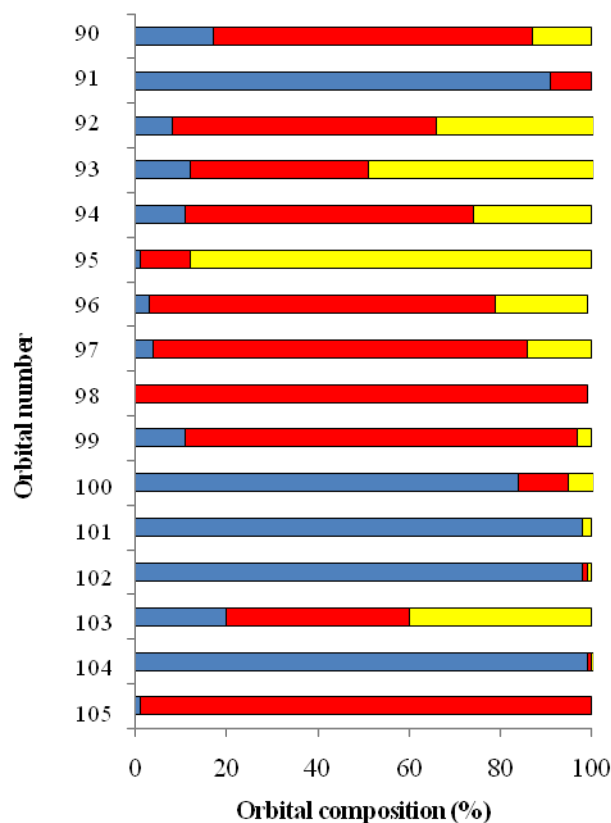
Figure 3.49. *Frontier molecular orbital (KS-MOs 90-105; HOMO = 99, LUMO = 100) composition calculated for 56 in the gas phase [fragments: platinum atom (yellow); S^S ligand (red); N^N ligand (blue)].*

As summarised in Table 3.34 for calculations performed in the gas phase, no significant differences can be found in the composition of frontier MOs for the twenty-one complexes studied. As concerns Series 1 (complexes **53-59**, Scheme 3.6), including complexes all featuring the same N^N ligand and differing in the nature of the E^E one, the LUMO composition is roughly the same for all complexes, while the HOMO undergoes slight changes upon varying the 1,2-dichalcogenolene ligand.

Table 3.34. *Calculated eigenvalues E (eV) and composition (%) of frontier KS-MOs for complexes **53-73** in the gas phase in terms of the central Pt atom and of the N^N and E^E ligands.*

		E	N^N	E^E	Pt
53	HOMO	-4.47	14	79	6
	LUMO	-2.64	83	10	6
54	HOMO	-4.86	14	80	6
	LUMO	-2.54	84	10	6
55	HOMO	-4.57	14	79	7
	LUMO	-2.69	84	10	6
56	HOMO	-4.49	11	86	3
	LUMO	-2.98	84	11	6
57	HOMO	-4.48	11	86	3
	LUMO	-2.98	84	11	6
58	HOMO	-4.49	11	86	3
	LUMO	-2.96	84	10	6
59	HOMO	-4.57	10	88	3
	LUMO	-3.02	85	9	6
60	HOMO	-4.44	14	80	6
	LUMO	-2.61	84	10	7
61	HOMO	-4.47	13	80	6
	LUMO	-2.64	84	9	6
62	HOMO	-4.53	13	80	7
	LUMO	-2.64	84	9	6
63	HOMO	-4.43	11	87	3
	LUMO	-2.93	84	10	6
64	HOMO	-4.44	10	87	3
	LUMO	-2.94	84	10	6
65	HOMO	-4.45	10	87	3
	LUMO	-2.91	85	9	6
66	HOMO	-4.53	9	88	3
	LUMO	-2.97	86	9	6
67	HOMO	-4.37	10	87	3
	LUMO	-2.80	85	9	6
68	HOMO	-4.33	10	87	3
	LUMO	-2.78	86	9	5
69	HOMO	-4.49	11	86	3
	LUMO	-2.98	84	11	6
70	HOMO	-4.39	12	86	3
	LUMO	-2.92	83	11	6
71	HOMO	-4.34	10	87	3
	LUMO	-2.84	85	9	6
72	HOMO	-4.20	8	89	3
	LUMO	-2.66	99	0	1
73	HOMO	-4.24	12	82	6
	LUMO	-2.38	86	8	5

Table 3.35. *Calculated eigenvalues E (eV) and composition (%) of frontier MOs for complexes **53-73** in CH₂Cl₂ in terms of the central Pt atom and of the N^N and E^E ligands.*

		E	N^N	E^E	Pt
53	HOMO	-4.87	7	84	9
	LUMO	-2.54	91	4	5
54	HOMO	-4.50	7	84	9
	LUMO	-2.68	91	4	5
55	HOMO	-4.91	7	83	10
	LUMO	-2.54	91	4	5
56	HOMO	-4.90	5	90	5
	LUMO	-2.68	92	3	4
57	HOMO	-4.89	5	90	5
	LUMO	-2.68	92	3	4
58	HOMO	-4.90	5	90	5
	LUMO	-2.67	92	3	4
59	HOMO	-5.00	4	91	5
	LUMO	-2.69	93	3	4
60	HOMO	-4.86	7	84	9
	LUMO	-2.50	92	4	5
61	HOMO	-4.87	7	84	9
	LUMO	-2.54	92	4	5
62	HOMO	-4.53	13	80	7
	LUMO	-2.64	84	9	6
63	HOMO	-4.88	4	91	5
	LUMO	-2.64	93	3	4
64	HOMO	-4.89	4	91	5
	LUMO	-2.64	93	3	4
65	HOMO	-4.90	4	90	5
	LUMO	-2.64	93	3	4
66	HOMO	-4.99	4	91	5
	LUMO	-2.65	93	3	4
67	HOMO	-4.87	4	90	5
	LUMO	-2.56	93	3	4
68	HOMO	-4.85	4	90	6
	LUMO	-2.50	94	3	4
69	HOMO	-4.84	4	90	5
	LUMO	-2.98	94	3	4
70	HOMO	-4.87	5	90	5
	LUMO	-2.75	92	3	5
71	HOMO	-4.86	5	90	5
	LUMO	-2.69	92	3	4
72	HOMO	-4.81	4	91	6
	LUMO	-2.37	99	0	0
73	HOMO	-4.74	6	85	9
	LUMO	-2.34	93	3	4

Calculations carried out in the presence of the reaction field due to different solvents for **56** show that both the composition and the eigenvalues of the frontier MOs are very scarcely affected by the nature of the solvent (Table 3.36).

Table 3.36. *Calculated eigenvalues E (eV) and composition (%) of frontier MOs for complexes **56** in different solvents,[a] in terms of the central Pt atom and of the N^N and E^E ligand.*

		E	N^N	S^S	Pt
CH_2Cl_2	HOMO	-4.90	5	90	5
	LUMO	-2.68	92	3	4
$CHCl_3$	HOMO	-4.81	5	90	5
	LUMO	-2.73	92	4	5
CH_3CN	HOMO	-4.99	4	90	6
	LUMO	-2.63	93	3	4
Acetone	HOMO	-4.97	5	90	5
	LUMO	-2.65	93	3	4
DMF	HOMO	-4.99	4	90	6
	LUMO	-2.63	93	3	4
DMSO	HOMO	-5.00	4	90	6
	LUMO	-2.63	93	3	4
THF	HOMO	-4.88	5	90	5
	LUMO	-2.69	92	3	4
Toluene	HOMO	-4.66	7	90	4
	LUMO	-2.83	89	6	5

[a] IEF-PCM SCRF model.

In Table 3.37 the HOMO-LUMO energy gaps calculated in the gas phase and in CH_2Cl_2 for the twenty-one model complexes are reported.

Table 3.37. *HOMO-LUMO energy gaps (eV) calculated for complexes **53-73** in the gas phase and in CH$_2$Cl$_2$.[a]*

	Gas phase	CH$_2$Cl$_2$
53	1.83	2.33
54	1.82	2.32
55	1.88	2.37
56	1.51	2.22
57	1.50	2.21
58	1.53	2.23
59	1.55	2.31
60	1.83	2.36
61	1.83	2.33
62	1.89	2.39
63	1.50	2.24
64	1.50	2.25
65	1.54	2.26
66	1.56	2.34
67	1.57	2.31
68	1.55	2.35
69	1.51	2.36
70	1.47	2.12
71	1.50	2.17
72	1.54	2.44
73	1.86	2.40

[a] IEF-PCM SCRF model.

In this context, it is worth recalling that, although Koopman's theorem does not apply to DFT, it is widely accepted that the energy difference ΔE between the HOMO and the LUMO can be considered as a valuable parameter, provided that similar systems are considered.[223] Among complexes featuring Ar,H-edt^{2-} ligands, **55** and **62** (where Ar = Pyr) show larger HOMO-LUMO energy gaps with respect to their phenyl- and naphthyl-substituted analogues. As regards the complexes containing Me-dmet^{2-} and Me-dset^{2-} ligands, the latter confers to complexes **59** and **66** a larger ΔE between the HOMO and the LUMO with respect to the corresponding sulphured complexes (Table 3.37). In both cases, these features are due to the stabilisation of the HOMO, and these considerations are in perfect agreement with experimental electrochemical data,

showing that, among complexes **53-55** and **60-62**, the ones featuring pyrenyl substituents are the most hardly oxidisable, suggesting their HOMO lies at lower energies (Table 3.27 and Figure 3.31), while complexes **56-58** and **63-65** undergo the oxidation process at less positive potentials with respect to **59** and **66** (Figure 3.31 and Table 3.27). Within Series 3 (Scheme 3.8), complexes **70** and **71** (featuring phenyl-substituted diimines) show smaller HOMO-LUMO energy gaps with respect to the corresponding complexes featuring unsubstituted N^N ligands, because of the stabilisation of the LUMO, and accordingly, experimental reduction potentials are less negative (Figure 3.32 and Table 3.27). Opposite considerations can be drawn for complexes with alkyl-substituted diimines, also in this case in agreement with electrochemical measurements (Figure 3.32 and Table 3.27). It is worth noting that when the presence of CH_2Cl_2 is taken into account, the HOMO-LUMO energy gap is systematically increased by about 0.8 eV with respect to the value calculated in the gas phase (Table 3.37). As predictable, a dependence of the ΔE between the HOMO and the LUMO on the nature of the solvent field applied can also be found, the HOMO-LUMO energy gap being larger in relatively polar solvents (ΔE = 2.22, 2.08, 2.36, 2.32, 2.19, 2.36, 2.37, and 1.83 eV in CH_2Cl_2, $CHCl_3$, CH_3CN, acetone, THF, DMF, DMSO, and toluene, respectively for **56**).

3.2.1.7.3. Charges

In Table 3.38, the results of a Mulliken charge analysis[224] are summarised for **53-73**. In particular, the charges Q on the central platinum ion, the coordinating N and E atoms (E = S, Se), and the whole ligands are reported. Although it is well known that Mulliken analysis overemphasises the charge separation,[225] an examination of the calculated charges allows to draw some general considerations. The 1,2-dichalcogenolato ligands, in agreement with their character of dichalcogenolates, feature for all complexes negative charges of about -0.6 e, while the diimines bear a positive charge of about 0.1-0.2 e, the remaining positive charge (0.3-0.4 e) being carried by the metal. Thus, all complexes feature a large charge separation between the two ligands of 0.6-0.8 e (Table 3.38). As concerns Series 1 (Scheme 3.6), the complexes featuring a R-dmet^{2-} ligand show negative charges on the S^S fragment slightly more negative than those calculated for complexes **53-55**, and accordingly, a larger charge separation can be found for these systems. Among complexes **56-59**, the selenated complex **59** features the smallest charge separation (Table 3.38). On the other hand, in complexes of Series 3 (Scheme 3.8), the substituted diimines are found to be more positively charged than unsubstituted ones, and subsequently the charge separation in the corresponding complexes is larger.

Table 3.38. *Mulliken charges Q (e) calculated on Pt, E1, E2, N1, N2, the dichalcogenolate (E^E), and the diimine (N^N) for **53-73** in the gas phase.*[a]

	Q(Pt)	Q(N1)	Q(N2)	Q(E1)	Q(E2)	Q(N^N)	Q(E^E)
53	0.376	-0.370	-0.371	-0.201	-0.208	0.124	-0.500
54	0.377	-0.370	-0.371	-0.201	-0.207	0.129	-0.506
55	0.371	-0.369	-0.369	-0.178	-0.216	0.135	-0.505
56	0.399	-0.371	-0.371	-0.180	-0.208	0.166	-0.565
57	0.398	-0.371	-0.371	-0.181	-0.205	0.166	-0.564
58	0.391	-0.370	-0.371	-0.182	-0.182	0.169	-0.560
59	0.332	-0.356	-0.355	-0.076	-0.128	0.179	-0.512
60	0.372	-0.355	-0.356	-0.207	-0.200	0.132	-0.504
61	0.372	-0.355	-0.356	-0.200	-0.206	0.138	-0.510
62	0.366	-0.354	-0.355	-0.177	-0.214	0.144	-0.510
63	0.393	-0.357	-0.358	-0.203	-0.246	0.175	-0.568
64	0.393	-0.356	-0.357	-0.179	-0.202	0.177	-0.570
65	0.387	-0.355	-0.356	-0.179	-0.179	0.179	-0.566
66	0.329	-0.342	-0.343	-0.129	-0.077	0.190	-0.519
67	0.396	-0.364	-0.363	-0.190	-0.258	0.198	-0.593
68	0.393	-0.369	-0.369	-0.216	-0.259	0.205	-0.598
69	0.392	-0.365	-0.365	-0.192	-0.262	0.217	-0.610
70	0.400	-0.375	-0.374	-0.182	-0.254	0.173	-0.573
71	0.396	-0.360	-0.361	-0.182	-0.209	0.190	-0.586
72	0.387	-0.347	-0.348	-0.196	-0.218	0.237	-0.624
73	0.370	-0.365	-0.365	-0.212	-0.225	0.165	-0.536

[a] Numbering Scheme as in Figure 3.46.

Table 3.39. *Mulliken charges Q (e) calculated on Pt, E1, E2, N1, N2, the dichalcogenolate ligand (E^E), and the diimine one (N^N) for **53-73** in CH$_2$Cl$_2$.[a]*

	Q(Pt)	Q(N1)	Q(N2)	Q(S1)	Q(S2)	Q(N^N)	Q(E^E)
53	0.355	-0.359	-0.359	-0.271	-0.271	0.333	-0.689
54	0.377	-0.360	-0.359	-0.270	-0.269	0.336	-0.713
55	0.351	-0.359	-0.359	-0.246	-0.281	0.334	-0.685
56	0.389	-0.360	-0.360	-0.240	-0.252	0.394	-0.783
57	0.389	-0.360	-0.360	-0.240	-0.249	0.394	-0.784
58	0.387	-0.360	-0.360	-0.239	-0.336	0.392	-0.779
59	0.333	-0.348	-0.347	-0.148	-0.183	0.401	-0.734
60	0.351	-0.346	-0.346	-0.268	-0.268	0.337	-0.688
61	0.351	-0.346	-0.346	-0.267	-0.266	0.340	-0.691
62	0.347	-0.346	-0.346	-0.277	-0.243	0.338	-0.685
63	0.383	-0.347	-0.347	-0.246	-0.349	0.397	-0.780
64	0.385	-0.347	-0.347	-0.245	-0.236	0.396	-0.782
65	0.384	-0.347	-0.347	-0.235	-0.237	0.394	-0.778
66	0.330	-0.336	-0.336	-0.181	-0.146	0.402	-0.732
67	0.384	-0.353	-0.354	-0.246	-0.257	0.412	-0.796
68	0.382	-0.361	-0.361	-0.246	-0.258	0.422	-0.804
69	0.379	-0.358	-0.358	-0.258	-0.246	0.424	-0.804
70	0.389	-0.365	-0.365	-0.240	-0.250	0.394	-0.783
71	0.387	-0.352	-0.353	-0.248	-0.238	0.398	-0.784
72	0.373	-0.343	-0.343	-0.246	-0.256	0.435	-0.809
73	0.342	-0.357	-0.357	-0.266	-0.289	0.413	-0.755

[a] Numbering Scheme as in Figure 3.46.

Calculations performed in CH_2Cl_2 show an increase of about 0.4 e in the charge separation between the ligands (Table 3.39).

The charge separation shows a solvent-dependence as well, as testified by calculations performed under the reaction field of different solvents for **56** (Table 3.40).

Table 3.40. *Mulliken charges Q (e) calculated on Pt, the dithiolate ligand (S^S), and the diimine one (N^N) for **56** in different solvents.[a]*

	Q(Pt)	Q(N^N)	Q(S^S)
CH_2Cl_2	0.389	0.394	-0.783
$CHCl_3$	0.392	0.363	-0.755
CH_3CN	0.385	0.421	-0.806
Acetone	0.386	0.415	-0.801
DMF	0.385	0.421	-0.807
DMSO	0.385	0.424	-0.809
THF	0.390	0.387	-0.777
Toluene	0.395	0.302	-0.697

[a] IEF-PCM SCRF model.

It is worth underlining that the trends of the atomic charges calculated through a Natural Population Analysis (NPA)[226] are in agreement with those found for the Mulliken analysis, both in the gas phase and in CH_2Cl_2 (Tables 3.41 and 3.42, respectively).

Table 3.41. *NPA charges Q (e) calculated on Pt, E1, E2, N1, N2, the dichalcogenolate (E^E), and the diimine (N^N) for **53-73** in the gas phase.*[a]

	Q(Pt)	Q(N1)	Q(N2)	Q(S1)	Q(S2)	Q(N^N)	Q(E^E)
53	0.083	-0.452	-0.452	-0.003	0.024	0.267	-0.350
54	0.084	-0.452	-0.452	-0.005	0.025	0.272	-0.356
55	0.080	-0.451	-0.452	0.005	0.013	0.278	-0.358
56	0.118	-0.450	-0.448	-0.021	0.030	0.304	-0.423
57	0.117	-0.445	-0.450	0.030	-0.019	0.304	-0.422
58	0.111	-0.450	-0.449	0.029	0.004	0.306	-0.418
59	0.051	-0.452	-0.454	0.074	0.133	0.305	-0.357
60	0.081	-0.449	-0.449	0.023	-0.004	0.274	-0.355
61	0.082	-0.449	-0.449	-0.005	0.025	0.279	-0.361
62	0.078	-0.448	-0.448	0.012	0.004	0.285	-0.363
63	0.114	-0.445	-0.448	0.030	-0.014	0.311	-0.425
64	0.115	-0.445	-0.448	-0.019	0.030	0.314	-0.429
65	0.109	-0.446	-0.447	0.028	-0.153	0.315	-0.425
66	0.049	-0.448	-0.451	0.074	0.132	0.314	-0.363
67	0.119	-0.444	-0.441	0.021	-0.029	0.334	-0.453
68	0.115	-0.453	-0.451	0.019	-0.031	0.344	-0.459
69	0.114	-0.449	-0.451	-0.035	0.015	0.357	-0.471
70	0.119	-0.454	-0.451	0.029	-0.023	0.311	-0.431
71	0.116	-0.447	-0.449	-0.026	0.025	0.329	-0.445
72	0.110	-0.442	-0.444	0.010	-0.032	0.375	-0.485
73	0.081	-0.452	-0.453	-0.028	0.002	0.311	-0.391

[a] Numbering Scheme as in Figure 3.46.

Table 3.42. *NPA charges Q (e) calculated on Pt, E1, E2, N1, N2, the dichalcogenolate (E^E), and the diimine (N^N) for* **53-73** *in CH$_2$Cl$_2$.*[a,b]

	Q(Pt)	Q(N1)	Q(N2)	Q(S1)	Q(S2)	Q(N^N)	Q(E^E)
53	0.081	-0.450	-0.450	-0.082	-0.048	0.459	-0.540
54	0.081	-0.450	-0.450	-0.046	-0.082	0.461	-0.543
55	0.079	-0.450	-0.449	-0.072	-0.061	0.460	-0.539
56	0.128	-0.446	-0.445	-0.042	-0.075	0.514	-0.642
57	0.128	-0.446	-0.445	-0.042	-0.074	0.515	-0.642
58	0.124	-0.446	-0.445	-0.042	-0.057	0.512	-0.636
59	0.061	-0.451	-0.450	0.057	0.019	0.506	-0.567
60	0.079	-0.447	-0.447	-0.047	-0.047	0.460	-0.539
61	0.080	-0.447	-0.447	-0.081	-0.045	0.462	-0.542
62	0.077	-0.447	-0.447	-0.058	-0.071	0.461	-0.539
63	0.123	-0.442	-0.443	-0.039	-0.066	0.514	-0.637
64	0.125	-0.442	-0.443	-0.071	-0.039	0.515	-0.640
65	0.123	-0.443	-0.443	-0.040	-0.055	0.512	-0.634
66	0.059	-0.447	-0.448	0.022	0.060	0.505	-0.564
67	0.127	-0.441	-0.439	-0.046	-0.079	0.528	-0.654
68	0.123	-0.452	-0.451	-0.049	-0.082	0.541	-0.663
69	0.120	-0.449	-0.450	-0.082	-0.049	0.543	-0.663
70	0.125	-0.450	-0.449	-0.041	-0.068	0.515	-0.640
71	0.123	-0.444	-0.446	-0.068	-0.041	0.520	-0.642
72	0.116	-0.443	-0.444	-0.049	-0.076	0.551	-0.666
73	0.072	-0.453	-0.453	-0.093	-0.070	0.486	-0.558

[a] Numbering Scheme as in Figure 3.46. [b] IEF-PCM SCRF model.

3.2.1.7.4. Time-Dependent DFT (TD-DFT) calculations

Time dependent DFT (TD-DFT) calculations were carried out on complexes **53-73** at their optimised geometries in their GSs, both in the gas phase and in CH_2Cl_2, at the same level of theory discussed above. As expected based on the UV-Vis-NIR spectroscopic measurements (Section 3.2.1.4), a comparison between simulated and experimental spectra shows a much better agreement for solvation calculations than for the ones performed in the gas phase, and thus just the results obtained by adopting the continuum SCRF approach will be discussed in this case.

As an example, in Table 3.43 the main vertical electronic transitions calculated for **56** in CH_2Cl_2 are summarised, along with the most relevant MO contributions to each one-electron excitation.

Table 3.43. *Principal electronic transitions (f > 0.015) calculated for **56** in CH$_2$Cl$_2$ at (IEF-PCM SCRF) TD-DFT level. For each transition, the excitation energy E (eV) the absorption wavelength λ (nm), the oscillator strenght f, and the molecular orbital composition of the excited-state functions, along with the fragments where the involved KS-MOs are mainly localised, are reported.*

Exc. State	E	λ	f	Composition[a]	%	Molecular fragments[b]
S1	1.675	740.0	0.144	99→100	99	S^S(90%)→N^N(92%)
S5	2.765	448.4	0.015	97→100	12	S^S(67%)+Pt(30%) →N^N(92%)
				99→102	86	S^S(90%)→N^N(98%)
S8	3.205	386.8	0.046	96→100	96	S^S(80%)→N^N(92%)
S10	3.664	338.8	0.227	99→104	95	S^S(90%)→S^S(99%)
S14	4.012	309.0	0.065	97→102	91	S^S(67%)+Pt(30%) → N^N(98%)
				96→101	5	S^S(80%)→N^N(89%)
S17	4.212	294.4	0.023	96→101	91	S^S(80%)→N^N(89%)
S20	4.302	288.2	0.055	94→100	36	N^N(92%)→ N^N(92%)
				96→102	58	S^S(80%)→ N^N(98%)
S23	4.465	277.6	0.186	93→100	57	Pt(50%)+S^S(37%)→ N^N(92%)
				94→100	13	N^N(92%)→ N^N(92%)
S24	4.479	276.8	0.265	93→100	18	Pt(50%)+S^S(37%)→ N^N(92%)
				94→100	37	N^N(92%)→ N^N(92%)
				96→102	24	S^S(80%)→ N^N(98%)
S26	4.532	273.6	0.213	93 →100	15	Pt(50%)+S^S(37%)→ N^N(92%)
				98→103	76	N^N(99%)→S^S(39%)+Pt(42%)
S27	4.547	272.7	0.142	92→100	80	S^S(47%)+Pt(34%)→ N^N(92%)

[a] The molecular orbitals are labelled according to Figure 3.49; [b] N^N = diimine ligand; S^S = 1,2-dithiolate ligand.

Electronic transitions calculated at TD-DFT level have been exploited to simulate the UV-Vis absorption spectra (Figure 3.50 for **56** in CH_2Cl_2). A comparison between the simulated and experimental spectra evidences that a very good agreement can be found.
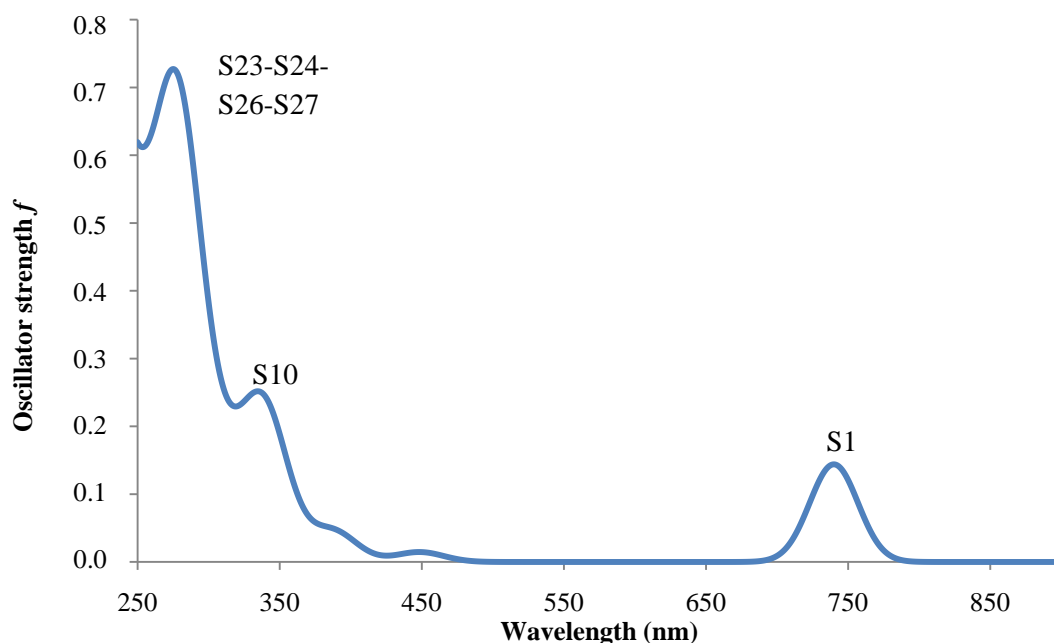
Figure 3.50. *Simulated UV-Vis-NIR spectrum (250-900 nm) of **56** in CH_2Cl_2 (IEF-PCM SCRF) based on TD-DFT calculations (Table 3.43).*

In particular, for all complexes the S0→S1 vertical transition, responsible for the solvatochromic absorption band evidenced experimentally in the visible region, should be attributed to an almost pure (92% for **56**, Table 3.43) one-electron excitation involving the frontier molecular-orbitals (KS-MOs 99 and 100 for **56**, Table 3.43), in agreement with what found in the literature. Thus, being the HOMO and the LUMO mostly localised on the S^S and N^N ligands, respectively, with similar contributions from the metal, this transition should be considered as an interligand charge-transfer (ILCT) process from the negatively charged 1,2-dichalcogenolato ligand to the diimine, featuring a positive partial charge (Section 3.2.1.7.3). Thus, the HOMO-LUMO

transition should result in a lowering of the charge separation in the first excited state as compared to the GS, in agreement with the negative solvatochromism observed experimentally discussed in Section 3.2.1.4. In Table 3.44, the wavelength of this transition calculated in CH_2Cl_2 for complexes **53-73** is reported, and a very good agreement between the trend of this value and that of the HOMO-LUMO energy gap calculated at the same level of theory (Table 3.37) can be observed ($R^2 = 0.97$).

Table 3.44. *TD-DFT λ_{max} values (nm) of the electronic transition S0→S1 calculated for **53-73** in CH_2Cl_2 (IEF-PCM SCRF model).*

53	703.06
54	705.53
55	690.92
56	739.98
57	742.60
58	736.25
59	708.10
60	696.96
61	699.17
62	685.44
63	734.79
64	732.68
65	727.20
66	700.04
67	706.49
68	694.30
69	688.74
70	775.91
71	754.46
72	667.10
73	701.20

For complexes featuring the same class of E^E ligands, a good agreement can be found between the experimental and calculated trends of the absorption wavelengths (Tables 3.29 and 3.44). In particular, as regards complexes **53-55** and **60-62**, the pyrenyl-substituted compounds feature the S0→S1 transition at shorter wavelengths with respect to complexes with Ar = Ph and Naph (Table 3.44), in agreement with the highest calculated HOMO-LUMO energy gaps (Table 3.37). Within complexes featuring a R-dmet^{2-}/R-dset^{2-} ligand, both experimental and calculated absorption bands fall at shorter wavelengths for complexes **59** and **66** with respect to sulphured analogues (Tables 3.29 and 3.44).

A linear correlation can also be found between the experimental and calculated trends of the absorption wavelengths within Series 3 (Scheme 3.8). In particular, complexes bearing 2,2′-bipyridine and 1,10-phenanthroline systems (blue and red symbols, respectively, in Figure 3.51) with phenyl substituents (**70** and **71**) feature both the experimental and calculated absorptions at longer wavelengths with respect to unsubstituted systems (**56** and **63**), due to their lower HOMO-LUMO energy gap (Table 3.37), while, on the contrary, λ_{max} is shorter for complexes bearing alkyl-substituted diimines (**67**-**69**, and **72**).
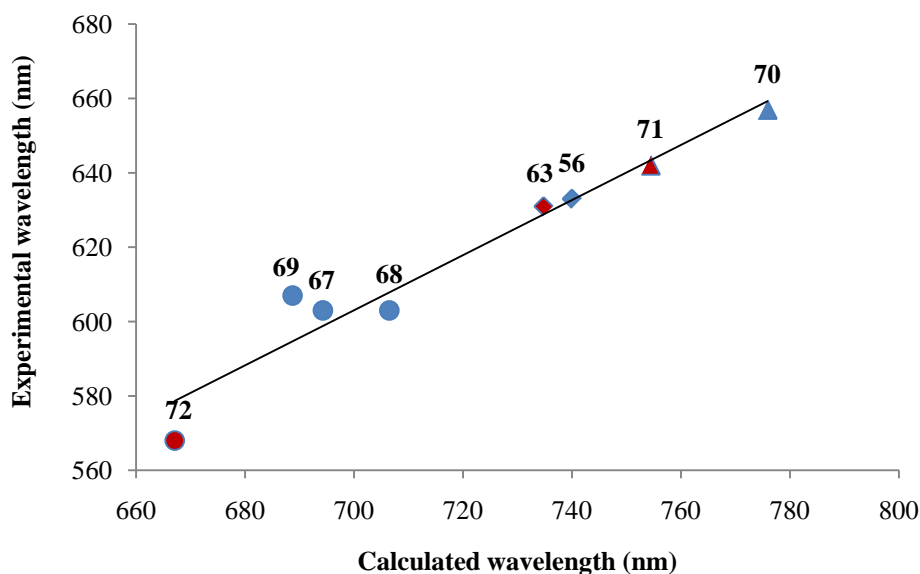
Figure 3.51. *Experimental and IEF-PCM TD-DFT calculated λ_{max} (nm) of the solvatochromic absorption band in the visible region for complexes **56**, **63**, and **67-72**, belonging to Series 3 ($R^2 = 0.94$; Tables 3.29 and 3.44). S^S = Me-dmet^{2-}; N^N = unsubstituted (rhombs) 2,2'-bipyridine (blue) or 1,10-phenanthroline (red) and alkyl (circles) and phenyl (triangles) derivatives.*

Moreover, calculations performed in different solvents for **56** (Table 3.45) show, as predictable, a dependence of the λ_{max} of this absorption on the nature of the solvent, according to the different values of the calculated HOMO-LUMO energy gaps discussed above (Table 3.37), and in agreement with the solvatochromism observed experimentally.

Table 3.45. *TD-DFT calculated λ_{max} (nm) of the solvatochromic absorption band for **56** in different solvents.[a]*

CH$_2$Cl$_2$	CHCl$_3$	CH$_3$CN	Acetone	THF	DMF	DMSO	Toluene
740	798	689	702	753	690	686	908

[a] IEF-PCM SCRF model.

In particular, it is worth noting that a linear correlation ($R^2 = 0.98$) holds between the experimental and calculated trends of λ_{max} for **56** in different solvents (Figure 3.52; Tables 3.29 and 3.45).
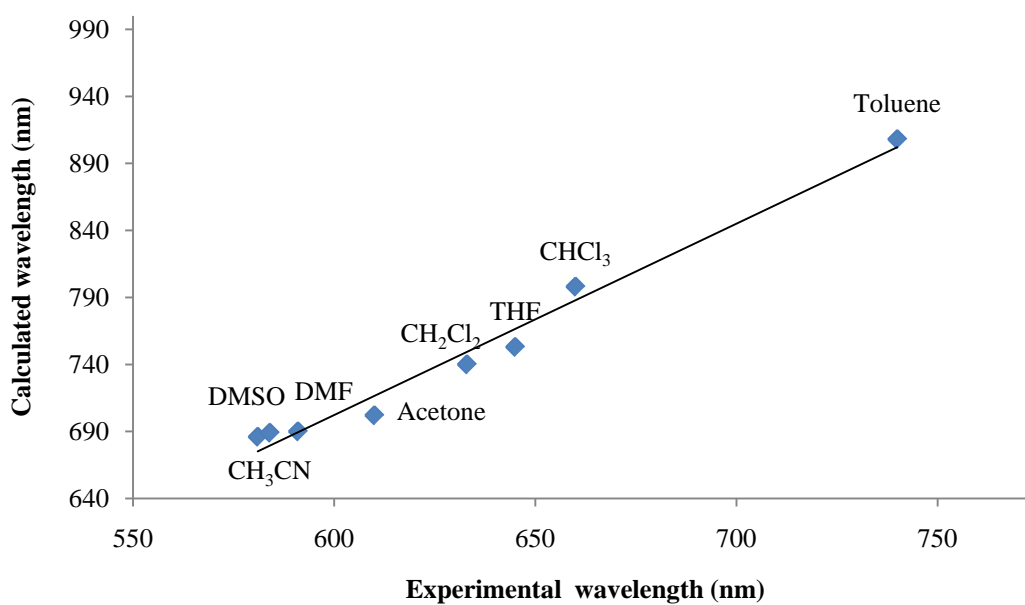
Figure 3.52. *Experimental and SCRF TD-DFT calculated λ_{max} (nm) of the solvatochromic absorption band in the visible region for **56** in different solvents (Tables 3.29 and 3.45).*

Concerning the experimental electronic absorptions featured by all complexes in the region 300-400 nm (Figures 3.34 and 3.35 for **53** and **56**, respectively) and calculated at TD-DFT level in the same spectral region (Figure 3.50 for **56**), they should be assigned to transitions due to monoelectronic excitations occurring between MOs mainly localised on the E^E ligands. In particular, for **56**, the most intense electronic transition calculated in this spectral region is S0→S10, mainly resulting from a one-electron excitation between KS-MOs 99 and 104 (HOMO→LUMO+4 excitation), both mainly localised on the S^S ligand (90 and 99%, respectively; Table 3.43 and Figure 3.50).

Finally, the absorptions found in the UV region falling in the range 250-300 nm in both UV-Vis-NIR experimental and TD-DFT calculated spectra are assigned to electronic transitions involving MOs mainly localised on the diimine (S1→S23/24/26/27 for **56**, Table 3.43 and Figure 3.50).

Thus, in the spectral region 250-300 nm, an overlap of absorptions due to excitations involving MOs localised both on the E^E and N^N ligands can be found. Nevertheless, the emissive processes occurring when the complexes are excited in this wavelength range (Section 3.2.1.6), should regard exclusively the excitations involving MOs localised on the N^N ligand, given the very similar emission profiles observed for all **53-73** complexes, which do not seem to be affected by the nature of the E^E ligand, at least as far as the emission energy is concerned.

3.2.1.7.5. Calculation of static first hyperpolarisability (β)

Static first hyperpolarisabilities (β_{tot}) and static dipole moments (μ) were calculated, at the same level of theory discussed above, for complexes **53-73,** both in the gas phase and in CH_2Cl_2, following the same procedure described for complexes **20-22** in Section 3.1.6.5. In order to have an absolute reference to evaluate the order of magnitude of the β_{tot} values, the same calculations were also undertaken, at the same level of theory, on [Pt(1,10-phen)(tdt)] (**75**) at the optimised geometry. In fact, this complex, to the best of our knowledge, among those whose β have been determined experimentally from EFISH measurements, showed the largest hyperpolarisability value reported so far (-37·10^{-30} esu, Section 1.3.2.4).[130c] The results are summarised in Table 3.46.

Table 3.46. *Static first hyperpolarisabilities β_{tot} (a.u. and esu) and static dipole moments μ (D) calculated for 53-73 and 75 in the gas phase and in CH_2Cl_2.*

	Gas phase			CH_2Cl_2[a]		
	$\beta_{tot} \cdot 10^4$ (a.u.)	$\beta_{tot} \cdot 10^{-30}$ (esu)	$\mid\mu\mid$ (D)	$\beta_{tot} \cdot 10^4$ (a.u.)	$\beta_{tot} \cdot 10^{-30}$ (esu)	$\mid\mu\mid$ (D)
53	2.01	174	2.85	3.46	299	4.43
54	1.71	147	4.98	3.45	298	7.63
55	1.76	152	2.29	3.09	267	3.07
56	4.16	360	7.46	4.68	404	11.31
57	4.25	367	7.41	4.74	409	11.22
58	4.29	370	7.98	4.61	398	4.93
59	4.26	368	7.45	3.97	343	11.08
60	2.40	208	4.77	3.74	323	7.37
61	2.06	178	5.16	3.73	322	7.77
62	2.13	184	2.62	3.36	290	3.50
63	4.89	423	5.67	4.83	418	8.59
64	4.94	427	7.59	4.79	414	11.32
65	4.95	428	8.15	4.68	404	12.34
66	4.81	416	7.95	4.06	351	11.66
67	4.30	371	8.01	3.88	335	11.79
68	4.65	402	9.25	3.82	330	13.51
69	5.31	459	6.98	3.94	340	9.95
70	7.68	664	7.85	8.00	691	11.58
71	7.68	664	6.65	6.99	604	9.62
72	5.34	461	6.57	3.38	292	9.29
73	2.65	229	6.22	3.60	311	9.12
75	2.33	201	1.80	3.42	296	3.10

[a] IEF-PCM SCRF model.

On passing from the gas phase to CH_2Cl_2, an increase in β_{tot} values is found for most complexes (β_{tot} = 147-664 and 267-690$\cdot 10^{-30}$ esu in gas phase and CH_2Cl_2, respectively).

Both in the gas phase and when the presence of the solvent is implicitly taken into account, complexes featuring R-dmet^{2-} and R-dset^{2-} ligands show larger hyperpolarisabilities with respect to the complexes containing the Ar,H-edt^{2-} ligands (Table 3.46). Within complexes featuring E^E ligands belonging to the same class, no significant changes can be observed in the value of β_{tot} upon changing the substituent at the 1,2-dichalcogenoelene core (Figure 3.53 for calculations performed in the gas phase on **53-59**).
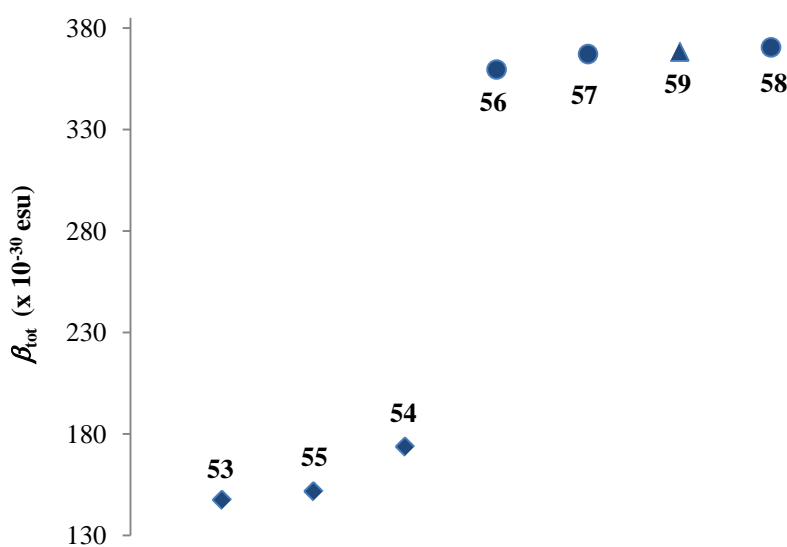
Figure 3.53. *Static first hyperpolarisabilities β_{tot} (esu) calculated for complexes 53-59 in the gas phase (Table 3.46): N^N = 2,2'-bipyridine; E^E = Ar,H-edt^{2-} (rhombs), R-dmet^{2-} (circles), Me-dset^{2-} (triangle).*

Larger differences are calculated in β_{tot} values when the N^N ligand is varied. In particular, complexes featuring 1,10-phenanthrolines show static hyperpolarisabilities systematically larger than corresponding complexes with 2,2′-bipyridines (Figure 3.54 for calculations performed in the gas phase on **56-59** and **63-66**).
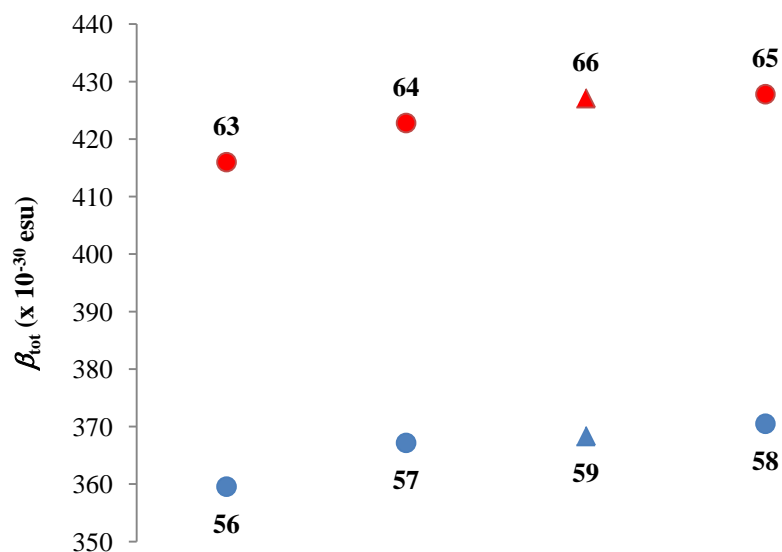
Figure 3.54. *Static first hyperpolarisabilities β_{tot} (esu) calculated for complexes **56-59** and **63-66** in the gas phase (Table 3.46). N^N = 2,2'-bipyridine (blue), 1,10-phenanthroline (red); S^S = R-dmet^{2-} (circles), Me-dset^{2-} (triangles).*

Moreover, complexes bearing substituted 2,2′-bipyridine and 1,10-phenanthroline ligands (blue and red symbols, respectively for gas phase calculations in Figure 3.55) feature larger values of β_{tot} with respect to unsubstituted ones, in particular as concerns aryl-substituted complexes **70** and **71** (Table 3.46).
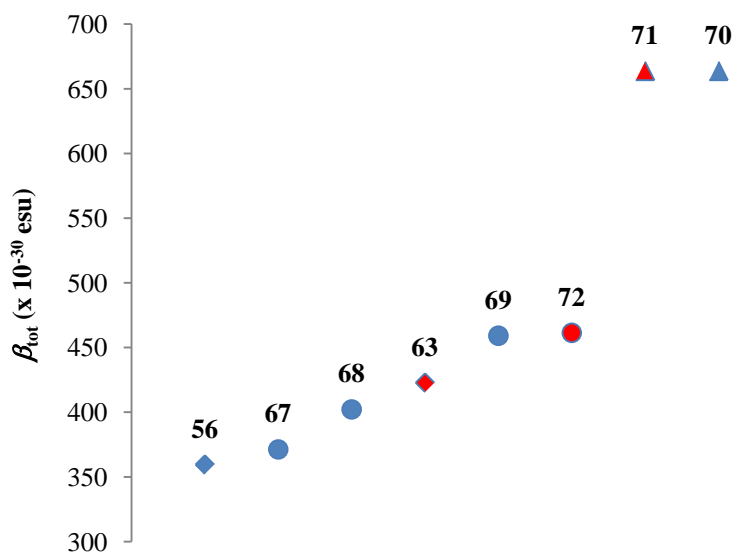
Figure 3.55. *Static first hyperpolarisabilities β_{tot} (esu) calculated for complexes **56**, **63** and **67-72** belonging to Series 3 in the gas phase (Table 3.46). S^S = Me-dmet^{2-}; N^N = unsubstituted (rhombs) 2,2'-bipyridine (blue) and 1,10-phenanthroline (red) and alkyl (circles) or phenyl (triangles) derivatives.*

Moreover, complexes **70** and **71** feature the largest values of calculated β_{tot} among the twenty-one complexes under study, thus suggesting these should be the best candidates for NLO applications. In this context, it is worth noting that the values of β_{tot} calculated for **53-73** are generally remarkably larger than that computed for **75** (by up to $450 \cdot 10^{-30}$ esu, Table 3.46), further suggesting the complexes considered in the present research project represent good candidates for applications in the field of NLO.

3.2.1.8. Photoconduction measurements

Given the wavelength-selective photoconductivity coupled to the near-IR absorption showed in the past by complexes belonging to the classes $[M(R,R'\text{-timdt})_2]^{x-}$ and $[M(R\text{-dmet})_2]^{x-}$, which allowed for the fabrication of solid-state photodetectors operating between the first and third optical-fibre windows,[91] preliminary photoconduction

measurements were conducted on one of the twenty-one [Pt(N^N)(E^E)] complexes synthesised, namely **54**, by the group of Prof. Sampietro, at the Politecnico di Milano. For these measurements, a prototype planar device similar to that depicted in Figure 3.56 was used.
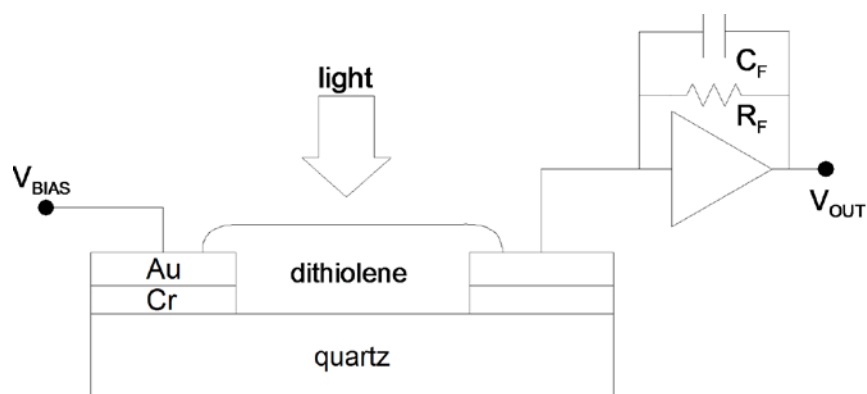
Figure 3.56. *Sketch of the typical planar detector prototype used for photoconduction measurements. The device is connected to a transimpedance amplifier.*

In this device, the active material is casted on a quartz substrate with lithographed gold/chromium electrodes, thus obtaining a metal-semiconductor-metal surface structure. Complex **54** was casted as a sonicated DMSO solution on a hot quartz substrate with interelectrode spacings of 6 μm. A detailed view of the sample casted on the electrodes' area is represented in Figure 3.57.
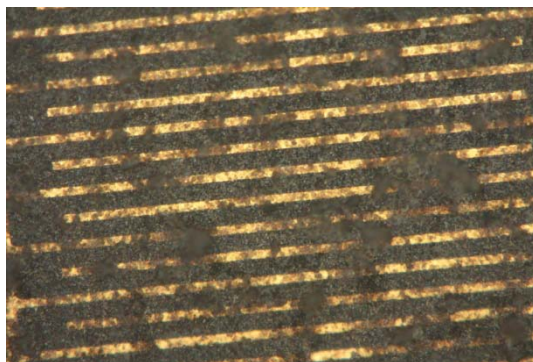
Figure 3.57. *Optical microscope picture (1000x magnification) of the prototype device obtained by casting **54** on the quartz substrate with lithographed gold/chromium electrodes, showing the interelectrode spacings.*

The device was irradiated with light pulses lasting 500 µs produced by a set of light emitting diodes (LEDs) differing in their wavelength (350-800 nm), and the resulting photocurrents were measured by biasing the device with a voltage source and connecting it to a transimpedance amplifier. In Figure 3.58, the efficiency η of photocurrent measurements as a function of incident wavelength λ_{LED} is reported, showing a wavelength selectivity of the photocurrent intensity, so that the device acts as an intrinsic wavelength-selective photodetector. Interestingly, in the visible region the highest photocurrent is recorded at about 600 nm, a wavelength corresponding to the λ_{max} of the solvatochromic absorption band in the visible region featured by **54** (Table 3.29).
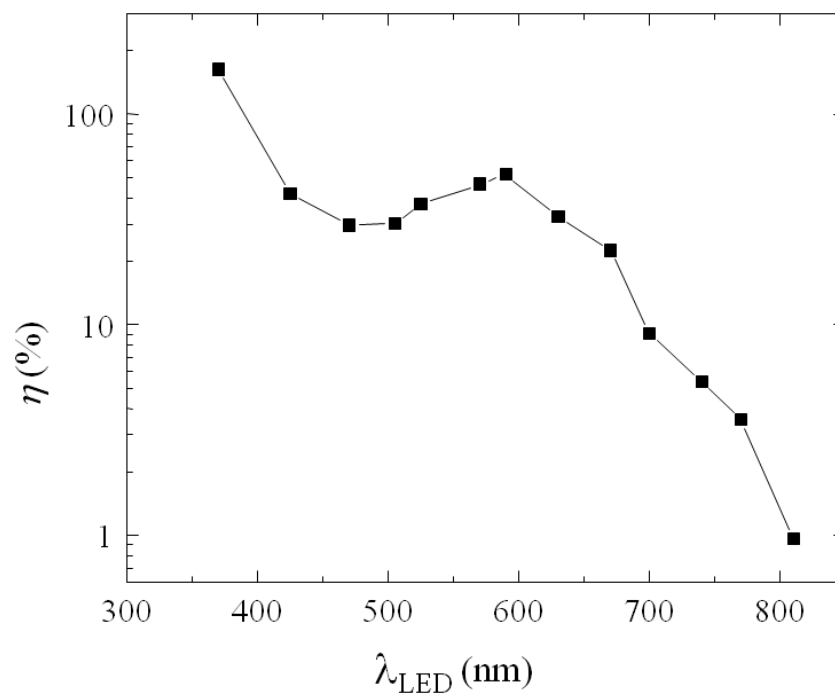
Figure 3.58. *Efficiency η (%) from photocurrent measurements as a function of the incident wavelength* λ_{LED} *(nm) for* **54**.

3.2.2. Synthesis and characterisation of [Au(Py^1)(mnt)] (76)

As already mentioned, the heteroleptic noncentrosymmetric complex [Au(Py^1)(mnt)] (**76**, Py^{1-} = 2-benzylpyridine, mnt^{2-} = maleonitrile-1,2-dithiolato) was synthesised during the present study, in order to explore further synthetic strategies for the preparation of NLO-active materials featuring 1,2-dithiolene ligands.

Very few reports on complexes of the type [Au(C^N)(S^S)] can be found in the literature, and in all cases the C^N ligand is a phenylpyridine (Figure 1.23).[129,148,227] As a consequence, the resulting complexes are completely planar but for the substituents, and, as already mentioned in Section 1.3.3, their spectroscopic features are generally analogous to those of corresponding [Au(N^N)(S^S)] complexes.[129]

3.2.2.1 Synthesis and Characterisation

The neutral complex was synthesised starting from the corresponding dichloro-complex [Au(Py^1)Cl$_2$] (**77**, previously reported by Prof. M. A. Cinellu)[228] by reaction with disodium maleonitrile-1,2-dithiolate, according to Scheme 3.15.
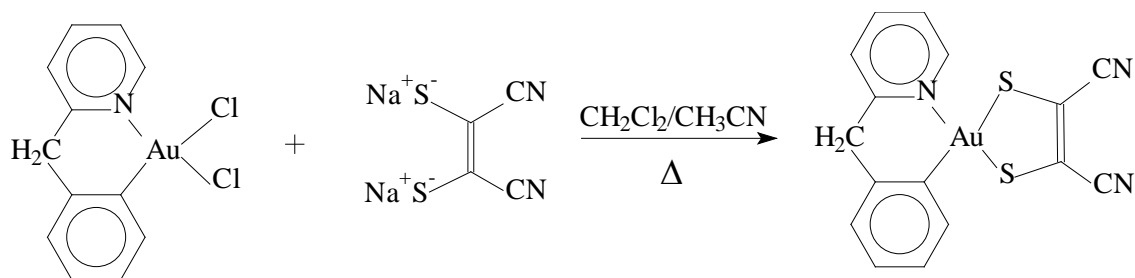
Scheme 3.15. *Synthetic route for the preparation of **76**.*

The reaction was carried out in CH$_2$Cl$_2$/CH$_3$CN at 130° C by adopting a pressure tube (Figure 3.59), and the product was obtained as a microcrystalline solid without further purification steps. Unfortunately, the crystals resulted not suitable for X-ray diffraction, and notwithstanding numerous attempts of crystallisation, no X-ray quality crystals were obtained.

Figure 3.59. *Pressure tube used for the synthesis of **76**.*

Cyclic voltammetry (CV) measurements performed in DMSO on **76** show a single irreversible reduction at -1.20 V vs the Fc$^+$/Fc couple (Figure 3.60).
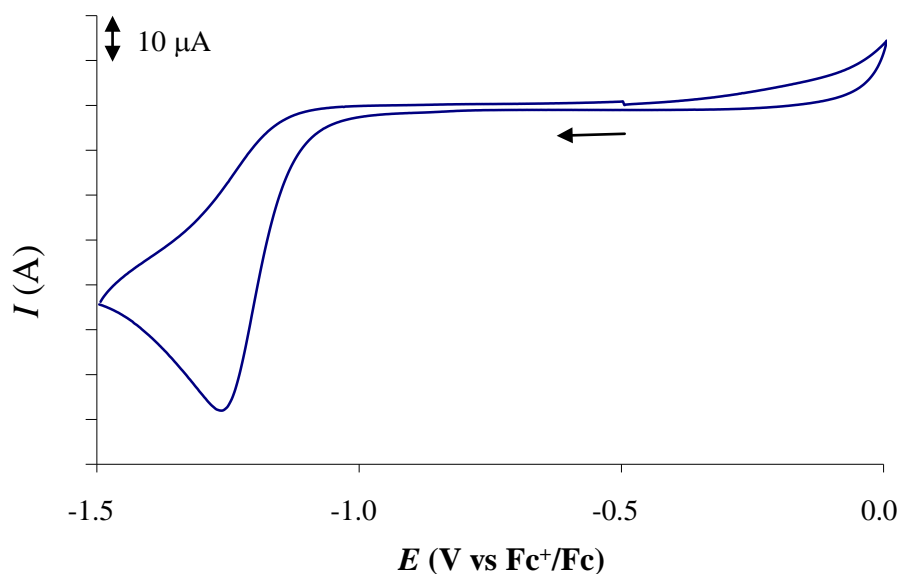
Figure 3.60. *Cyclic voltammetry recorded for a anhydrous DMSO solution of 76 at a platinum electrode [298 K; scan rate 20 mV s^{-1}; supporting electrolyte (TBA$^+$)(BF$_4^-$) 0.1 M)].*

A similar electrochemical behavior is shown by the precursor **77**, with the irreversible reduction occurring at an almost identical potential (-1.19 V vs the Fc$^+$/Fc couple). This suggests that the reduction process is centred on the 2-benzylpyridine system.

The UV-Vis-NIR absorption spectrum (260-1100 nm) recorded for **76** in DMF shows two main absorption bands with λ_{max} at 268 and 349 nm ($\varepsilon = 35000$ and 8000 M^{-1} cm^{-1}, respectively, Figure 3.61), and no absorptions in the visible region, in contrast with what previously reported for other [Au(N^C)(S^S)] and [Au(N^N)(S^S)] reported so far, such as **19** and [Au(2,2′-bipy)(tdt)].[129]
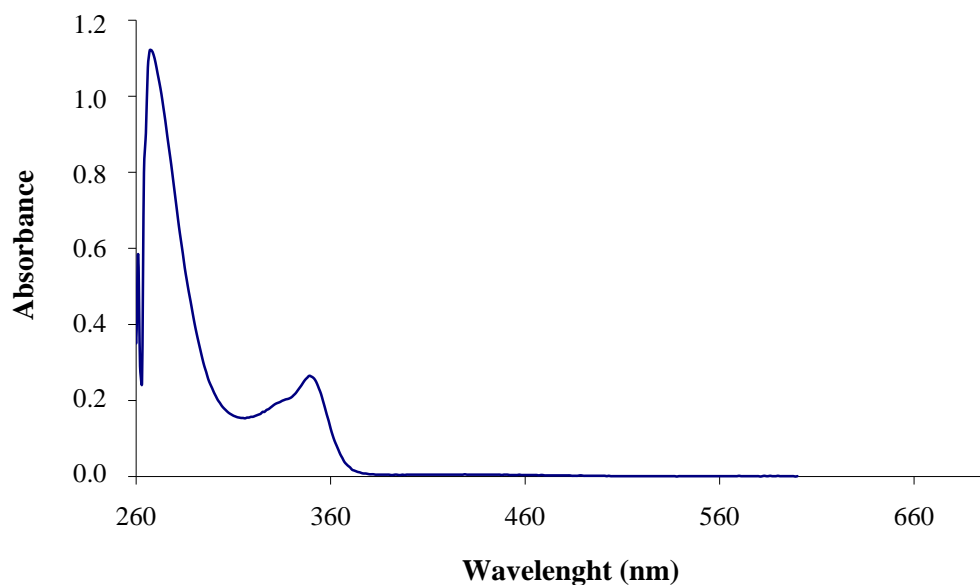
Figure 3.61. *UV-Vis absorption spectrum (260-720 nm) recorded for **76** in DMF.*

Fluorescence measurements carried out in DMSO, in the range λ_{exc} = 260-350 nm, showed an emission profile in the visible region, with maxima at λ_{em} = 372 and 390 nm. (Quantum yield $\Phi = 9.9 \cdot 10^{-3}$; Figure 3.62). Emission processes in the same spectral region were reported for the related complex **19**, but in the case of this system fluorescence was reported to occur in the solid state only, and was not observed in solution.[129] On the other hand, the luminescence features of **76** are very similar to those of [Pt(N^N)(E^E)] complexes described above (Section 3.2.1.6).
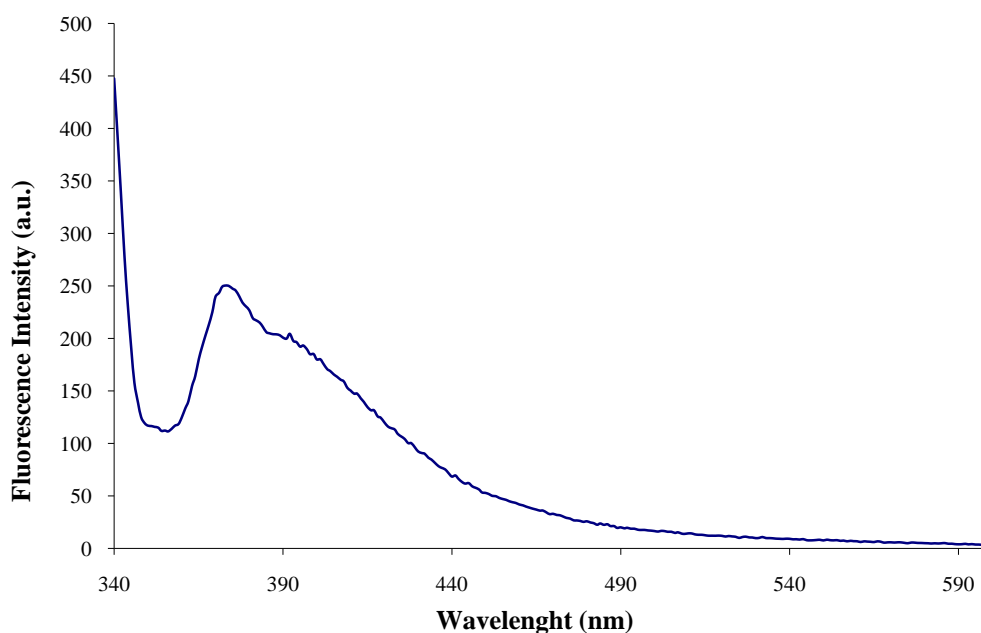
Figure 3.62. *Emission spectrum recorded for **76** in DMSO solution (λ_{exc} = 299 m).*

3.2.2.2. DFT calculations

An examination of the literature shows that, to the best of our knowledge, no computational investigation has been reported to date on complexes belonging to the general class [Au(C^N)(S^S)].

Theoretical DFT calculations were performed in the gas phase on **76** at the same level of theory adopted for complexes **53-73** (PBE0 functional; Ahlrichs BSs for C, N, S, H and CRENBL+ECP BSs for gold). The optimised geometry is depicted in Figure 3.63, showing that the central metal ion is coordinated by the (C^N)(S^S) system in a square–planar fashion. As predictable, the optimised structure is not completely planar, due to a torsion of the 2-benzylpyridine rings with respect to the coordination core of about 45° (dihedral angles S1-Au-N1-C10 and S2-Au-C3-C8 in Figure 3.63, Table 3.47), allowed by the presence of the methylene bridging group.

Selected optimised bond lengths and angles are listed in Table 3.47, along with corresponding average experimental values extracted from the few structural reports found in the CCDC for similar systems.[229]
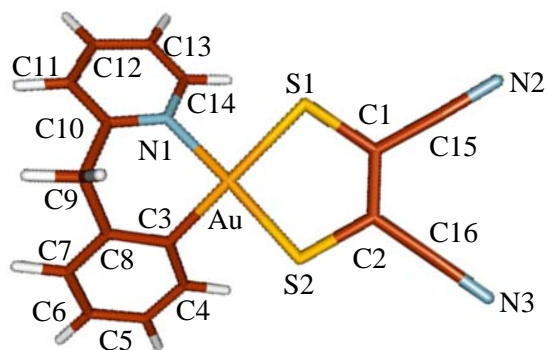
Figure 3.63. *Molecular drawing and atom labeling scheme of **76** at the optimised geometry.*

Table 3.47. *Selected optimised bond lengths (Å), angles and dihedrals (°) for **76** and relative average experimental values for analogue [Au(C^N)(S^S)] systems reported in the literature.*

	Optimised	Experimental[a]
Au-S1	2.366	2.333
Au-S2	2.279	2.288
Au-N1	2.106	2.072
Au-C3	2.056	2.072
S1- C1	1.756	1.748
S2-C2	1.744	1.738
C1-C2	1.368	1.363
ES-Au-S2	90.42	90.96
N1-Au-C3	87.93	81.34
S1-Au-N1-C10	136.63	/
S2-Au-C1-C8	138.56	/

[a] Mean values on six crystal structures deposited at the CCDC (Ref. 229).

Optimised metric parameters are in very good agreement with the experimental ones used for the comparison, and show that the two Au-S distances in the complex are in every case remarkably different. In particular, the Au-S distance *trans* to the Au-C bond (Au-S1 in Figure 3.63) is longer than the other one by about 0.1 Å. As expected, C-S and C-C bond lengths at the maleonitrile-1,2-dithiolate ligand are consistent with a ene-1,2-dithiolato limit form for this ligand.

In Figure 3.64 the KS-MO scheme calculated fo **76** in its ground state (*A*) is depicted, while in Figure 3.65 the contributions from the central gold atom and the two ligands to the composition of selected frontier MOs are summarised.
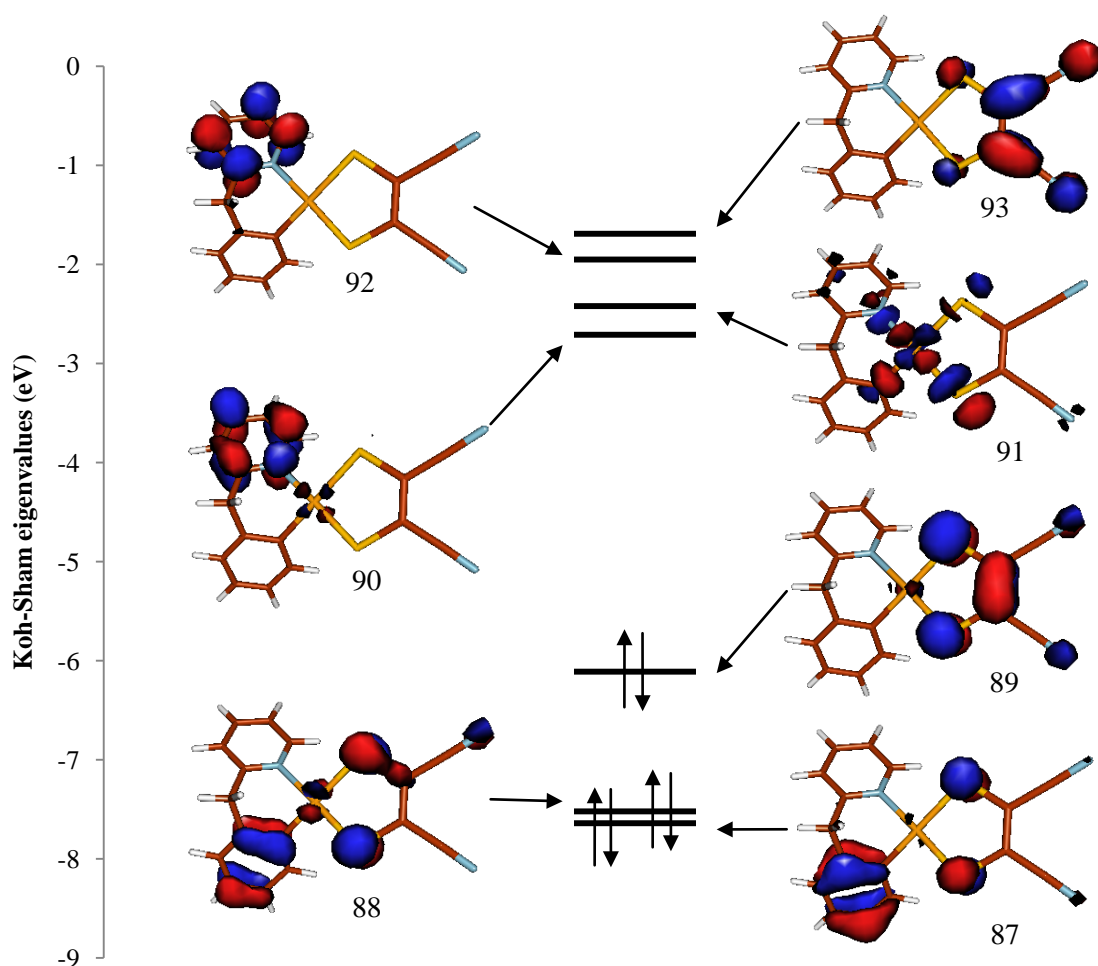
Figure 3.64. *KS-MO scheme and isosurface drawings calculated for **76**. Contour value = 0.05 e.*

In this complex, the HOMO (orbital 89 in Figures 3.64 and 3.65) is a π MO mainly localised on the S^S ligand, with only a minor participation of Au 5*d* character (7%), while the LUMO (orbital 90 in Figures 3.64 and 3.65) is almost exclusively located on the pyridine ring of the C^N ligand, and a contribution by the metal similar to that observed for the HOMO (7%) was calculated. Notably, the localisation of these molecular orbitals, as well as the entity of the contribution from the atomic orbitals of the metal, closely resemble those calculated for [Pt(N^N)(S^S)] complexes. The nature of the LUMO is consistent with the conclusions drawn from experimental cyclic voltammetry measurements (see above).
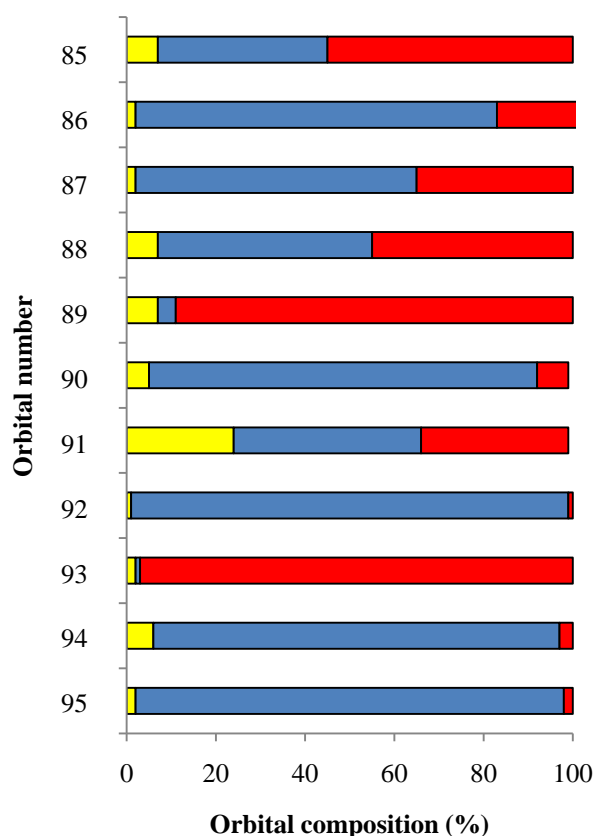
Figure 3.65. *Frontier molecular orbital (KS-MOs 85-95; HOMO = 89, LUMO = 90) composition calculated for 76 [fragments: gold atom (yellow); C^N ligand (blue); S^S ligand (red)].*

In Table 3.48, the results from a Mulliken population analysis are summarised for **76**. In particular, the charges Q carried by the central gold ion, the coordinating N, C, and S atoms and the ligands are reported. According to the results described for diimine-dithiolate complexes (Section 3.1.6.3), the mnt^{2-} ligand features a negative charge of about -0.4 e, while the C^N has a positive charge of 0.137 e, the remaining charge (0.290 e) being carried by the metal. Thus, similarly to what observed for [Pt(N^N)(S^S)] complexes, a charge separation of about 0.55 e is present between the two ligands (Table 3.48).

Table 3.48. *Mulliken charges Q (e) calculated on Au, S1, S2, N1, C3, the dithiolate ligand (N^N), and the 2-benzylpyridine (C^N) for* **76**.[a]

Q(Au)	0.290
Q(S1)	-0.019
Q(S2)	0.145
Q(N1)	-0.470
Q(C3)	-0.183
Q(C^N)	0.137
Q(S^S)	-0.427

[a] Numbering scheme as in Figure 3.63.

Time-dependent DFT (TD-DFT) calculations were also performed on complex **76** at its optimised geometry in its GS (*A*) at the same level of theory discussed above, and the main calculated vertical transitions are listed in Table 3.49, while in Figure 3.66 is depicted the simulated spectrum based on these calculations.

Table 3.49. *Principal electronic transitions (f > 0.05) calculated for **76** at TD-DFT level. For each transition, the excitation energy E (eV), the absortion wavelength (nm), the oscillator strenght f, and the molecular orbital composition of the excited-state functions, along with the fragments where the involved KS-MOs are mainly localised, are reported.*

Exc. State	E	λ	f	Composition[a]	%	Molecular fragments[b]
S5	3.844	322.7	0.068	89→93	78	S^S(89%)→S^S(97%)
S12	4.564	271.6	0.052	85→91	38	S^S(55%)+C^N(38%)→C^N(42%)+S^S(33%)
				89→94	55	S^S(89%)→C^N(91%)
S13	4.722	262.6	0.068	89→95	53	S^S(89%)→C^N(96%)
				89→94	18	S^S(89%)→C^N(91%)
				85→91	13	S^S(55%)+C^N(38%) →C^N(42%)+S^S(33%)
S15	4.828	256.8	0.246	88→92	66	C^N(48%)+S^S(45%)→C^N(98%)
S21	5.109	242.7	0.180	85→93	29	S^S(55%)+C^N(38%) →S^S(97%)
				87→93	13	C^N(63%)→ C^N(35%) →S^S(97%)
				88→93	41	C^N(48%)+S^S(45%)→ S^S(97%)
S25	5.394	229.8	0.086	82→90	50	C^C(43%)+S^S(45%)→ C^N(87%)
				83→90	12	C^N(66%)+S^S(27%)→ C^N(87%)
S33	5.915	209.6	0.077	79→90	37	Au(42%)+C^N(32%)→ C^N(87%)
				81→90	21	S^S(91%)→ C^N(87%)
				82→91	10	C^C(43%)+S^S(45%)→ C^N(42%)+S^S(33%)
S35	6.002	206.6	0.075	79 →91	19	Au(42%)+C^N(32%)→ C^N(42%)+S^S(33%)
				84→93	21	S^S(90%)→ S^S(97%)
				81→91	9	S^S(91%)→ C^N(42%)+S^S(33%)

[a] The molecular orbitals are labelled according to Figure 3.65; [b] C^N = 2-benzylpyridine; S^S = maleonitrile-1,2-dithiolate.

The simulated spectrum shows two main absorption bands in the spectral region 200-350 nm, in agreement with experimental data of **76** (Figure 3.61), although the transitions energies are slightly overestimated.
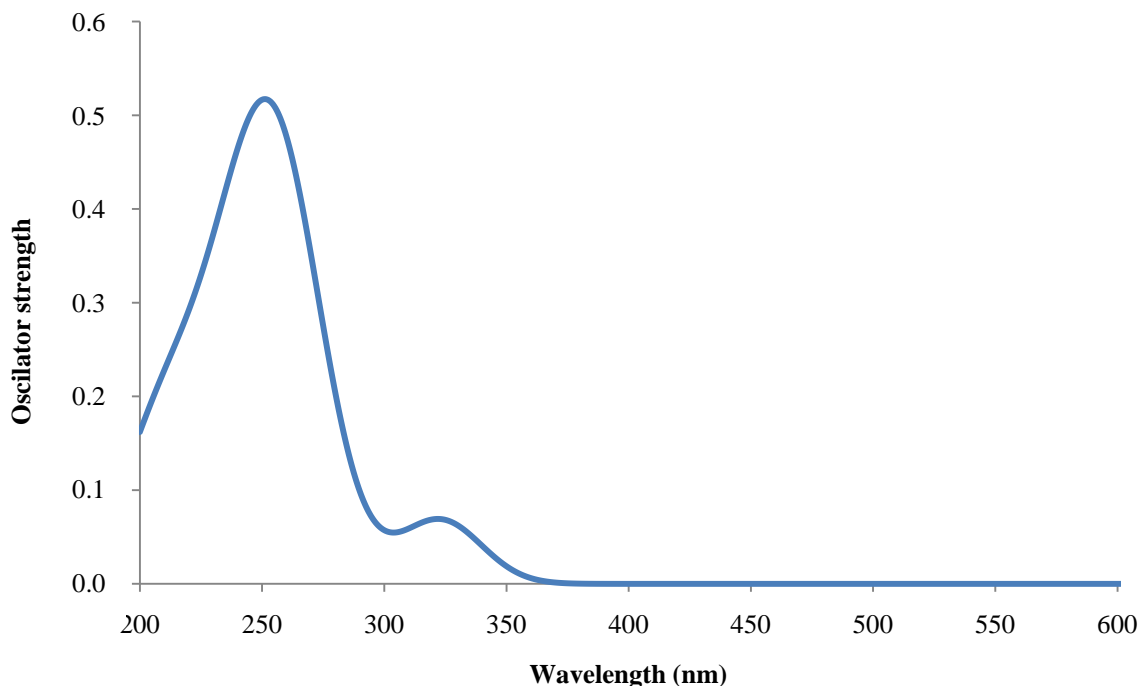
Figure 3.66. *Simulated UV-Vis spectrum (200-600 nm) based on TD-DFT calculations performed on **76** (Table 3.49).*

The absorption band at the lowest energy shown by **76** is assigned to the vertical electronic transition S0→S5, predominantly (78%) HOMO→ LUMO+3 in character, and thus occurring between MOs mainly localised on the maleonitrile-1,2-dithiolate ligand (89→93 excitation; Figure 3.65 and Table 3.49). The absorption at about 250 nm is calculated to derive from the overlap of several electronic transitions occurring in the range 4.5-6.0 eV.

Finally, also for this complex the first static hyperpolarisability (β_{tot}) was calculated at DFT level, and a value of $10 \cdot 10^{-30}$ esu was found. Thus, as compared to [Pt(N^N)(S^S)]

complexes **53-73** (Table 3.46), **76** seems to be a less promising candidate for NLO applications.

4. Conclusions

This PhD thesis has been focused on the synthesis and characterisation of new noncentrosymmetric complexes featuring 1,2-dichalcogenolene ligands, in order to investigate their potential NLO applications.

Bis-complexes of d^8 metals belonging to different classes were prepared and studied separately, in order to explore their structure-property relationships. The results obtained can be summarised as follows.

(i) Three new Au^{III} complexes featuring the asymmetrically substituted arylethylene-1,2-dithiolato ligands Ar,H-edt^{2-} (Ar = Ph, Naph, Pyr) were synthesised, and the effect of varying both the substituent Ar at the 1,2-dithiolene ligands and the total charge of the complex on the electrochemical and absorption and emission spectroscopic features of these systems was studied. Remarkably, an unprecedented investigation on the fluorescence features of gold(III) *bis*(1,2-dithiolene) complexes was performed, revealing interesting potential controlled emission features, and demonstrating that both the low energy NIR-absorption and emission properties of [Au(Ar,H-edt)$_2$]$^{x-}$ complexes are tunable by varying their oxidation state. These features were investigated by means of DFT and TD-DFT calculations, and the potential NLO features of the complexes were evaluated through the theoretical calculation of the first static hyperpolarisability β. The values obtained are comparable to those calculated for other NLO-active materials, and also in this case a dependence of the β value on the ligands' substituents and the total charge of the complex was observed and rationalised.

As a result, the [Au(Ar,H-edt)$_2$]$^{x-}$ complexes combine in a single molecular material the linear and nonlinear optical properties of the dithiolene core with the fluorescent features of the aryl substituents, and both properties can be tuned by varying Ar and *x*.

(ii) Twenty new diimine-dithiolate complexes [Pt(N^N)(E^E)] (E = S, Se) were synthesised by systematically varying both the diimine N^N and the 1,2-dichalcogenolate E^E, leading to the preparation of an homogeneous series of complexes whose properties were extensively studied by both experimental and theoretical means. Remarkably, two complexes featuring 1,2-diselenolene ligands were synthesised, only another [Pt(N^N)(Se^Se)] system having been reported so far in the literature. The electrochemical and spectroscopic characterisation of the complexes allowed to rationalise the effects induced by the different ligands on their chemical-physical features, and to correlate the redox potentials and the position of the characteristic solvatochromic absorption featured by these complexes. An in-depth DFT study allowed for the rationalisation of their optical properties, and a dependence of the first static hyperpolarisability value on the nature of the ligands was found, so that the structural features conferring the best SONLO properties were individuated. Further properties exploitable for ICT applications, such as photoconductivity, were also studied, resulting in very promising preliminary results.

iii) Two very original complexes were obtained: an unusual cyclometalated compound of the type [Au(C^N)(S^S)], and a [Pt(N^N)(S^S)] complex containing a ferrocenyl-substituted 1,2-dithiolene ligand, which represents the first platinum(II) complex featuring this ligand, whose peculiar redox behavior, due to the presence of the redox-active ferrocenyl substituent, was explained by means of spectroelectrochemical measurements. DFT calculations allowed also in this case for the study of the optical nonlinearities of the complexes, further contributing to the understanding of the effect induced by the variation of the ligands on heteroleptic *mono*-(1,2-dithiolene) complexes.

Summarily, a wide range of noncentrosymmetric complexes featuring 1,2-dichalcogene ligands with promising NLO applications were obtained, and the experimental and theoretical study of their structural, spectroscopic, and electrochemical properties deepened the knowledge on these complexes and outlined useful guidelines for further studies in this field.

5. Experimental

5.1. Instrumentation

5.1.1. Microanalytical measurements

Melting point measurements were carried in capillaries. Elemental analyses were performed with an EA1108 CHNS-O Fisons instrument ($T = 1000$ °C) for all of the products but for **73**, which was analysed by the Microanalytical Service of the Department of Chemistry of the University of Sheffield (U.K.).

5.1.2. FT-IR Spectroscopy

Infrared spectra were recorded with a Thermo-Nicolet 5700 spectrometer at room temperature: KBr pellets with a KBr beam-splitter and KBr windows (4000–400 cm^{-1}, resolution 4 cm^{-1}) were used.

5.1.3. ^{1}H NMR Spectroscopy

^{1}H NMR measurements were recorded on a Varian INOVA 400 MHz spectrometer at 298 K and referenced to $Si(CH_3)_4$.

5.1.4. Mass spectroscopy

The mass spectrum of **73** was recorded at the University of Sheffield (U.K.) on a Fisons/BG Prospec 3000 instrument operating in fast atom bombardment mode with *m*-nitrobenzyl alcohol as matrix.

5.1.5. UV-Vis-NIR Spectroscopy

Absorption spectra were recorded at 298 K in a quartz cell of 10.00 mm optical path with a Varian Cary 500 (200–2000 nm) or a Thermo Evolution 300 (190–1100 nm) spectrophotometer.

5.1.6. Emission spectroscopy

Uncorrected emission spectra were collected at 298 K with a Varian Cary Eclipse spectrophotometer equipped with a Xenon lamp. Quantum yields were determined relative to 2-aminopyridine in sulphuric acid 0.5 M aqueous solution and anthracene in ethyl alcohol for complexes **20-22** and **53-73/76**, respectively, by using Equation 5.1:[230]

$$\Phi_S = \Phi_R \frac{I_S}{I_R} \frac{\eta_S^2}{\eta_R^2} \tag{5.1}$$

where Φ = sample or reference fluorescence quantum yield; I = integrated fluorescence of the sample or reference; η = refractive index of the sample of reference solvent.

The integrated fluorescence of both the samples and the references were evaluated through the software Fytik[231] by decomposing the emission spectra in their Gaussian components.

5.1.7. Electrochemistry

Cyclic (scan rate 25–1000 mV s^{-1}) and differential pulsed voltammetry measurements were performed in anhydrous solvents in a Metrohm voltammetric cell, with a combined working and counter platinum electrode and a standard Ag/AgCl reference electrode with a Metrohm Autolab PGSTAT 10 potentiostat (supporting electrolyte $(TBA^+)(PF_6^-)$ 0.10 M): reported data are referred to the Fc^+/Fc reversible couple. HOMO and LUMO energy levels, referred to ferrocene were calculated, for reversible

processes, from the reduction and oxidation onsets (E_{onset}^{rd} and E_{onset}^{ox}, respectively) for

the one-electron processes through the equations $-E_{HOMO} = 4.80 + E_{onset}^{ox}$ and $-E_{LUMO} =$

$4.80 + E_{onset}^{rd}$, respectively.[192]

5.1.8. Spectroelectrochemistry

UV-Vis-NIR spectroelectrochemical measurements were performed at the University of

Sheffield in dry CH_2Cl_2 [supporting electrolyte $(TBA^+)(PF_6^-)$ 0.10 M], using an

optically transparent thin-layer electrode (OTTLE) cell fitted with platinum gauze,

platinum wire, and Ag/AgCl working, counter, and reference electrodes, respectively,

and mounted in a Cary 5000 spectrometer. The temperature was maintained at 273 K

throughout data collection. Potentials were applied using an EG&G model 273A

potentiostat linked to a computer with EG&G model 273 research electrochemistry

software.

5.1.9. X-ray diffraction

X-ray structure determinations for $(TBA^+)(\mathbf{21}^-)$, **26**, and **34** were carried out at the

EPSRC UK National Crystallography service, University of Southampton (U.K.).

Measurements were collected at 120(2) K by means of combined $\varPhi$ and $\varOmega$ scans with a

Bruker Nonius KappaCCD area detector situated at the window of a rotating anode

(graphite $Mo_{K\alpha}$ radiation, $\lambda = 0.71073$ Å). The structures were solved by direct methods

with SHELXS-97 and refined on F^2 by using SHELXL-97.[232] X-ray single-crystal

diffraction data for **57**, **58**, **59,** and **64** were collected at the University of St. Andrews

(U.K.). Data collections were performed on a SMART CCD area detector

diffractometer with graphite-monochromated $Mo_{K\alpha}$ radiation. Data collection was

performed at 93(2) K for **57**, and at 125(2) K for **58**, **59** and **64**. The structures were solved by direct methods with SHELXS-97 and refined on F^2 by using SHELXL-97.[232] X-ray structure determinations for **67** and **69** were carried out at the University of Rennes 1. Measurements were collected at 150(2) K with a Bruker-AXS diffractometer (Mo$_{K\alpha}$ radiation). The structures were solved by direct methods using the SIR97 program,[233] and then refined with full-matrix least-square methods based on F^2 (SHELXL-97)[232] with the aid of the WINGX program.[234] All the structures were validated by using the programs CheckCIF[235] and enCIFer.[236]

5.1.10. *Photoconduction measurements*

Photoconduction measurements were performed by Prof. M. Sampietro at the Politecnico di Milano (Milan, Italy). Prototype planar devices were prepared by casting a sonicated solution of the active material on a quartz substrate with previously lithographed gold/chromium electrodes, thus obtaining a metal-semiconductor-metal surface structure with interelectrode spacings of 6 μm. The devices were irradiated with light pulses lasting 500 μs produced by a set of light emitting diodes (LEDs), and the resulting photocurrents were measured by biasing the device with a voltage source and connecting it to a transimpedance amplifier. Output voltage was recorded by means of an Tektronix DPO4054 oscilloscope, from which the device photocurrent was numerically obtained on the basis of the feedback impedance of the amplifier. All measurements were performed in vacuum at a pressure below 10^{-5} mbar. The light intensity of each LED was measured by means of a silicon photodiode.

5.2. Synthesis

All operations were carried out under inert atmosphere. All the solvents were purchased from Aldrich and Merck, and when necessary, they were purified according to standard techniques. The degree of purity of each synthesised compound was checked by CHNS , ^{1}H NMR,[237] and TLC analysis.

2-Bromo-2′-acetophenone, 2-bromo-2′-acetonaphthone, 1-(bromoacetyl)pyrene, K_2PtCl_4, $KAuCl_4$, disodium 1,2-maleonitrile-1,2-dithiolate (Na$_2$mnt) and the diimines 2,2′-bipyridine (bipy), 1,10-phenanthroline (phen), 4,4′-dimethyl-2,2′-bipyridine (4,4′-Me$_2$-bipy), 5,5′-dimethyl-2,2′-bipyridine (5,5′-Me$_2$-bipy), 4,4′-di-*tert*-butyl-2,2′-bipyridine (4,4′-*t*Bu$_2$-bipy), 4,4′-diphenyl-2,2′-bipyridine (4,4′-Ph$_2$-bipy), 4,7-diphenyl-1,10-phenanthroline (4,7-Ph$_2$-phen), and 3,4,7,8-tetramethyl-1,10-phenanthroline (3,4,7,8-Me$_4$-phen), were used as received from Aldrich without further purification.

5.2.1. Synthesis and characterisation of ligands and precursors

The precursors of the ligands belonging to the class R-dmet^{2-}/R-dset^{2-} [*N*-methyl-4,5-*bis*(2′-cyanoethylthio)-1,3-thiazol-2-thione (**49**), *N*-ethyl-4,5-*bis*(2′-cyanoethylthio)-1,3-thiazol-2-thione (**50**), *N*-phenyl-4,5-*bis*(2′-cyanoethylthio)-1,3-thiazol-2-thione (**51**) and *N*-methyl-4,5-*bis*(2′-cyanoethylseleno)-1,3-thiazol-2-thione (**52**)] were synthesised according to literature procedures.[28,79,172] The diimine-dichloro platinum complexes [Pt(2,2′-bipy)Cl$_2$] (**41**), [Pt(1,10-phen)Cl$_2$] (**42**), [Pt(4,4′-Me$_2$-bipy)Cl$_2$] (**44**), [Pt(5,5′-Me$_2$-bipy)Cl$_2$] (**43**), [Pt(4,4′-*t*Bu$_2$-bipy)Cl$_2$] (**45**), [Pt(4,4′-Ph$_2$-bipy)Cl$_2$] (**46**), [Pt(4,7-Ph$_2$-phen)Cl$_2$] (**47**) and [Pt(3,4,7,8-Me$_4$-phen)Cl$_2$] (**48**) were prepared by the method of Morgan, by heating a mixture of the diimine suspended in a solution of 1 equivalent of K_2PtCl_4 in H_2O with an excess of HCl until the water solution was colorless (2-48 h), as also reported by Eisenberg and by Gillard.[127,210] The precursor of the ligand Fc,H-edt^{2-}

(Ferrocenyl-1,3-dithiol-2-one, **74**) was obtained following the general method reported by Gareau for the synthesis of 1,3-dithiol-2-ones,[19] by reacting ethynylferrocene (synthesised as reported by Wang)[211] with diisopropyl xanthogen disulfide in the presence of AIBN as radical initiator.[238] The complex $[Au(Py^1)(Cl_2)]$ (**77**; Hpy^1 = 2-benzylpyridine) was synthesised as reported in the literature.[197] The precursors of the ligands $Ar,H\text{-edt}^{2-}$ [Ar = Ph (**26**), 2-Naph (**27**), 1-Pyr (**28**)] were obtained by reacting α-haloketones bearing the desidered aryl substituent with isopropylxanthate, leading to the corresponding α-ketoxanthate esters, which undergo cyclisation in strongly acidic media to give a 1,3-dithiol-2-one.

5.2.1.1. Synthesis of isopropyl Xanthate

1.00 g of KOH (17.9 mmol) were refluxed for 60 minutes in 200 mL of isopropyl alcohol. After filtration on celite, 5 mL of CS_2 (83.10 mmol, d = 1.266 g/cm^3) in 15 mL of the same solvent at 0 °C were added dropwise. The reaction was cooled in ice for 30 minutes, then 30 mL of diethyl ether were added. The reaction mixture was left under stirring for 60 minutes, and the resulting precipitate recovered by filtration and dried under reduced pressure. Yield: 2.91 g (91.7%); m.p. > 240 °C; FTIR: $\tilde{v}$ = 1052 (vs), 1085 (vs), 1130 (s), 1148 (s), 1183 (s), 1371 (w), 2970 cm^{-1} (w); ^{1}H NMR ($CDCl_3$): δ = 5.456, 1.160 ppm; elemental analysis calcd (%) for $C_4H_7S_2O$: C 27.25, H 4.05, S 36.79; found: C 27.25, H 4.19, S 30.82.

5.2.1.2. Synthesis of O-Isopropyl S-Phenyl Dithiocarbonate (23)

A solution of 2-bromo-2′-acetophenone (4.15 g, 20.86 mmol) in acetone (40 mL) was added dropwise to potassium isopropyl xanthate (3.64 g, 20.86 mmol) dissolved in the same solvent (200 mL). After one hour of stirring, the solution was filtered through celite. After concentration under reduced pressure, an equivalent volume of water was

added. The product was filtered, washed with water and subsequently with hexane, and dried under reduced pressure. Yield: 4.50 g (84%); m.p. 65 °C; FTIR: $\tilde{v}$ = 750 (s), 872 (m), 904 (m), 984 (m), 1047 (m), 1093 (m), 1228 (s), 1325 (m), 1352 (m), 1373 (m), 1447 (s), 1578 (m), 1594 (m), 1692 (vs), 2930 (vw), 2987 (w), 3061 cm^{-1} (w); ^{1}H NMR (CDCl$_3$): δ = 8.005, 7.986, 7.582, 7.475, 5.658, 4.608, 1.342, 1.326 ppm; elemental analysis calcd (%) for C$_{12}$H$_{14}$O$_2$S$_2$: C 56.67, H 5.55, S 25.21; found: C 56.60, H 5.65, S 24.39.

5.2.1.3. Synthesis of O-Isopropyl S-Naphthacyl Dithiocarbonate (24)

The synthesis was carried out as described for *O*-isopropyl-*S*-phenyldithiocarbonate (**23**) starting from 2-bromo-2′-acetonaphthone (2.04 g, 8.20 mmol). Yield: 2.24 g (92%); m.p. 99 °C; FTIR: $\tilde{v}$ = 823 (w), 1026 (w), 1050 (s), 1094 (s), 1128 (vw), 1146 (w), 1224 (vs), 1347 (w), 1624 (w), 1692 (s), 2919 (vw), 2980 cm^{-1} (vw); ^{1}H NMR (CDCl$_3$): δ = 8.449, 8.249, 8.161, 8.055, 4.855, 4.687 ,1.385, 1.364 ppm; elemental analysis calcd (%) for C$_{16}$H$_{16}$O$_2$S$_2$: C 63.13, H 5.30, S 21.06; found: C 63.06, H 5.77, S 21.57.

5.2.1.4. Synthesis of O-Isopropyl S-Pyrenacyl Dithiocarbonate (25)

The synthesis was carried out as described for *O*-isopropyl-*S*-phenyldithiocarbonate (**23**) starting from 1-(bromoacetyl)pyrene (2.01 g, 3.10 mmol). Yield: 0.81 g (68%); m.p. 116–118 °C; FTIR: $\tilde{v}$ = 842 (vs), 959 (vw), 991 (w), 1045 (vs), 1087 (s), 1177 (w), 1216 (vw), 1234 (m), 1258 (vw), 1371 (vw), 1383 (w), 1371 (vw), 1592 (w), 1676 (m), 2987 cm^{-1} (vw); ^{1}H NMR (CDCl$_3$): δ = 8.939, 8.908, 8.440, 8.238, 8.179, 8.059, 5.739, 4.850, 1.386, 1.365 ppm; elemental analysis calcd (%) for C$_{22}$H$_{18}$S$_2$O$_2$: C 69.81, H 4.79, S 16.94; found: C 69.02, H 5.12, S 17.33.

5.2.1.5. Synthesis of Phenyl-1,3-dithiol-2-one (26)

Perchloric acid (3.0 mL, 65% w/w) was slowly added to a solution of *O*-isopropyl *S*-phenyl dithiocarbonate (**23,** 2.53 g, 9.96 mmol) in a 1:2 diethyl ether/chloroform mixture (18 mL). The reaction mixture was heated at reflux for one hour and then poured into ice. The organic phase, extracted with chloroform, was dried over Na_2SO_4. After filtration, the solvent was removed under reduced pressure. Crystals suitable for X-ray diffraction were obtained by slowly cooling a water/MeCN (1:1 v/v) saturated solution of the product. Yield: 1.66 g (86%); m.p. 90 °C; FTIR: $\tilde{v}$ = 743 (vs), 874 (s), 1074 (m), 1099 (m), 1443 (m), 1487 (m), 1578 (vw), 1647 (s), 1697 (vw), 1749 (w), 1958 (vw), 3089 cm^{-1} (vw); ^{1}H NMR (CDCl$_3$): δ = 7.393, 7.366, 6.807 ppm; elemental analysis calcd (%) for $C_9H_6S_2O$: C 55.64, H 3.11, S 33.01; found: C 55.69, H 3.19, S 32.60.

5.2.1.6. Synthesis of Naphthyl-1,3-dithiol-2-one (27)

The synthesis was carried out as described for phenyl-1,3-dithiol-2-one (**26**) starting from *O*-isopropyl *S*-naphthacyl dithiocarbonate (**24**, 2.51 g, 8.24 mmol). Yield: 1.72 g (86%); m.p. 145 °C; FTIR: $\tilde{v}$ = 754 (m), 776 (m), 860 (m), 888 (m), 1204 (w), 1361 (vw), 1633 (vs), 1503 (vw), 1708 (vw), 1741 (vw), 3051 (vw), 3089 cm-1 (vw); ^{1}H NMR (CDCl$_3$): δ = 8.253, 8.222, 7.944, 7.920, 7.350 ppm; elemental analysis calcd (%) for $C_{13}H_8S_2O$: C 63.91, H 3.30, S 26.24; found: C 63.56, H 3.55, S 25.49.

5.2.1.7. Synthesis of 1-Pyrenyl-1,3-dithiol-2-one (28)

The synthesis was carried out as described for phenyl-1,3-dithiol-2-one (**26**) starting from *O*-isopropyl *S*-pyrenacyl dithiocarbonate (**25**, 0.70 g, 1.86 mmol). Yield: 0.55 g (93%); m.p. 130 °C; FTIR: $\tilde{v}$ = 711 (s), 748 (w), 816 (w), 844 (vs), 1644 (s), 1685 (m), 2962 (w), 3038 cm^{-1} (w); ^{1}H NMR (CDCl$_3$): δ = 8.054, 8.056, 7.950, 7.890, 7.826,

7.729, 6.568 ppm; elemental analysis calcd (%) for $C_{19}H_{10}S_2O$: C 71.67, H 3.17, S 20.14; found: C 69.39, H 3.36, S 19.61.

5.2.2. Synthesis and characterisation of the 1,2-dithiolene complexes

5.2.2.1. Synthesis of (TBA$^+$)[Au(Ar,H-edt)$_2$]$^-$ complexes (Ar = Ph, 2-Naph, 1-Pyr)

The complexes were synthesised by reacting the 1,3-dithiol-2-one, obtained as previously reported (Sections 5.2.1.5-5.2.1.7), treated with strong bases to give the corresponding ethylene-1,2-dithiolates, with potassium tetrachloroaurate in the presence of tetrabutylammonium iodide. This leads to the formation of the desired gold *bis*(1,2-dithiolene) complexes as monoanions counterbalanced by tetrabutylammonium (TBA$^+$) cations.

5.2.2.1.1. Synthesis and characterisation of (TBA$^+$)[Au(Ph,H-edt)$_2$]$^-$ (TBA$^+$)(20$^-$)

An ethyl alcohol solution of KOH (40 mL; 0.17 g, 3.1 mmol) was added dropwise to 4-phenyl-1,3-dithiol-2-one (**26**, 30 mL EtOH; 0.25 g, 1.30 mmol) under an inert N_2 atmosphere. After addition of solutions of KAuCl$_4$ (15 mL; 0.25 g, 0.67 mmol) and (TBA$^+$)(I$^-$) (15 mL; 0.25 g, 0.69 mmol) in ethyl alcohol, the volume of the reaction mixture was reduced and the precipitate collected by filtration. Yield 0.12 g (24%); m.p. 128 °C; FTIR: $\tilde{v}$ = 691 (s), 746 (s), 1140 (vs), 1375 (vw), 1440 (w), 1484 (s), 1538 (s), 1571 (w), 1590 (w), 1718 (s), 2870 (vw), 2958 cm^{-1} (vw); UV-Vis-NIR (CH$_2$Cl$_2$): λ (ε) = 269 (35000), 296 sh (32000), 346 nm (12800 M^{-1} cm^{-1}); Fluorescence (CH$_2$Cl$_2$; λ_{exc} = 299 nm; slit = 10x10): λ_{em} = 390 nm, Φ = 2.4·10^{-3}; elemental analysis calcd (%) for $C_{32}H_{48}NS_4Au$: C 49.79, H 6.27, N 1.81, S 16.61; found: C 49.66, H 5.51, N 1.51, S 15.15; CV (CH$_2$Cl$_2$): $E_{1/2}$ vs Fc$^+$/Fc (scan rate 100 mV s^{-1}) = -2.013, -0.127 V.

5.2.3.1.2. Synthesis and characterisation of (TBA⁺)[Au(Naph,H-edt)₂]⁻ (TBA⁺)(21⁻)

The complex was synthesised as described for (TBA⁺)(20⁻) starting from naphthyl-1,3-dithiol-2-one (27, 0.25 g, 1.03 mmol). Crystals suitable for X-ray diffraction were obtained by slow evaporation of a CH_2Cl_2 solution of the complex. Yield: 0.16 g (36%); m.p. 186 °C; FTIR: $\tilde{v}$ = 748 (m), 780 (m), 815 (m), 855 (vw), 1123 (vw), 1379 (w), 1479 (w), 1456 (w), 1498 (m), 1531 (m), 1571 (w), 1592 (m), 2869 (vw), 2957 (w), 3050 cm⁻¹ (vw); UV-Vis-NIR (CH_2Cl_2): λ (ε) = 247 (65500), 295 sh (36000), 365 nm (13000 M⁻¹ cm⁻¹); Fluorescence (CH_2Cl_2; λ_{exc} = 290 nm; slit = 10x10): λ_{em} = 426 nm, Φ = 9.4·10⁻⁴; elemental analysis calcd (%) for $C_{40}H_{52}NS_4Au$: C 55.09, H 6.01, N 1.61, S 14.71; found: C 54.57, H 6.33, N 1.67, S 14.38; CV (CH_2Cl_2): $E_{1/2}$ vs Fc⁺/Fc (scan rate 100 mV s⁻¹) = -2.011, -0.120 V.

5.2.3.1.3. Synthesis and characterisation of (TBA⁺)[Au(Pyr,H-edt)₂]⁻ (TBA⁺)(22⁻)

The complex was synthesised as described for (TBA⁺)(20⁻) starting from 1-pyrenyl-1,3-dithiol-2-one (28, 0.25g, 0.78 mmol). Yield: 0.14 g (18%); m.p. 121 °C; FTIR: $\tilde{v}$ = 816 (m), 841 (m), 1020 (w), 1097 (w), 1134 (w), 1260 (m), 1454 (vw), 1695 (vw), 2870 (vw), 2960 (vw), 3037 cm⁻¹ (vw); UV-Vis-NIR (CH_2Cl_2): λ (ε) = 245 (99000), 282 (67500), 352 (43500), 435 sh nm (7400 M⁻¹ cm⁻¹); Fluorescence (CH_2Cl_2; λ_{exc} = 343 nm; slit = 10x10): λ_{em} = 465 nm, Φ = 1.0·10⁻³; elemental analysis calcd (%) for $C_{52}H_{20}NS_4Au$: C 61.22, H 5.53, N 1.37, S 12.57; found: C 61.01, H 5.40, N 1.14, S 12.30; CV (CH_2Cl_2): $E_{1/2}$ vs Fc⁺/Fc (scan rate 100 mV s⁻¹) = -2.038, -0.134 V.

5.2.2.2. Synthesis of Platinum(diimine)(dithiolate) complexes [Pt(N^N)(S^S)]

The Pt(diimine)(dithiolate) complexes were prepared by displacement of the two chlorides in the corresponding Pt(diimine)Cl$_2$ precursors with the desired dithiolate chelating ligand.

5.2.2.2.1. Synthesis and characterisation of [Pt(2,2'-bipy)(Ph,H-edt)] (53)

To a solution of 4-phenyl-1,3-dithiol-2-one (**26**, 0.06 g, 0.31 mmol) in 15 mL of dry ethyl alcohol a solution of KOH in the same solvent (15 mL; 0.07 g, 1.25 mmol) was added dropwise under a N$_2$ inert atmosphere. A suspension of [Pt(2,2′-bipy)Cl$_2$] (**41**, 0.13 g, 0.31 mmol) in 20 mL of dry THF was then added dropwise, and the reaction mixture was left under magnetic stirring for one week, resulting in the formation of a dark precipitate, which was collected by filtration and washed with ethyl alcohol and water. Yield: 0.10 g (52%); m.p. >240 °C; FTIR: $\tilde{v}$ = 415 (s), 445 (w), 454 (w), 553 (w), 612 (w), 619 (w), 645 (w), 671 (w), 684 (m), 716 (m), 742 (vs), 793 (m), 831 (w), 922 (m), 1032 (w), 1070 (w), 1124 (w), 1163 (m), 1260 (w), 1276 (w), 1315 (m), 1429 (w), 1446 (m), 1469 (s), 1486 (m), 1530(s), 1571 (w), 1591 (m), 3049 cm^{-1} (vw); UV-Vis-NIR (DMSO): λ (ε) = 257 (24000), 299 (34000), 327 (14000), 344 (11000), 604 nm (7000 M^{-1} cm^{-1}); Fluorescence (DMSO): λ_{exc} = 360 nm; slit = 5x5): λ_{em} = 374, 395 nm, Φ = 8.39·10^{-3}; ^{1}H NMR (DMSO-d_6): δ = 9.368, 9.245, 8.767, 8.480, 7.892, 7.716, 7.384, 7.248, 7.013 ppm; elemental analysis calcd (%) for C$_{18}$H$_{14}$N$_2$S$_2$Pt: C 41.77, H 2.73, N 5.41, S 12.39; found: C 41.23, H 2.85, N 5.04, S 11.99; CV (DMF): $E_{1/2}$ vs Fc$^+$/Fc (scan rate 100 mV s^{-1}) = -1.739, -0.135 V.

5.2.2.2.2. Synthesis and characterisation of [Pt(2,2'-bipy)(Naph,H-edt)] (54)

The complex was synthesised as described for [Pt(2,2′-bipy)(Ph,H-edt)] (**53**) starting from naphthyl-1,3-dithiol-2-one (**27**, 0.09 g, 0.35 mmol). Yield: 0.13 g (67%); m.p.

>240 °C; FTIR: $\tilde{v}$ = 475 (s), 718 (m), 748 (s), 761 (m), 811 (m), 1098 (vs), 1260 (m), 1384 (m), 1430 (w), 1446 (m), 1468 (m), 1508 (w), 1523 (m), 1561 (w), 1571 (w), 1594 (m), 1603 (m), 1619 (m), 1624 (m), 1638 (w), 1648 (w), 1655 (w), 1686 (w), 1719 (w), 1735 (w), 2345 (m), 2364 (m), 2926 (w), 2962 (w), 3057 cm^{-1} (vw); UV-Vis-NIR (DMSO): λ (ε) = 261 (27000), 301 (30000), 344 (11000), 381 (8000), 603 nm (6000 M^{-1} cm^{-1}); Fluorescence (DMSO; λ_{exc} = 359 nm; slit = 5x5): λ_{em} = 374, 395 nm, Φ = 1.08·10^{-2}; ^{1}H NMR (DMSO-d_6): δ = 9.426, 9.265, 8.785, 8.500, 8.315, 8.001, 7.941, 7.894, 7.588, 7.533, 7.250 ppm; elemental analysis calcd (%) for C$_{22}$H$_{16}$N$_2$S$_2$Pt: C 46.56, H 2.84, N 4.94, S 11.30; found: C 45.43, H 2.93, N 4.77, S 11.14; CV (DMF): $E_{1/2}$ vs Fc$^+$/Fc (scan rate 100 mV s^{-1}) = -1.727, -0.135 V.

5.2.2.2.3. Synthesis and characterisation of [Pt(2,2'-bipy)(Pyr,H-edt)] (55)

The complex was synthesised as described for [Pt(2,2′-bipy)(Ph,H-edt)] (**53**) starting from 1-pyrenyl-1,3-dithiol-2-one (**28**, 0.11 g, 0.35 mmol). Notwithstanding the numerous attempts to purify the complex, it was not possible to obtain the product in a pure solid with a satisfying elemental analysis. Yield: 0.15 g ; m.p. >240 °C; FTIR: $\tilde{v}$ = 413 (s), 156 (w), 645 (w), 655 (w), 681 (w), 717 (s), 737 (w), 760 (vs), 799 (w), 818 (w), 844 (s), 882 (w), 932 (w), 964 (w), 1026 (m), 1045 (m), 1072 (m), 1112 (m), 1127 (m), 1165 (s), 1243 (m), 1271 (w), 1450 (s), 1470 (s), 1498 (w), 1560 (w), 1605 (s), 3045 cm^{-1} (vw); UV-Vis-NIR (DMSO): λ = 270, 280, 320, 336, 351, 379, 592 nm; CV (DMF): $E_{1/2}$ vs Fc$^+$/Fc (scan rate 100 mV s^{-1}) = -1.620, -0.075 V.

5.2.2.2.4. Synthesis and characterisation of [Pt(2,2'-bipy)(Me-dmet)] (56)

A dry ethyl alcohol solution of NaOEt (15 mL, 2.80 mmol) was added dropwise to a solution of *N*-methyl-4,5-*bis*(2′-cyanoethylthio)-1,3-thiazol-2-thione in the same solvent (**49,** 15 mL; 0.11 g, 0.35 mmol) under a N$_2$ inert atmosphere. A suspension of [Pt(2,2′-

bipy)Cl$_2$] (**41**, 0.11 g, 0.35 mmol) in 20 mL of dry THF was then added dropwise, and the reaction mixture was left under stirring for one week, resulting in the formation of a dark precipitate, which was collected by filtration and washed with EtOH and H$_2$O. Yield: 0.11 g (66%); m.p. >240 °C; FTIR: $\tilde{v}$ = 534 (s), 713 (s), 748 (s), 936 (m), 1073 (m), 1085 (m), 1143 (s), 1316 (m), 1347 (s), 1432 (w), 1148 (s), 1472 (s), 1508 (s), 1605 (vs), 2346 (vw), 2817 (w), 3029 (vw), 3073 (vw), 3111 cm^{-1} (vw); UV-Vis-NIR (DMSO): λ (ε) = 260 (24000), 288 (20000), 315 (9000), 328 (10000), 378 (12000), 581 nm (4300 M^{-1} cm^{-1}); Fluorescence (DMSO; λ_{exc} = 335 nm; slit = 5x5): λ_{em} = 374, 395 nm, Φ = 1.85·10^{-2}; ^{1}H NMR (DMSO-d_6): δ = 9.065, 8.980, 8.774, 8.495, 7.883, 3.650 ppm; elemental analysis calcd (%) for C$_{14}$H$_{11}$S$_4$N$_3$Pt: C 30.88, H 2.04, N 7.72, S 23.55; found: C 29.80, H 1.92, N 7.36, S 21.67; CV (DMF): $E_{1/2}$ vs Fc$^+$/Fc (scan rate 100 mV s^{-1}) = -2.267, -1.608, -0.003 V.

5.2.2.2.5. Synthesis and characterisation of [Pt(2,2′-bipy)(Et-dmet)] (57)

The complex was synthesised as described for [Pt(2,2′-bipy)(Me-dmet)] (**56**) starting from *N*-ethyl-4,5-*bis*(2′-cyanoethylthio)-1,3-thiazol-2-thione (**50**, 0.15 g, 0.36 mmol). X-ray-quality crystals were obtained by slow infusion of diethyl ether into a THF solution of the complex. Yield: 0.09 g (44%); m.p. >240 °C; FTIR: $\tilde{v}$ = 715 (s), 749 (vs), 758 (s), 791 (m), 826 (w), 894 (s), 989 (w), 1016 (m), 1106 (m), 1143 (vs), 1243 (s), 1293 (m), 1316 (w), 1377 (s), 1432 (w), 1448 (s), 1471 (s), 1504 (s), 1606 (s), 2932 (w), 2974 (w), 3070 cm^{-1} (m); UV-Vis-NIR (DMSO): λ (ε) = 260 (24000), 291 (22000), 315 (10000), 327 (11000), 379 (13000), 582 nm (4500 M^{-1} cm^{-1}); Fluorescence (DMSO; λ_{exc} = 341 nm; slit = 5x5): λ_{em} = 375, 405 nm, Φ = 7.21·10^{-3}; ^{1}H NMR (DMSO-d_6): δ = 9.066, 9.990, 8.504, 7.894, 4.337, 1.408 ppm; elemental analysis calcd (%) for C$_{15}$H$_{13}$S$_4$N$_3$Pt: C 32.25, H 2.35, N 7.52, S 22.96; found: C 31.36, H 1.92, N

7.14, S 21.50; CV (DMF): $E_{1/2}$ vs Fc$^+$/Fc (scan rate 100 mV s^{-1}) = -2.255, -1.608, 0.008 V.

5.2.2.2.6. Synthesis and characterisation of [Pt(2,2'-bipy)(Ph-dmet)] (58)

The complex was synthesised as described for [Pt(2,2′-bipy)(Me-dmet)] (**56**) starting from *N*-phenyl-4,5-*bis*(2′-cyanoethylthio)-1,3-thiazol-2-thione (**51**, 0.14 g, 0.33 mmol). X-ray-quality crystals were obtained by slow infusion of *n*-hexane into an acetone solution of the complex. Yield: 0.13 g (66%); m.p. >240 °C; FTIR: $\tilde{v}$ = 411 (m), 455 (w), 501 (w), 629 (s), 702 (vs), 715 (m), 753 (s), 804 (w), 877 (s), 1019 (m), 1066 (s), 1124 (w), 1159 (m), 1264 (s), 1322 (s), 1384 (w), 1431 (m), 1446 (s), 1471 (s), 1506 (m), 1591 (m), 1604 cm^{-1} (m); UV-Vis-NIR (DMSO): λ (ε) = 259 (22000), 288 (22000), 316 (10000), 327 (10000), 392 (10000), 580 nm (4000 M^{-1} cm^{-1}); Fluorescence (DMSO; λ_{exc} = 334 nm; slit = 5x5): λ_{em} = 375, 405 nm, Φ = 1.21·10^{-2}; ^{1}H NMR (DMSO-d_6): δ = 9.021, 9.007, 8.756, 8.478, 7.890, 7.781, 7.272, 7.666, 7.474 ppm; elemental analysis calcd (%) for C$_{19}$H$_{13}$S$_4$N$_3$Pt: C 37.61, H 2.16, N 6.93, S 21.14; found: C 38.17, H 2.35, N 6.53, S 20.41; CV (DMF): $E_{1/2}$ vs Fc$^+$/Fc (scan rate 100 mV s^{-1}) = -2.267, -1.620, 0.044 V.

5.2.2.2.7. Synthesis and characterisation of [Pt(2,2'-bipy)(Me-dset)] (59)

A dry ethyl alcohol solution of NaOEt (15 mL; 3.64 mmol) was added dropwise to a solution of *N*-methyl-4,5-*bis*(2′-cyanoethylseleno)-1,3-thiazol-2-thione in the same solvent (**52,** 15 mL; 0.18 g, 0.45 mmol) under a N$_2$ inert atmosphere. A suspension of [Pt(2,2′-bipy)Cl$_2$] (**41**, 0.19 g, 0.45 mmol) in 20 mL of dry THF was then added dropwise, and the reaction mixture was left under stirring for one week, after which the solvent was removed under reduced pressure. The crude product obtained was then dissolved in 600 mL of CH$_2$Cl$_2$, filtered, and 100 mL of *n*-hexane were added dropwise,

Experimental

resulting in the precipitation of a dark solid, which was collected by filtration. X-ray-quality crystals were obtained by slow infusion of petroleum ether into a CH_2Cl_2 solution of the complex. Yield: 0.02g (9%); m.p. >240 °C; FTIR: $\tilde{v}$ = 411 (w), 481 (w), 517 (s), 638 (w), 712 (s), 747 (vs), 761 (m), 789 (w), 906 (w), 925 (w), 990 (m), 1068 (m), 1124 (vs), 1158 (w), 1246 (w), 1316 (m), 1336 (m), 1384 (w), 1432 (w), 1446 (s), 1471 (s), 1498 (m), 1604 (m), 3068 cm^{-1} (vw); UV-Vis-NIR (DMSO): $\lambda\,(\varepsilon)$ = 257 (17000), 277 (16000), 302 (16000), 331 (6000), 371 (11000), 569 nm (3500 $M^{-1}\,cm^{-1}$); Fluorescence (DMSO; λ_{exc} = 341 nm; slit = 5x5): λ_{em} = 373, 393 nm, Φ = 8.21·10^{-3}; elemental analysis calcd (%) for $C_{14}H_{11}N_3S_2Se_2Pt$: C 26.34, H 1.74, N 6.58, S 10.05; found: C 25.76, H 1.63, N 6.02, S 9.04; CV (DMF): $E_{1/2}$ vs Fc$^+$/Fc (scan rate 100 mV s^{-1}) = -2.243, -1.608, 0.044 V.

5.2.2.2.8. Synthesis and characterisation of [Pt(1,10-phen)(Ph,H-edt)] (60)

To a solution of 4-phenyl-1,3-dithiol-2-one (**26**, 0.06 g, 0.29 mmol) in 15 mL of dry EtOH an ethyl alcohol solution of KOH (15 mL; 0.06 g, 1.18 mmol) was added dropwise under a N_2 inert atmosphere. A suspension of [Pt(1,10-phen)Cl$_2$] (**42**, 0.13 g, 0.30 mmol) in 20 mL of dry THF was then added dropwise, and the reaction mixture was left under stirring for one week, resulting in the formation of a dark precipitate, which was collected by filtration and washed with EtOH and H_2O. Yield: 0.10 g (61%); m.p. >240 °C; FTIR: $\tilde{v}$ = 420 (m), 506 (m), 613 (w), 620 (w), 650 (w), 669 (w), 693 (s), 709 (vs), 726 (w), 746 (vs), 783 (w), 834 (vs), 903 (w), 922 (m), 1032 (w), 1073 (w), 1092 (w), 1151 (w), 1202 (m), 1219 (m), 1296 (m), 1316 (w), 1346 (w), 1414 (m), 1428 (s), 1449 (w), 1485 (m), 1525 (s), 1571 (w), 1589 (m), 1627 (w), 3058 cm^{-1} (vw); UV-Vis-NIR (DMSO): $\lambda\,(\varepsilon)$ = 271 (38000), 347 (10000), 606 nm (5400 $M^{-1}\,cm^{-1}$); Fluorescence (DMSO; λ_{exc} = 359 nm; slit = 5x5): λ_{em} = 374, 400 nm, Φ = 1.34·10^{-2}; ^{1}H NMR (DMSO-d_6): δ = 9.798, 9.654, 9.537, 9.146, 9.085, 8.737, 8.281, 8.261, 7.852,

7.402, 7.261, 7.004 ppm; elemental analysis calcd (%) for $C_{20}H_{14}N_2S_2Pt$: C 44.36, H 2.61, N 5.17, S 11.84; found: C 43.26, H 2.61, N 5.82, S 10.68; CV (DMF): $E_{1/2}$ vs Fc^+/Fc (scan rate 100 mV s^{-1}) = -1.716, -0.147 V.

5.2.2.2.9. Synthesis and characterisation of [Pt(1,10-phen)(Naph,H-edt)] (61)

To a solution of naphthyl-1,3-dithiol-2-one (**27**, 0.07 g, 0.29 mmol) in 15 mL of dry EtOH an ethyl alcohol solution of KOH (15 mL; 0.06 g, 1.16 mmol) was added dropwise under a N_2 inert atmosphere. A suspension of [Pt(1,10-phen)Cl$_2$] (**42**, 0.13 g, 0.29 mmol) in 20 mL of dry THF was then added dropwise, and the reaction mixture was left stirring for one week, after which the solvent was removed under reduced pressure. The solid obtained was then dissolved in 200 mL of CH_2Cl_2, filtered, and 350 mL of *n*-hexane were added dropwise, resulting in the precipitation of a dark solid, which was collected by filtration. Yield: 0.04 g (24%); m.p. >240 °C; FTIR: $\tilde{v}$ = 464 (m), 560(w), 553 (w), 523 (w), 651 (w), 707 (vs), 725 (w), 745 (m), 780 (m), 809 (m), 824 (s), 849 (m), 872 (w), 915 (w), 1093 (w), 1144 (w), 1202 (m), 1258 (w), 1292 (w), 1343 (w), 1385 (w), 1429 (s), 1450 (w), 1501 (w), 1521 (m), 1569 (w), 1593 (m), 1619 cm^{-1} (w); UV–Vis-NIR (DMSO): λ (ε) = 271 (43000), 353 (9000), 378 (9000), 603 nm (3600 M^{-1} cm^{-1}); Fluorescence (DMSO; λ_{exc} = 349 nm; slit = 5x5): λ_{em} = 374, 400 nm, Φ = 1.52·10^{-2}; ^{1}H NMR (DMSO-d_6): δ = 9.707, 9.661, 9.557, 9.167, 9.097, 98.375, 8.243, 8.038, 7.956, 7.891, 7.594, 7.537, 7.231 ppm; elemental analysis calcd (%) for $C_{24}H_{16}N_2S_2Pt$: C 48.73, H 2.71, N 4.74, S 10.85; found: C 47.23, H 2.41, N 4.90, S 11.51; CV (DMF): $E_{1/2}$ vs Fc^+/Fc (scan rate 100 mV s^{-1}) = -1.728, -0.159 V.

5.2.2.2.10. Synthesis and characterisation of [Pt(1,10-phen)(Pyr,H-edt)] (62)

The complex was synthesised as described for [Pt(1,10-phen)(Ph,H-edt)] (**60**) starting from 1-pyrenyl-1,3-dithiol-2-one (**28**, 0.14 g, 0.33 mmol). Notwithstanding the

numerous attempts to purify the complex, it was not possible to obtain the product as a pure solid with a satisfying elemental analysis. Yield: 0.12g; m.p. >240 °C; FTIR: $\tilde{v}$ = 707 (vs), 725 (m), 777 (m), 839 (vs), 884 (w), 995 (w), 1035 (w), 1092 (w), 113 (w), 1153 (m), 1028 (w), 1220 (w), 1039 (w), 1347 (w), 1409 (w), 1427 (s), 1456 (w), 1494 (w), 1515 (m), 1558 (w), 1578 (m), 1605 (m), 1627 (w), 3082 cm^{-1} (w); UV-Vis-NIR (DMSO): λ = 270, 330, 348, 389, 596 nm; CV (DMF): $E_{1/2}$ vs Fc$^+$/Fc (scan rate 100 mV s^{-1}) = -1.620, -0.075 V.

5.2.2.2.11. Synthesis and characterisation of [Pt(1,10-phen)(Me-dmet)] (63)

An ethyl alcohol solution of NaOEt (15 mL; 2.48 mmol) was added dropwise to *N*-methyl-4,5-*bis*(2′-cyanoethylthio)-1,3-thiazol-2-thione (**49,** 15 mL dry EtOH; 0.09 g, 0.31 mmol) under a N$_2$ inert atmosphere. A suspention of [Pt(1,10-phen)Cl$_2$] (**42**, 0.14 g, 0.31 mmol) in 20 mL of dry THF was then added dropwise, and the reaction mixture was left stirring for one week, resulting in the formation of a dark precipitate, which was collected by filtration and washed with EtOH and H$_2$O. Yield: 0.12g (70%); m.p. >240 °C; FTIR: $\tilde{v}$ = 412 (m), 504 (m), 535 (s), 666 (w), 706 (vs), 725 (m), 756 (m), 833 (vs), 919 (m), 942 (s), 1016 (m), 1074 (m), 1140 (s), 1217 (w), 1203 (w), 1301 (w), 1345 (s), 1431 (s), 1432 (w), 1057 cm^{-1} (s); UV-Vis-NIR (DMSO): λ (ε) = 267 (51000), 379 (14000), 581 nm (5000 M^{-1} cm^{-1}); Fluorescence (DMSO; λ_{exc} = 337 nm; slit = 5x5; M): λ_{em} = 372, 405 nm, Φ = 8.21·10^{-3}; ^{1}H NMR (DMSO-d_6): δ = 9.818, 9.445, 9.361, 9.153, 8.403, 8.235, 3.624 ppm; elemental analysis calcd (%) for C$_{16}$H$_{11}$N$_3$S$_4$Pt: C 33.80, H 1.95, N 7.39, S 22.56; found: C 34.20, H 1.82, N 7.38, S 21.85; CV (DMF): $E_{1/2}$ vs Fc$^+$/Fc (scan rate 100 mV s^{-1}) = -1.620, -0.015 V.

5.2.2.2.12. Synthesis and characterisation of [Pt(1,10-phen)(Et-dmet)] (64)

The complex was synthesised as described for [Pt(1,10-phen)(Me-dmet)] (**63**) starting from *N*-ethyl-4,5-*bis*(2′-cyanoethylthio)-1,3-thiazol-2-thione (**50**, 0.15 g, 0.33 mmol). X-ray-quality crystals were obtained by slow infusion of diethyl ether into a CH_2Cl_2 solution of the complex. Yield: 0.16 g (82%); m.p. >240 °C; FTIR: $\tilde{v}$ = 505 (w), 527 (m), 548 (m), 654 (m), 708 (s), 768 (w), 793 (w), 837 (vs), (s), 1014 (m), 1065 (m), 1106 (w), 1143 (s), 1221 (w), 1246 (m), 1292 (m), 1379 (s), 1430 (s), 1503 (w), 1633 (w), 2968 cm^{-1} (w); UV-Vis-NIR (DMSO): λ (ε) = 264 (34000), 378 (12000), 579 nm (4000 M^{-1} cm^{-1}); Fluorescence (DMSO; λ_{exc} = 350 nm; slit = 5x5): λ_{em} = 375, 391, 404, 433 nm, Φ = 9.15·10^{-3}; ^{1}H NMR (DMSO-d_6): δ = 9.800, 9.338, 9.271, 9.119, 8.388, 8.276, 8.196, 4.34, 1.420 ppm; elemental analysis calcd (%) for $C_{17}H_{13}S_4N_3Pt$: C 35.04, H 2.24, N 7.21, S 22.01; found: C 35.25, H 2.63, N 6.59, S 20.75; CV (DMF): $E_{1/2}$ vs Fc^+/Fc (scan rate 100 mV s^{-1}) = -1.620, -0.027 V.

5.2.2.2.13. Synthesis and characterisation of [Pt(1,10-phen)(Ph-dmet)] (65)

The complex was synthesised as described for [Pt(1,10-phen)(Me-dmet)] (**63**) starting from *N*-phenyl-4,5-*bis*(2′-cyanoethylthio)-1,3-thiazol-2-thione (**51**, 0.14 g, 0.32 mmol). Yield: 0.18 g (88%); m.p. >240 °C; FTIR: $\tilde{v}$ = 419 (w), 453 (w), 501 (m), 532 (w), 628 (s), 702 (vs), 725 (m), 767 (m), 835 (s), 877 (s), 1016 (m), 1066 (s), 1095 (w), 1165 (w), 1222 (w), 1268 (s), 1324 (m), 1413 (w), 1429 (s), 1452 (w), 1494 (s), 1592 (w), 1618 cm^{-1} (w); UV-Vis-NIR (DMSO): λ (ε) = 265 (36000), 391 (11000), 581 nm (4600 M^{-1} cm^{-1}); Fluorescence (DMSO; λ_{exc} = 337 nm; slit = 5x5): λ_{em} = 373, 403, 419 nm, Φ = 2.76·10^{-2}; ^{1}H NMR (DMSO-d_6): δ = 9.290, 9.090, 9.039, 8.351, 8.190, 8.086, 7.749, 7.684, 7.504 ppm; elemental analysis calcd (%) for $C_{21}H_{13}N_3S_4Pt$: C 39.99, H 2.07, N 6.66, S 20.34; found: C 38.97, H 2.20, N 6.44, S 20.80; CV (DMF): $E_{1/2}$ vs Fc^+/Fc (scan rate 100 mV s^{-1}) = -1.632, 0.020 V.

5.2.2.2.14. Synthesis and characterisation of [Pt(1,10-phen)(Me-dset)] (66)

The complex was synthesised as described for [Pt(1,10-phen)(Me-dmet)] (**63**) starting from *N*-methyl-4,5-*bis*(2′-cyanoethylseleno)-1,3-thiazol-2-thione (**52**, 0.14 g, 0.30 mmol). Yield: 0.11 g (55%); m.p. >240 °C; FTIR: $\tilde{v}$ = 502 (w), 517 (s), 650 (w), 705 (vs), 724 (m), 754 (w), 787 (w), 831 (s), 916 (m), 990 (s), 1063 (m), 1126 (s), 1151 (w), 1217 (w), 1294 (w), 1340 (m), 1430 (m), 1502 (m), 1578 cm^{-1} (w); UV-Vis-NIR (DMSO): λ (ε) = 271 (41000), 374 (16000), 570 nm (5000 M^{-1} cm^{-1}); Fluorescence (DMSO; λ_{exc} = 279 nm; slit = 5x5): λ_{em} = 375, 395 nm, Φ = 1.18·10^{-2}; elemental analysis calcd (%) for C$_{16}$H$_{11}$N$_3$S$_2$Se$_2$Pt: C 29.01, H 1.67, N 6.34, S 9.68; found: C 30.93, H 2.38, N 7.21, S 8.40; CV (DMF): $E_{1/2}$ vs Fc$^+$/Fc (scan rate 100 mV s^{-1}) = -1.620, -0.027 V.

5.2.2.2.15. Synthesis and characterisation of [Pt(5,5′-Me$_2$-bipy)(Me-dmet)] (67)

The complex was synthesised as described for [Pt(2,2′-bipy)(Me-dmet)] (**56**) starting from [Pt(5,5′-Me$_2$-bipy)Cl$_2$] (**43**, 0.11 g, 0.25 mmol). X-ray-quality crystals were obtained by slow infusion of diethyl ether into a CH$_2$Cl$_2$ solution of the complex. Yield: 0.06 g (42%); m.p. >240 °C; FTIR: $\tilde{v}$ = 665 (w), 713 (m), 809 (vs), 830 (w), 938 (s), 1015 (w), 1086 (m), 1143 (s), 1255 (m), 1300 (w), 1336 (s), 1382 (m), 1475 (s), 1507 (s), 1577 (w), 1607 (w), 1655 cm^{-1} (w); UV-Vis-NIR (DMSO): λ (ε) = 259 (28000), 292 (21000), 323 (12000), 334 (15000), 378 (12000), 567 nm (4700 M^{-1} cm^{-1}); Fluorescence (DMSO; λ_{exc} = 337 nm; slit = 5x5): λ_{em} = 372, 391 nm, Φ = 8.84·10^{-3}; ^{1}H NMR (DMSO-d_6): δ = 8.798, 8.744, 8.629, 8.325, 3.700. 2.619 ppm; elemental analysis calcd (%) for C$_{16}$H$_{15}$S$_4$N$_3$Pt: C 33.57, H 2.64, N 7.34, S 22.40; found: C 32.36, H 2.39, N 7.01, S 21.02; CV (DMF): $E_{1/2}$ vs Fc$^+$/Fc (scan rate 100 mV s^{-1}) = -1.727, -0.027 V.

5.2.2.2.16. Synthesis and characterisation of [Pt(4,4′-Me$_2$-bipy)(Me-dmet)] (68)

The complex was synthesised as described for [Pt(2,2′-bipy)(Me-dmet)] (**56**) starting from [Pt(4,4′-Me$_2$-bipy)Cl$_2$] (**44**, 0.15 g, 0.34 mmol). Yield: 0.18 g (90%); m.p. >240 °C; FTIR: $\tilde{v}$ = 515 (s), 537 (s), 668 (w), 827 (s), 872 (w), 934 (m), 1033 (w), 1088 (m), 1145 (vs), 1222 (w), 1251 (w), 1304 (w), 1339 (m), 1378 (w), 1427 (m), 1489 (w), 1513 (m), 1618 (s), 3028 cm^{-1} (vw); UV-Vis-NIR (DMSO): λ (ε) = 261 (24000), 281 (24000), 311 (9000), 324 (9000), 379 (12000), 563 nm (4500 M^{-1} cm^{-1}); Fluorescence (DMSO; λ_{exc} = 339 nm; slit = 5x5): λ_{em} = 375, 399 nm, Φ = 1.12·10^{-2}; elemental analysis calcd (%) for C$_{16}$H$_{15}$N$_3$S$_4$Pt: C 33.66, H 2.64, N 7.34, S 22.39; found: C 34.53, H 1.64, N 7.45, S 23.98; CV (DMF): $E_{1/2}$ vs Fc$^+$/Fc (scan rate 100 mV s^{-1}) = -1.740, -0.015 V.

5.2.2.2.17. Synthesis and characterisation of [Pt(4,4'-tBu$_2$-bipy)(Me-dmet)] (69)

The complex was synthesised as described for [Pt(2,2′-bipy)(Me-dmet)] (**56**) starting from [Pt(4,4′-*t*Bu$_2$-bipy)Cl$_2$] (**45**, 0.14 g, 0.23 mmol). X-ray-quality crystals were obtained by slow infusion of petroleum ether into a CH$_2$Cl$_2$ solution of the complex. Yield: 0.10 g (65%); m.p. >240 °C; FTIR: $\tilde{v}$ =668 (w), 735 (w), 837 (s), 877 (m), 902 (w), 941 (s), 1014 (w), 1086 (m), 1143 (vs), 1203 (w), 1253 (m), 1309 (w), 1343 (s), 1364 (w), 1417 (s), 1458 (w), 1490 (w), 1512 (m), 1541 (w), 1560 (w), 1616 (s), 2960 (m) cm^{-1} ; UV-Vis-NIR (DMSO): λ (ε) = 258 (24000), 291 (24000), 313 (9000), 325 (10000), 379 (13000), 564 nm (5000 M^{-1} cm^{-1}); Fluorescence (DMSO; λ_{exc} = 341 nm; slit = 5x5): λ_{em} = 375, 399 nm, Φ = 1.55·10^{-2}; ^{1}H NMR (DMSO-d_6): δ = 8.970, 8.891, 8.772, 7.917, 3.392, 1.547 ppm; elemental analysis calcd (%) for C$_{22}$H$_{27}$S$_4$N$_3$Pt: C 40.23, H 4.14, N 6.40, S 19.53; found: C 41.46, H 4.60, N 6.73, S 18.80; CV (DMF): $E_{1/2}$ vs Fc$^+$/Fc (scan rate 100 mV s^{-1}) = -1.692, -0.015 V.

5.2.2.2.18. Synthesis and characterisation of [Pt(4,4'-Ph$_2$-bipy)(Me-dmet)] (70)

The complex was synthesised as described for [Pt(2,2′-bipy)(Me-dmet)] (**56**) starting from [Pt(4,4′-Ph$_2$-bipy)Cl$_2$] (**46**, 0.12 g, 0.20 mmol). Yield: 0.08 g (56%); m.p. >240 °C; FTIR: $\tilde{v}$ = 412 (m), 473 (w), 535 (m), 629 (w), 638 (w), 691 (s), 723 (w), 756 (s), 835 (m), 878 (m), 938 (m), 1014 (w), 1078 (m), 1142 (vs), 1257 (w), 1341 (s), 1412 (s), 1505 (m), 1541 (m), 1613 cm^{-1} (s); UV-Vis-NIR (DMSO): λ (ε) = 264 (38000), 300 (34000), 341 (15000), 381 (15000), 608 nm (5600 M^{-1} cm^{-1}); Fluorescence (DMSO; λ_{exc} = 350 nm; slit = 5x5): λ_{em} = 372, 391 nm, Φ = 1.84·10^{-2}; ^{1}H NMR (DMSO-d_6): δ = 9.241, 9.013, 8.943, 8.196, 8.061, 7.749, 3.648 ppm; elemental analysis calcd (%) for C$_{24}$H$_{19}$S$_4$N$_3$Pt: C 42.85, H 2.85, N 6.24, S 19.06; found: C 43.69, H 2.73, N 6.37, S 20.12; CV (DMF): $E_{1/2}$ vs Fc$^+$/Fc (scan rate 100 mV s^{-1}) = -2.112, -1.561, -0.040 V.

5.2.2.2.19. Synthesis and characterisation of [Pt(3,7-Ph$_2$-phen)(Me-dmet)] (71)

The complex was synthesised as described for [Pt(2,2′-bipy)(Me-dmet)] (**56**) starting from [Pt(4,7-Ph$_2$-phen)Cl$_2$] (**47**, 0.11 g, 0.19 mmol). Yield: 0.10 g (72%); m.p. >240 °C; FTIR: $\tilde{v}$ = 489 (w), 533 (m), 577 (w), 637 (m), 666 (m), 701 (s), 729 (m), 763 (s), 833 (m), 934 (m), 1018 (w), 1084 (m), 1144 (vs), 1228 (m), 1339 (s), 1400 (w), 1423 (s), 1443 (w), 1508 (m), 1558 (w), 1600 (w), 1621 cm^{-1} (w); UV-Vis-NIR (DMSO): λ (ε) = 274 (39000), 298 (39000), 341 (16000), 377 (18000), 794 nm (5700 M^{-1} cm^{-1}); Fluorescence (DMSO; λ_{exc} = 338 nm; slit = 5x5): λ_{em} = 373, 394 nm, Φ = 1.83·10^{-2}; elemental analysis calcd (%) for C$_{26}$H$_{19}$S$_4$N$_3$Pt: C 44.82, H 2.75, N 6.03, S 18.41; found: C 46.34, H 3.14, N 6.50, S 17.82; CV (DMF): $E_{1/2}$ vs Fc$^+$/Fc (scan rate 100 mV s^{-1}) = -1.561, -0.002 V.

5.2.2.2.20. Synthesis and characterisation of [Pt(3,4,7,8-Me$_4$-phen)(Me-dmet)] (72)

The complex was synthesised as described for [Pt(2,2′-bipy)(Me-dmet)] (**56**) starting from [Pt(3,4,7,8-Me$_4$-phen)Cl$_2$] (**48**, 0.11 g, 0.22 mmol). Yield: 0.08 g (58%); m.p.

>240 °C; FTIR: $\tilde{v}$ = 472 (w), 533 (m), 580 (w), 708 (s), 800 (m), 901 (w), 935 (m), 1011 (w), 1084 (m), 1143 (vs), 1336 (s), 1385 (m), 1431 (m), 1508 (s), 1541 (w), 1560 (w), 1577 (w), 1625 (m), 1647 (s), 1654 (w), 1701 (w), 1718 (w), 1735 cm^{-1} (w); UV-Vis-NIR (DMSO): λ (ε) = 265 (15000), 285 (16000), 378 (6000), 549 nm (3700 M^{-1} cm^{-1}); Fluorescence (DMSO; λ_{exc} 345 = nm; slit = 5x5): λ_{em} = 384, 402 nm, Φ = 6.45·10^{-3}; elemental analysis calcd (%) for C$_{20}$H$_{19}$N$_3$S$_4$Pt: C 38.45, H 3.06, N 6.73, S 20.53; found: C 38.65, H 3.13, N 6.61, S 18.24; CV (DMF): $E_{1/2}$ vs Fc$^+$/Fc (scan rate 100 mV s^{-1}) = -1.789 V.

5.2.2.2.21. Synthesis and characterisation of [Pt(4,4'-tBu$_2$-bipy)(Fc,H-edt)] (73)

The complex was synthesised as described for [Pt(4,4′-tBu$_2$-bipy)(Me-dmet)] (**69**) starting from ferrocenyl-1,3-dithiol-2-one (**74**, 65 mg, 0.21 mmol). Yield: g 0.09 (60%); m.p. >240 °C; FTIR: $\tilde{v}$ = 419 (w), 465 (m), 491 (s), 515 (w), 564 (w), 599 (s), 643 (m), 736 (m), 767 (s), 798 (m), 815 (w), 834 (vs), 850 (w), 865 (w), 876 (w), 903 (w), 951 (m), 999 (m), 1022 (m), 1034 (vw), 1049 (m), 1129 (w), 1205 (s), 1265 (w), 1313 (w), 1358 (m), 1370(w), 1395 (w), 1416 (vs), 1463 (m), 1479 (m), 1535 (w), 1555 (w), 1589 (w), 1614 (vs), 1655 (w), 2869 (w), 2955 (m), 3089 cm^{-1} (w); UV-Vis-NIR (DMSO): λ (ε) = 256 (21000), 296 (29000), 413 (1800), 611 nm (5400 M^{-1} cm^{-1}); Fluorescence (DMSO; λ_{exc} = 351 nm; slit = 5x5): λ_{em} = 372, 392, 409 nm, Φ = 1.37·10^{-2}; elemental analysis calcd (%) for C$_{30}$H$_{34}$N$_2$S$_2$PtFe: C 48.84, H 4.65, N 3.80, S 8.69; found: C 48.44, H 4.53, N 3.67, S 8.61; CV (CH$_2$Cl$_2$): $E_{1/2}$ vs Fc$^+$/Fc (scan rate 100 mV s^{-1}) = -1.472, 0.216, 0.613, 0.773 V; Mass spectrum: *m/z* 737 (M$^+$).

5.2.2.3. Synthesis and characterisation of [Au(Py^1)(mnt)] (76)

11 mg ($2.52 \cdot 10^{-5}$ mol) of [Au(Py^1)(Cl$_2$)] (**77**) were reacted with 1 equivalent (4.7 mg) of disodium 1,2-maleonitrile-1,2-dithiolate in 30 mL of a CH$_2$Cl$_2$/MeCN mixture (1:2 v/v) for 10 minutes in an Aldrich pressure tube at 130 ℃. After cooling, the resulting yellow precipitate was filtered off and washed with H$_2$O. Yield: 1 mg (8%); m.p. >240 ℃; FTIR: $\tilde{v}$ = 497 (m), 552 (m), 622 (s), 669 (w), 710 (w), 752 (vs), 959 (w), 1022 (w), 1035 (w), 1155 (w), 1169 (w), 1226 (w), 1384 (m), 1430 (w), 1438 (w), 1459 (w), 1489 (w), 1508 (s), 1541 (w), 1560 (w), 1610 (w), 1637 (w), 1648 (w), 1654 (w), 1717 (w), 2211 cm^{-1} (m); UV-Vis-NIR (DMF): λ (ε) = 268 (35000), 334 sh (6000), 349 nm (8000 M^{-1} cm^{-1}); Fluorescence (DMSO; λ_{exc} = 339 nm; slit = 5x5): λ_{em} = 377, 406 nm, Φ = $9.88 \cdot 10^{-3}$; elemental analysis calcd (%) for C$_{16}$H$_{10}$N$_3$SAu: C 38.03, H 1.99, N 8.31, S 12.69; found: C 37.52, H 1.36, N 8.16, S 11.16; CV (DMSO): E_{pa} vs Fc$^+$/Fc (scan rate 100 mV s^{-1}) = -1.20 V.

5.3. Theoretical Calculations

Theoretical calculations were performed at the DFT level with the Gaussian suite of programs (in the editions G03, Rev. E.01, or G09, Rev. A.02)[239,240] on a 64-bit E4 workstation equipped with four quad-core AMD Opteron processors and 16 Gb of RAM and running the OpenSuSE 10.2 Linux operating system. As a general procedure, geometry were optimised starting from structural data, when available. The nature of the minima of each optimised structure was verified by harmonic frequency calculations (*freq=raman* keyword). Natural and Mulliken atomic charges were calculated at the optimised geometries. When required, electronic transition energies and oscillator strength values were calculated at TD-DFT level. The electronic spectra were simulated

by a convolution of Gaussian functions centred at the calculated excitation energies. The programs Gaussview 5.0,[241] Gabedit 2.1.0[242] and Molden 4.7-4.9[243] were used to investigate the charge distributions and molecular orbital shapes. The software GaussSum 2.1[244] was used to calculate the molecular orbital contributions (MOC) from groups of atoms, along with the contribution of singly excited configurations to each electronic transition, and to generate all the necessary data to simulate absorption spectra.

5.3.1. Calculations on [Au(Ar,H-edt)$_2$]$^{x-}$ complexes (20^{x-}-22^{x-}) (x = 0-2)

Theoretical calculations were performed on the *cis* and *trans* isomers of complexes **20**$^{x-}$, **21**$^{x-}$ and **22**$^{x-}$ adopting the mPW1PW[198] hybrid functional. Schäfer, Horn, and Ahlrichs double-ζ plus polarisation all-electron basis sets[199] were used for C, H, and S, whereas the LanL2DZ (d,p)[200] basis set with relativistic effective core potentials[200] was adopted for the heavier Au species. Geometry optimisations were performed on the *cis* and *trans* isomers, and were regularised by letting the model complexes belong to an ideal C_2 point group, with the Au(C$_2$S$_2$)$_2$ planar core lying on the *xy* plane and the *y* axis crossing the C-C bond middle points. PES scanning was performed for the three complexes (*cis* and *trans* isomers) by imposing the rotation of the phenyl ring (between -90 and 90°, steps of 10°) and optimising the resulting geometry at each rotational step (*opt=modredundant* keyword).

5.3.2. Calculations on [Pt(N^N)(S^S)] complexes (53-73, 75) and [Au(Py^1)(mnt)] (76)

Theoretical calculations were performed adopting the PBE0 (PBE1PBE)[220] hybrid functional. Schäfer, Horn, and Ahlrichs double-ζ plus polarisation all-electron basis

sets[199] were used for C, H, N, S, Se and Fe, whereas the CRENBL[221] basis set with relativistic effective core potentials[200] was adopted for the heavier Pt and Au species.[245] The choice of this computational setup derives from a series of preliminary calculations performed on **56** and **59**, the results of which are summarised in Annex A. Geometry optimisations were regularised by letting the model complexes belong to an ideal C_s (for **56-59**, **63-72** and **75**) or C_1 (for **53-55**, **60-62**, **73**, and **76**) point group. For the geometry optimisation of the complexes, tight SCF convergence criterion (*SCF=tight* keyword) and fine numerical integration grids [*Integral(FineGrid)* keyword] were used. In order to determine the influence of the solvent on the properties of the complexes, solvation calculations were also carried out at the same level of theory, by using the IEF-PCM model of SCRF theory[222] [*SCRF=(solvent=)* keyword]. The programs Gabedit 2.1.0[242] and Molden 4.7[243] were used to investigate the charge distributions and molecular orbital shapes. The software GaussSum 2.1[244] was used to calculate the molecular orbital contributions (MOC) from groups of atoms, along with the contribution of singly excited configurations to each electronic transition, and to generate all the necessary data to simulate absorption spectra.

Annex A

A.1. Preliminary calculations performed on 56

As mentioned in Sections 3.2.1.7 and 5.3.1, the theoretical investigation performed on [Pt(N^N)(S^S)] complexes **53-73** was preceded by a series of preliminary calculations aimed at identifying a proper computational setup for these systems. Complex **56** was chosen as a benchmark compound, and both the functional and the basis set (BS) for the metal atom were systematically varied, while Ahlrich's double-ζ basis set with polarisation functions[199] was adopted for light atomic species in all calculations. The functionals tested include: (i) pure functionals such as PW91PW91,[246] PBEPBE,[247] wPBEhPBE,[248] and PBEhPBE;[249] (ii) the hybrid functionals B3LYP,[250] PBE0 (PBE1PBE),[220] PBEh1PBE,[249] and mPW1PW;[198] (iii) pure functionals implemented with the long-range correction by Hirao and coworkers,[251] namely LC-PBEhPBE, LC-PBEPBE, and LC-PW91PW91; (iv) and long-range corrected functionals such as LC-wPBE,[251] CAM-B3LYP,[252] and wB97X.[253] As regards BSs, CRENBL,[221] LanL2DZ,[200] LanL2TZ,[254] SBKJC VDZ,[255] and Stuttgardt RSC 1997[256] BSs, all with Effective Core Potentials (ECPs),[200] were tested.

In the first part of this study, the geometry of **56** was optimised employing the CRENBL+ECP[257] and Ahlrichs pVDZ BSs on Pt and light atomic species, respectively, and by systematically varying the functional. These calculations were performed both in the gas phase and by simulating the presence of CH_2Cl_2 by means of the IEF-PCM approach of SCRF theory. In Table A.1, selected average optimised bond lengths obtained in the gas phase with the fifteen functional adopted are listed. An examination of the results clearly shows that DFT provides very reliable estimates of the selected bond distances, with average bond lengths values of 2.29(2), 2.05(2), 1.74(1), and

1.36(2) Å for Pt-S, Pt-N, C-S, and C-C distances, respectively. In order to evaluate the closeness between calculated and experimental metric parameters, both absolute and relative differences were evaluated. In Table A.1 the sum of the relative deviations (SRD) over the four selected distances is reported (the crystal data of **57**, differing from **56** just for the presence of an ethyl in place of a methyl substitutent at the 1,2-dithiolene ligand, were exploited for this purpose). These data show that the optimised geometries in best agreement with experimental ones were obtained by adopting the long-range corrected functionals and the mPW1PW, PBE0, and PBEh1PBE ones, the Pt-S distances being particularly affected by the functional.

Table A.1. *Selected average experimental bond lengths (Å) for* **57**, *corresponding optimised distances (Å) obtained with different functionals on* **56**, *and sum of relative deviations (SRD).[a,b]*

	Pt-S	Pt-N	C-S	C-C	SRD$\cdot 10^{-2}$
wB97X	2.297	2.082	1.747	1.350	3.79
LC-wPBE	2.276	2.055	1.726	1.338	2.29
CAM-B3LYP	2.296	2.067	1.748	1.351	3.03
PW91PW91	2.296	2.067	1.748	1.351	5.17
LC-PW91PW91	2.254	2.025	1.726	1.338	3.50
PBEPBE	2.300	2.045	1.740	1.384	5.19
LC- PBEPBE	2.253	2.023	1.727	1.339	3.51
PBEhPBE	2.306	2.05	1.741	1.384	5.50
LC- PBEhPBE	2.254	2.024	1.727	1.339	3.42
wPBEhPBE	2.306	2.050	1.741	1.384	5.50
mPW1PW	2.285	2.043	1.736	1.362	3.22
PBE0	2.282	2.040	1.735	1.363	3.36
PBEh1PBE	2.286	2.043	1.735	1.363	3.39
B3LYP	2.310	2.068	1.747	1.367	4.94
Experimental values	2.2715	2.0465	1.7515	1.341	/

[a] Atom labelling scheme as in Figure 3.22. [b] CRENBL+ECP BS for Pt.

Furthermore, time-dependent DFT (TD-DFT) calculations were carried out on **56** at the geometries optimised with the different functionals, and the results obtained by adopting the IEF-PCM model of the SCRF approach were compared with the experimental spectroscopic features of **56** in CH_2Cl_2. In particular, the energy of the S0→S1 transition (mainly deriving from the HOMO→LUMO excitation), responsible for the experimental solvatochromic absorption (Section 3.2.1.7.3), was analysed, and the results are listed in Table A.2.

Table A.2. *Absorption maxima λ_{max} (nm) for the electronic transition S0→S1 calculated at IEF-PCM SCRF TD-DFT level for **56** with different functionals, corresponding experimental value, and difference between experimental and calculated data $\Delta\lambda_{max}$ (nm).*[a]

	λ_{max}	$\Delta\lambda_{max}$
Experimental	633	/
wB97X	381	-252
LC-wPBE	359	-274
CAM-B3LYP	489	-144
PW91PW91	1077	444
LC-PW91PW91	343	-290
PBEPBE	1076	443
LC- PBEPBE	344	-289
PBEhPBE	1085	452
LC- PBEhPBE	344	-289
wPBEhPBE	1085	452
mPW1PW	359	-244
PBE0	739	106
PBEh1PBE	740	107
B3LYP	826	193

[a] CRENBL+ECP BS for Pt

The data clearly show that the energy of this transition is over- or under-stimated by all calculations (-290 nm < $\Delta\lambda_{max}$ < 452 nm), but the lowest absolute values of $\Delta\lambda_{max}$ (106-107 nm) are found for calculations performed with PBE0 and PBEh1PBE functionals. Thus, given the combined results of geometry optimisation and TD-DFT calculations,

the functional PBE0 was chosen to perform the DFT calculations on all [Pt(N^N)(E^E)] complexes included in the present study.

Calculations were then performed on **56** by adopting the PBE0 functional, in combination with four different BSs, all featuring ECPs, in order to compare the results of these calculations with the ones obtained by employing the CRENBL+ECP basis set. Also in this case, a geometry optimisation was performed for each BS both in the gas phase and by adopting the IEF-PCM approach (CH$_2$Cl$_2$), followed by TD-DFT calculations. The results were evaluated by comparing selected optimised bond lengths with corresponding experimental values of **57**, and S0→S1 transition energies with experimental λ_{max} of the solvatochromic absorption band. The results are listed in Tables A.3 and A.4.

Table A.3. *Selected average experimental bond lengths (Å) for* **57**, *corresponding optimised distances (Å) obtained with different basis sets (all featuring ECPs) on* **56**, *and sum of relative deviations (SRD).*[a,b]

	Pt-S	Pt-N	C-S	C-C	SRD·10^{-2}
Experimental	2.271	2.046	1.751	1.341	/
CRENBL	2.282	2.040	1.735	1.363	3.36
LANL2DZ	2.300	2.050	1.733	1.363	4.14
LANLDTZ	2.277	2.031	1.732	1.363	3.79
SBKJC VDZ	2.292	2.054	1.733	1.363	4.00
Stuttgardt RSC 1997	2.290	2.051	1.734	1.362	3.63

[a] Atom labelling scheme as in Figure 3.22. [b] PBE0 functional.

The results obtained from the geometry optimisations indicate that calculations performed by adopting the CRENBL+ECP basis set feature the best agreement between experimental and calculated data, thus confirming the previous results.[257] On the other hand, regarding TD-DFT calculations, no significant differences can be observed in the

energy of the S0→S1 electronic transition calculated with the five BSs under exam (less than 15 nm, $\Delta\lambda_{max}$ = 100-112 nm), thus suggesting that excited state calculations are not particularly affected by the identity of the BS employed. Thus, given the very good agreement between experimental and optimised geometries obtained by employing the CRENBL+ECP BS, it was chosen to perform DFT calculations on all [Pt(N^N)(E^E)].

Table A.4. *Absorption maxima λ_{max} (nm) of the electronic transition S0→S1 calculated for* **56** *at IEF-SCRF TD-DFT level with different BSs (all with ECPs) in CH_2Cl_2, corresponding experimental value, and difference between experimental and calculated data $\Delta\lambda_{max}$ (nm).[a]*

	λ_{max}	$\Delta\lambda_{max}$
Experimental	633	/
CRENBL	739	106
LANL2DZ	733	100
LANL2TZ	733	100
SBKJC VDZ	736	103
Stuttgardt RSC 1997	745	112

[a] PBE0 functional.

A.2. Calculations performed on 59 with CRENBL+ECP on Se

As already mentioned in Section 5.3.1, the geometry of **59** was optimised also by adopting the CRENBL+ECP BS instead of the full-electron Ahlrichs pVDZ BS for Se, in order to account for the relativistic effects for this heavy atomic species. In Table A.5 selected optimised bond lengths obtained in the gas phase with the two basis sets are listed, along with corresponding experimental values and the sum of relative deviations (SRD). Given the very small difference between the two values of SRD obtained (less than 1×10^{-3}), the improvement conferred by ECPs to the agreement between experimental and calculated data was considered negligible, and thus the Ahlrichs BS

was employed on all atomic species but the metals to perform the DFT calculations on

59, analogously to all other [Pt(N^N)(E^E)] complexes included in this study.

Table A.5. *Selected average experimental bond lengths (Å) for **59**, corresponding optimised distances (Å) obtained with full electron Ahlrichs pVDZ and CRENBL basis sets, and sum of relative deviations (SRD).[a,b]*

	Experimental	Ahlrichs pVDZ	CRENBL+ECP
Pt-Se	2.387	2.386	2.403
Pt-N	2.068	2.058	2.053
C-Se	1.902	1.875	1.887
C-C	1.319	1.359	1.356
SRD	/	$4.94 \cdot 10^{-2}$	$4.90 \cdot 10^{-2}$

[a] Atom labelling scheme as in Figure 3.22. [b] PBE0 functional.

References and Notes

[1] J. A. McCleverty, *Prog. Inorg. Chem.,* **1968**, *10,* 49.

[2] (a) W. H. Mills, R. E. D. Clarck, *J. Chem. Soc.*, **1963**, 175; (b) R. E. D. Clarck, *Analyst*, **1936**, *60*, 242; (c) R. E. D. Clarck, *Analyst*, **1937**, *62*, 661.

[3] G. Bähr, H. Schleitzer, *Chem. Ber.,* **1957**, *90,* 438.

[4] D. B. Stevancevic, V. C. Drazic, *Bull. Inst. Nucl. Sci. "Boris Kidrich"*, **1959**, *9*, 69.

[5] G. N. Schrauzer, V. P. Mayweg, *J. Am. Chem. Soc.,* **1962**, *84*, 3221.

[6] H. B. Gray, R. Willimas, I. Bernal, E. Billig, *J. Am. Chem. Soc.,* **1962**, *84*, 3596.

[7] This is testified, as an example, by the recent publication of the volume "Dithiolene Chemistry-Synthesis, Properties, and Applications" (E. I. Stiefel ed., *Progr. Inorg. Chem.,* **2004**, *52*) and the Special Issue "Dithiolenes and non-innocent redox-active ligands" in *Coord. Chem. Rev.,* **2010**, *254*.

[8] F. J. Hine, A. J. Taylor, C. D. Garner, *Coord. Chem. Rev.,* **2010**, *254*, 1570.

[9] (a) A. Davison, E. T. Shawl, *Chem. Commun.,* **1967**, 670; (b) A. Davison, E. T. Shawl, *Inorg. Chem.,* **1970**, *9*, 1820.

[10] See for example: (a) G. Matsubayashi, S. Tanaka, A. Yokozawa, *J. Chem. Soc., Dalton Trans.,* **1992**, 1827; (b) S. Ford, C. P. Morley, M. Di Vaira, *Inorg. Chem.,* **2004**, *43*, 7101; (c) M. Nomura, T. Cauchy, M. Geoffroy, P. Adkine, M. Formiguè, *Inorg. Chem.,* **2006**, *45*, 8194; (d) C. C. McLauchlan, S. D. Robowski, J. A. Ibers, *Inorg. Chem.,* **2001**, *40*, 1372; (e) R.-M. Olk, B. Olk, J. Rohloff, J. Reinhold, J. Sieler, K. Trübenbach, R. Kimrse, E. Hoyer, *Z. Anorg. Allg. Chem.,* **1992**, *609*, 103.

[11] (a) T. Klapötke, H. Köpf, P. Gowik, *Polyhedron*, **1987**, *6*, 1923; (b) R. D. McCullough, J. A. Belot, J. Seth, A. L. Rheingold, G. P. A. Yap, D. O. Cowan, *J. Mater. Chem.,* **1995**, *5*, 1581; (c) W. A. Flomer, J. W. Kolis, *Inorg. Chem.,* **1989**, *28*, 2513; (d) D. M. Giolando, T. B. Rauchfuss, A. L. Rheingold, *Inorg. Chem.,* **1987**, *26*, 1636.

[12] M.C. Aragoni, M. Arca, F. Demartin, F. A. Devillanova, A. Garau, F. Isaia, F. Lelj, V. Lippolis, G. Verani, *J. Am. Chem. Soc.,* **1999**, *121*, 7098.

[13] T. B. Rauchfuss, *Progr. Inorg. Chem.,* **2004**, *52*, 1.

[14] G. C. Papavassiliou, S. Y. Yiannoupoulos, J. S. Zambounis, *Chem. Scr.,* **1987**, *27*, 265.

[15] N. D. Lowe, C. D. Garner, *J. Chem. Soc., Dalton Trans.,* **1993**, 2197.

[16] D. J. Sandman, G. W. Allen, L. A. Acampora, J. C. Stark, S. Jansen, M. T. Jones, G. J. Ashwell, B. M. Foxman, *Inorg. Chem.,* **1987**, *26*, 1664.

[17] E. S. Davies, R. L. Beddoes, D. Collinson, A. Dinsmore, A. Docrat, J.A. Joule, C. R. Wilson, C. D. Garner, *J. Chem. Soc., Dalton Trans.,* **1997**, 3985.

[18] (a) H. Sugimoto, M. Harihara, M. Shiro, K. Sugimoto, K. Tanaka, H. Miyake, H. Tsukube, *Inorg. Chem.,* **2005**, *44*, 6386; (b) J. M. Tunney, A. J. Blake, E. S. Davies, J. McMaster, C. Wilson, C. D. Garner, *Polyhedron*, **2006**, *25*, 591.

[19] Y. Gareau, A. Beuchemin, *Heterocycles,* **1998**, *48*, 2003.

[20] R. K. Brown, T. J. Bergendahl, J .S. Wood, J. H. Waters, *Inorg. Chim. Acta*, **1983**, *68*, 79.

[21] F. Wudl, E. T. Zellers, S. D. Cox, *Inorg. Chem.,* **1985**, *24*, 2864.

[22] A. Davison, R. H. Holm, *Inorg. Synth.,* **1967**, *10*, 8.

References and Notes

---

[23] (a) G. Steimecke, H. J. Sieler, R. Kirmse, E. Hoyer, *Phosphorus and Sulphur,* **1979**, *7*, 49; (b) R.-M. Olk, W. Dietzsch, E. Hoyer, *Synth. React. Inorg. Met.-Org. Chem.,* **1984**, *14*, 915; (c) G. Matsubayashi, A. Yokozawa, *J. Chem. Soc., Dalton Trans.,* **1990**, 3535; (d) G. Matsubayashi, A. Yokozawa, *J. Chem. Soc., Dalton Trans.,* **1990**, 3013; (e) G. Matsubayashi, K. Akiba, *J. Chem. Soc., Dalton Trans.,* **1990**, 115; (f) R.-M. Olk, W. Dietzsch, E. Hoyer, G. Steimecke, *Patent DD236100,* **1986**; (g) M. Kodani, K. Takimiya, Y. Aso, T. Otsubo, T. Nakayashiki, Y. Misaki, *Synthesis,* **2001**, 1614; (h) E. Cerrada, M. Laguna, *Can. J. Chem.,* **1998**, *76*, 1033.

[24] R.-M. Olk, W. Dietzsch, R. Kirmse, J. Stack, E. Hoyer, *Inorg. Chim. Acta,* **1987**, *128*, 251.

[25] (a) K. Hartke, T. Kissel, J. Quante, and R. Matusa, *Chem. Ber.*, **1980**, *113*, 1898; (b) J. P. Cornelissen, B. Pomarede, A. L. Spek, D. Reefman, J. P. Haasnoot, J. Reedijk, *Inorg. Chem.,* **1993**, *32*, 3720.

[26] (a) F. Bigoli, P. Deplano, F.A. Devillanova, V. Lippolis, P. J. Lukes, M. L. Mercuri, M. A. Pellinghelli, E. F. Trogu, *J. Chem. Soc., Chem. Commun.,* **1995**, 371; (b) F. Bigoli, P. Deplano, F.A. Devillanova, V. Lippolis, P. J. Lukes, M. L. Mercuri, M. A. Pellinghelli, E. F. Trogu, J. M. Williams, *Inorg. Chem.,* **1997**, *36*, 1218; (c); F. Bigoli, P. Deplano, M. L. Mercuri, M. A. Pellinghelli, G. Pintus, E. F. Trogu,, G. Zonnedda, H. H. Wang, J. M. Williams, *Inorg. Chim. Acta*, **1998**, *273*, 175; (d) M. Arca, F. Demartin, F. A. Devillanova, A. Garau, F. Isaia, F. Lelj, V. Lippolis, S. Pedraglio, G. Verani, *J. Chem. Soc., Dalton Trans.,* **1998**, 3731; (e) F. Bigoli, S. Curreli, P. Deplano, L. Leoni, M. L. Mercuri, M. A. Pellinghelli, A. Serpe, E. F. Trogu, *J. Chem. Soc., Dalton Trans.,* **2002**, 1985.

[27] M. C. Aragoni, M. Arca, F. A. Devillanova, F. Isaia, V. Lippolis, A. Mancini, L. Pala, A. M. Z. Slawin, J. D. Woollins, *Inorg. Chem.,* **2005**, *44*, 9610.

[28] (a) S. Eid, M. Formigué, T. Roisnel, D. Lorcy, *Inorg. Chem.,* **2007**, *46*, 10647; (b) S. Eid, M. Guerro, D. Lorcy, *Tetrahedron Lett.*, **2006**, *47*, 8333.

[29] G. Periyasamy, N. A. Burton, I. H. Hillier, M. A. Vicent, H. Disley, J. McMaster, C. D. Garner, *Faraday Discuss.,* **2007**, *135*, 469.

[30] K. Jørgeson, *Coord. Chem. Rev.,* **1966**, *1*, 164.

[31] M. D. Ward, J. A. McCleverty, *J. Chem. Soc., Dalton Trans.,* **2002**, 275.

[32] G. Bruno, M. Almeida, F. Artizzu, J. C. Dias, M. L. Mercuri, L. Pilia, C. Rovira, X. Ribas, A. Serpe, P. Deplano, *Dalton. Trans.,* **2010**, *39*, 4566.

[33] H. Alves, D. Simão, I. C. Santos, V. Gama, R. Y. Henriques, H. Novais, M. Almeida, *Eur. J. Inorg. Chem.,* **2004**, 1318.

[34] H. Sugimoto, M. Tarumizu, K. Tanaka, H. Miyake, H. Tsukube, *Dalton Trans.,* **2005**, 3558.

[35] (a) H. Fujiwara. E. Ojima, H. Kobayashi, T. Courcet, I. Malfant, P. Cassoux, *Eur. J. Inorg. Chem.,* **1998**, 1631; (b) Y. Ji, J.-L. Zuo, L. Chen, Y.-Q. Tian, Y. Song, Y.-Z. Li, X.-Z- You, *J. Phys. Chem. Sol.,* **2005**, *66*, 207; (c) J. Morgado, L. C. Santos, M. T. Duarte, L. Alcacer, M. Almeida, *Chem. Commun.,* **1996**, 1837.

[36] U. Zoller, *Compr. Heterocycl. Chem. II,* **1996**, *1B*, 1113.

[37] U. T. Mueller-Westerhoff, B. Vance, *Compr. Coord. Chem.,* **1987**, *2*, 597.

[38] (a) G. N. Schrauzer, V. P. Mayweg, *J. Am. Chem. Soc.,* **1965**, *87*, 1483; (b) G. N. Schrauzer, V. P. Mayweg, W. Heinrich, *Inorg. Chem.,* **1965**, *4*, 1615.

[39] S. Sheibe, B. J. Pedersen, S.-O. Lawesson, *Bull. Soc. Chim. Belg.,* **1978**, *87*, 229.

[40] U. T. Mueller-Westerhoff, B. Vance, D. I. Yoon, *Tetrahedron*, **1991**, *110*, 115.

[41] (a) C. M. Bolinger, T. B. Rauchfuss, S. R. Wilson, *J. Am. Chem. Soc.,* **1981**, *103*, 5620; (b) T. B. Rauchfuss, *Inorg. Chem.,* **2004**, *43*, 14.

[42] (a) C. M. Bolinger, T. B. Rauchfuss, *Inorg. Chem.,* **1982**, *21*, 3947; (b) R.-M. Olk, W. Dietzsch, J. Kahlmeier, P. Jörchel, R. Kirmse, J. Sieler, *Inorg. Chim. Acta,* **1997**, *254*, 375; (c) F. Bigoli, P. Cassoux, P. Deplano, M. L. Mercuri, M. A. Pellinghelli, G. Pintus, A. Serpe, E. F. Trogu, *J. Chem. Soc., Dalton Trans.,* **2000**, 4639.

[43] (a) L. Ambrosio, M. C. Aragoni, M. Arca, F. A. Devillanova, M. B. Hursthouse, S. L. Huth, F. Isaia, V. Lippolis, A. Mancini, A. Pintus, *Chem. Asian J.,* **2010**, *5*, 1395; (b) M. C. Aragoni, M. Arca, F. A. Devillanova, F. Isaia, V. Lippolis, A. Pintus, *Chem. Asian J.,* **2011**, *6,* 198.

[44] (a) R. Eisenberg, J. A. Ibers, R. J. H. Clark, H. B. Gray, *J. Am. Chem. Soc.,* **1964**, *86*, 113; (b) R. Eisenberg, J. A. Ibers, *Inorg. Chem.,* **1965**, *4*, 605.

[45] (a) R. Eisenberg, *Progr. Inorg. Chem.,* **1970**, *12*, 295; (b) S. A. Baudron, N. Avarvari, P. Batail, *Inorg. Chem.,* **2005**, *44*, 3380; (c) T. Arliguie, P. Thuéry, M. Formigué, M. Ephritikhine, *Eur. J. Inorg. Chem.,* **2004**, 4502; (d) R. P. Burns, C. A. McAuliffe, *Adv. Inorg. Chem. Radiochem.,* **1979**, *22*, 303; (e) F.-Y. Dong, J.-M. Dou, D.-C. Li, X.-K. Gao, D.-Q. Wang, *J. Mol. Struct.,* **2005**, *738*, 79.

[46] C. L. Beswick, J. Schulman, E. I. Stiefel, *Progr. Inorg. Chem.,* **2004**, *52*, 55.

[47] CCDC ConQuest version v. 5.31 updated to Feb. 2010.

[48] In *bis*(1,2-dithiolene) complexes, the M-S distances range between 2.101 and 2.563 Å. Ni complexes show the shortest average M-S bond distances recorded, while the complexes based on Mn, Hg, Cd, and Ag feature the longest ones (Figure 1.4). Within the series containing the complexes of a single element, a correlation can be generally found between the average M-S bond length and the charge of the complex, negatively charged complexes typically featuring longer M-S distances.[46]

[49] (a) X. Ribas, J. C. Dias, J. Morgado, K. Wurst, I. C. Santos, M. Almeida, J. Vidal-Gancedo, J. Veciana, C. Rovira, *Inorg. Chem.,* **2004**, *43*, 3631; (b) X. M. Ren, T. Akutagawa, S. Nishihara, T. Nakamura, *Synth. Met.,* **2005**, *150*, 57.

[50] (a) P. I. Clemenson, *Coord. Chem. Rev.,* **1990**, *106*, 171; (b) X. Ribas, J. C. Dias, J. Morgado, K. Wurst, E. Molins, E. Ruiz, M. Almeida, J. Veciana, C. Rovira, *Chem. Eur. J.,* **2004**, *10*, 1691.

[51] Y.-K. Han, D.-K. Seo, H. Kang, W. Kang, D.-Y. Noh, *Inorg. Chem.,* **2004**, *43*, 7294.

[52] (a) M. A. Ansari, C. H. Mahler, J. A. Ibers, *Inorg. Chem.,* **1989**, *28*, 2669; (b) R. B. King, *J. Organomet. Chem.,* **2001**, *623*, 95; (c) X. Ribas, J. C. Dias, J. Morgado, K. Wurst, M. Almeida, T. Parella, J. Veciana, and C. Rovira, *Angew. Chem. Int. Ed.,* **2004**, *13*, 4049.

[53] (a) E. I. Stiefel, G. F. Brown, *Inorg. Chem.,* **1972**, *11*, 434; (b) G. F. Brown, E. I. Stiefel, *Inorg. Chem.,* **1973**, *12*, 2140.

[54] M. L. Kirk, R. L. McNaughton, M. E. Helton, *Progr. Inorg. Chem.,* **2004**, *52*, 111.

[55] S. I. Shupack, E. Billig, R. J. H. Clark, R. Williams, H. B. Gray, *J. Am. Chem. Soc.*, **1964**, *86*, 4594.

[56] S. Alvarez, R. Vicente, R. Hoffman, *J. Am. Chem. Soc.,* **1985**, *107, 6253.*

[57] See for example the following recent reviews: (a) S. Sproules, K. Wieghardt, *Coord. Chem. Rev.,* **2010**, *254*, 1358; (b) S. Zàliš, R. F. Winter, W. Kaim, *Coord. Chem. Rev.,* **2010**, *254*, 1383; (c) A. B. P. Lever, *Coord. Chem. Rev.,* **2010**, *254*, 1397.

References and Notes

---

[58] (a) I. Malfant, N. Cordente, P. G. Lacroix, C. Lepetit, *Chem. Mater.*, **1998**, *10*, 4079; (b) P. Rosa, L. Ricard, P. Le Floch, F. Mathey, G. Sini, O. Eisenstein, *Inorg. Chem.,* **1998**, *37*, 3154.

[59] B. S. Lim, D. V. Fomitchev, R. H. Holm, *Inorg. Chem.,* **2001**, *40*, 4257.

[60] B. Garreau-de Bonneval, K. I. Moineau-Chane Ching, F. Alary, T.-T. Bui, L. Valade, *Coord. Chem. Rev.,* **2010**, *254*, 1457.

[61] A. L. Bach, R. H. Holm, *J. Am. Chem. Soc.,* **1966**, *88*, 5201.

[62] V. Bachler, G. Olbrich, F. Neese, K. Wieghardt, *Inorg. Chem.,* **2002**, *41*, 4179.

[63] L. Noodelman, *J. Chem. Phys.,* **1981**, *74*, 5737.

[64] (a) L. Serrano-Andres, A. Avramopoulos, J. B. Li, P. Labeguerie, D. Begue, V. Kello, M. G. Papadopoulos, *J. Chem. Phys.,* **2009**, *131*, 134312; (b) F. Alary, J.-L. Heully, A. Scemama, B. Garreau de Bonneval, K. I. Chane-Ching, M. Caffarel, *Theor. Chem. Acc.,* **2010**, *126*, 275.

[65] K. Ray, T. Petrenko, K. Wieghardt, F. Neese, *Dalton Trans.,* **2007**, 1552.

[66] G. Bruno, M. Almeida, D. Simao, M. L. Mercuri, L. Pilia, A. Serpe, P. Deplano, *Dalton Trans.,* **2009**, 495.

[67] K. Wang, *Progr. Inorg. Chem.,* **2004**, *52*, 267.

[68] W. E. Geiger Jr., F. Barriere, R. J. LeSuer, S. Trupia, *Inorg. Chem.,* **2001**, *40*, 2472.

[69] G. N. Schrauzer, V. P. Mayweg, H. W. Finck, W. Heinrich, *J. Am. Chem. Soc.,* **1966**, *88*, 4604.

[70] (a) U. T. Mueller-Westerhoff, B. Vance, D. I. Yoon, *Tetrahedron,* **1991**, *47*, 909; (b) U. T. Mueller-Westerhoff, D. I. Yoon, K. P. Lourde, *Mol. Cryst. Liq. Cryst.,* **1990**, *183*, 29.

[71] S. B. Wilkes, I. R. Butler, A. E. Underhill, A. Kobayashi, H. Kobayashi, *Chem. Commun.,* **1994**, 53.

[72] H.-J. Lee, D.-Y. Noh, *Synth. Met.,* **1999**, *102*, 1696.

[73] F. Barriere, N. Camire, W. E. Geiger, U. T. Mueller-Westerhoff, R. Sanders, *J. Am. Chem. Soc.,* **2002**, *124*, 7262.

[74] (a) C. Faulmann, P. Cassoux, *Progr. Inorg. Chem.,* **2004**, *52*, 399; (b) U. T. Mueller Westerhoff, R. W. Sanders, *Patent US 2003225296,* **2003.**

[75] (a) S. Kokatam, K. Ray, J. Pap, E. Bill, W. E. Geiger, R. J. LeSuer, P. H. Rieger, T. Weyhermüller, F. Neese, K. Wieghardt, *Inorg. Chem.,* **2007**, *46*, 1100; (b) R. Perochon, L. Piekara-Sady, W. Junga, R. Clérac, M. Formigué, *Dalton Trans.,* **2009**, 3052.

[76] Z. S. Herman, R. F. Kirchner, G. H. Loew, U. T. Mueller-Westerhoff, A. Nazzal, M. C. Zerner, *Inorg. Chem.,* **1982,** *21,* 36.

[77] J.-L. Zuo, T.-M. Yao, F. You, X.-Z. You, H.-K. Fun, B.-C. Yip, *J. Mater. Chem.,* **1996**, *6*, 1633.

[78] M. C. Aragoni, M. Arca, T. Cassano, C. Denotti, F. A. Devillanova, R. Frau, F. Isaia, F. Lelj, V. Lippolis, L. Nitti, P. Romaniello, R. Tommasi, G. Verani, *Eur. J. Inorg. Chem.,* **2003**, 1939.

[79] N. Tenn, N. Bellec, O. Jeannin, L. Piekara-Sady, P. Auban-Senzier, J. Iniguez, E. Canadell, D. Lorcy, *J. Am. Chem. Soc.,* **2009**, *46*, 16961.

[80] U. T. Mueller-Westerhoff, R. W. Sanders, *Organomet.,* **2003**, *22*, 4778.

[81] D. J. Harrison, A. G. De Crisci, A. J. Lough, M. J. Kerr, U. Fekl, *Inorg. Chem.,* **2008**, *47*, 10199.

[82] T. M. Yao, J.-L. Zuo, X.-Z. You, X.-Y. Huang, *Polyhedron*, **1995**, *14*, 1487.

[83] M. C. Aragoni, M. Arca, M. Caironi, C. Denotti, F. A. Devillanova, E. Grigiotti, F. Isaia, F. Laschi, V. Lippolis, D. Natali, L. Pala, M. Sampietro, P. Zanello, *Chem. Commun.,* **2004**, 1882.

[84] A. J. Scroggie, G. D'Alessandro, N. Langford, G.-L. Oppo, *Opt. Commun.,* **1999**, *160*, 119.

[85] (a) K. H. Drexhage, U. T. Mueller-Westerhoff, *IEEE J. Quant. Electr.,* **1972**, *QE-8*, 759; (b) K. H. Drexhage, U. T. Mueller-Westerhoff, *US Patent 3743964,* **1973.**

[86] Y. R. Shen, *The Principles of Nonlinear Optics,* Wiley, New York, **1984.**

[87] (a) K. Base, M. T. Tierney, A. Fort, J. Muller, M. W. Grinstaff, *Inorg. Chem.,* **1999**, *338*, 287; (b) H. Le Bolzec, T. Renouard, *Eur. J. Inorg. Chem.,* **200**, 229.

[88] (a) S. N. Oliver, C. S. Winter, R. J. Manning, J. D. Rush, C. A. S. Hill, A. E. Underhill, in *Nonlinear Optical Properties of Inorganic Materials V, vol. 110,* D. J. Williams (ed), **1992**; (b) G. J. Gall, T. A. King, S. N. Oliver, C. A. Capozzi, A. B. Seddon, C. A. S. Hill, A. E. Underhill, *Proc. SPIE Int. Soc. Opt. Eng.,* **1994**, *2288*, 372.

[89] See for example Fuji photofilm co., ltd., *European Patent EP1057622A2*, **2000**.

[90] *Proceeding of SPIE Photonics,* **2004**, *5464*, 165.

[91] (a) M. C. Aragoni, M. Arca, T. Cassano, C. Denotti, F. A. Devillanova, F. isaia, V. Lippolis, D. Natali, L. Nitti, M. Sampietro, R. Tommasi, G. Verani, *Inorg. Chem. Commun.,* **2002**, *5*, 869; (b) D. Natali, M. Sampietro, M. Arca, C. Denotti, F. A. Devillanova, *Synth. Met.,* **2003**, *137*, 1489; (c) M. Caironi, D. Natali, M. Sampietro, M. Ward, A. Meacham, F. A. Devillanova, M. Arca, C. Denotti, L. Pala, *Synth. Met.,* **2005**, *153*, 273; (d) M. C. Aragoni, M. Arca, F. A. Devillanova, F. Isaia, V. Lippolis, A. Mancini, L. Pala, G. Verani, T. Agostinelli, M. Caironi, D. Natali, M. Sampietro, *Inorg. Chem. Comm.,* **2007**, *10*, 191.

[92] (a) A. Davison, J. A. McCleverty, E. T. Shawl, E. J. Whartom, *J. Am. Chem. Soc.,* **1967**, *89*, 830; (b) J. G. M. Van Der Linden, H. G. J. Van de Roer, *Inorg. Chim. Acta,* **1971**, *5*, 254; (c) J. G. M. Van Der Linden, *J. Inorg. Nucl. Chem.,* **1972**, *34*, 1645; (d) T. R. Miller, I. G. Dance, *J. Am. Chem. Soc.,* **1973**, *95*, 6970; (e) A. L. Balch, *Inorg. Chem.,* **1971**, *10*, 388.

[93] (a) N. G. Connelly, J. A. McCleverty, C. J. Winscom, *Nature*, **1967**, *216*, 999; (b) J. A. McCleverty, N. M. Atherton, N. G. Connelly, C. J. Winscom, *J. Chem. Soc. A,* **1969**, 2242; (c) J. A. McCleverty, B. Ratcliff, *J. Chem. Soc. A,* **1970**, 1631.

[94] (a) G. N. Schrauzer, H. N. Rabinowitz, *J. Am. Chem. Soc.,* **1968**, *90*, 4297; (b) G. N. Schrauzer, R. K. Y. Ho, R. P. Mourillo, *J. Am. Chem. Soc.,* **1970**, *92*, 3508; (c) G. N. Schrauzer, C. Zhang, E. O. Schlemper, *Inorg. Chem.,* **1990**, *29*, 3371.

[95] R. M. Wing, G. C. Tustin, W. H. Okamura, *J. Am. Chem. Soc.,* **1970**, *92*, 1935.

[96] M. A. Mazid, M. T. Razi, P. J. Sadler, *Inorg. Chem.,* **1981**, *20*, 2872.

[97] G. N. Schrauzer, C. Zhang, R. Chadha, *Inorg. Chem.,* **1990**, *29*, 4140.

[98] R. Kato, *Chem. Rev.,* **2004**, *104*, 5319.

[99] (a) R. Llusar, C. Vicent, *Coord. Chem. Rev.,* **2010**, *254*, 1534; (b) S. Dagleish, N. Robertson, *Coord. Chem. Rev.,* **2010**, *254*, 1549.

[100] H. M. McConnell, R. Lynden-Nell, *J. Chem. Phys.,* **1962**, *36*, 2393.

[101] (a) L. Alcacer, H. Novais, F. Pedroso, S. Flandrois, C. Coulon, D. Chasseau, J. Gaultier, *Solid State Commun.,* **1980**, *35*, 945; (b) R. D. McDonald, N. Harrison, J. Singleton, A. Bangura, P. A. Goddard, A. P. Ramirez, X. Chi, *Phys. Rev. Lett.,* **2005**, *94,* 106404.

[102] M. M. Ahmad, D. J. Turner, A. E. Underhill, C. S. Jacobsen, K. Mortensen, K. Carneiro, *Phys. Rev. B*, **1984**, *29*, 4796.

References and Notes

---

[103] (a) J. W. Bray, H. R. Hart Jr., L. V. Interrante, I. S. Jacobs, J. S. Kasper, G. D. Watkins, S. H. Wee, J. C. Bonner, *Phys. Rev. Lett.,* **1975**, *35*, 744; (b) I. S. Jacobs, J. W. Bray, H. R. Hart Jr, L. V. Interrante, J. S. Kasper, G. D. Watkins, D. E. Prober, J. C. Bonner, *Phys. Rev. B*, **1976**, *14*, 3036.

[104] J. M. Williams, J. R. Ferrero, R. J. Thorn, K. D. Carlson, U. Geiser, H. H. Wang, A. M. Kini, M.-H. Wangbo, *Organic Superconductors (Including Fullerenes),* Prentice-Hall, Englewood Cliffs, NJ, **1992**.

[105] J. C. Dias, X. Ribas, J. Morgado, J. Seiça, E. B. Lopes, I. C. Santos, R. T. Henriques, M. Almeida, K. Wurst, P. Floury-Leylekian, E. Canadell, J. Vidal-Gancedo, J. Veciana, C. Rovira, *J. Mater. Chem.,* **2005**, *15*, 3187.

[106] (a) N. J. Harris, A. E. Underhill, *J. Chem. Soc., Dalton Trans.,* **1987**, 1683; (b) W. B. Heuer, P. J. Squattrito, B. M. Hoffman, J. A. Ibers, *J. Am. Chem. Soc.,* **1988**, *110*, 792.

[107] L. Valade, M. Bousseau, A. Gleizes, P. Cassoux, *J. Chem. Soc., Chem. Commun.,* **1983**, 110.

[108] L. Brossard, M. Ribault, M. Bousseau, L. Valade, P. Cassoux, *C. R. Acad. Sci., Ser. II*, **1986**, *302*, 205.

[109] In particular, beside $(TTF)[Ni(dmit)_2]$, twelve more *bis*(1,2-dithiolene) complexes exhibiting superconducting properties have been reported to date, namely α-(EDT-TTF)$[Ni(dmit)_2]$, $(Me_4N)[Ni(dmit)_2]_2$, α'-(TTF)$[Pd(dmit)_2]_2$, α-(TTF)$[Pd(dmit)_2]_2$, β-$(Me_4N)[Pd(dmit)_2]_2$, $(Et_2Me_2N)[Pd(dmit)_2]_2$, β'-$(Et_2Me_2P)[Pd(dmit)_2]_2$, β'-$(Me_4Sb)[Pd(dmit)_2]_2$, β'-$(Me_4As)[Pd(dmit)_2]_2$, β'-$(Et_2Me_2As)[Pd(dmit)_2]_2$, β'-$(Et_2Me_3As)[Pd(dmit)_2]_2$, β'-$(Et_4P)[Pd(dmit)_2]_2$, Ref. 110.

[110] (a) H. Tajima, M. Inokuchi, A. Kobayashi, T. Otha, R. Kato, H. Kobayashi, H. Kuroda, *Chem. Lett.,* **1993**, 1235; (b) A. Kobayashi, H. Kim, Y. Sasaki, R. Kato, H. Kobayashi, S. Moriyama, Y. Nishio, K. Kajita, W. Sasaki, *Chem. Lett.,* **1987**, 1819; (c) L. Brossard, H. Hurdequint, M. Ribault, L. Valade, L.-P. Legros, P. Cassoux, *Synth. Met.,* **1988**, *27*, B157; (d) L. Brossard, M. Ribault, L. Valade, P. Cassoux, *J. Phys. (Paris),* **1989**, *50*, 1521; (e) A. Kobayashi, H. Kobayashi, A. Miyamoto, R. Kato, R. A. Clark, A. E. Underhill, *Chem. Lett.,* **1991**, 2163; (f) H. Kobayashi, K. Bun, T. Naito, R. Kato, A. Kobayashi, *Chem. Lett.,* **1992**, 1909; (g) R. Kato, Y. Kashimura, S. Aonuma, N. Hanasaki, H. Tajima, *Solid State Commun.,* **1998**, *105*, 561; (h) R. Kato, N. Tajima, M. Tamura, J.-I. Yamaura, *Phys. Rev. B,* **2002**, *66*, 020508; (i) A. Tajima, A. Nakao, R. Kato, *J. Phys. Soc. Jpn.,* **2005**, *74*, 412; (j) R. Kato, A. Tajima, A. Nakao, *J. Am. Chem. Soc.,* **2006**, *128*, 10016.

[111] (a) A. E. Pullen, R.-M. Olk, *Coord. Chem. Rev.,* **1999**, *188*, 211; (b) P. Cassoux, *Coord. Chem. Rev.,* **1999**, *185*; (c) N. Robertson, L. Cronin, *Coord. Chem. Rev.,* **2002**, *227*, 93; (d) J. Morgado, L. Alcacer, R. T. Henriques, M. Almeida, *Synth. Met.,* **1999**, *103*, 2123.

[112] W. B. Heuer, B. M. Hoffman, *J. Chem. Soc., Chem. Commun.,* **1986**, 174.

[113] (a) P. Cassoux, L. Valade, H. Kobayashi, A. Kobayashi, R. A. Clark, A. E. Underhill, *Coord. Chem. Rev.,* **1991**, *9*, 1909; (b) L. Ouahab, *Chem. Mater.,* **1997**, *9*, 1909; (c) E. Canadell, *Coord. Chem. Rev.,* **1999***, 186*, 629; (d) P. Basu, J. F. Stolz, M. T. Smith, *Curr. Sci.,* **2003**, *84*, 1412; (d) D. Belo, M. Almeida, *Coord. Chem. Rev.,* **2010**, *254*, 1479; (e) S. Rabaça, M. Almeida, *Coord. Chem. Rev.,* **2010**, *254*, 1493; (f) H.-B. Duan, X.-M. Ren, Q.-J. Meng, *Coord. Chem. Rev.,* **2010**, *254*, 1509;

[114] (a) T. Akutagawa, K. Matsuura, A. Hashimoto, T. Nakamura, *Inorg. Chem.,* **2005**, *44,* 4454; (b) X. M. Ren, H. Okudera, J. L. Xie, Q. J. Meng, *J. Mol. Struct.,* **2005**, *733*, 119; (c) H.-R. Wen, J.-L. Zuo, T. A. Scott, H.-C. Zhou, X.-Z. You, *Polyhedron*, **2005**, *24*, 671; (d) S. S. Stanisland, W. Fujita, Y. Umezono, K. Awaga, P. J. Camp, S. J. Clark, N. Robertson, *Inorg. Chem.,* **2005**, *44*, 546.

[115] L. V. Interrante, J. W. Bray, H. R. Hart Jr, L. S. Jacobs, J. S. Kasper, P. A. Piacente, J. C. Bonner, *Lect. Notes Phys.,* **1979**, *96*, 55.

[116] H. Imai, T. Inabe, T. Otsuka, T. Okuno, K. Agawa, *Synth. Met.,* **1997**, *85*, 1705.

[117] (a) D. Arcon, A. Lappas, S. Margadonna, K. Prassides, E. Ribera, J. Veciana, C. Rovira, R. T. Henriques, M. Almeida, *Phys. Rev. B,* **1999**, *60,* 4191*;* (b) X. Ribas, A. Sironi, N. Masciocchi, E. B. Lopes, M. Almeida, J. Veciana, C. Rovira, *Inorg. Chem.,* **2005**, *44*, 2358; (c) R. Wesolowski, J. T. Haraldsen, J. L. Musfeldt, T. Barnes, M. Mas-Torrent, C. Rovira, R. T. Henriques, M. Almeida, *Pyhs. Rev. B*, **2003**, *68*, 134405; (d) R. Wesolowski, J. T. Haraldsen, J. L. Musfeldt, T. Barnes, M. Mas-Torrent, c. Rovira, R. T. Henriques, M. Almeida, *Pyhs. Rev. B*, **2000**, *70*, 059901.

[118] (a) H. Nakajima, M. Katshara, M. Ashizawa, T. Kawamoto, T. Mori, *Inorg. Chem.,* **2004**, *43*, 6075; (b) N. C. Schiødt, R. Sessoli, F. C. Krebs, *Inorg. Chem.,* **2004**, *43*, 1986; (c) X. M. Ren, H. Okudera, R. K. Kremer, Y. Song, C. He, Q. J. Meng, P. H. Wu, *Inorg. Chem.,* **2004***, 43*, 2569; (d) W. E. Broderick, J. A. Thompson, M. R. Godfrey, M. Sabat, B. M. Hoffman, E. P. Day, *J. Am. Chem. Soc.,* **1989**, *111*, 7656; (e) S. Rabaça, R. Meira, L. C. J. Pereira, M. T. Duarte, J. J. Novoa, V. Gama, *Inorg. Chim. Acta,* **2001**, *326*, 89.

[119] (a) M. L. Allan, A. T. Coomber, I. R. Marsden, J. H. F. Martens, R. H. Friend, A. Charlton, A. E. Underhill, *Synth. Met.,* **1993**, *56*, 3317; (b) A. T. Coomber, D. Beljonne, R. H. Friend, J. L. Bredas, A. Charlton, N. Robertson, A. E. Underhill, M. Kurmoo, P. Day, *Nature*, **1996**, *380*, 144.

[120] C. Faulamnn, A. E. Pullen, E. Riviere, S. Dorbes, F. Senoca, E. Coronado, P. Cassoux, *Eur. J. Inorg. Chem.,* **2003**, 2880.

[121] P. Deplano, L. Pilia, D. Espa, M. L. Mercuri, A. Serpe, *Coord. Chem. Rev.,* **2010**, *254*, 1434.

[122] F. Bigoli, C.-T. Chen, W.-C. Wu, P. Deplano, M. L. Mercuri, M. A. Pellinghelli, L. Pilia, G. Pintus, A. Serpe, E. F. Trogu, *Chem. Commun.,* **2001**, 2246.

[123] (a) F. Bigoli, P. Deplano, M. L. Mercuri, M. A. Pellinghelli, L. Pilia, G. Pintus, A. Serpe, E. F. Trogu, *Inorg. Chem.,* **2002,** *41*, 524**;** (b) S. Currelli, P. Deplano, C. Faulmann, A. Ienco, C. Mealli, M. L. Mercuri, L. Pilia, G. Pintus, A. Serpe, E. F. Trogu, *Inorg. Chem.,* **2002**, *41*, 5241; (c) C.-T. Chen, S.-Y. Liao, K.-J. Lin, L.-L. Lai, *Adv. Mater.,* **1998**, *3*, 335; (d) R. Kato, Y. Kashimura, H. Sawa, Y. Okano, *Chem. Lett.,* **1997**, 921; (e) Y. Kashimura, Y. Okano, J.-I. Yamaura, R. Kato, *Synth. Met.,* **1999**, 2123; (f) E. Watanabe, M. Fujiwara, J.-I. Yamaura, R. Kato, *J. Mater. Chem.,* **2001**, *11*, 2131; (g) G. C. Papavassiliou, G. C. Anyfantis, B. R. Steele, A. Terzis., C. P. Raptopolou, G. Tatakis, G. Chaidogiannos, N. Glezos, Y. Weng, Y. Yoshino, K. Murata*, Z. Naturforsch.*, **2007**, *62b*, 679; (h) G. C. Anyfantis, G. C. Papavassiliou, P. Aloukos, S. Couris, Y. F. Weng, H. Yoshino, K. Murata, *Z. Naturforsch.,* **2007**, *62b*, 200; (i) P. Aloukos, S. Couris, J. B. Koutselas, G. C. Anyfantis, C. Papavassiliou, *Chem. Phys. Lett.,* **2006**, *428*, 109; (j) G. C. Anyfantis, G. C. Papavassoliou, A. Terzis, C. P. Raptopoulou, Y. F. Weng, H. Yoshino, K. Murata, *Z. Naturforsch.*, **2006**, *61b*, 1007; (k) G. C. Anyfantis, G. C. Papavassiliou, N. Assimomytis, A. Terzis, V. Psycharis, C. P. Raptopolou, P. Kyritsis, V. Thoma, L. B. Koutselas, *Solid State Sci.,* **2008**, *10*, 1729; (l) C.-C. Wang, W.-C. Wu, G.-H. Lee, C.-T. Chen, *J. Chin. Chem. Soc.,* **2002**, *49*, 805; (m) P. Deplano, L. Marchiò, M. L. Mercuri, L. Pilia, G. Pintus, A. Serpe, E. B. Yagubskii, *Monatsch. Chem.,* **2009**, *140*, 775; (n) S. Dagleish, C. A. Morrison, D. S. Middlemiss, A. R. Mount, A. Collins, L. Pilia, M. L. Mercuri, A.

References and Notes

Serpe, P. J. Murphy, N. Robertson, *J. Mater. Chem.,* **2009**, *19*, 6149; (o) A. Vogler, H. Kunkely, *Angew. Chemie Int. Ed. Engl.,* **1982**, *21*, 77.

[124] (a) C. Papavassiliou, G. C. Anyfantis, A. Terzis, V. Psycharis, P. Krystis, P. Paraskevopolou, *Z. Naturforsch.*, **2008**, *63b*, 1377; (b) G. C. Papavassiliou, G. C. Anyfantis, *Z. Naturforsch.,* **2005**, *60b,* 811; (c) M. C. Aragoni, M. Arca, C. Denotti, F. A. Devillanova, E. Grigiotti, F. Isaia, F. Laschi, V. Lippolis, L. Pala, A. M. Z. Slawin, P. Zanello, J. D. Woollins, *Eur. J. Inorg. Chem.,* **2003**, 1291; (d) L. Pilia, F. Artizzu, C. Faulmann, M. L. Mercuri, A. Serpe, P. Deplano, *Inorg. Chem. Commun.,* **2009**, *12*, 490.

[125] (a) C. Zhan, W. Xu, D. Zhang, D. Li, Z. Lu, Y. Nie, D. Zhu, *J. Mater. Chem.,* **2002**, *12*, 2945; (b) C. S. Winter, S. N. Oliver, J. D. Rush, C. A. S. Hill, A. E. Underhill, *J. Appl. Phys.,* **1992,** *71*, 512.

[126] (a) E. Coronado, J. R. Galàn-Mascaros, C. J. Gòmez-Garcìa, V. N. Laukhin, *Nature*, **2000**, *408*, 447; (b) H. Hiraga, H. Miyasaka, K. Nakata, T. Kajiwara, S. Takaishi, Y. Oshima, H. Nojiri, M. Yamshita, *Inorg. Chem.,* **2007**, *46*, 9661; (c) H. Kisch, B. Eisen, R. Dinnebier, K. Shankland, W. I. F. Davis, F. Knoch, *Chem. Eur. J.,* **2001**, *7*, 738; (d) E. Coronado, P. Day, *Chem. Rev.,* **2004**, *104*, 5419; (e) T. Enoki, A. Miyazaki, *Chem. Rev.,* **2004**, *104*, 5449.

[127] S. D. Cummings, R. Eisenberg, *J. Am. Chem. Soc.,* **1996**, *118*, 1949.

[128] (a) C. G. Pierpont, R. Eisenberg, *Inorg. Chem.,* **1970**, *9*, 2218; (b) G. P. Khare, R. Eisenberg, *Inorg. Chem.,* **1970**, *9*, 2211; (c) Y. Liu, Z. Peng, D. Li, Y. Zhou, *Spectrochim. Acta A,* **2008**, *69*, 471.

[129] M. A. Mansour, R. J. Lachicotte, H. J. Gysling, R. Eisenberg, *Inorg. Chem.,* **1998**, *37*, 4625.

[130] (a) P. J. Gronlund, J. A. Burt, W. F. Wacholtz, *Inorg. Chim. Acta,* **1995**, *357*, 1198; (b) K. Halvorsen, W. F. Wacholtz, G. Crosby, *Inorg. Chim. Acta,* **1995**, *228*, 81; (c) S. D. Cummings, L.-T. Cheng, R. Eisenberg, *Chem. Mater.,* **1997**, *9,* 440; (d) C. M. Liu, D.-Q. Zhang, Y.-L. Song, C.-L. Zhan, Y.-L. Li, D. B. Zhu, *Eur. J. Inorg. Chem.,* **2002**, 1591; (e) Q.-H. Wang, D.-L. Long, H.-M. Hu, Y. Cui, J.-S. Huang, *J. Coord. Chem.*, **2000**, *49*, 201; (f) D. M. Hatch, W. F. Wacholtz, J. T. Mague, *Acta Cryst, Sect. C*, **2003**, *59*, m452; (g) S. V. Vitushkina, V. A.Starodub, O. S.Pyshkin, *Koord. Khim.,* **2006**, *32*, 247; (f) W. Guo, Z. Peng, D. Li, Y. Zhou, *Polyhedron*, **2004**, *23*, 1701.

[131] L.-L. Wen, Z.-H. Peng, B.-G. Zhang, Y.-H. Zhou, *J. Mol. Struct.,* **2004**, *694*, 223.

[132] (a) K. Natsuaki, M. Nakano, G. Matsubayashi, R. Arakawa, *Inorg. Chim. Acta*, **2000**, *299*, 112; (b) A. Islam, H. Sugihara, K. Hara, L. P. Singh, R. Katoh, M. Yanagida, Y. Takahashi, S. Murata, H. Arakawa, *J. Photochem. Photobiol.,* **2001**, *145*, 135.

[133] (a) W.-Y. Guo, Z.-H. Peng, C.-G. Wang, Y.-H. Zhou, *J. Coord. Chem.,* **2006**, *59*, 1213.

[134] M L. Calatayud, J. Sletten, I. Castro, M. Julve, G. Seitz, K. Mann, *Inorg. Chim. Acta*, **2003**, *353*, 159.

[135] S. M. Dibrov, R. E. Bachman, *Inorg. Chim. Acta,* **2004**, *357*, 1198.

[136] A. Vogler, H. Kunkley, *J. Am. Chem. Soc.,* **1981**, *103*, 1559.

[137] (a) C.-T. Chen, T.-Y. Jeremy Lin, C.-H. Chen, K.-J. Lin, *J. Chin. Chem. Soc.,* **2000**, *47*, 197; (b) W.-Y. Guo, Z.-H. Peng, C.-G. Wang, Y.-H. Zhou, *J. Coord. Chem.,* **2006**, *59*, 1213.

[138] As regards the M-S bond lengths, considerations similar to those deduced for homoleptic *bis*(1,2-dichalcogenolene) complexes can be made: M-S distances range between 2.122[137a] and 2.58[131] Å. Ni complexes show the shortest average M-S bond distances recorded, while the cadmium complexes feature the longest ones. On the other hand, M-N distances ranging between 1.926[139] and 2.361[131] Å are reported, and also in this case the shortest bond lengths are observed in Ni complexes and the longest ones in Cd

complexes. As regards angles, S-M-S angles have been found to range between 83.27[130b] and 98.39,[130a] while N-M-N angles range between 70.08[131] and 83.37° (Figure 1.15).[139]

[139] T. M. Cocker, R. E .Bachman, *Mol. Cryst. Liq. Cryst. Sci. Technol., Sect. A,* **2004**, *408*,1.

[140] J. S. Pap, F. L. Benedito, E. Bothe, E. Bill, S. DeBeer George, T. Weyhermuller, K. Wieghardt, *Inorg. Chem.,* **2007**, *46*, 4187.

[141] J. Moussa, M. N. Rager, K. Boubekeur, H. Amouri, *Eur. J. Inorg. Chem.,* **2007**, 2648.

[142] Y. Ji, R. Zhang, Y.-J. Li, Y.-Z. Li, J.-L. Zuo, X.-Z. You, *Inorg. Chem.,* **2007**, *46*, 866.

[143] B. W. Smucker, J. M. Hudson, M. A. Omary, K. R. Dunbar, *Inorg. Chem.,* **2003**, *42*, 4714.

[144] S. Parsons, Z. Zhang, P. J. Sadler, A. Daweson, R. Johnstone, *Private Communication*, **2006**.

[145] W. Liu, R. Wang, X.-H. Zhou, J.-L. Zuo, X.-Z. You, *Organometallics,* **2008**, *27*, 126.

[146] R. Sakamoto, M. Murata, S. Kume, H. Sampei, M. Sugimoto, H. Nishihara, *Chem. Commun.,* **2005**, 125.

[147] J.-L. Zuo, R.-G. Xiong, X.-Z. You, X.-Y. Huang, *Inorg. Chim. Acta*, **1995**, *237*, 117.

[148] (a) K. Kubo, M. Nakano, H. Tamura, G.-E. Matsubayashi, *Eur. J. Inorg. Chem.,* **2003**, 4093; (b) K. Kubo, M. Nakano, H. Tamura, G.-E. Matsubayashi, *Inorg. Chim. Acta*, **2002**, *336*, 120.

[149] Also in this case, the longest M-S and M-N distances are observed for Cd complexes,[128a] while the shortest ones are featured by the Co complexes.[130f]

[150] (a) J. A. Zuleta, J. M. Bevilacqua, D. M. Proserpio, P. D. Harvey, R. Eisenberg, *Inorg. Chem.,* **1992** *31*, 2396; (b) S. D. Cummings, R. Eisenberg, *Inorg. Chem.,* **1995***, 34*, 2007.

[151] C. Makedonas, C. A. Mitsopoulou, *Eur. J. Inorg. Chem.,* **2007**, 110.

[152] C. A. Mitsopoulou, *Coord. Chem. Rev.,* **2010**, *254*, 1448.

[153] C. Makedonas, C. A. Mitsopoulou, *Inorg. Chim. Acta,* **2007**, *360*, 3997.

[154] W. L. Fleeman, W. B. Connick, *Comments. Inorg. Chem.,* **2002**, *23*, 205.

[155] Y. Zhang, K. D. Ley, K. Schanze, *Inorg. Chem.,* **1996**, *35*, 7102.

[156] C.-T. Chem, S.-Y. Liao, K.-J. Lin, L.-L. Lai, *Adv. mater.,* **1995**, *3*, 334.

[157] C. A. Bignozzi, R. Argazzi, C. J. Kleverlaan, *Chem. Soc. Rev.,* **2000**, *29*, 87.

[158] E. A. M. Geary, L. J. Yellowlees, L. A. Jack, I. D. H. Oswald, S. Parsons, N. Hirata, J. R. Durrant, N. Robertson, *Inorg. Chem.,* **2005**, *44*, 242.

[159] (a) A. Islam, H. Sugihara, K. Hara, L. P. singh, R. KAtoh, M. Yanagida, Y. Takahshi, S. Murata, H. Arakawa, *Inorg. Chem.,* **2001**, *40*, 5371; (b) E. A. M. Geary, N. Hirata, J. Clifford, J. R. Durrant, S. Parsons, A. Dawson, L. J. Yellowlees, N. Robertson, *Dalton Trans.,* **2003**, 3757; (c) E. A. M. Geary, K. L. McCall, A. Turner, P. R. Murray, E. J. L. McInnes, L. A. Jack, L. J. Yellowlees, N. Robertson, *Dalton Trans.,* **2008**, 3701.

[160] M. Hissler, J. E. McGarrah, W. B. Connick, D. K. Geiger, S. D. Cummings, R. Eisenberg, *Coord. Chem. Rev.,* **2000**, *208*, 115.

[161] J. Zhang, P. Du, J. Schneider, P. Jarosz, R. Eisenberg, *J. Am. Chem. Soc.,* **2007**, *129*, 7726.

[162] K. Kubo, M. Nakano, H. Tamura, G. Matsubayashi, *Inorg. Chim. Acta,* **2000**, *311*, 6

[163] Y. Ji, R. Zhang, X.-B. Du, J.-L. Zuo, X.-Z. You, *Dalton Trans.,* **2008**, 2578.

[164] C. A. Mitsopolou, C. E. Dagas, C. Makedonas, *J. Inorg. Biochem.,* **2008**, *102*, 77.

[165] P.-I. Kvam, M. V. Puzyk, V. S. Cotlyr, J. Songstad, K. P. Balashev, *Acta Chem. Scand.,* **1997**, *50*, 6.

[166] C. A. Goddard, R. H. Holm, *Inorg. Chem.,* **1999**, *38*, 5389.

References and Notes

[167] C. L. Beswick, E. I. Stiefel, private communications.

[168] (a) J. Locke, J. A. McCleverty, E. J. Wharton, C. J. Winscom, *Chem. Comm.,* **1966**, 677; (b) J. A. McCleverty, N. M. Atherton, J. Locke, E. J. Wharton, C. J. Winscom, *J. Am. Chem. Soc.,* **1967**, *89*, 6082.

[169] S. K. Ibrahim, C. J. Pickett, *J. Chem. Soc., Chem. Commun.,* **1991**, 246.

[170] M. Nomura, T. Cauchy, M. Formigué, *Coord. Chem. Rev.,* **2010**, *254*, 1406.

[171] A. Sugimori, T. Akiyama, M. Kajitani, T. Sugiyama, *Bull. Chem. Soc. Jpn.,* **1996**, *117*, 69.

[172] S. Eid, T. Roisnel, D. Lorcy, *J. Organomet. Chem.*, **2008**, *693*, 2755.

[173] (a) S. P. Kaiwar, A. Vodacek, N. V. Blough, R. S. Pilato, *J. Am. Chem. Soc.,* **1997**, *119*, 3311; (b) K. A. Van Houten, K. A. Walters, K. S. Schanze, R. S. Pilato, *J. Fluoresc.,* **2000**, *10*, 35.

[174] Y. Kostov, K. A. Van Houten, P. Harms, R. S. Pilato, G. Rao, *Appl. Spectrosc.¸* **2000**, *54*, 864.

[175] S. D. Cummings, R. Eisenberg, *Progr. Inorg. Chem.,* **2004**, *52*, 315.

[176] (a) S. J. N. Burgmayer, *Progr. Inorg. Chem.,* **2004**, *52*, 491; (b) J. McMaster, J. M. Tunney, C. D. Garner, *Progr. Inorg. Chem.,* **2004**, *52*, 539; (c) C. D. Garner, L. J. Stewart, *"Metal ions in Biological Systems",* M. Dekker Inc. ed. (New York), **2002**, *vol. 39*, 699; (d) J. McMaster, J. H. Enemark, *Curr. Opin. Chem. Biol,* **1998**, *2*, 201.

[177] (a) R. Hille, *Chem. Rev.*, **1996**, *96,* 2757; (b) *"Molybdenum Enzymes, Cofactors and Model System "*, E. I. Stiefel, D. Coucouvanis, W. E. Newton eds., *American Chemical Society*, *Washington DC*, **1993**, 535.

[178] M. J. Romão, *Dalton Trans.,* **2009**, 4053, and references therein.

[179] C. D. Garner, R. Banham, S. J. Cooper, E. S. Davies, L. J. Stewart, in *"Handbook on Metalloproteins 2"*, I. Bertini, A. Sigel, H. Sigel eds., *M. Dekker Inc., New York*, **2001**, 539.

[180] J. McMaster, J. M. Tunney, C. D. Garner, *Cheminform.*, **2004**, *35*.

[181] (a) F. E. Inscore, R. Mcnaughton, B. L. Wescott, M. E. Helton, R. Jones, I. K. Dahwan, J. H. Enemark, M. L. Kirk, *Inorg. Chem.,* **1999**, *38*, 1401; (b) Y. Izimu, T. Glaser, K. Rose, J. McMaster P. Basu, J. H. Enemark, B. Hedman, K. O. Hodgson, E. I. Solomon, *J. Am. Chem. Soc.,* **1999**, *121*, 10035; (c) S. P. Greatbanks, I. H. Hillier, C. D. Garner, J. A. Joule, J. A. Joule, *J. Chem. Soc., Perkin Trans.,* **1997**, *2*, 1529.

[182] (a) T. Cassano, R. Tommasi, L. Nitti, M. C. Aragoni, M. Arca, C. Denotti, F. A. Devillanova, F. Isaia, V. Lippolis, F. Lelj, P. Romaniello, *J. Chem. Phys.,* **2003**, *118*, 5995; (b) T. Cassano, R. Tommasi, M. Arca, F. A. Devillanova, F. Lelj, *Recent Res. Devel. Chem. Phyisics,* **2004**, *5*, 553; (c) T. Cassano, R. Tommasi, M. Arca, F. A. Devillanova, *J. Phys.: Condens. Mater*, **2006**, *18*, 5279.

[183] P. Romaniello, F. Lelj, *J. Molec. Struct.: THEOCHEM*, **2003**, *636*, 23.

[184] (a) L. Pala*, "Nuovi bis(1,2-ditioleni) ad elevata delocalizzazione elettronica: sintesi, caratterizzazione spettroscopica, elettrochimica e cacoli DFT", PhD thesis*, University of Cagliari, **2005**; (b) L. Ambrosio, *"Nuovi bis(1,2-ditioleni) metallici [M(Ar,H-edt)₂]: sintesi, caratterizzazione strutturale, elettrochimica, spettroscopica e calcoli DFT (M = Ni, Cu, Au)", Master's Degree thesis*, University of Cagliari, **2006**; (c) M. C. Aragoni, M. Arca, F. A. Devillanova, V. Lippolis, F. Isaia, A. Pintus, G. Verani, unpublished results.

[185] (a) S. P. Kaiwar, J. K. Hsu, A. Vodacek, G. Yap, L. M. Liable-Sands, A. L. Rheingold, R. S. Pilato, *Inorg. Chem.*, **1997**, *36*, 2406; (b) S. P. Kaiwar, A. Vodacek, N. V. Blough, R. S. Pilato, *J. Am. Chem. Soc.*, **1997**, *119*, 9211; V. Madhu, S. K. Das, *Inorg. Chem.*, **2008**, *47*, 5055; (c) R. S. Pilato, K. A. van Houten, *Prog. Inorg. Chem.*, **2004**, *52*, 369.

[186] V. Madhu, S. K. Das, *Inorg. Chem.*, **2006**, *45*, 10037.

[187] The crystal structures of 1,3-dithiol-2-ones considered are those having the following refcodes in the Cambridge Crystallografic Database: BATPIW, BATTEW, CALVEQ, CUNQUX, FIYHUR, GIWDAS, KAMSOE, KEKWOM, MIYDON, QUHNAT, QEHNEX, QIBQAT, RIPLOS, ULEWIR, YAYZIH, YEGXOX10, and ZAMMUV.

[188] V. Madhu, S. K. Das, *Inorg. Chem.*, **2008**, *47*, 5055.

[189] S. Rabaça, A. C. Cerdeira, A. I. S. Neves, S. I. G. Dias, C. Mézière, I. C. Santos, L. C. J. Pereira, M. Formigué, R. T. Henriques, M. Almeida, *Polyhedron,* **2009**, *28*, 1069.

[190] (a) K. Ray, T. Weyhermüller, A. Goossens, M. W. J. Craié, K. Wieghardt, *Inorg. Chem.*, **2003**, *42*, 4082; (b) K. Ray, T. Weyhermüller, F. Neese, K. Wieghardt, *Inorg. Chem.*, **2005**, *44*, 5345.

[191] (a) X. Liu, I. Wallman, E. Boudinov, J. Kielstrup-Hansen, M. Schiek, A. Lutzen, H.-G. Rubaham, *Org. Electron.,* **2010**, *11*, 1096; (b) R. Soumya, M. Charette, S. P. Finkelstein, *PCT Int. Appl.,* **2009**, WO 2009088975 A2 20090716.

[192] (a) G. C. Papavassiliou, G. C. Anyfantis, C. P. Raptopoulou, V. Psycharis, N. Ioannidis, V. Petrouleas, P. Paraskevopoulou, *Polyhedron*, **2009**, *28*, 3368; (b) D. M. D. Leeuw, M. M. J. Simenon, A. R. Brown, R. E. F. Einerhand, *Synth. Met.*, **1997**, *87*, 53.

[193] (a) A. L. Balch, I. G. Dance, R. H. Holm, *J. Am. Chem. Soc.*, **1968**, *90*, 1139 ; (b) J. C. Fitzmaurice, A. M. Z. Slawin, D. J. Williams, J. D. Woollins, A. J. Lindsay, *Polyhedron*, **1990**, *9*, 1561; (c) O. Jeannin, M. Formigué, *New J. Chem.*, **2006**, *30*, 1774.

[194] M. La Deda, I. Aiello, A. Grisolia, M. Ghedini, M. Amati, F. Lelj, *Dalton Trans.*, **2006**, 330.

[195] (a) W. Koch, M. C. Holthausen, "*A Chemist's Guide to Density Functional Theory*", 2nd ed., Wiley-VCH, Weinheim, Germany, **2002**; (b) F. Neese, *Coord. Chem. Rev.*, **2009**, *253*, 526.

[196] (a) M. C. Aragoni, M. Arca, F. Demartin, F. A. Devillanova, F. Lelj, F. Isaia, V. Lippolis, A. Mancini, L. Pala, G. Verani, *Eur. J. Inorg. Chem.*, **2004**, 3099; (b) P. Romaniello, F. Lelj, M. Arca, F. A. Devillanova, *Theor. Chem. Acc.,* **2007**, *117*, 621.

[197] (a) M. A. Cinellu, G. Minghetti, F. Cocco, S. Stoccoro, A. Zucca, M. Manassero, M. Arca, *Dalton Trans.*, **2006**, 5703; (b) C. Gabbiani, A. Casini, L. Messori, A. Guerri, M. A. Cinellu, G. Minghetti, M. Corsini, C. Rosani, P. Zanello, M. Arca, *Inorg. Chem.*, **2008**, *47*, 2368.

[198] C. Adamo, V. Barone, *J. Chem. Phys.*, **1998**, *108*, 664.

[199] A. Schäfer, H. Horn, R. Ahlrichs, *J. Chem. Phys.*, **1992**, *97*, 2571.

[200] (a) T. H. Dunning, Jr., P. J. Hay in "*Methods of Electronic Structure, Theory*", Vol. 2, H. F. Schaefer III ed., Plenum Press, **1977**; (b) J.V. Ortiz, P. J. Hay, R. L. Martin, *J. Am. Chem. Soc.*, **1992**, *114*, 2736.

[201] R. Kirmse, M. Kampf, R.-M. Olk, M. Hildebrand, H. Krautscheid, *Z. Allg. Chem.*, **2004**, *630*, 1433.

[202] R. L. Schlupp, A. H. Maki, *Inorg. Chem.*, **1974**, *13*, 44.

[203] A similar analysis performed on **22** in its *cis* conformation, showed a rotational barrier (about 8 kcal mol^{-1}) more than double than that calculated for **20** and **20**$^-$.

[204] Calculations were carried out on the neutral and monoanionic species investigated experimentally by UV-Vis and emission spectroscopy (Sections 3.1.4 and 3.1.5). TD-DFT investigation on **20** and **20**$^-$ were carried out previously.[184b]

[205] M. Kasha, *Discuss. Faraday Soc.*, **1950**, *9*, 14.

[206] M. P. Cifuentes, M. G. Humphrey, *J. Organomet. Chem.*, **2004**, *689,* 3968.

References and Notes

---

[207] D. A. Kleinman, *Phys. Rev.*, **1962**, *126*, 1977.

[208] P. J. Mendes, A. J. P. Carvalho, J. P. P. Ramalho, *Theochem*, **2009**, *900*, 110.

[209] (a) I. R. Whittall, M. G. Humphrey, *Organometallics,* **1996**, *15*, 573; (b) M. G. Humphrey, *Gold Bull.*, **2000**, *33*, 97; (c) S. K. Hurst, M. P. Cifuentes, A. M. McDonagh, M. G. Humphrey, M. Samoc, B. Luther-Davies, I. Asselberghs, A. Persoons, *J. Organomet. Chem.*, **2002**, *642*, 259; (d) G. Yang, Z. Su, C. Qin, Y. Zhao, *J. Chem. Phys.*, **2005**, *123*, 134302-1-5; (e) S.-L. Sun, C.-S. Qin, Y.-Q. Qiu, G.-C. Yang, Z.-M. Su, *J. Organomet. Chem.*, **2009**, *694*, 1266.

[210] (a) G. T. Morgan, F. H. Burstall, *J . Chem. Soc.,* **1934**, 965; (b) E. Bielli, P. M. Gidney, R. D. Gillard, B. T. Heaton, *J. Chem. Soc., Dalton Trans.*, **1974**, 2133.

[211] J. S. Wu, C. Y. Chi, X. H. Wang, X. J. Zhao, J. Li, F. S. Wang, *Chin. Chem. Lett.,* **2001**, *12*, 387.

[212] J. Tang, X.-F. Liu, L.-Y. Zhang, X.-L. Xu, P.-R. Zhang, *Synth. Commun.,* **2000**, *30*, 1657.

[213] K. Griesbaum, *Angew. Chem., Int. Ed. Engl.,* **1970**, *9*, 273.

[214] J. Weinstein, M.T. Tierney, E.S. Davies, K. Base, A. A. Robeiro, M. W. Grinstaff, *Inorg. Chem.,* **2006**, *45*, 4544.

[215] A. Bondi, *J. Phys. Chem.*, **1964**, *68*, 441.

[216] Solvent parameters: toluene (0.172), THF (0.494), chloroform (0.610), dichloromethane (0.765), acetone (0.797), DMF (0.901), DMSO (0.973), acetonitrile (1.000).

[217] (a) J. A. Zuleta, J. M. Bevilacqua, R. Eisenberg, *Coord. Chem. Rev.,* **1991**, *111*, 237; (b) J. M. Bevilacqua, R. Eisenberg, *Inorg. Chem.*, **1994**, *33*, 2913.

[218] Notably, the emission profile of complexes **53-73** is also very similar to that found for the corresponding dichlorocomplexes [Pt(N^N)Cl$_2$], thus suggesting the E^E ligand is not involved in the emissive processes.

[219] A linear correlation (R^2 = 0.85) was also observed between the value of Φ determined for complexes of Series 1 (**53-59**, Scheme 3.6) and the ones of Series 2 (**60-66**, Scheme 3.7) featuring the same E^E ligands.

[220] C. Adamo, V. Barone, J. Chem. Phys., **1999**, 110, 6158.

[221] W.C. Ermler, R.B. Ross, P.A. Christiansen, *Int. J. Quant. Chem.*, **1991**, *40*, 829.

[222] J. Tomasi, B. Mennucci, R. Cammi, *Chem. Rev.*, **2005**, *105*, 2999.

[223] (a) T. Koopmans, *Physica*, **1934**, *1*, 104; (b) P. Politzer, A. A. Fakher, *Theor. Chem. Acc.,* **1998**, *99,* 83; (c) S. Hamel, P. Duffyc, M. E. Casidad, D. R. Salahub, *J. Electron. Spectrosc. & Rel. Phenom.,* **2002**, *123*, 345; (d) G. Zhang, C. B. Musgrave, *J. Phys. Chem A*, **2007**, *111*, 1554.

[224] R. S. Mulliken, *J. Chem. Phys.,* **1955**, *23*, 1833.

[225] D. C. Young, *"Computational Chemistry: A Practical Guide for Applying Techniques to the Real World Problems",* Wiley and Sons eds., **2001**.

[226] A. E. Reed, R. B. Weinstock, F. Weinhold, *J. Chem. Phys.*, **1985**, *83,* 735.

[227] (a) K. Kubo, A. Nakao, Y. Ishii, M. Tamura, R. Kato, G. E. Matsubayashi, *J. Low Temp. Phys.,* **2006**, *142*, 413; (b) K. Kubo, A. Nakao, Y. Ishii, R. Kato, G.-E. Matsubayashi, *Synth. Met.,* **2005**, *153*, 425.

[228] G. Sanna, M. I. Pilo, N. Spano, G. Minghetti, M. A. Cinellu, A. Zucca, R, Seeber, *J. Organomet. Chem.,* **2001**, *622*, 47.

[229] The crystal structures considered are those having the following refcodes in the Cambridge Crystallographic Database: AMEXIZ, HIRZIR, TAFJEQ, YEDPON, YEDPUT, and YEDQAA.

250

[230] J. R. Lakiwicz, *"Principles of Fluorescence Spectroscopy"*, Kluwer Academic Publishing/Plenum, New York, **1999**.

[231] Fityk 0.8, http://www.unipress.waw.pl/fityk/.

[232] G. M. Sheldrick, University of Göttingen, Germany, **1997**.

[233] A. Altomare, M. C. Burla, M. Camalli, G. Cascarano, C. Giacovazzo, A. Guagliardi, A. G. G. Moliterni, G. Polidori, R. *Spagna, J. Appl. Cryst.*, **1999**, *32*, 115.

[234] L. J. Farrugia, *J. Appl. Cryst.*, **1999**, *32*, 837.

[235] CheckCIF program (http://checkcif.iucr.org/).

[236] F. H. Allen, O. Johnson, G. P. Shields, B. R. Smith, M. Towler, *J. Applied Cryst.*, **2004**, *37*, 335.

[237] ^{13}C NMR could not be recorded on the products due to solubility reasons, and for the same reason the ^1H NMR analysis could not be performed on some of the synthesised complexes.

[238] M. J. Morris et al., unpublished results.

[239] Gaussian 03, Revision E.01, M. J. Frisch, G. W. Trucks, H. B. Schlegel, G. E. Scuseria, M. A. Robb, J. R. Cheeseman, J. A. Montgomery, Jr., T. Vreven, K. N. Kudin, J. C. Burant, J. M. Millam, S. S. Iyengar, J. Tomasi, V. Barone, B. Mennucci, M. Cossi, G. Scalmani, N. Rega, G. A. Petersson, H. Nakatsuji, M. Hada, M. Ehara, K. Toyota, R. Fukuda, J. Hasegawa, M. Ishida, T. Nakajima, Y. Honda, O. Kitao, H. Nakai, M. Klene, X. Li, J. E. Knox, H. P. Hratchian, J. B. Cross, V. Bakken, C. Adamo, J. Jaramillo, R. Gomperts, R. E. Stratmann, O. Yazyev, A. J. Austin, R. Cammi, C. Pomelli, J. W. Ochterski, P. Y. Ayala, K. Morokuma, G. A. Voth, P. Salvador, J. J. Dannenberg, V. G. Zakrzewski, S. Dapprich, A. D. Daniels, M. C. Strain, O. Farkas, D. K. Malick, A. D. Rabuck, K. Raghavachari, J. B. Foresman, J. V. Ortiz, Q. Cui, A. G. Baboul, S. Clifford, J. Cioslowski, B. B. Stefanov, G. Liu, A. Liashenko, P. Piskorz, I. Komaromi, R. L. Martin, D. J. Fox, T. Keith, M. A. Al-Laham, C. Y. Peng, A. Nanayakkara, M. Challacombe, P. M. W. Gill, B. Johnson, W. Chen, M. W. Wong, C. Gonzalez, and J. A. Pople, Gaussian, Inc., Wallingford CT, **2004**.

[240] Gaussian 09, Revision A.02, M. J. Frisch, G. W. Trucks, H. B. Schlegel, G. E. Scuseria, M. A. Robb, J. R. Cheeseman, G. Scalmani, V. Barone, B. Mennucci, G. A. Petersson, H. Nakatsuji, M. Caricato, X. Li, H. P. Hratchian, A. F. Izmaylov, J. Bloino, G. Zheng, J. L. Sonnenberg, M. Hada, M. Ehara, K. Toyota, R. Fukuda, J. Hasegawa, M. Ishida, T. Nakajima, Y. Honda, O. Kitao, H. Nakai, T. Vreven, J. A. Montgomery, Jr., J. E. Peralta, F. Ogliaro, M. Bearpark, J. J. Heyd, E. Brothers, K. N. Kudin, V. N. Staroverov, R. Kobayashi, J. Normand, K. Raghavachari, A. Rendell, J. C. Burant, S. S. Iyengar, J. Tomasi, M. Cossi, N. Rega, J. M. Millam, M. Klene, J. E. Knox, J. B. Cross, V. Bakken, C. Adamo, J. Jaramillo, R. Gomperts, R. E. Stratmann, O. Yazyev, A. J. Austin, R. Cammi, C. Pomelli, J. W. Ochterski, R. L. Martin, K. Morokuma, V. G. Zakrzewski, G. A. Voth, P. Salvador, J. J. Dannenberg, S. Dapprich, A. D. Daniels, Ö. Farkas, J. B. Foresman, J. V. Ortiz, J. Cioslowski, and D. J. Fox, Gaussian, Inc., Wallingford CT, **2009**.

[241] Æ. Frisch, H.P. Hratchian, R.D. Dennington II, T.A. Keith, John Millam, A.B. Nielsen, A.J. Holder, J. Hiscocks. Gaussian, Inc. GaussView Version 5.0., **2009**.

[242] Gabedit is a free Graphical User Interface for computational chemistry packages written by Abdul-Rahman Allouche. http://gabedit.sourceforge.net.

[243] G. Schaftenaar, J. H. Noordik, *J. Comput.-Aided Mol. Des.*, **2000**, *14*, 123.

[244] N. M. O'Boyle, A. L. Tenderholt, K. M. Langner, *J. Comput. Chem.*, **2008**, *29*, 839.

[245] Basis sets were obtained from Basis Set Exchange and Basis Set EMSL Library; (a) D. Feller, *J. Comput. Chem.,* **1996**, *17*, 1571; (b) K. L. Schuchardt, B. T. Didier, T. Elsethagen, L. Sun, V. Gurumoorthi, J. Chase, J. Li, T. L. Windus, *J. Chem. Inf. Model,* **2007**, *47*, 1045.

[246] K. Burke, J. P. Perdew, Y. Wang, in "*Electronic Density Functional Theory: Recent Progress and New Directions*", J. F. Dobson, G. Vignale, M. P. Das eds. (Plenum), **1998**.

[247] J. P. Perdew, K. Burke, M. Ernzerhof, *Phys. Rev. Lett.*, **1997,** *78* 1396.

[248] T. M. Henderson, A. F. Izmaylov, G. Scalmani, G. E. Scuseria, *J. Chem. Phys.*, **2009**, *131*, 044108.

[249] M. Ernzerhof, J. P. Perdew, *J. Chem. Phys.*, **1998**, 109.

[250] A. D. Becke, *J. Chem. Phys.*, **1993**, *98*, 5648.

[251] H. Iikura, T. Tsuneda, T. Yanai, K. Hirao, *J. Chem. Phys.* ,**2001**, *115, 3540.

[252] T. Yanai, D. Tew, N. Handy, *Chem. Phys. Lett.*, **2004**, *393*, 57.

[253] J.-D. Chai, M. Head-Gordon, *J. Chem. Phys.*, **2008**, *12*, 084106.

[254] L. E. Roy, P. J. Hay, and R. L. Martin, *J. Chem. Theory Comput.,* **2008**, *4*, 10290.

[255] W. J. Stevens, M. Krauss, H. Basch, P. G. Jasien, *Can. J. Chem.,* **1992**, *70*, 612.

[256] M. Kaupp, P. V. R. Schleyer, H. Stoll, H. Preuss, *J. Chem. Phys.*, **1991**, *94*, 1360.

[257] This basis set was chosen based on the good results obtained in the case of different gold complexes with variously substituted 2,2′-bipyridine donors (Ref. 197).